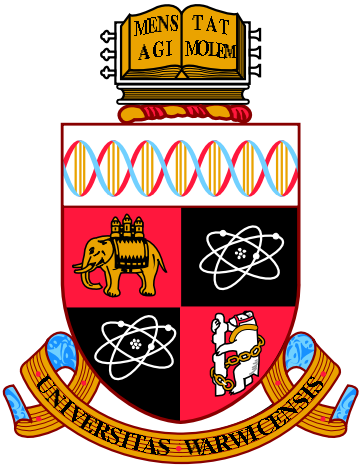

Correlation, concurrency, and clustering in network models of epidemics in human populations

by

Trystan Stewart Leng

Thesis

Submitted to the University of Warwick

for the degree of

Doctor of Philosophy

Mathematics for Real-world Systems Centre for Doctoral Training

April 2021

Contents

List of Tables

List of Figures

Acknowledgments

Firstly, I would like to thank my supervisor Matt Keeling for his support, wisdom, and patience. I'm still astounded at the insights you can provide in an hour-long meeting to a problem I've been pondering for weeks. Above all, thank you for being a kind and caring supervisor, who has made these last few years so enjoyable.

I would like to thank the numerous people who have discussed various aspects of this PhD with me, including (but almost certainly not limited to) Lorenzo Pellis, Mike Tildesley, Ed Hill, Connor White, and Xavier Didelot. In particular, I would like to thank Mark Jit and Yoon Choi at Public Health England for the conversations that provided the motivation for Chapter 5, and Stefan Flasche, whose support and guidance was invaluable to the research underlying Chapter 6.

The biggest thanks must go to my mother, father, and brothers Rhodri and Owain, for their unwavering support throughout this thesis and throughout my life. Everything I know about writing, rigour, and debate, I have learned from you.

Finally, I would like to thank every friend who has had to endure me discussing mathematical modelling, sexual networks, social bubbles, or any combination of the three. I would especially like to thank my only contact through the last year's various lockdowns, Marianne Etheridge, for reminding me that the world is bigger than these four walls and this laptop.

Declarations

The work presented here is my own, except where stated otherwise. This thesis has been composed by myself and has not been submitted for any other degree or professional qualification. The work presented (including data generated and data analysis) was carried out by the author except in the cases outlined below:

- The stochastic simulations in Chapter 3 were undertaken by M.J. Keeling.
- The age-stratified household composition data used in Chapter 6 was extracted and processed by J. Hilton.
- Figures 6.1, 6.4, 6.7 and 6.9 were visualised by S. Flasche.

Chapter 3 has been published as:

- **T. Leng** and M. J. Keeling. Improving pairwise approximations for network models with susceptible-infected-susceptible dynamics. *Journal of Theoretical Biology*, 500, p.110328, 2020.

Chapter 4 has been published as:

- **T. Leng** and M. J. Keeling. Concurrency of partnerships, consistency with data, and control of sexually transmitted infections. *Epidemics*, 25:35-46, 2018.

Chapter 6 has been published as:

- **T. Leng**, C. White, J. Hilton, A. Kucharski, L. Pellis, H. Stage, N.G. Davies, M.J. Keeling, and S. Flasche. The effectiveness of social bubbles as part of a Covid-19 lockdown exit strategy, a modelling study. *Wellcome Open Research*, 5(213), p.213, 2020.

Abstract

The spread of an epidemic can be conceptualised as a process on a network, where vertices refer to individuals and where edges refer to epidemiologically relevant connections between individuals. Understanding the impact of network structure on epidemiological outcomes is a central task in mathematical epidemiology. Accordingly, a range of mathematical models incorporating network structure have been designed. In this thesis, we develop a range of network models in the context of epidemics in human populations.

Firstly, we consider a novel moment-closure approximation for a disease with susceptible-infected-susceptible dynamics. For diseases without immunity, the possibility of re-infection can introduce *correlations* in infection status between indirectly connected individuals, limiting the accuracy of moment-closure approaches. By incorporating these correlations into a model, we introduce an improvement to the standard pairwise approximation for two different network structures: the isolated open triple and the k-regular network.

Secondly, we assess the importance of including *concurrent* sexual partnerships, partnerships that overlap in time, when modelling the control of sexually transmitted infections. We do this in two distinct settings, firstly developing nested pair-formation models before developing an individual-based dynamic network model of a heterosexual population. In both instances we find that while concurrency can have a large impact on epidemiological dynamics, the inclusion of concurrency in models matched to prevalence data has only a modest impact on control measures.

Thirdly, we consider the extent to which the *clustering* imposed by social bubbles, where two households form an exclusive social group, is an effective way of increasing social contact while minimising the resulting increase in transmission in the context of COVID-19. Using a stochastic, generation-based network model of household and bubble contacts, we find that social bubble strategies are effective at minimising transmission when compared to unclustered increases in contacts.

Chapter 1

Introduction

Our lives are defined by our relationships with others - or at least this much is true when it comes to the spread of infectious diseases. The process of a pathogen spreading is inherently relational - infectious diseases spread *from* an infected individual *to* an uninfected individual. This transfer requires the two individuals to be in some sense 'connected' - though what counts as a connection depends on the pathogen in question. At least in theory, by understanding the totality of such connections, we can begin to understand the spread of any epidemic, and by tracing these connections we can begin to control the spread of any epidemic. We refer to this totality of connections as a *network*.

In most cases, a network approach to modelling epidemics faces myriad difficulties. For many pathogens, even defining the underlying network of connections would be difficult or impossible. If a pathogen can survive while airborne over long distances, or can survive remotely on inanimate surfaces, an individual will inevitably be connected to contacts they have no direct knowledge of. Other pathogens are transmitted via vectors, such as malaria and mosquitoes, or can be transmitted through animal reservoirs, such as rabies and dogs. In such cases, the relevant contacts include non-human, and therefore practically untraceable, connections.

For pathogens requiring relatively close human-to-human contact for transmission, the varied and fleeting nature of people's ordinary social interactions makes reconstructing this network of connections a daunting task. In most cases, the data practically obtainable are egocentric accounts of only a fraction of relevant contacts, and are insufficient to faithfully reconstruct the underlying epidemiologically relevant contact network from.

Yet if we are able to capture this contact structure, network modelling approaches can play an integral role in both understanding the dynamics of epidemics and predicting the impact of control measures. Here, we consider two distinct scenarios that are particularly suited to a network approach. These scenarios are outlined below, and are the subject of this thesis.

1.1 Sexually transmitted infections and the structure of sexual networks

Sexually transmitted infections (STIs) are pathogens that are primarily transmitted via unprotected sex. With STIs, the connection between networks and the spread of epidemics is at its clearest. An individual's epidemiologically relevant contacts are simply their partners in sexually active relationships. These contacts often persist over long durations compared to other social contacts. While the contact networks relevant to the spread of a respiratory pathogen often change within the space of a day, people may have the same sexual partner over a period of weeks, months, or even years. This is particularly true in the heterosexual population, where relatively long partnerships and serial monogamy is the prevailing social norm in the UK [Johnson et al., 2001]. As many STIs are often symptomless, or at least symptomless in the early stages of infections, sexual behaviour can continue unaltered.

Syphilis is a bacterial STI that, although initially painless, can be fatal if untreated. In previous generations, syphilis infection was commonplace. Over 20,000 diagnoses were made in the UK at the peak of infections in 1946 [Mohammed et al., 2018], and the disease was reported to have afflicted several famous figures, including the philosopher Friedrich Nietzsche, the painter Edouard Manet, and the gangster Al Capone [Sarbu et al., 2014]. Like many bacterial infections, the treatment of syphilis was transformed by the discovery of antibiotics - a previously incurable disease was now easily remedied by a course of antibiotics prescribed by a doctor. The introduction of such treatment, in part, led to a large reduction in the prevalence of syphilis - by 1995, there were fewer than 300 diagnoses in the UK. Yet this respite was not to last. At the turn of the millennium, syphilis diagnoses in the UK began to rise, and have not stopped rising since, with almost 8,000 diagnoses in 2019 in England alone [Office for National Statistics, 2020b].

The recent trend of syphilis is echoed by the trends of other STIs in the UK; diagnosed cases in England of both chlamydia and gonorrhoea have increased by 46% and 277% since 2010 respectively [Office for National Statistics, 2020b]. This is despite the fact that these STIs are currently easily treatable. To those interested in public health, two questions naturally arise: firstly, what is causing this increase in cases and secondly, how do we stop it?

We have the potential to treat or prevent infection for many STIs. For the human papillomavirus (HPV), responsible for the majority of cases of cervical cancer [Muñoz et al., 2003], a vaccine is available and vaccination campaigns have been rolled out across many countries [Markowitz et al., 2012]. Vaccines are being developed for other STIs, including the human immunodeficiency virus (HIV) [Bekker et al., 2018] and chlamydia [Abraham et al., 2019], and have been suggested as potential control measures against others [Gottlieb et al., 2014]. For those in groups considered at risk of contracting HIV, routinely taking pre-exposure prophylaxis (PrEP) medication can significantly reduce an individual's chance of contracting

the virus [McCormack et al., 2016]. For other STIs, where treatments are available, methods that identify and contact individuals likely exposed to infection can be an effective way to reduce cases [Eames and Keeling, 2002]. To best deploy the many tools we have to control the spread of STIs, we must be able to forecast their likely impact, and to do so we must know what features of the real-world have a significant impact on such forecasts.

Because it is obvious who should count as an epidemiologically relevant contact, we are able to collect data on the underlying network of sexual contacts. Because sexual contacts are, compared to contacts relevant to respiratory pathogens, sparse and longlasting, the impact of network structure is pronounced [Keeling et al., 2016]. Therefore, an understanding of the impact different aspects of network structure have, and an understanding of how correlations build up across sexual networks, is key to understanding the spread of STIs. Further, understanding the impact network structure can have on the control of STIs is paramount when planning public health strategies.

STIs and sexual networks are the focus of Chapters 3, 4, and 5 of this thesis. For many STIs, recovery from infection does not lead to immunity. This possibility of reinfection provides a further source of *correlations* between the infection status of individuals within a sexual network, over and above the correlations that result from disease dynamics where reinfection is not possible. Chapter 3 aims to understand these correlations, and utilise them to improve approximate network models of STI spread. Chapters 4 and 5 consider the impact of *concurrent* partnerships, sexual partnerships that overlap in time. By designing models that can be matched to observed levels of concurrent partnerships, we assess the importance of capturing *concurrency* in models forecasting the control of STIs.

1.2 COVID-19 and the role of social structure

In normal times, people's social lives are varied and variable - varied in that people have different social contacts corresponding to different aspects of their lives (e.g. friends, family, colleagues), and variable in that the social connections people make may vary substantially from day to day. Consequently, accurately recalling one's social contacts is a non-trivial task in and of itself. Even with perfect recall, it is not always clear who should count as an epidemiologically relevant contact in the context of respiratory pathogens. As Eames et al. [2015] pose, if you have travelled on a bus, should every other person on the bus count as a relevant contact, or only those in close proximity to you? In part because of the difficulty in accurately defining the underlying relevant contact network, the field of epidemiology concerning the spread of respiratory pathogens has often utilised methods that do not explicitly consider contact network structure.

However, these are not normal times. At the time of writing, we are in the midst of a global pandemic of severe acute respiratory syndrome coronavirus 2 (SARS-CoV-2), the pathogen responsible for coronavirus disease 2019 (COVID-19) [Wu et al., 2020]. To counter the spread of this pathogen, to protect health services from being overrun, and ultimately to save lives, unprecedented social restrictions have been placed on populations across the world [Hsiang et al., 2020]. These non-pharmaceutical interventions have included general social distancing measures, the closure of schools, non-essential shops, bars, and restaurants, asking all those who can to work from home, and the prohibition of households from mixing socially. Collectively, these restrictions have been referred to as 'lockdowns'.

Under lockdown restrictions, and assuming that restrictions are being adhered to, people's social networks are radically transformed. Previously varied and transitory, social contacts within a lockdown situation are limited, fixed, and centred around households [Jarvis et al., 2020]. Yet because of this, we are able to cap-

ture a large number of epidemiologically relevant contacts. This overhaul must have an impact on the spread of epidemics - indeed, that is why such measures are introduced. By utilising this information effectively, there is the potential to understand in finer detail the epidemiological consequences of lockdown policies, as well as what interventions are likely most effective in controlling the spread of this pandemic.

People's social lives are important to them. The isolation imposed by lockdown policies will likely have a detrimental impact on the mental health of many. Exploiting the implications of network structure may provide us ways to expand our social lives, and return a semblance of normality to those that need it most. *Clustering* the social contacts of individuals has been suggested as a potential solution, with the aim of minimising the resulting increase in transmission from allowing individuals to expand their social lives [Block et al., 2020; Willem et al., 2021]. To understand the extent to which this approach is beneficial, one must understand the impact that the resulting network structure implied by relaxation has on the spread of an epidemic. The impact of one such strategy, known as the 'social bubble' strategy, in the context of a lockdown in the UK, is the focus of Chapter 6.

1.3 Mathematical models

Mathematical models play a central role in the study of epidemics. These tools, abstractions of real-world systems simplified and rewritten in the language of mathematics, play two distinct roles. By simplifying the process of epidemics to core aspects, researchers gain an *understanding* of why epidemics unfold in the way they do, and the impact different features have on epidemiological outcomes. By incorporating aspects of the real-world that have a significant impact on the spread of epidemics into sophisticated models, researchers are able to *predict* the course of

epidemics, and crucially the impact of possible control strategies. Often, these two aims are in conflict, and a model most useful for understanding is in general not the model with the best predictive accuracy, and vice versa [Keeling and Rohani, 2011]. Yet they also complement one another: for example, to create accurate *predictive* models to forecast the spread of epidemics, one must *understand* what features of the real-world have a significant impact on the spread of epidemics.

Since the seminal works of Kermack and McKendrick [1927], the mathematical study of epidemics has traditionally used models that do not explicitly account for the underlying structure of contact networks. By adapting and refining these models, researchers have been able to understand the behaviour of epidemics and predict their spread. Today, models of this type are still widely used, and play a key role in public health [Rozhnova et al., 2019; Keeling et al., 2021; Chin et al., 2020]. However, to understand the impact network structure has, and the impact of this structure on control measures, methods that take into account network structure must be developed.

In response, a range of mathematical models incorporating network structure have emerged [Keeling and Eames, 2005; Danon et al., 2011; Kiss et al., 2017]. Despite the progress in many areas, many challenges remain in implementing a network approach to modelling the spread of epidemics [Eames et al., 2015; Pellis et al., 2015a]. This thesis aims to resolve some of these challenges in specific contexts. The structure of this thesis is outlined below.

1.4 Thesis outline

In Chapter 2, we survey the relevant academic literature concerning the application of network models to the spread of epidemics on human populations. We begin by introducing network theory, available data on sexual and social networks, and

briefly introduce the development of epidemic models without network structure. Then, we consider the development of static network models that aim to capture or understand the correlations in infection status between infectious individuals, before considering the development of dynamic network models that aim to capture the impact that concurrent partnerships, partnerships that overlap in time, have on the spread of STIs. Finally, we consider the impact that clustering has on the spread of pathogens, the clustering imposed by household structure, and the models capturing this structure.

Incorporating waning immunity into network models remains a key challenge for network epidemic models, as the possibility of reinfection can lead to correlations in infection status of indirectly connected individuals [Pellis et al., 2015a]. In Chapter 3, we develop a static network modelling approach for diseases with susceptible-infected-susceptible (SIS)-dynamics that improves upon previous models by incorporating the *correlation* between infection statuses of individuals into pairwise approximations. We introduce improved pairwise approximations in two distinct but related contexts, first introducing an approximation for the disease states of an isolated open triple before introducing an analogous approximation for k-regular networks. Doing so, we gain an insight into the errors introduced by previous approximations, and obtain models capable of closer matching the prevalence levels obtained from more detailed models and stochastic simulations.

Clarifying the impact of network properties on epidemiological outcomes has also been identified as a remaining challenge in the field [Pellis et al., 2015a]. Doing so is necessary to understand the features of network features that have a substantive impact on outcomes, to inform the level of detail required in models for public health. In Chapter 4, we use a dynamic network model to assess the importance of explicitly matching models to observed levels of *concurrency* when modelling the control of STIs by vaccination. Specifically, we compare the required levels of vaccination to eliminate a disease with SIS-dynamics in three nested pair-formation

models - one where infection can only be transmitted via a stable sexual partnership, one where single individuals can also acquire infection via casual partnerships with other single individuals, and one that incorporates concurrent partnerships by allowing individuals in stable partnerships to acquire infection via casual partnerships. We find that, at a fixed transmission rate, concurrency has a large impact on required levels of vaccination, but when models are matched to prevalence data, models require similar levels of vaccination to eliminate the disease from the population. This result suggests that models that accurately capture concurrency may not always be needed to forecast the impact of control measures against STIs.

The impact of concurrency in models matched to prevalence data is explored further in Chapter 5. In this chapter, we introduce a stochastic individual-based dynamic network model of a heterosexual population that is capable of being fitted to behavioural data collected from egocentric surveys of sexual partnerships, including yearly degree distributions and yearly levels of concurrency. We compare the results from this model to two alternative models that represent the opposite extremes of assumptions concerning concurrent partnerships - one that assumes individuals are serially monogamous, and one that assumes the rate individuals form partnerships is independent of the number of partnerships they are currently involved in. We fit each model to data from the National Survey of Sexual Attitudes and Lifestyle (Natsal), and find that while the instantaneous network structure of each model differs considerably, the impact of control measures is similar across models when matched to prevalence data. Doing so, we not only introduce a flexible framework for modelling dynamic heterosexual networks, but provide a further evaluation of the importance of matching models of STI control to observed levels of concurrency.

Designing network-based interventions that utilise and exploit network structure to aid the control of epidemics is another key challenge identified by Pellis et al. [2015a].

In Chapter 6, we move away from STIs, and consider the application of network models to respiratory pathogens. Specifically, we use a stochastic generation-based static network model to assess the impact of allowing households to form 'social bubbles', exclusive groups of two households that are allowed to socialise freely with one another, on transmission of SARS-CoV-2. By creating a synthetic population sampled from the household composition distribution of the most recent census of England and Wales, we assess the impact of different social bubble strategies that target different subsets of households on both transmission and mortality. We find that, when restricted to households that are likely to benefit most, social bubbles have only a limited impact on transmission. We assess the specific impact the *clustering* imposed by social bubbles has by comparing social bubble scenarios against counterfactual situations where individuals make comparable numbers of infectious contacts, but in an unclustered fashion. We find that social bubble strategies are an effective way of increasing contacts while minimising increases in transmission and fatalities compared to unclustered increases in contacts.

Together, this thesis develops a variety of network approaches to modelling the spread of epidemics. By doing so, we not only advance the field of network epidemiology in specific areas; we also demonstrate the wealth and diversity of network approaches to modelling epidemics, their capacity to answer a range of theoretical and applied questions, and the details that must be taken into account when designing network models. We conclude this thesis in Chapter 7, where we offer some final thoughts on the implications of our results, the limitations of our approaches, and potential areas for future work.

Chapter 2

Background

In this chapter, we survey the academic literature concerning the application of network approaches to epidemic modelling on human populations. In Section 2.1, we provide a brief introduction to network theory and its numerous applications. In Section 2.2, we consider the data available that describes sexual network structure and social network structure. In Section 2.3, we consider the development of epidemic models without explicit network structure. In Section 2.4, we consider the *correlations* imposed by network structure in epidemic models, and the development of approximate static network models that aim to understand these correlations. In Section 2.5, we consider the impact *concurrency* has on the spread of sexually transmitted infections (STIs), and the range of dynamic network models developed to understand its effects. In Section 2.6, we explore the impact that *clustering* has on the spread of epidemics on networks, the clustering imposed by household structure, and the models including such structure.

2.1 A brief introduction to networks

A network is an abstract representation of a system consisting of elements that in some sense interact or are connected with one another. Using terminology from graph theory, the elements are referred to as *vertices*, V, while the connections are referred to as *edges*, E. The network (or *graph* in graph theory) is given by the set of these vertices and edges, which can be represented graphically as dots and lines:

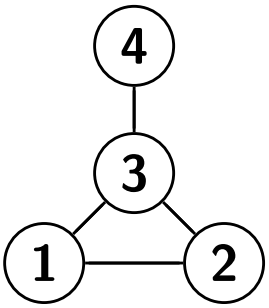

Figure 2.1: **An example network.** The numbers within each vertex represent the relevant row/column of each individual in the adjacency matrix that defines it, given in Equation (2.2).

Networks are a convenient representation of systems whose behaviour depends on the structure of these interactions. While the nature of the elements and connections may differ drastically from real-world application to real-world application, these different systems may share a common structure, and therefore the same suite of tools may be useful across disparate disciplines. Indeed, the study of networks has been developed and applied across the sciences and social sciences - from the structure of the world wide web [Albert et al., 1999] to the stability of food webs [Johnson et al., 2014]; from the role of gene regulatory networks [Davidson and Levin, 2005] to the patterns of academic citations [Price, 1965]; from optimising transport networks [Von Ferber et al., 2009] to understanding neural networks [Bassett and Sporns, 2017].

Given its wide and varied applications, a slew of terminology has been developed for similar or equivalent concepts. In this thesis, vertices are typically referred to as individuals and edges between vertices as connections. This is the most natural terminology due to our focus on human populations. In some instances, however, the terminology of vertices and edges is used when it is more natural to the application.

While networks can be represented graphically, other representations of a network are much more convenient mathematically and computationally. Networks can be represented as *adjacency matrices*. Assuming all edges are of equal strength, an adjacency matrix A is defined as:

$$A_{ij} = \begin{cases} 1 \text{ if individual } j \text{ is connected to individual } i, \\ 0 \text{ otherwise} \end{cases} \tag{2.1}$$

The network from Figure 2.1 can be represented by the following adjacency matrix:

$$A = \begin{pmatrix} 0 & 1 & 1 & 0 \\ 1 & 0 & 1 & 0 \\ 1 & 1 & 0 & 1 \\ 0 & 0 & 1 & 0 \end{pmatrix} \tag{2.2}$$

For networks where edges are *undirected*, as in Figure 2.1, adjacency matrices are symmetric, i.e. $A = A^T$. Undirected networks are a natural representation of *contact* networks in the context of epidemiology - if you have been in close contact long enough to be able to infect someone, it is natural to assume they have been in close contact long enough to be able to infect you. In contrast, directed networks are

not symmetric, i.e. $A_{ij} = 1 \not\Rightarrow A_{ji} = 1$. Directed networks are a natural representation of *transmission* networks in the context of epidemiology, where connections denote transmission events - transmitting infection to someone does not necessarily mean they will transmit infection to you. While transmission networks are of practical interest in the context of contact tracing, the structure of these transmission networks are determined by the underlying contact network. Because of this, network models of epidemics focus on capturing the structure of contact, and hence undirected, networks (with some exceptions, such as Sharkey et al. [2006]). In contact networks, individuals are typically not be considered epidemiologically relevant contacts of themselves, and hence $A_{ii} = 0$. The above definition of an adjacency matrix can be extended to include weighted or multiple edges [Newman, 2010], though this is not considered here.

Many quantities and measures have been defined that capture properties both at the level of individuals and at the level of the network as a whole [Newman, 2010]. We restrict our discussion to three concepts of interest to this thesis: the degree of an individual, the degree distribution of a network, and the clustering coefficient of a network. The *degree* of an individual i in a network is the number of connections i has to other individuals. For an undirected network of n individuals, the degree of an individual i, denoted k_i can be expressed in terms of the adjacency matrix A:

$$k_i = \sum_{j=1}^{n} A_{ij} \tag{2.3}$$

By calculating the proportion of individuals of each degree, we obtain the *degree distribution* of a network, which equivalently can be thought of as the probability distribution of randomly choosing an individual with degree k. Degree distributions are important when modelling, for two reasons. Firstly, observed degree distribu-

tions of social networks have a non-random structure. If individuals' social contacts were random, i.e. connections between every individuals existed with some probability p, the degree distribution of social networks would be binomially distributed, which tends to the Poisson distribution as network size increases [Newman, 2003]. However, social networks are typically characterised by having a *heavy tail* of highly connected individuals, with a degree distribution that can be approximated by a power-law distribution [Liljeros et al., 2001; Schneeberger et al., 2004]. Secondly, in many cases degree distribution data is the only source of data practically obtainable for social networks [Danon et al., 2011].

The level of clustering within a network is also of practical interest to many applications. The global clustering coefficient, ϕ, of an undirected network can be defined in terms of open and closed triples (which are shown graphically in Figure 2.2), as in Newman [2010]:

$$\phi = \frac{\text{\# of closed triples}}{\text{\# of open and closed triples}} \tag{2.4}$$

As an undirected network is defined uniquely by an adjacency matrix A, ϕ can be obtained from the formula below [Keeling and Eames, 2005]:

$$\phi = \frac{\sum_{i,j,k} A_{ij}A_{jk}A_{ki}}{\sum_{j \neq k} A_{ij}A_{ki}} = \frac{tr(A^3)}{||A^2|| - tr(A^2)} \tag{2.5}$$

where tr denotes the *trace* of a matrix A and where $||.||$ denotes the sum of all elements in the matrix. The concept of clustering is particularly relevant to the study of epidemics on networks - due to its presence in social networks and its relative absence in sexual networks. While the above measures are not used explicitly in this thesis, the concept of clustering is relevant to many of the chapters. For example, Chapter 3 focusses on open triples to model unclustered populations, while

Chapter 6 focusses on social networks comprising of household contacts, i.e. highly clustered networks.

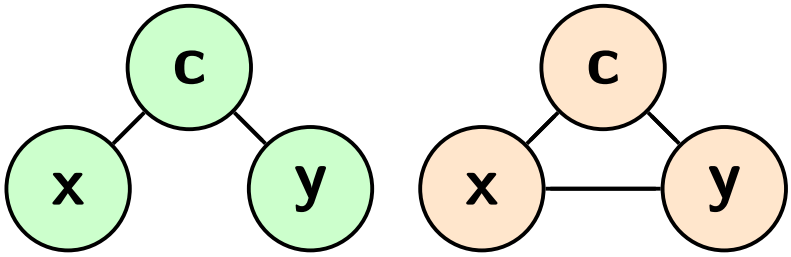

Figure 2.2: **Network representation of open and closed triples.** In open triples, individuals x and y are only indirectly connected via individual c. In contrast, x and y share a direct connection in closed triples.

2.2 Social and sexual network data

Both applied and theoretical models of epidemics on networks must consider the structure of social networks. Applied models must be matched to epidemiologically relevant network data, whereas theoretical models must consider the general features present in real-world data to ascertain whether they are epidemiologically relevant. Working optimally, there should be a symbiosis between theoretical and applied work. Data collection can be used to inform researchers about the network structure present in real-world social networks, while theoreticians can ascertain the extent to which network features have an epidemiological impact. These efforts inform both applied modellers of what must be included in detailed models for public health, and also informs future data collection on potentially important network features to measure. Accordingly, various studies have sought to ascertain the structure of epidemiologically relevant networks, using a variety of methods [Klovdahl et al., 1994; Johnson et al., 2001; Mossong et al., 2008]. Of course, what counts as an epidemiologically relevant contact depends on the infectious disease in question, which in turn impacts the most suitable data collection method.

2.2.1 Sexual network data

For STIs, who should count as epidemiologically relevant is straightforward - infection is spread through active sexual partnerships, particularly between those engaging in condomless intercourse. To ascertain whether such a contact has occurred, participants of a data collection study are simply asked, either through interviews or surveys. To obtain a more detailed understanding of the structure of sexual networks, collection methods have been developed that involve contacting the contacts of initial participants, such as snowball sampling [Goodman, 1961] or respondent-driven sampling [Heckathorn, 1997]. While several studies have used these techniques to collect sexual network data in high-risk groups [Klovdahl, 1985; Klovdahl et al., 1994; Wylie and Jolly, 2001], this approach has several limitations. Sexual behaviours and sexual partnerships are a sensitive topic, particularly in the context of studying the spread of STIs. Because of this, both recruiting individuals onto a study and obtaining accurate information about partnerships from recruited individuals can be a challenge, particularly if they are concerned about their anonymity. These approaches also have a more theoretical limitation; methods that rely on contacting the partners of participants only reveal the network structure of one connected component, when it is possible in reality that many disconnected components exist [Danon et al., 2011]. The network characteristics of the obtained component may differ from the network as a whole, and disconnected components sampled at one time may connect at a later time. These approaches can also be extremely time-consuming and labour intensive, making them unsuitable for capturing the network structure of sexual networks at a population level.

A more common data source to inform public health models for STIs are *egocentric surveys*. These typically ask a representative sample of the target population questions about both the number and characteristics of their epidemiologically relevant contacts. These surveys attempt to capture the network structure of a population at an individual level, and do not consider network properties that require

knowledge of contacts of contacts, such as levels of clustering. For STIs in the UK, the decennial National Survey of Sexual Attitudes and Lifestyle (Natsal) is a comprehensive survey asking a wide range of questions concerning individuals' sexual behaviour [Johnson et al., 2001; Mercer et al., 2013]. Similar surveys have been used in other countries [Lewin et al., 1998], and for men who have sex with men (MSM) specifically [Dodds et al., 2000; Weiss et al., 2020]. The Natsal studies have formed the basis of many modelling studies central to STI control policy, in particular studies assessing the impact of vaccination programmes against the human papillomavirus (HPV) [Jit et al., 2008; Choi et al., 2010; Datta et al., 2019].

These studies reveal many aspects of sexual network structure pertinent to mathematical modelling. A frequently observed feature of sexual networks is a *heavy-tailed* degree distribution of sexual partnerships, which in many cases can be approximated by a power-law [Liljeros et al., 2001; Schneeberger et al., 2004], and is a feature apparent from the Natsal studies. This distribution implies that the lion's share of sexual contacts are undertaken by a relatively small group of individuals. Because of this, sexual networks are often referred to as possessing a 'core group' of individuals - individuals who are active enough within a population to transmit an infection to more than one individual [Yorke et al., 1978]. The studies confirm that, in the UK, serial monogamy is the prevailing social norm. This is not a feature of sexual networks universally - in some cultures polygyny is practiced [Reniers and Watkins, 2010], while populations of MSM often have more lax social conventions surrounding monogamy [Parsons et al., 2013]. However, the studies do confirm that the heterosexual UK population is not entirely monogamous - a modest but substantial proportion (14.6% of men and 9.0% of women) of the population report being involved in a *concurrent* partnership every year [Johnson et al., 2001], defined as being in more than one sexually active partnership at the same time. By recording the age of respondents, and asking about the ages of contacts, the Natsal studies have helped understand sexual mixing patterns between age groups [Smid

et al., 2018], and while the studies are cross-sectional rather than longitudinal, they ask questions about the number of partnerships in different timeframes, and the duration of partnerships, making them a rich source of data for modelling networks that change dynamically through time.

The reconstruction of heterosexual networks from egocentric data raises unique difficulties. Within a closed population, the number of heterosexual partnerships involving a woman is necessarily equal to the number of heterosexual partnerships involving a man. In a representative sample of the population, and assuming that the size of the population of sexually active men and women is approximately equal, then the average number of heterosexual partnerships reported by women should approximately equal the average number reported by men. However, studies have consistently shown that men report a higher average number of partners than women [Mercer et al., 2013; Mitchell et al., 2019]. A number of hypotheses have been suggested to explain this discrepancy, including the undersampling of female sex workers [Brewer et al., 2000], cognitive biases in rounding errors [Brown and Sinclair, 1999], and social factors facilitating either the overestimation of partnerships by men or the understatement of partnerships by women [Alexander and Fisher, 2003]. In any case, models fitted to egocentric heterosexual must capture the data available for both sexes while resolving this discrepancy in some way [Garnett and Anderson, 1994].

2.2.2 Social network data

For the underlying contact networks relevant to respiratory pathogens, who should count as an epidemiologically relevant contact becomes harder to define. Typically, researchers define criteria about the proximity, duration, and type of contact to ascertain whether a contact counts as relevant. As for STIs, participants may be asked through interviews or surveys about those contacts (e.g. Mossong et al.

[2008]). Unlike with STIs, sensors or mobile devices may be used to automatically infer social contacts (e.g. Salathé et al. [2010]). Both approaches face significant challenges. While some contacts relevant to respiratory pathogens are extremely longlasting, such as household or family members, others are fleeting, such as one-time contacts in a bar or on public transport. Because of this, participants may struggle to recall all relevant contacts accurately. For contact networks inferred via technological means, a high uptake is required to obtain meaningful information, and there are ethical and practical concerns about researchers having access to such data [Eames et al., 2015].

Egocentric surveys have been undertaken that detail the properties of people's social contacts relevant to respiratory pathogens, notably the Polymod surveys [Mossong et al., 2008] for influenza and the CoMix surveys for COVID-19 [Jarvis et al., 2020]. These surveys typically involve individuals recording a diary of their social contacts over a defined period of time. These studies tell us important features of social networks. For example, social networks are highly assortative by age, and mixing patterns are consistent across many European countries [Mossong et al., 2008]. However, egocentric data is *ipso facto* unable to tell us about the level of clustering within social networks. While the reconstruction of sexual networks from egocentric data under the assumption that clustering of contacts is rare is reasonable, doing so for social networks would be a significant departure from reality. The clustering of contacts is a hallmark of social networks - this has been consistently observed in small-scale studies of social networks [Goodreau et al., 2009], but is also something obvious to us from our everyday lives. Because of this, studies utilising these studies, more often than not, circumvent this complication by using these data to infer mixing patterns in models of populations with no explicit network structure [Wallinga et al., 2006; Baguelin et al., 2010; Keeling et al., 2021], the methods outlined in Section 2.3.

Other studies have attempted to capture the relevant contact networks in specific

settings, such as schools [Salathé et al., 2010; Conlan et al., 2011] and hospitals [Isella et al., 2011]. Such data may be used to inform network models of diseases within particular settings, but these studies account for only a subset of epidemiologically relevant contacts. For example, those in school will interact with others outwith the school setting, and these contacts may impact on resulting epidemiological dynamics. The importance of capturing extraneous connections, and the implications external network structure has on the seeding of epidemics within structured environments, is raised by Eames et al. [2015] as a key challenge when measuring contact networks.

By restricting our attention to household contacts, and under the assumption that those sharing a household are in close enough contact to be epidemiologically relevant, we are able to gain a source of data that does account for the clustering of contacts. In the UK, a census of household composition is undertaken every 10 years, the most recent census of England and Wales occurring in 2011 [Office for National Statistics, 2020a]. For this census, the full data on household contacts (as opposed to a sample obtained from egocentric methods) is obtainable. These data contain fine-scale information about households by geographical area, and also contain the composition of households by age and size. While censuses provide a rich data set of social contacts, the obvious limitation is that, at least in normal times, household contacts represent only a fraction of people's epidemiologically relevant contacts.

2.3 Modelling epidemics without network structure

Historically, the field of mathematical epidemiology has used methods that do not incorporate explicit network structure. The early models formulated by Kermack and McKendrick [1927] assumed that individuals mix randomly as in the mixing patterns of molecules in an ideal gas. Consequently, the rate of social contact of

any individual is homogeneous and constant across the population. Such contacts are also assumed to be instantaneous. Each individual is considered as belonging to a discrete *state* signifying their infectious status. While the original works of Kermack and McKendrick [1927] describe a general modelling framework where the infectivity of an infectious individual and their chances of recovery or death vary over the course of an individual's infectious period, a special case of their model was popularised by Anderson and May [1979] that assumed transmission and recovery/removal occur at constant rates. In this model, known commonly as the Susceptible-Infected-Removed (SIR) model, individuals are classified as either being susceptible, denoted by S, infectious, denoted by I, or removed (or recovered), denoted by R. The number or proportion of individuals in each state is then aggregated into a *compartment*. Assuming a constant rate of recovery from the infectious state, the rate of change between compartments is captured in the following system of ordinary differential equations (ODEs), here expressed in more familiar notation, as in Keeling and Rohani [2011].

$$\frac{dS}{dt} = -\beta SI \tag{2.6}$$

$$\frac{dI}{dt} = \beta SI - \gamma I \tag{2.7}$$

$$\frac{dR}{dt} = \gamma I \tag{2.8}$$

Here, γ denotes the rate of recovery, i.e. the inverse of infectious period, and β denotes the product of the contact rate and transmission probability. β can be thought of as a term that informs us about the number of contacts an individual has: the higher number of contacts individuals have in the population, the higher β.

The success of this paradigm is due to its flexibility. Since its inception, this frame-

work has been refined to incorporate multiple heterogeneities in mixing patterns between different subgroups of a population [Hethcote and Yorke, 1984; Grenfell and Harwood, 1997; Keeling and Rohani, 2011]. Provided there is relevant data available, these mixing patterns can be encoded in a matrix known as the Who Acquires Infection From Whom (WAIFW) matrix [Keeling and Rohani, 2011]. The framework has also been extended to incorporate much more realistic disease dynamics than those of the original SIR-model [Anderson, 1988; Grenfell et al., 2001].

This approach also allows for the calculation and definition of the basic reproduction number, R_0, a term central to the mathematical study of epidemiology, defined as the average number of secondary infections caused by a primary infected individual in a completely susceptible population. Importantly, R_0 exhibits a thresholding property - $R_0 > 1$ is required for an epidemic to spread throughout the population. For a randomly mixing population at the infinite population limit, R_0 can be calculated by finding the dominant eigenvalue of the next generation matrix [Diekmann et al., 1990].

As many STIs do not lead to immunity after recovery from infection, these equations must be adapted, to a susceptible-infected-susceptible (SIS)-model:

$$\frac{dS}{dt} = \gamma I - \beta SI \tag{2.9}$$

$$\frac{dI}{dt} = \beta SI - \gamma I \tag{2.10}$$

These deterministic models without explicit network structure, often referred to as random-mixing models or mean-field models, were used to glean some of the earliest results on the spread of STIs [Cooke and Yorke, 1973; Yorke et al., 1978; Hethcote and Yorke, 1984], finding that the disease dynamics of STIs imply an endemic prevalence of infection within the population, and that STI epidemics are

driven by a core group of highly active individuals.

The SIS-paradigm is still widely used to approximate the infection dynamics of bacterial STIs, such as chlamydia, gonorrhoea, and syphilis, both in models with and without explicit network structure [Kretzschmar et al., 2009; Chesson et al., 2016; Smid et al., 2018], often with the inclusion of separate compartments for symptomatic and asymptomatic infection [Tuite et al., 2018; Rönn et al., 2020]. The dynamics of human papillomavirus (HPV) have also been modelled under the SIS-paradigm [Ribassin-Majed et al., 2014; Taira et al., 2004], although this may be an idealisation of the true dynamics [Beachler et al., 2016], and other studies have modelled HPV as having different epidemiological dynamics [Horn et al., 2013]. However, this paradigm is not appropriate for all STIs, and in particular is unsuitable when modelling the dynamics of HIV, where recovery does not occur. While the assumption of SIS-dynamics is still widely used, other approaches that include greater realism have been developed including the addition of an incubation period [Whittles et al., 2019], the modelling of within-host dynamics (particularly for HIV) [Perelson and Ribeiro, 2013], and site-specific infection [Jenness et al., 2017].

While mean-field models do not consider network structure explicitly, they assume some implicit network dynamics, either through the absence or through the presence of risk structure within the population. At the infinite population limit, social contacts occurring at a constant rate implies that the degree distribution of contacts would be Poisson distributed [Newman, 2003], a departure from the observed degree distributions of sexual and social networks. Further, under this framework, infectious contacts are instantaneous; as contacts only last an instant, it is hard to even define the concepts of concurrency or clustering.

Despite this, models without explicit network structure have continued to be deployed and refined, and are still a vital tool for public health. There are often advantages to taking this approach. As previously stated, the underlying network

of epidemiologically relevant contacts is unclear or unfeasible to collect data on for most pathogens acting on humans. Further, models without network structure can often be parameterised robustly from incomplete data; in contrast, omitting certain edges from network models can have a significant impact on modelled epidemic outcomes [Watts and Strogatz, 1998]. In the absence of reliable network data, with the impact of some features of network structure still relatively poorly understood, it is often pragmatic to take such an approach. However, if one is interested in the correlations between the infection status of individuals, or the impact of network features on the spread of infection, such as concurrency or clustering, a network approach to modelling is unavoidable.

2.4 Correlations and static network models

In recent years, both analytical and simulation models incorporating network structure have been developed. There has been much work on providing a rigorous underlying framework for population-level models, such as mean-field models as well as models incorporating network structure, from network models concerning the infection status of individuals.

The spread of epidemics can be conceptualised as a stochastic process on a fixed network. Assuming that individuals can be labelled as belonging to discrete disease states, and assuming that transmission of infection across connected contacts and recovery from infection happen at constant rates, i.e. that both transmission and recovery are Poisson processes, the underlying process is *Markovian* [Kiss et al., 2017]. Accordingly, the probability that the underlying process is in any particular state can be obtained by (numerically) solving the system's Master equations. While these are idealisations, these assumptions are common throughout both the theoretical and applied epidemiological literature (although alternative non-Markovian frameworks have been developed by some, such as Pellis et al. [2015b], Kiss et al.

[2015b], and Van Mieghem and Van de Bovenkamp [2013]). In this thesis, the assumption that transitions between states occur at a constant rate, sometimes referred to as the *Markovian* assumption, is made throughout.

While the above framework has provided a useful tool for small networks, these exact methods are inevitably constrained computationally. As each state of the system must be recorded, and the state of the system depends on the state of each individual, the number of equations required to describe the underlying system grows exponentially with network size. For example, considering a disease with SIS-dynamics acting on a network of 100 individuals would require 2^{100} equations. While methods such as lumping [Simon et al., 2011] have been developed that allow larger network sizes to be considered for specific network configurations, these exact methods remain unable to handle networks of the sizes required for public health.

Using this framework, one is able to obtain equations describing the rate of change of the expected infection status of particular individuals. The behaviour of epidemics at a population level, in terms of the expected number or proportion of individuals in certain states, has been derived from understanding the behaviour of epidemics at an individual level. Of particular importance are the results of Simon et al. [2011] and Taylor et al. [2012]. By considering the probability of individuals being either susceptible or infected, Simon et al. [2011] derive exact expressions for the expected number of susceptible and infected individuals in an arbitrary network for a disease with SIS-dynamics. Letting $|S|$ denote the expected number of susceptible individuals, $|I|$ denote the expected number of infected individuals, $|SI|$ denote the expected number of susceptible-infected pairs, and letting τ and γ denote transmission and recovery rates respectively, the time evolution of $|S|$ and $|I|$ is given exactly by the following system of ODEs:

$$|\dot{S}| = \gamma|I| - \tau|SI| \tag{2.11}$$

$$|\dot{I}| = \tau|SI| - \gamma|I| \tag{2.12}$$

From this equation, we are able to recover the standard SIS-model by assuming that infected individuals are distributed randomly throughout the population. Assuming that an individual has an average of n neighbours, a susceptible individual will have an average of nI/N infected neighbours in a population of N individuals [Kiss et al., 2017]. Doing so, we obtain the following approximation:

$$|SI| = \frac{n}{N}|S||I| \tag{2.13}$$

By substituting this into Equations (2.11) and (2.12), we obtain a *closed* set of equations. The assumption that infected individuals are distributed randomly throughout the population implies that the infection status of individuals within a pair is independent of one another. However, between connected individuals, we should expect some correlation - we expect an individual with an infectious contact to be more likely to be infectious than an individual with only uninfectious contacts. Accordingly, models that try and account for these correlations have been developed. Above, we approximate the behaviour of *pairs* in terms of *individuals*. Instead, we could consider the rate of change of pairs, shown rigorously by [Taylor et al., 2012]:

$$|SI| = \gamma(|II| - |SI|) + \tau(|SSI| - |ISI| - |SI|) \tag{2.14}$$

$$|II| = -2\gamma|II| + 2\tau(|ISI| + |SI|) \tag{2.15}$$

$$|SS| = 2\gamma|SI| - 2\tau|SSI| \tag{2.16}$$

Here, this equation describing the rate of change of pairs depends on the infection status of *triples*. Inspecting the rate of change of triples, we find that these depend upon order-four terms [House et al., 2009], which in turn depend on the disease state of yet higher order structures. *Moment-closure* methods approximate behaviour of the system by approximating the disease state of higher-order structures in terms of lower-order structures, as in Equation (2.13). In general, closing a system at a higher-order one obtains a more accurate model. Many studies have utilised moment-closure methods to incorporate network structure into their models - first motivated from considerations at the population level [Keeling, 1999; Rand, 1999; Keeling and Eames, 2005] before being developed from considering dynamics at the individual level [Sharkey, 2008; Taylor et al., 2012; Sharkey et al., 2015]. However, the question of just how approximate these approximate models are is a pertinent one. To answer this, research at both the individual-level [Sharkey, 2011; Sharkey et al., 2015; Pellis et al., 2015b] and at the population-level [House and Keeling, 2011b; Keeling et al., 2016] has been developed to understand the correlations induced by network structure and the errors introduced by moment-closure approximations.

There has been significant analytical success in the moment-closure approach for diseases with SIR-dynamics. Of note, for diseases with SIR-dynamics acting on unclustered (tree-like) networks, a closure at the level of *triples* leads to a closed set of equations that describe the dynamics of the underlying system *exactly* [Sharkey et al., 2015]. Kiss et al. [2015a] extend this framework to consider more realistic

network structures including loops, Trapman [2007] define the reproduction number of pairwise approximations for diseases with SIR-dynamics, while House [2015] provide algebraic moment-closures for such diseases based on Lie algebras. This framework has also been extended to consider non-Markovian infection periods [Wilkinson and Sharkey, 2014; Pellis et al., 2015b].

However, for diseases with SIS-dynamics, results have been more limited. The correlations imposed by reinfection reduce the analytical tractability of these models. While progress has been made in providing a rigorous basis for such models [Taylor et al., 2012; Taylor and Kiss, 2014], and there has been progress in defining more accurate moment-closure approximations for diseases with SIS-dynamics [House et al., 2009; Lindquist et al., 2011; Keeling et al., 2016; Simon and Kiss, 2016], a more detailed understanding of the correlations between connected individuals and methods that account for or incorporate such correlations is still required.

There have been other approaches to modelling disease with SIS-dynamics on static networks. This disease dynamic has been considered in the theoretical literature as the *contact process* [Liggett, 2013], although results considering the contact process have tended to focus on global theoretical properties rather than results directly relevant to epidemiology. Explicit simulation of diseases on networks has been used to explore the effect of various aspects of network structure on disease spread [Moore and Newman, 2000; Read and Keeling, 2003; Meyers et al., 2005]. More recently, other static network modelling approaches have been developed [Floyd et al., 2012; Lee et al., 2013; Wilkinson and Sharkey, 2013].

2.5 Concurrency and dynamic network models

While static network models are a natural starting point to understand the impact network structure has, in many cases the formation and dissolution of partnerships

is a key determinant of epidemiological dynamics. While it is still common for mathematical models to assume that contacts are fixed throughout an epidemic, such models can incorrectly predict the outcomes of epidemics on models where partnerships are transient [Volz and Meyers, 2009; Bansal et al., 2010; Whittles et al., 2019]. Accordingly, a range of *dynamic* network models, both deterministic [Miller et al., 2012; Hansson et al., 2019] and stochastic [Jenness et al., 2018; Whittles et al., 2019], have been developed. These are particularly useful when considering the spread of STIs, where partnership turnover has a significant impact on epidemiological outcomes.

In the heterosexual population of the UK, the prevailing social norm around sexual relationships is serial monogamy - the majority of individuals are involved in at most one active partnership at any given time. Through the exclusivity of monogamous partnerships, constituent individuals are shielded from acquiring new infections from the population at large, and if one individual is infected, the maximum number of people they can pass the disease onto over the period of the relationship is 1. However, the population is not strictly monogamous [Johnson et al., 2001], and sexual networks in other contexts often do not have the same expectation of exclusivity within relationships [Reniers and Watkins, 2010; Parsons et al., 2013]. If relationships are non-exclusive, large connected components of individuals become possible, and infection is potentially able to traverse large paths within the network. Consequently, there has been considerable interest in the impact of *concurrent partnerships*, partnerships that overlap in time, on the spread of STIs. Using a deterministic model, Watts and May [1992] found that levels of concurrency can have a large impact on the early growth rate of an epidemic, a finding corroborated by the stochastic simulation studies of Kretzschmar and Morris [1996] and Morris and Kretzschmar [1995, 1997], while the models of Bauch and Rand [2000], Eames and Keeling [2004], and Morris and Kretzschmar [2000] show that concurrency significantly increases the final size of epidemics compared to populations that are serially

monogamous. More recent studies have continued to explore the impact of concurrent partnerships on disease dynamics [Kim et al., 2010; Armbruster et al., 2017]. However, while modelling studies have demonstrated the potential impact of concurrent partnerships on epidemiological dynamics, empirical studies on its influence have been mixed [Kretzschmar et al., 2010; Reniers and Watkins, 2010], perhaps due to the interplay between concurrency and other network properties.

A difficulty that arises from egocentric surveys is the measuring of levels of concurrency within a network. While Kretzschmar and Morris [1996] detail instantaneous metrics of levels of concurrency, the data obtainable from egocentric surveys is often the proportion of respondents who have had a concurrent partnership in a specified time-frame [Johnson et al., 2001]. In the Natsal surveys, whether an individual has engaged in a concurrent partnership in the previous year is inferred from the start and end months of individuals' last three sexual relationships - though some assumption must be made about whether one partnership that ends in the same month as another starts is concurrent or not.

A popular deterministic approach to modelling dynamic networks is to extend the deterministic mean-field framework described in Section 2.3 by explicitly accounting for partnership formation and dissolution, collectively referred to as *pair formation models* [Kretzschmar and Heijne, 2017], first introduced to the epidemiological literature by Dietz and Hadeler [1988]. Under such a framework, both partnership formation and partnership dissolution are Poisson processes and hence can be formulated as a system of ODEs. As an extension of the deterministic mean-field framework, significant analytical insights are tractable from pair-formation models, with methods to obtain R_0 described by Diekmann et al. [1991] and Kretzschmar et al. [1994]. For diseases with SIS or SIS-like dynamics, where individuals can potentially be re-infected by the same partner within a relationship multiple times, alternative reproduction numbers have been defined and derived. This includes the case reproduction number introduced by Heijne et al. [2013], which defines the av-

erage number of secondary cases from an initially infected individual. Figure 2.3 is a schematic of a pair-formation model of a disease with SIS-dynamics for a serially monogamous population.

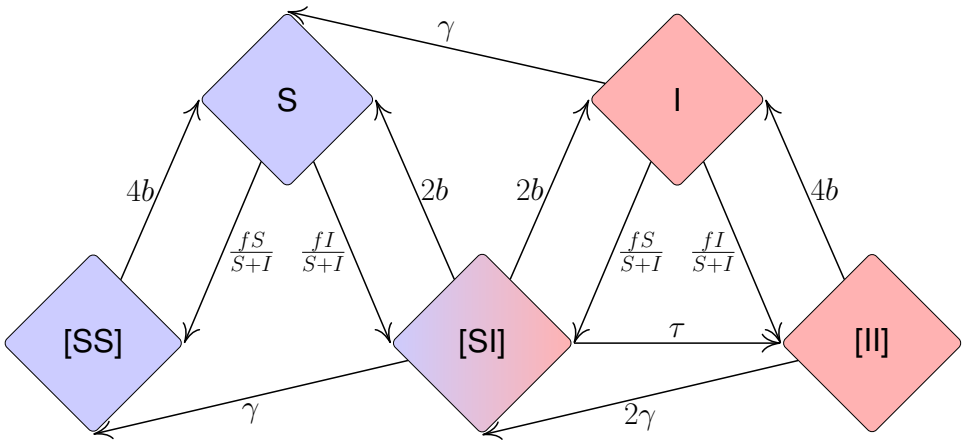

Figure 2.3: **A flow-chart of a pair-formation model assuming serial monogamy**. This chart depicts a pair-formation model for a disease with SIS-dynamics in a serially monogamous population.

This framework is a flexible way of obtaining relatively simple models that are capable of incorporating many of the heterogeneities relevant to the spread of STIs, and has been used to model the impact of real-world public health interventions [Heijne et al., 2011; Powers et al., 2011]. Pair-formation model approaches have shown that if there are short gaps between partnerships, reinfection within partnerships can sustain the transmission of low-prevalence STIs with SIS-dynamics [Chen and Ghani, 2010].

Pair-formation models are not immediately suited to deal with concurrent partnerships - if individuals are allowed to form more than one partnership, the infection status of pairs will depend on triples, as in Section 2.4. However, by including casual partnerships as instantaneous additional mean-field contacts, pair-formation models can account for concurrent partnerships in a limited capacity. This approach is taken by Xiridou et al. [2003, 2004] to assess the relative contribution

of steady and casual partnerships to the spread of HIV. Another approach developed by Leung et al. [2012, 2015] assumes that individuals have a fixed number of 'binding sites' for partnerships, allowing individuals to potentially form concurrent partnerships, under the assumption that the rate individuals form additional partnerships is independent of the number of partnerships they are already in. While each approach has limitations, both provide further evidence that concurrency can play an important role in epidemiological dynamics.

While the impact concurrency can have on the spread of epidemics is clear, the importance of explicitly including concurrency in population-level models for public health remains relatively unexplored. Such models are often calibrated to prevalence data, and are matched to available real-world data available from egocentric surveys like Natsal. In the context of school networks, Nath et al. [2018] show that models matched to local network data and calibrated to prevalence can sometimes differ in epidemiological outcomes. Models used to forecast the spread of STIs make a range of different assumptions surrounding concurrency. Some do not account for concurrency - either using mean-field models [Barnabas et al., 2006; Ribassin-Majed et al., 2014], or assuming serial monogamy [Datta et al., 2019]. Other models do include concurrent partnerships, but are not matched to concurrency data directly [Gray et al., 2009; Choi et al., 2010]. While the models of Jenness et al. [2017] and Goodreau et al. [2018] account for concurrency, they only account for instantaneous levels of concurrency, rather than observed levels over a period of time. It is unclear whether models matched to the proportion of individuals involved in a concurrrent partnership at a snapshot in time also match, for example, the proportion of individuals who have been involved in a concurrent partnership over the past year. Hence, understanding the impact that concurrency has in models that are matched to observed levels of concurrency and prevalence data remains an important question.

2.6 Clustering and household models

The previous sections have focussed on networks that are typically unclustered. In exclusively heterosexual populations, triangles of three connected individuals are impossible, and higher order loops are presumably rare. Triangles can occur in homosexual populations, and as MSM relationships are varied in the degree to which they are monogamous, clustering may sometimes be more common [Parsons et al., 2013]. In contrast to sexual networks, the clustering of social contacts is a hallmark of social networks. Because of this, much research has considered the impact of clustering on the spread of infectious diseases.

Clustering has been incorporated into both static and dynamic deterministic network models using moment-closure methods. Yet incorporating clustering accurately into moment-closure models remains challenging. For tree-like networks, the moment-closure approach can provide an exact description of the underlying disease dynamics for certain types of disease dynamics [Sharkey et al., 2015]. However, inevitable correlations between individuals within closed loops limits the analytical tractability of this approach on clustered networks. To close a model at the level of triples, one must approximate the behaviour of open and closed triples (Figure 2.2). While the choice of closure for open triples is straightforward, the correct approximation for closed triangles is less obvious. Originally, this was done by invoking the *Kirkwood* approximation for closed triples [Kirkwood, 1935; Keeling, 1999]. Assuming that individuals x, c and y comprise a closed triple, letting $[A_x]$ denote the probability that individual x is in state A, and letting $[A_x B_c]$ denote the probability that individual x is in state A and individual c in state B and so on, the Kirkwood approximation of the probability that the closed triple is in a particular state is given by the following equation:

$$[A_x B_c C_y] \approx \frac{[A_x B_c][B_c C_y][A_x C_y]}{[A_x][B_c][C_y]} \tag{2.17}$$

However, this approximation has been criticised because of a lack of accuracy and because it does not result in a proper distribution over system states [Pellis et al., 2015b]. More recently, improved closures for closed triangles have been developed [House and Keeling, 2010; Rogers, 2011], although the Kirkwood approximation is often still used [House and Keeling, 2011a]. Moment-closure methods provide reasonable approximations of underlying disease dynamics in networks with low to medium levels of clustering, but their efficacy at approximating the dynamics of epidemics on more highly clustered networks is relatively unexplored.

While imperfect, models utilising moment-closures have played a valuable role in understanding the impact of clustering on both the spread of infectious diseases and the success of control measures. Static network models have shown that, because individuals infected after the first generation have a reduced number of new susceptible contacts, the average number of secondary infections from an infected individual is smaller in clustered populations [Keeling, 1999; Keeling and Eames, 2005]. Consequently, both the early growth rate and full R_0 is lower in clustered populations [House and Keeling, 2011a]. Further, the efficacy of contact tracing is often increased in clustered populations [House and Keeling, 2010]. These studies corroborate similar findings through explicit stochastic simulation or other approaches [Huerta and Tsimring, 2002; Miller, 2009; Badham and Stocker, 2010].

A certain level of clustering is imposed by the household structure of a population - individuals live in households with other individuals, who are likely to be considered close contacts for many pathogens. The clustering imposed by this structure slows the spread of epidemics [Volz et al., 2011]. A field of models, known as *household models*, has been developed to account for the specific effects of this type of clus-

tering. Typically, such models account for disease dynamics at two levels - within the household and between households [Ball et al., 1997]. There are a range of household modelling approaches, from analytical approaches [Ball and Neal, 2002; House and Keeling, 2008; Hilton and Keeling, 2019] to detailed simulations used for public health [Ferguson et al., 2005; Cauchemez et al., 2008].

A specific challenge for household models is the definition of reproduction numbers. In models that assume random-mixing, it can be assumed in the early stages of an epidemic that the proportion of the population who are not susceptible to infection, either because they are infected or they have recovered, is negligible. Consequently, the next-generation approach outlined by Diekmann et al. [1990] is a reliable way of obtaining the average number of infections caused by an infected individual. However, this method relies on the infection status of individuals within the population to be uncorrelated [Diekmann and Heesterbeek, 2000]. In the context of households, the depletion of susceptibles even in the early stages of an epidemic is never negligible, and the clustering imposed by households inevitably leads to correlations in infection status. While R_0 can still be defined in the standard way [Ball et al., 1997], it describes the average number of infections caused by an individual in a fully susceptible population. However, while infection may spread quickly within a household, the depletion of susceptibles may mean an epidemic cannot take off. Therefore, the standard conception of R_0 is no longer a useful parameter for household models, as it does not exhibit the thresholding properties that make it a quantity of interest in epidemiology [Pellis et al., 2012]. Because of this, alternative metrics that do exhibit this thresholding property have been proposed: Ball et al. [1997] propose the average number of households infected by an infected household, Pellis et al. [2012] define a reproduction number that effectively averages over household members infected in different generations of an epidemic, while House and Keeling [2011a] compare the ratio between individuals infected in subsequent generations after infection correlations have equilibrated.

Recently, it has been suggested that clustering itself could be utilised as an effective control measure against epidemics, either by encouraging individuals to form social connections with the contacts of their contacts [Block et al., 2020], or by restricting individual's social contacts to another clustered group, such as a household [Willem et al., 2021; Danon et al., 2020]. To understand the effectiveness of these approaches, models must be developed that incorporate the data available on the structure of contacts within the population, that infer the resulting clustered contacts implied by any such strategy, and that compare epidemiological outcomes against counterfactual models where individuals increase their contacts in an unclustered fashion.

Chapter 3

Correlations: improving pairwise approximations for network models with susceptible-infected-susceptible dynamics

The research in this chapter has been presented in Leng and Keeling [2020].

3.1 Introduction

The spread of any epidemic can be conceptualised as a process on a network, where individuals are represented as vertices and epidemiologically relevant contacts as edges between vertices. An abundance of different network-based approaches to disease spread have been developed over the years, varying in scope, application, and sophistication. These range from, at one extreme, Markovian state-based models, where the probability of a system being in a certain state is given exactly by its master equations (see Kiss et al. [2017] for an introduction to such methods), to

explicit stochastic simulations of epidemics on networks (see Goodreau et al. [2017] and Whittles et al. [2019] for recent examples) at the other. Both approaches have limitations. The exponentially increasing state-space with network size for state-based models mean these exact descriptions are computationally unfeasible for most networks of real-world interest; and while stochastic simulations can deal with networks of these sizes, such methods offer little or no analytical tractability, making sensitivity to network structure hard to quantify and the causal determinants of the resulting dynamics hard to identify.

One network approach that aims to bridge this gap is *moment-closure approximation*, which is the focus of this chapter. In a population, the rate of change of the number of infected individuals will depend upon how many susceptible-infected pairs there are. The rate of change of these pairs, in turn, depends upon the number of triples, and so on up to the full size of the population. Moment-closure approximation methods obtain a closed set of ordinary differential equations (ODEs) for the disease dynamics by approximating the dynamics of higher-order moments (e.g. triples) in terms of lower-order moments (e.g. singletons and pairs). By doing so, one obtains a relatively simple ODE model that retains much of the tractability of mean-field approximation models (the standard approach to modelling the spread of infectious diseases) but that also explicitly accounts for some aspects of network structure. Hence, there has been much interest and research into such methods, and into the errors such approximations introduce into a model [Sharkey, 2011; Taylor et al., 2012; Keeling et al., 2016; Pellis et al., 2015b].

There has been considerable progress in this moment-closure method for diseases that can be modelled via the susceptible-infected-recovered (SIR) paradigm: the determinants of errors in such methods are detailed by Sharkey [2011]; the exactness of a closure at the level of triples for tree-like networks is proven by Sharkey et al. [2015]; this framework is extended by Kiss et al. [2015a] to more realistic network structures that include loops; Trapman [2007] defines a reproduction number for

pairwise approximation; House [2015] provides an algebraic moment-closure for such diseases based on Lie algebraic methods; while Pellis et al. [2015b] explore the exactness of closures when infective periods are of a constant duration.

By comparison, progress has been modest for diseases with susceptible-infected-susceptible (SIS) dynamics, equivalent to the network-based contact process [Liggett, 2013], where recovery from infection does not lead to immunity. Despite its lower dimensionality than the SIR model, the possibility of reinfection can cause correlations between indirectly connected individuals to accrue over time. Consequently, moment-closure approximations on networks with SIS-dynamics are in general not exact, and their analytical tractability is limited. Of the progress that has been made: important formal results on their derivability from exact state-based models have been achieved by Taylor et al. [2012] and Taylor and Kiss [2014]; Keeling et al. [2016] compare three systematic moment-closure approximations against stochastic simulations; House et al. [2009] develop a motif-based approach that outperforms simpler methods for particular network topologies; while Simon and Kiss [2016] develop a compact pairwise approximation that agrees well with ODE models of a much higher dimensionality.

Capturing network structure is at its most important when edges between vertices are sparse but relatively long lasting. This, alongside the more well-defined nature of epidemiologically relevant contacts, means that moment-closure methods are potentially most valuable for understanding the spread of sexually transmitted infections (STIs). However, most STIs are modelled using the SIS-paradigm (though notably not HIV). Thus, both understanding the errors introduced by moment-closure approximations for diseases with SIS-dynamics, and improving upon these approximations, is vital for the successful application of such methods to public-health problems.

In this chapter, we introduce improvements to the standard pairwise approxima-

tion for diseases with SIS-dynamics. In particular, we do this for the isolated open triple and for k-regular networks, by explicitly obtaining equations for the rates of change of the errors between triples and their standard pairwise approximation. By applying a closure to these equations, we obtain a closed set of equations that better approximate the true dynamics of infection, with only a modest increase in dimensionality. In the case of the isolated open triple, such a model is exact, while for k-regular networks, closures at the level of order-four structures have to be applied. Specifically, in Section 3.2 we discuss the isolated open triple, obtaining exact expressions for the appropriate errors and their rates of change, thus obtaining an exact set of equations describing the disease dynamics on this network topology. In Section 3.3, we use the results from the isolated open triple to inform our improved approximation on k-regular networks, i.e. networks with no loops and where each individual has k neighbours. In Section 3.4, we consider both higher-order moment-closure approximations and explicit stochastic simulations for this type of network, to act as benchmarks for our improved pairwise approximation. In Section 3.5, we compare this improved approximation to the standard pairwise approximation, to higher-order approximation models, and to stochastic simulations. In Section 3.6, we discuss some of the limitations to such an approach, and highlight some potential areas where we believe further research could be fruitful.

3.2 The isolated open triple

In this section, we consider the errors introduced by performing pairwise approximation on *isolated open triples* for a disease with SIS-dynamics. We define an isolated open triple as a central individual c connected to two neighbouring individuals x and y, where x and y remain unconnected, as illustrated in Figure 3.1. By investigating this topology, the errors introduced by a pairwise approximation that result from the disease dynamics of the triple itself are not obfuscated by errors

introduced via transmission events to the open triple from external connections, and exact results using the master equation approach [Kiss et al., 2017] can be generated.

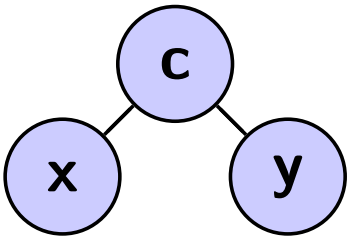

Figure 3.1: **Graphical representation of the isolated open triple.** A central vertex c connected to two other vertices x and y. For the SIS model such triples have eight possible states.

We consider a diseases with SIS-dynamics, that is, upon recovery from infection (I) an individuals returns to the susceptible (S) class. We can described this process on the 3-network in terms of its states, of which there are eight - corresponding to whether each individual belongs to the S or I class - so a particular state $A \in \{S, I\}^3$. We denote the probability of being in a certain state $\mathbb{P}(x = X, c = C, y = Y)$ as $[X_x C_c Y_y]$, where $X, C, Y \in \{S, I\}$. If we consider recovery from infection, γ, and transmission across partnerships, τ, to be Poisson processes, then the above situation is a continuous-time Markov process, and can be fully described by its Master equations (see Kiss et al. [2017], Chapter 2 for an introduction to this approach).

We set initial probabilities of each state by assuming random initial conditions, i.e. by taking $I_0 \sim U(0, 1)$ and setting $[I_x I_c I_y]_0 = I_0 \times I_0 \times I_0$ and so on. Note, under this assumption, we have the symmetries $[S_x S_c I_y] = [I_x S_c S_y]$ and $[S_x I_c I_y] = [I_x I_c S_y]$. Thus, the dynamics of the isolated open triple are fully and exactly described by the following six ODEs:

Model 1 - The isolated open triple

$$[S_x\dot{S}_cS_y] =\gamma(2[S_xS_cI_y] + [S_xI_cS_y]) \tag{3.1}$$

$$[S_x\dot{S}_cI_y] = [I_x\dot{S}_cS_y] =\gamma([S_xI_cI_y] + [I_xS_cI_y] - [S_xS_cI_y]) - \tau[S_xS_cI_y] \tag{3.2}$$

$$[S_x\dot{I}_cS_y] =\gamma(2[S_xI_cI_y] - [S_xI_cS_y]) - 2\tau[S_xI_cS_y] \tag{3.3}$$

$$[S_x\dot{I}_cI_y] = [I_x\dot{I}_cS_y] =\gamma([I_xI_cI_y] - 2[S_xI_cI_y]) + \tau([S_xS_cI_y] + [S_xI_cS_y] - [S_xI_cI_y]) \tag{3.4}$$

$$[I_x\dot{S}_cI_y] =\gamma([I_xI_cI_y] - 2[I_xS_cI_y]) - 2\tau[I_xS_cI_y] \tag{3.5}$$

$$[I_x\dot{I}_cI_y] = -3\gamma[I_xI_cI_y] + 2\tau([S_xI_cI_y] + [I_xS_cI_y]) \tag{3.6}$$

Note that the disease-free state $[S_xS_cS_y]$ is absorbing, and so given long enough this system will always evolve to this state. Hence, without an external source of infection, a disease cannot persist indefinitely with an isolated open triple (or indeed, within any isolated graph of finite topology). If we wish to consider initial conditions that do not assume random mixing, e.g. pure initial conditions, eight equations are required:

$$[S_x\dot{S}_cS_y] =\gamma([S_xS_cI_y] + [I_xS_cS_y] + [S_xI_cS_y]) \tag{3.7}$$

$$[S_x\dot{S}_cI_y] =\gamma([S_xI_cI_y] + [I_xS_cI_y] - [S_xS_cI_y]) - \tau[S_xS_cI_y] \tag{3.8}$$

$$[I_x\dot{S}_cS_y] =\gamma([I_xI_cS_y] + [I_xS_cI_y] - [I_xS_cS_y] - \tau[I_xS_cS_y] \tag{3.9}$$

$$[S_x\dot{I}_cS_y] =\gamma([S_xI_cI_y] + [I_xI_cS_y] - [S_xI_cS_y]) - 2\tau[S_xI_cS_y] \tag{3.10}$$

$$[S_x\dot{I}_cI_y] =\gamma([I_xI_cI_y] - 2[S_xI_cI_y]) + \tau([S_xS_cI_y] + [S_xI_cS_y] - [S_xI_cI_y]) \tag{3.11}$$

$$[I_x\dot{I}_cS_y] =\gamma([I_xI_cI_y] - 2[I_xI_cS_y]) + \tau([I_xS_cS_y] + [S_xI_cS_y] - [I_xI_cS_y]) \tag{3.12}$$

$$[I_x\dot{S}_cI_y] =\gamma([I_xI_cI_y] - 2[I_xS_cI_y]) - 2\tau[I_xS_cI_y] \tag{3.13}$$

$$[I_x\dot{I}_cI_y] = -3\gamma[I_xI_cI_y] + \tau([S_xI_cI_y] + [I_xI_cS_y] + 2[I_xS_cI_y]) \tag{3.14}$$

3.2.1 The pairwise approximation for the isolated open triple

Returning to the homogeneous initial condition, we now introduce the pairwise approximation for the open triple. It is important to note that we are considering a *local* moment-closure approximation, i.e. we are tracking the dynamics and errors introduced for a particular subgraph, as opposed to a *global* moment-closure approximation, where we apply closures at a population level.

We begin by considering equations for the probability of individuals (vertices of the open triple) being in a certain state $A \in \{S, I\}$, where we denote $\mathbb{P}(a = A)$ as $[A_a]$. ODEs describing the rate of change of these states can be obtained by summing the rates of change from the appropriate triples, e.g. $[\dot{S_x}] = [S_x\dot{S_c}S_y] + [S_x\dot{S_c}I_y] + [S_x\dot{I_c}S_y] + [S_x\dot{I_c}I_y]$. We observe that the state of an individual depends on the probability of pairs of individuals being in certain states: we denote $\mathbb{P}(a = A, b = B)$ as $[A_aB_b]$ and also obtain these by summing the appropriate triples. We arrive at the following equations:

$$[\dot{S_x}] = [\dot{S_y}] = \gamma[I_x] - \tau[S_xI_c] \tag{3.15}$$

$$[\dot{S_c}] = \gamma[I_c] - 2\tau[I_xS_c] \tag{3.16}$$

$$[S_x\dot{I_c}] = [I_c\dot{S_y}] = \gamma([I_xI_c] - [S_xI_c]) + \tau([S_xS_cI_y] - [S_xI_c]) \tag{3.17}$$

$$[I_x\dot{S_c}] = [S_c\dot{I_y}] = \gamma([I_xI_c] - [I_xS_c]) - \tau([I_xS_cI_y] + [I_xS_c]) \tag{3.18}$$

where $[I_a] = 1 - [S_a]$ and $[I_aI_b] = [I_b] - [S_aI_b] = [I_a] - [I_aS_b]$. Thus, we see that the rate of change of the probability of the infection status of individuals depends on the infection status of certain pairs, which themselves depend on the infection status of certain triples. This set of equations is unclosed, as we do not have expressions representing the time evolution of the disease status of these triples. Typically, studies have obtained a closed set of equations by assuming that the

infection status of individuals x and y are conditionally independent given the infection status of individual c [Sharkey, 2008, 2011; Pellis et al., 2015b]. That is, the following assumption is made:

$$[S_xS_cI_y] \approx \frac{[S_xS_c][S_cI_y]}{[S_c]} \qquad [I_xS_cI_y] \approx \frac{[I_xS_c][S_cI_y]}{[S_c]} = \frac{[I_xS_c]^2}{[S_c]} \tag{3.19}$$

Observing that $[S_xS_c] = [S_x] - [S_xI_c]$, and that $[S_c] = [S_xS_c] - [I_xS_c]$, we obtain a closed set of three equations, which we refer to as the *pairwise approximation for the isolated open triple*, given in full below:

Model 2 - The pairwise approximation for the isolated open triple

$$\dot{[S_xS_c]} = \dot{[S_cS_y]} = \gamma([I_xS_c] + [S_xI_c]) - \tau\frac{[S_xS_c][S_cI_y]}{[S_c]} \tag{3.20}$$

$$\dot{[S_xI_c]} = \dot{[I_cS_y]} = \gamma([I_xI_c] - [S_xI_c]) + \tau\left(\frac{[S_xS_c][S_cI_y]}{[S_c]} - [S_xI_c]\right) \tag{3.21}$$

$$\dot{[I_xS_c]} = \dot{[S_cI_y]} = \gamma([I_xI_c] - [I_xS_c]) - \tau\left(\frac{[I_xS_c]^2}{[S_c]} + [I_xS_c]\right) \tag{3.22}$$

where $[I_xI_c] = 1 - [S_xS_c] - [S_xI_c] - [I_xS_c]$ and $[S_c] = [S_xS_c] + [I_xS_c]$.

3.2.2 Quantifying errors

We can now compare the pairwise approximation model (Equations (3.20) to (3.22)) to the exact model (Equations (3.1) to (3.6)). The approximate model captures the dynamics of the system at low values of the transmission rate τ, but if τ is sufficiently high, the approximate model behaves qualitatively different to the exact model - there is no absorbing state, and we have a non-zero stationary probability of individuals being infected (Figure 3.2).

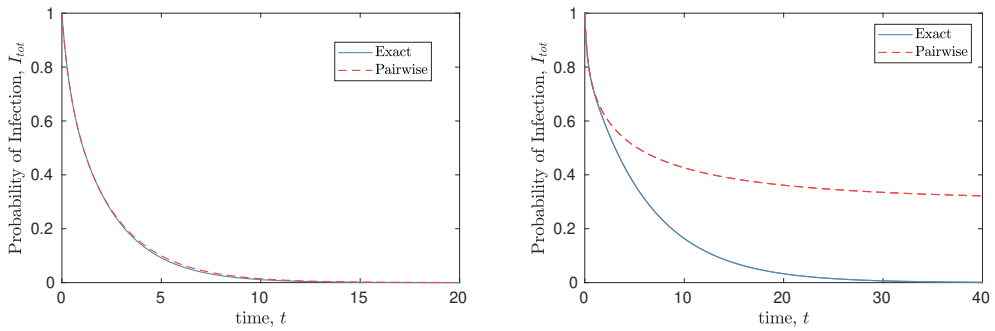

Figure 3.2: **Comparing exact and pairwise models for the isolated open triple**. In (a), we see at low values of transmission between connected individuals ($\tau = 1$), the pairwise approximation (red) captures the probability of an individual being infected (given by $I_{tot} = ([I_x] + [I_c] + [I_y])/3$) of the exact model (blue) reasonably well. In (b), we see that for higher values of τ (here $\tau = 3$), the pairwise model evolves to a non-zero stationary probability of individuals being infected, while the exact model always proceeds to the disease-free equilibrium. For all plots, we set $\gamma = 1$.

While in Model 1 $[S_x S_c S_y]$ never decreases, in Model 2 its approximation $[S_x S_c][S_c S_y]/[S_c]$ can decrease. This decrease occurs because of the rate of change of $[I_c]$ to $[S_c]$. In Model 1, this only affects the transition to the state $[S_x S_c S_y]$ from the state $[S_x I_c S_y]$, which only ever increases the probability of $[S_x S_c S_y]$. However, in Model 2 the decoupling of the two pairs and single means that this transition, with certain within pair correlations, can lead to a decrease in $[S_x S_c][S_c S_y]/[S_c]$.

Comparing the exact value for triples with their approximation at any given time, we observe this approximation underestimates the probability of the state $[I_x S_c I_y]$, and overestimates the probability of the state $[S_x S_c I_y]$. Indeed, the underestimate of $[I_x S_c I_y]$ is exactly the overestimate of $[S_x S_c I_y]$ (Figure 3.3).

To understand why, consider the quantities $\alpha_{[S_x S_c I_y]} := [S_x S_c I_y][S_c] - [S_x S_c][S_c I_y]$ and $\alpha_{[I_x S_c I_y]} := [I_x S_c I_y][S_c] - [I_x S_c]^2$, borrowing notation from Sharkey et al. [2015], which quantify the difference between triples and their approximations. By expanding $[S_c] = [S_x S_c S_y] + 2[S_x S_c I_y] + [I_x S_c I_y]$, $[S_x S_c] = [S_x S_c S_y] + [S_x S_c I_y]$, and

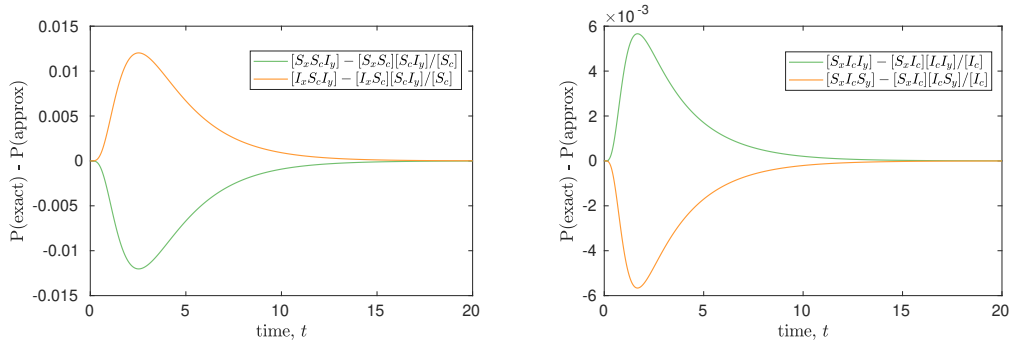

(a) (b)

Figure 3.3: **Comparing exact and approximated probability of isolated open triples**. In (a), we see that the approximation overestimates the probability of being in state $[S_xS_cI_y]$, and underestimates the probability of an isolated open triple being in state $[I_xS_cI_y]$. Similarly, (b) we see this approximation underestimates the probability of $[S_xI_cI_y]$ and overestimates the probability of $[S_xI_cS_y]$. In both cases, the overestimate of one is equal to the underestimate of the other. In both plots we set $\tau = 1, \gamma = 1$.

$[S_cI_y] = [S_xS_cI_y] + [I_xS_cI_y]$ and cancelling the appropriate terms, we arrive at the fact that both quantities are equal but opposite in sign, and thus we now define α_S as:

$$\alpha_S = \alpha_{[I_xS_cI_y]} = -\alpha_{[S_xS_cI_y]} = [S_xS_cS_y][I_xS_cI_y] - [S_xS_cI_y]^2 \tag{3.23}$$

Noting further that $\alpha_{[S_xS_cS_y]} = \alpha_S$, while clearly $\alpha_{[I_xS_cS_y]} = \alpha_{[S_xS_cI_y]} = -\alpha_S$, we observe that the difference between true and approximate triple values for all triples with susceptible central individuals depends upon one quantity α_S. Similarly, the difference between true and approximate triple values of all triples with infected central individuals depends only on one quantity, which we denote α_I:

$$\alpha_I = [I_x I_c I_y][S_x I_c S_y] - [S_x I_c I_y]^2 \tag{3.24}$$

3.2.3 Improving the pairwise approximation

If instead of using the approximations from Equation (3.19), we let $[S_x S_c I_y] = ([S_x S_c][S_c I_y] - \alpha_S)/[S_c]$ in Equation (3.17), and let $[I_x S_c I_y] = ([I_x S_c]^2 + \alpha_S)/]S_c]$ in Equation (3.18), we obtain the rates of change of pairs in terms of singletons, pairs, and α_S. To obtain a closed set of equations, we must consider $\dot{\alpha_S}$, where the rates of change of triples can be obtained from the exact model.

$$\begin{aligned}
\dot{\alpha_S} =& [S_x \dot{S_c} S_y][I_x S_c I_y] + [I_x \dot{S_c} I_y][S_x S_c S_y] - 2[S_x \dot{S_c} I_y][S_x S_c I_y] && (3.25)\\
=& \gamma(\phi_S - 2\alpha_S) - 2\tau\alpha_S && (3.26)\\
\text{where } \phi_S =& [S_x S_c S_y][I_x I_c I_y] + [S_x I_c S_y][I_x S_c I_y] - 2[S_x S_c I_y][S_x I_c I_y] && (3.27)\\
=& \frac{1}{[S_c][I_c]}(([S_x S_c][I_x I_c] - [I_x S_c][S_x I_c])^2 + \alpha_I[S_c]^2 + \alpha_S[I_c]^2) && (3.28)
\end{aligned}$$

Thus, the rate of change of α_S depends in turn on the rate of change of α_I, which is given by:

$$\begin{aligned}
\dot{\alpha_I} =& [I_x \dot{I_c} I_y][S_x I_c S_y] + [S_x \dot{I_c} S_y][I_x I_c I_y] - 2[S_x \dot{I_c} I_y][S_x I_c I_y] && (3.29)\\
=& -4\gamma\alpha_I + 2\tau(\phi_I - \alpha_I) && (3.30)\\
\text{where } \phi_I =& 2[S_x I_c S_y][I_x S_c I_y] - 2[S_x S_c I_y][S_x I_c I_y] && (3.31)\\
=& \frac{2}{[S_c][I_c]}([S_x I_c]^2[I_x S_c]^2 - [S_x S_c][I_x S_c][S_x I_c][I_x I_c] + [I_x S_c][S_c]\alpha_I + [S_x I_c][I_c]\alpha_S) && (3.32)
\end{aligned}$$

We insist that ϕ_S and ϕ_I are 0 if either $[S_c] = 0$ or $[I_c] = 0$. Using the above equations, we arrive at a closed set of equations that describes exactly the disease dynamics of the open triple, without any reference to the particular states of triples themselves, by tracking the error terms α_S and α_I. Model 3 below describes in full this improved pairwise model, with ϕ_S and ϕ_I described as above:

Model 3 - Improved pairwise model of the isolated open triple

$$\dot{[S_x S_c]} = \gamma([I_x S_c] + [S_x I_c]) - \tau \frac{[S_x S_c][I_x S_c] - \alpha_S}{[S_c]} \tag{3.33}$$

$$\dot{[S_x I_c]} = \gamma([I_x I_c] - [S_x I_c]) + \tau \left(\frac{[S_x S_c][I_x S_c] - \alpha_S}{[S_c]} - [S_x I_c] \right) \tag{3.34}$$

$$\dot{[I_x S_c]} = \gamma([I_x I_c] - [I_x S_c]) - \tau \left(\frac{[I_x S_c]^2 + \alpha_S}{[S_c]} + [I_x S_c] \right) \tag{3.35}$$

$$\dot{\alpha_S} = \gamma(\phi_S - 2\alpha_S) - 2\tau\alpha_S, \text{ with } \phi_S \text{ as in Equation (3.28)} \tag{3.36}$$

$$\dot{\alpha_I} = -4\gamma\alpha_I + 2\tau(\phi_I - \alpha_I), \text{ with } \phi_I \text{ as in Equation (3.32)} \tag{3.37}$$

By including α_S and α_I and their time-evolution in Model 3, we obtain a system of ODEs that describes exactly the dynamics of the open triple. However, it is worth noting that this new model is of no lower dimensionality than Model 1. Despite this, we believe this is still a valuable model to have obtained explicitly. There are two principal reasons for this: firstly, by creating a system where errors α_S and α_I are tracked explicitly, we can obtain results and gain an understanding about the ways in which the standard pairwise approximation (which ignores the action of α_S and α_I) fails to capture the disease dynamics of the isolated open triple; and secondly, the derivation of this model informs our strategy of how to derive an improved pairwise approximation for k-regular networks, where there is a significant reduction in dimensionality.

Upon numerical evaluation, interesting results about the error terms α_S and α_I

arise. When considering the whole state space, both error terms can be either negative or positive ($\alpha_S, \alpha_I \in [-1/4\ 1/4]$). However, this is not the case when starting from either random or pure initial conditions; in both scenarios, $\alpha_S \geq 0$ and $\alpha_I \leq 0$. This is numerically demonstrated in Figure 3.4.

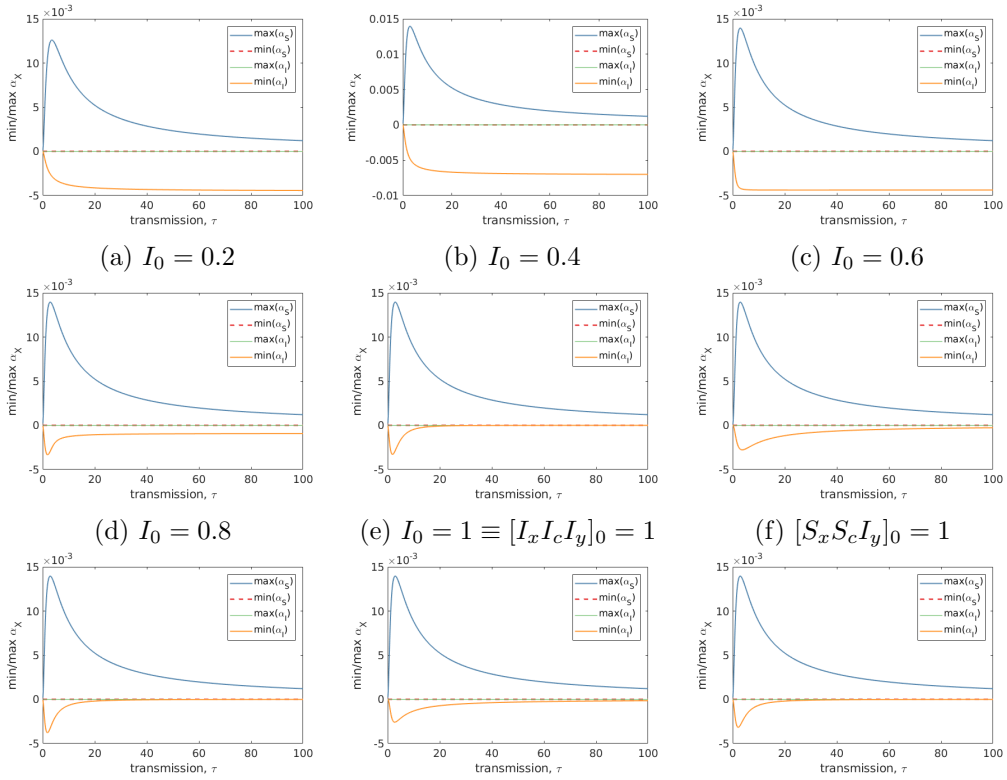

(a) $I_0 = 0.2$ (b) $I_0 = 0.4$ (c) $I_0 = 0.6$

(d) $I_0 = 0.8$ (e) $I_0 = 1 \equiv [I_x I_c I_y]_0 = 1$ (f) $[S_x S_c I_y]_0 = 1$

(g) $[I_x S_c I_y]_0 = 1$ (h) $[S_x I_c S_y]_0 = 1$ (i) $[S_x I_c I_y]_0 = 1$

Figure 3.4: **Numerical demonstration of the bounds $\alpha_S \geq 0, \alpha_I \leq 0$ for the isolated open triple.** We consider how $min(\alpha_X)$ and $max(\alpha_X)$, $X \in \{S, I\}$ vary with the transmission rate τ for the isolated open triple, for a range of different initial conditions - both random (a–e) and pure (e–i). These plots demonstrate the bounds $\alpha_S \geq 0$ and $\alpha_I \leq 0$ hold in general for the isolated open triple. In all plots we set $\gamma = 1$.

Consequently, assuming random or pure initial conditions, we arrive at the following bounds:

$$\frac{[S_xS_c]^2}{[S_c]} \leq [S_xS_cS_y] \qquad \frac{[I_xI_c]^2}{[I_c]} \geq [I_xI_cI_y]$$
$$\frac{[I_xS_c]^2}{[S_c]} \leq [I_xS_cI_y] \qquad \frac{[S_xI_c]^2}{[I_c]} \geq [S_xI_cS_y]$$
$$\frac{[S_xS_c][S_cI_y]}{[S_c]} \geq [S_xS_cI_y] \qquad \frac{[S_xI_c][I_cI_y]}{[I_c]} \leq [S_xI_cI_y]$$

Of these, the bound $[I_xI_c]^2/[I_c] \geq [I_xI_cI_y]$ is of particular interest. In previous moment-closure studies, it has been suggested heuristically that moment-closure models *underestimate* the probability of $[I_xI_cI_y]$ triples [Taylor et al., 2012]. This does hold if the system is closed at the level of individuals, i.e. if we assume that the infection status of neighbours are independent. The above result demonstrates that the opposite is true if the system is closed at the level of pairs: $\mathbb{P}(x = I, y = I|c = I) \leq \mathbb{P}(x = I|c = I) \times \mathbb{P}(y = I|c = I)$.

To explore whether α_S and α_I were uniquely defined for given values of $[S_xS_c]$ and $[S_cI_y]$, we ran Model 3 for a range of initial conditions. varying I_0 from 0 to 1. For each of these model runs, we plotted the 3-D trajectory of $([S_xS_c], [S_cI_y], \alpha_X)$, with $[S_xS_c]$ values on the x-axis, $[S_cI_y]$ values on the y-axis and $\alpha_X,\ X \in \{S, I\}$ values on the z-axis. By conjoining adjacent trajectories, we could then visualise α_S or α_I as a surface. For random initial conditions, α_S and α_I appear to be uniquely defined by the pairs $[S_xS_c]$ and $[S_cI_y]$, in other words α_S and α_I appear to be *functions* of $[S_xS_c]$ and $[S_cI_y]$ (explored in the supplementary information of Leng and Keeling [2020]). In theory, given values of $[S_xS_c]$ and $[S_cI_y]$, one could determine the values of α_S and α_I exactly, consequently reducing the dimensionality of Model 3, as equations for their time evolution would no longer be necessary.

3.3 k-regular Networks

In Section 3.2, we considered the accuracy of the standard pairwise approximation on the isolated open triple, and derived a closed exact set of equations describing the errors such an approximation makes. We could do so because we could compute exactly the probability of the states of the open triple (Model 1), and working backwards we could derive expressions for $\dot{\alpha_S}$ and $\dot{\alpha_I}$ solely in terms of $[S_xS_c]$, $[S_cI_y]$, α_S, and α_I - i.e. solely in terms of pairs and error terms. Informed by these results, we move on to consider pairwise approximations for k-regular networks. k-regular networks are defined as networks in which each individual has k neighbours. Here, we consider k-regular networks which are infinite and contain no loops. Diseases with SIS-dynamics on k-regular networks have been studied before are referred to in the theoretical literature as the contact process on the homogeneous tree T_{k-1} [Liggett, 2013]. Being infinite, the disease dynamics on such a network cannot be described exactly by a closed set of ODEs, unless a closure at some level is exact, as in Sharkey et al. [2015] for diseases with SIR-dynamics. As stated previously, the possibility of reinfection induces correlations between distantly connected individuals, meaning the method used by Sharkey et al. [2015] is not successful for diseases with SIS-dynamics. However, one can close the system at a higher level than pairs and by doing so, we can obtain expressions for $\dot{\alpha_S}$ and $\dot{\alpha_I}$ solely in terms of pairs and error terms. While these are still approximations to the true disease dynamics on a k-regular network, doing so makes a considerable improvement on the standard pairwise approximation. This is the strategy we employ in this section.

While k-regular networks are clearly idealisations far removed from any real-world sexual network, we believe that they are a useful example to study for a number of reasons. The impact of a small number of contacts, and the resulting dynamical correlations between non-adjacent individuals, is still relatively poorly understood [Keeling et al., 2016]. In these idealised networks, the errors such correlations in-

troduce into moment-closure approximations are at their most pronounced, and are not muddied by errors introduced from other sources, such as clustering or heterogeneity. While heterogeneity in the number of contacts individuals have is apparent in any real-world sexual network, and is important to capture when modelling STIs, the effect of heterogeneity has been studied extensively [Eames and Keeling, 2002; Simon and Kiss, 2016], and can oftentimes be modelled by introducing multiple risk-groups into a mean-field approximation model (e.g. Edwards et al. [2010]). Additionally, in the case of an infinite network, each individual has exactly the same properties, allowing us to bridge the gap from local to global moment-closure approximation.

In this section, we define *global* moment-closures for k-regular networks. That is, we define a closure in terms of population-level quantities rather than for the probabilities of particular individuals being in certain states. Accordingly, we use the notation $[S]$ to represent the *proportion* of individuals who are susceptible, $[SI]$ to represent the *proportion* of pairs where one individual is susceptible and one individual is infected, and so on. While it is standard within the moment-closure literature to refer to *numbers* of these quantities, we find that dealing with proportions avoids much of the combinatorial rigmarole involved, and has a more obvious correspondence with the methods described in Section 3.2. The following results hold true whether referring to proportions or numbers - in Appendix A.1 we provide a conversion table to transform the results from this section to numbers, and provide the model derived in this section in terms of numbers.

While the derivation of this moment-closure is independent to that of the previous section, and can be treated as a separate modelling exercise, we will observe that there are clear analogies between the two. This correspondence occurs because k-regular networks are isotropic - number of partnerships, as well as transmission and recovery rates, are homogeneous across the population. An alternative conceptualisation is that if we were to randomly sample one individual (or a higher-order

motif) from a k-regular network, the probability of it being in a given state is directly equal to the proportion of the population in that state. Conversely, if we consider a population of infinitely many isolated open triples from Section 3.2, then the proportion in a given state is equal to the probability of one triple being in that state. Therefore while Section 3.2 is formulated in terms of probabilities and Section 3.3 is formulated in terms of proportions, we are effectively modelling interchangeable quantities.

3.3.1 Mean-field and pairwise approximations for k-regular networks

For a disease with SIS-dynamics, the following equation describes the rate of change of $[S]$ for any network [Simon et al., 2011]:

$$[\dot{S}] = \gamma[I] - \lambda[SI] = \gamma(1 - [S]) - \lambda[SI] \tag{3.38}$$

In the case of k-regular networks, $\lambda = k\tau$. By assuming the disease status of constituent individuals in pairs are uncorrelated, i.e. $[SI] \approx [S][I]$, we arrive at the mean-field approximation for the k-regular network, which is equivalent to the standard SIS-model:

Model 4 - The mean-field approximation for k-regular networks

$$[\dot{S}] = \gamma[I] - k\tau[S][I] = \gamma(1 - [S]) - k\tau[S](1 - [S]) \tag{3.39}$$

If instead we want to close the system at a higher-order moment, we must consider the rate of change of $[SI]$:

$$[\dot{SI}] = \gamma([II] - [SI]) - \tau[SI] + (k-1)\tau[SSI] - (k-1)\tau[ISI] \tag{3.40}$$

To close this system of equations, we must approximate the proportion of triples $[SSI]$ and $[ISI]$. We use the standard pairwise approximation of Rand [1999] and Keeling [1999], commonly attributed to Kirkwood [1935]. Using straight line brackets to denote *numbers* of individuals, etc. this is expressed as:

$$|ABC| \approx \frac{(k-1)}{k}\frac{|AB||BC|}{|B|} \iff [ABC] \approx \frac{[AB][BC]}{[B]} \tag{3.41}$$

When terms are expressed in terms of numbers this must be scaled by the factor $(k-1)/k$; this scaling factor disappears for k-regular networks when expressed in terms of proportions. This can be shown by converting either formulation of the approximation to the other using the conversion table given in Table A.1. Using this approximation, we obtain:

Model 5 - The pairwise approximation for k-regular networks

$$[\dot{SS}] = 2\gamma[SI] - 2(k-1)\tau\frac{[SS][SI]}{[S]} \tag{3.42}$$

$$[\dot{SI}] = \gamma([II] - [SI]) - \tau[SI] + (k-1)\tau\frac{[SS][SI]}{[S]} - (k-1)\tau\frac{[SI]^2}{[S]} \tag{3.43}$$

where $[S] = [SS] + [SI]$, $[I] = 1 - [S]$, $[IS] = [SI]$, and $[II] = 1 - [SS] - 2[SI]$.

3.3.2 Improving pairwise approximations for k-regular networks

Once again, we can look to improve the pairwise approximation by considering the rate of change of triples. Reintroducing subscripts (the position of individuals is illustrated in Figure 3.5), the state of $x - c - y$ triples depend upon topologies consisting of four connected individuals: line graphs of length 4 $[A_a X_x C_c Y_y]$ and $[X_x C_c Y_y B_b]$, capturing the external force of infection acting upon individuals on the periphery of the triple, and star graphs with three outer individuals, $[X_x C_c Y_y Z_z]$, capturing the external force of infection upon the central individual.

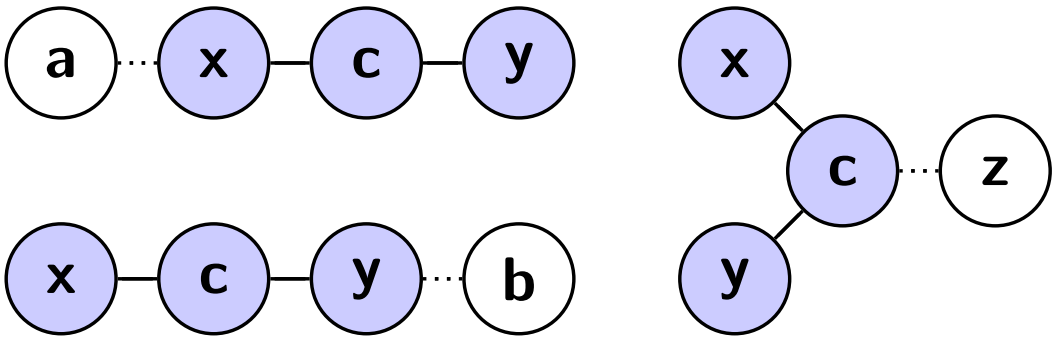

Figure 3.5: **Dependence on order-four structures in a k-regular network.** The state $[X_x C_c Y_y]$ of our triple of interest (shaded in blue) depends on the state of two order-four network structures - length four line-graphs $[A_a X_x C_c Y_y]$ and $[X_x C_c Y_y B_b]$ and the 'star' graph with three outer individuals $[X_x C_c Y_y Z_z]$. The positions of a, b, and z relative to the triple of interest are shown visually here. N.B. that $[X_x C_c Y_y B_b] \equiv [B_a Y_x C_c X_y]$, meaning only one length-four line graph term is necessary in the equations below.

The rates of change of the states of triples in a k-regular network depend upon the state of order-four network structures: line-graphs of length four ($[A_a X_x C_c Y_y], [X_x C_c Y_y B_b]$) and star graphs with three outer individuals ($[X_x C_c Y_y Z_z]$). Assuming random initial conditions, because of the symmetry of the system $[X_x C_c Y_y B_b] = [B_a Y_x C_c X_y]$, only one length four line-graph term is needed in the equations below. Given that $[SSI] = [ISS]$ and $[SII] = [IIS]$, the rates of change of these triples are described by six ODEs, which can be derived from the system of equations (12) described by

House et al. [2009] by omitting terms that include closed loops and by converting the equations from numbers to proportions via Table A.1.

$$\begin{aligned}
[S\dot{S}S] =& \gamma(2[SSI] + [SIS]) - \tau(k-2)[S_xS_cS_yI_z] - 2\tau(k-1)[I_aS_xS_cS_y] && (3.44)\\
[S\dot{S}I] =& \gamma([SII] + [ISI] - [SSI]) - \tau[SSI] && (3.45)\\
& - \tau(k-2)[S_xS_cI_yI_z] + \tau(k-1)([I_aS_xS_cS_y] - [I_aS_xS_cI_y])\\
[I\dot{S}I] =& \gamma([III] - 2[ISI]) - 2\tau[ISI] - \tau(k-2)[I_xS_cI_yI_z] && (3.46)\\
& + 2\tau(k-1)[I_aS_xS_cI_y]\\
[S\dot{I}S] =& \gamma(2[SII] - [SIS]) - 2\tau[SIS] + \tau(k-2)[S_xS_cS_yI_z] && (3.47)\\
& - 2\tau(k-1)[I_aS_xI_cS_y]\\
[S\dot{I}I] =& \gamma([III] - 2[SII]) + \tau([SIS] + [SSI] - [SII]) && (3.48)\\
& + \tau(k-2)[S_xS_cI_yI_z]) + \tau(k-1)([I_aS_xI_cS_y] - [I_aS_xI_cI_y])\\
[I\dot{I}I] =& -3\gamma[III] + \tau(2[SII] + 2[ISI]) + \tau(k-2)[I_xS_cI_yI_z] && (3.49)\\
& + 2\tau(k-1)[I_aS_xI_cI_y]
\end{aligned}$$

As before, we define α values as the difference between triple values and their standard pairwise approximation. Once again, the following relations hold:

$$\begin{aligned}
[S] =& [SSS] + 2[SSI] + [ISI] && (3.50)\\
[SS] =& [SSS] + [SSI] && (3.51)\\
[SI] =& [SSI] + [ISI] && (3.52)
\end{aligned}$$

Thus, as for the isolated open triple, the difference between triple values and pairwise approximations depend only upon two quantities: α_S and α_I, which are as defined in Equation (3.23) and Equation (3.24). We can use Equations (3.44) to (3.49) to obtain expressions for $\dot{\alpha_S}$ and $\dot{\alpha_I}$ for this type of network:

$$\dot{\alpha_S} = [S\dot{S}S][ISI] + [I\dot{S}I][SSS] - 2[S\dot{S}I][SSI] \tag{3.53}$$

$$= \gamma(\Phi_S - 2\alpha_S) + \tau(\beta_S - 2\alpha_S) \tag{3.54}$$

$$\text{where } \beta_S = 2(k-1)([I_a S_x S_c I_y][SS] - [I_a S_x S_c S_y][SI]) \tag{3.55}$$

$$+ (k-2)(2[S_x S_c I_y I_z][SSI] - [S_x S_c S_y I_z][ISI] - [I_x S_c I_y I_z][SSS])$$

$$\dot{\alpha_I} = [I\dot{I}I][SIS] + [S\dot{I}S][III] - 2[S\dot{I}I][SII] \tag{3.56}$$

$$= -4\gamma\alpha_I + \tau(\beta_I + 2\Phi_I - 2\alpha_I) \tag{3.57}$$

$$\text{where } \beta_I = 2(k-1)([I_a S_x I_c I_y][SI] - [I_a S_x I_c S_y][II]) \tag{3.58}$$

$$- (k-2)(2[S_x S_c I_y I_z][SII] - [I_x S_c I_y I_z][SIS] - [S_x S_c S_y I_z][III])$$

Despite being calculated for triples within a k-regular network, we find that $\Phi_S = \phi_S$ and $\Phi_I = \phi_I$ as previously defined for the isolated open triple in Equations (3.28) and (3.32), and so use the ϕ_S and ϕ_I terms henceforth. We therefore obtain a closed set of equations by once again setting

$$[ABA] \approx \frac{[AB]^2 + \alpha_B}{[B]} \qquad [ABC] \approx \frac{[AB][BC] - \alpha_B}{[B]} \tag{3.59}$$

But now we must also make some approximation for order four terms. We do this by making the following closures:

$$[A_x S_c B_y I_z] \approx \frac{[ASB][BSI][ASI][S]}{[AS][BS][IS]} \tag{3.60}$$

$$[I_a S_x A_c B_y] \approx \frac{[ISA][SAB]}{[SA]} \tag{3.61}$$

Thus, we can again express $\dot{\alpha_S}$ and $\dot{\alpha_I}$ as (complicated) functions of $[SS], [SI], \alpha_S$ and α_I. Using this, we arrive at a system of four ODEs, which we call the improved pairwise approximation for k-regular networks:

Model 6 - The improved pairwise approximation for k-regular networks

$$[\dot{SS}] = 2\gamma[SI] - 2(k-1)\tau\frac{[SS][SI] - \alpha_S}{[S]} \tag{3.62}$$

$$[\dot{SI}] = \gamma([II] - [SI]) - \tau[SI] + (k-1)\tau\frac{[SS][SI] - \alpha_S}{[S]} - (k-1)\tau\frac{[SI]^2 + \alpha_S}{[S]} \tag{3.63}$$

$$\dot{\alpha_S} = \gamma(\phi_S - 2\alpha_S) + \tau(\beta_S - 2\alpha_S) \tag{3.64}$$

$$\dot{\alpha_I} = -4\gamma\alpha_I + \tau(\beta_I + 2\phi_I - 2\alpha_I) \tag{3.65}$$

where ϕ_S and ϕ_I are defined as in Section 3.2.

3.4 Higher-order moment-closure approximations

To assess the accuracy gained by modelling the error terms α_S and α_I, we compare our model to higher-order moment-closures. The first of these we refer to as a *neighbourhood* closure, previously described by Lindquist et al. [2011] and Keeling et al. [2016], where we model a central individual and their number of infected neighbours explicitly. This system is described by $2 \times (k+1)$ ODEs. The second of these we refer to as an *extended triple closure*, where we explicitly model a central triple and every neighbour of this triple. This system is described by 2^{3k-1} equations (though its dimensionality can be reduced by accounting for symmetries). In both cases, we approximate the external force of infection on outer individuals by exploiting the symmetry of the topology of the k-regular network. While each model is still an approximation towards the true dynamics of a k-regular network,

in virtue of closing the system at a higher order, these models are expected to have a greater accuracy. From these higher-order models, we can also obtain estimates of the terms α_S and α_I, with which we can compare the α terms obtained from the improved pairwise model for the k-regular network (Model 6).

3.4.1 The neighbourhood closure

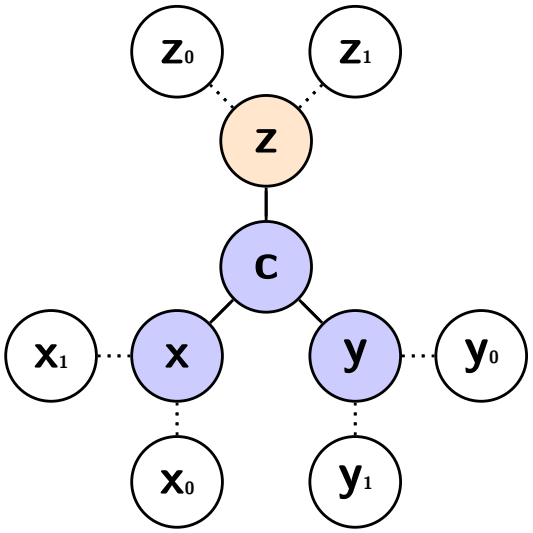

Figure 3.6: **The external force of infection on a neighbourhood.** Here we illustrate the external force of infection on a neighbourhood in the neighbourhood approximation for k-regular networks, for the example of $k = 3$. Shaded blue is our triple of interest, shaded in orange are any additional individuals that are modelled explicitly, while shaded in white are individuals not explicitly modelled who exert a force of infection on the explicitly modelled neighbourhood. In this approximation, we model a central individual c, and the number of infected neighbours c as (here shown by x, y, and z). The external force of infection on the explicitly modelled neighbourhood will depend upon order-six structures: $[X_x C_c Y_y Z_z X_{0_{x_0}} X_{1_{x_1}}]$, $[X_x C_c Y_y Z_z Y_{0_{y_0}} Y_{1_{y_1}}]$, and $[X_x C_c Y_y Z_z Z_{0_{z_0}} Z_{1_{z_1}}]$. To close the system, we make the approximation that, e.g. $[X_x C_c Y_y Z_z X_{0_{x_0}} X_{1_{x_1}}] \approx ([X_x C_c Y_y Z_z] \times [X_x C_c X_{0_{x_0}} X_{1_{x_1}}])/[X_x C_c]$.

For the neighbourhood closure, we model a central individual and their number of infected neighbours explicitly. Visually then, we are modelling a star topology. The rate of change of state of the 'star' will depend upon both the internal configurations

and the immediate neighbours of the star. We show this visually in Figure 3.6.

To close this system of equations, we make the assumption that the configuration of two overlapping 'stars' are conditionally independent given the infection status of the two shared individuals of the combined configuration. As we only need to consider the effect of an external force of infection if the relevant neighbour is susceptible (S), there are only two quantities relevant to the external force of infection on that individual, depending on the infection status of the original central individual (S or I), which denote λ_S and λ_I accordingly. These terms are constructed by summing all configurations of the external neighbours including an infected individuals, multiplied by the number of infected external neighbours in that configuration, divided by the sum of all possible configurations of external neighbours. Denoting a central individual in state $A \in \{S, I\}$ with $i \in \{0, 1, ..., k\}$ infected neighbours as $[A_i]$, the neighbourhood model can thus be described by the following set of equations:

Model 7 - The neighbourhood approximation model for k-regular networks

$$[\dot{S}_i] = \begin{cases} 0, i < 0 \\ \gamma([I_i] + (i+1)[S_{i+1}] - i[S_i]) - \tau i[S_i] + \lambda_S((k-i+1)[S_{i-1}] - (k-i)[S_i]), 0 \leq i \leq k \\ 0, i > k \end{cases} \tag{3.66}$$

$$[\dot{I}_i] = \begin{cases} 0, i < 0 \\ \gamma(i+1)([I_{i+1}] - [I_i]) + \tau i[S_i] + (\lambda_I + \tau)((k-i+1)[I_{i-1}] - (k-i)[I_i]), 0 \leq i \leq k \\ 0, i > k \end{cases} \tag{3.67}$$

where λ_S and λ_I are given by:

$$\lambda_S = \tau \frac{\sum_{i=0}^{k-1} i(k-i)[S_i]}{\sum_{i=0}^{k-1} (k-i)[S_i]} \tag{3.68}$$

$$\lambda_I = \tau \frac{\sum_{i=0}^{k-1} i(i+1)[S_{i+1}]}{\sum_{i=0}^{k-1} (i+1)[S_{i+1}]} \tag{3.69}$$

To obtain estimates for α_S (and α_I) from this model, we must derive the proportion of triples implied by the assumptions of the neighbourhood model. This can be calculated as follows. For a given triple $[XCY]$, we let l indicate whether X and Y are infected. (If $X = Y = S$, $l = 0$. If $X = S$ and $Y = I$, or $X = I$ and $Y = S$, $l = 1$. If $X = Y = I$, $l = 2$.) In the neighbourhood model we explicitly model a central individual and the number of its k immediate neighbours who are infected. $[XCY]$ will occur as subgraphs of configurations that comprise C_l to C_{k+l-2}. Assuming there are i additional infected individuals surrounding c (in addition to those specified by X and Y), there are $\binom{k}{i+l}$ different configurations such that a central individual C has $i+l$ infected neighbours. Of these, there are $\binom{k-2}{i}$ configurations once the position of the [XCY] subgraph is determined, as there are $k-2$ positions left to fill with i infected individuals. Hence $\binom{k-2}{i}$ / $\binom{k}{i+l}$ of $[C_{i+l}]$ contain $[XCY]$, and so we arrive at the formula:

$$[XCY] = \sum_{i=0}^{k-2} \frac{\binom{k-2}{i}}{\binom{k}{i+l}} [C_{i+l}] \tag{3.70}$$

3.4.2 The extended triple closure

For the extended triple closure, we model a triple and each of its neighbours explicitly. For a k-regular network, $3k-1$ individuals are modelled explicitly, meaning 2^{3k-1} equations are required to describe this model. The state of this system will

depend on the infection status of the neighbours of these neighbours, i.e. the rate of change of states in the extended triple depend upon order $4k - 2$ configurations (illustrated in Figure 3.7). We approximate these external forces on the extended triple by assuming that the state of these higher-order structures amount to overlapping extended triple topologies conditionally independent given the state of their shared individuals, of which there are $2k$.

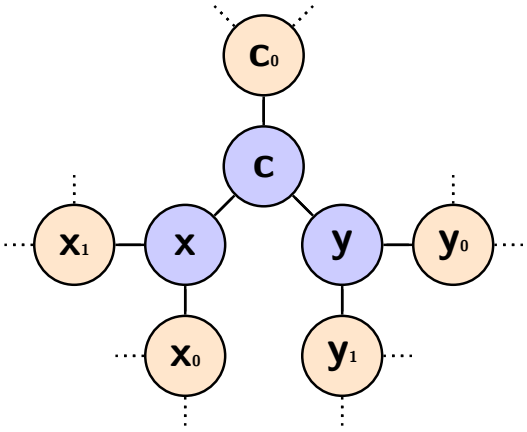

Figure 3.7: **A graphical representation of the extended triple approximation.** Here we visualise the extended open triple model for $k = 3$. Shaded blue is our triple of interest, shaded in orange are any additional individuals that are modelled explicitly, while dotted lines show connections to individuals not explicitly modelled that exert an external force of infection upon the topology. The state of this topology will depend upon order 10 structures.

By accounting for symmetries in the extended triple topology, one could reduce the dimensionality of this system. However, the method constructing the set of ODEs algorithmically described below models each state explicitly. Writing an algorithm that accounts for such symmetries, while possible, would be somewhat cumbersome, and as such we did not decide to pursue this. We approximate the external forces on this topology by assuming that the higher-order structures that the rate of change of states depend on can be approximated by conjoined extended triple topologies conditionally independent on the state of shared individuals.

We construct the extended triple model in two steps. Firstly, we construct a model

with SIS-dynamics on the finite topology of the extended triple. To construct this model, we provide an algorithm for constructing SIS-models on graphs with any arbitrary finite topology. Secondly, we add on external force of infection to this model, which we achieve via *relabelling*.

An algorithm for constructing SIS-models on graphs with arbitrary topology

Here, we outline an algorithm for constructing a model with SIS-dynamics on networks of arbitrary topology. We can rewrite the full equations for the open triple in matrix form as follows: if we let

$$\underline{x} = \{[SSS], [SSI], [SIS], [SII], [ISS], [ISI], [IIS], [III]\}^T$$

Then

$$\frac{d\underline{x}}{dt} = \gamma \underline{\underline{R}}\underline{x} + \tau \underline{\underline{N}}\underline{x} \tag{3.71}$$

States are ordered in this way so that they are interpreted as a binary string (e.g. $[SSS]$ as 000). For the open triple, $\underline{\underline{R}}$ and $\underline{\underline{N}}$ are given by:

$$\underline{\underline{R}} = \begin{bmatrix} 0 & 1 & 1 & 0 & 1 & 0 & 0 & 0 \\ 0 & -1 & 0 & 1 & 0 & 1 & 0 & 0 \\ 0 & 0 & -1 & 1 & 0 & 0 & 1 & 0 \\ 0 & 0 & 0 & -2 & 0 & 0 & 0 & 1 \\ 0 & 0 & 0 & 0 & -1 & 1 & 1 & 0 \\ 0 & 0 & 0 & 0 & 0 & -2 & 0 & 1 \\ 0 & 0 & 0 & 0 & 0 & 0 & -2 & 1 \\ 0 & 0 & 0 & 0 & 0 & 0 & 0 & -3 \end{bmatrix}$$

$$\underline{\underline{N}} = \begin{bmatrix} 0 & 0 & 0 & 0 & 0 & 0 & 0 & 0 \\ 0 & -1 & 0 & 0 & 0 & 0 & 0 & 0 \\ 0 & 0 & -2 & 0 & 0 & 0 & 0 & 0 \\ 0 & 1 & 1 & -1 & 0 & 0 & 0 & 0 \\ 0 & 0 & 0 & 0 & -1 & 0 & 0 & 0 \\ 0 & 0 & 0 & 0 & 0 & -2 & 0 & 0 \\ 0 & 0 & 1 & 0 & 1 & 0 & -1 & 0 \\ 0 & 0 & 0 & 1 & 0 & 2 & 1 & 0 \end{bmatrix}$$

Thus, we need an algorithm to construct matrices $\underline{\underline{R}}$ and $\underline{\underline{N}}$ for an arbitrary graph topology, defined by its adjacency matrix $\underline{\underline{A}}$. Such an algorithm is detailed below:

1. Start with empty matrices $\underline{\underline{R}}$ and $\underline{\underline{N}}$ of size $2^a \times 2^a$, where a is the length of $\underline{\underline{A}}$.

2. Interpret each possible state of A as a vector $\underline{b}$, with a 0 in position i of $\underline{b}$ representing that $i = S$ in that state, and with a 1 in position i of $\underline{b}$ representing that $i = I$ in that state. The column corresponding to a given state in $\underline{\underline{N}}$ and $\underline{\underline{R}}$ is given by $d = 1 + \underline{b}$ *(with $\underline{b}$ interpreted as a binary number.)*

3. For each vector b, go through each entry i. If $b(i) = 1$, then $\underline{\underline{R}}(d, d) = \underline{\underline{R}}(d, d) - 1$. Let e be the number obtained by changing $b(i)$ from 1 to 0, and $\underline{\underline{R}}(e, d) = \underline{\underline{R}}(e, d) + 1$

4. For each vector b, go through each entry j. If $b(j) = 0$, go through each entry k of b. If $b(k) = 1$ and $\underline{\underline{A}}(j, k) = 1$, then $\underline{\underline{N}}(d, d) = \underline{\underline{N}}(d, d) - 1$. Let e be the number obtained by changing $b(j)$ from 0 to 1, and $\underline{\underline{N}}(e, d) = \underline{\underline{N}}(e, d) + 1$

Using this algorithm, we can construct a model with SIS-dynamics on the finite topology of the extended triple.

Relabelling - an example

To consider the external force of infection acting upon a particular state of the external triple, we must consider the external force of infection on the susceptible neighbours of that particular configuration. To evaluate this, we must consider the states in which this neighbour has no susceptible external partners, up to the state in which this neighbour has all susceptible external partners. We can achieve this by *relabelling* the system to give us equations describing the probability of being in said states.

Let us consider an example for a 3-regular network. Suppose we want to consider the external force of infection on the state $A = [S_x S_c S_y; S_{x_0} I_{x_1} I_{c_0} I_{y_0} I_{y_1}]$, with subscripts designating the positions described in Figure 3.7. We include the semicolon to distinguish between the central triple and its neighbours. The only external force acting on this topology will be upon x_0, who is susceptible, by any external infected neighbour of x_0. Thus, the rate of change of $[S_x S_c S_y; S_{x_0} I_{x_1} I_{c_0} I_{y_0} I_{y_1}]$ will depend upon some order 10 terms: $[S_x S_c S_y; S_{x_0} I_{x_1} I_{c_0} I_{y_0} I_{y_1}; I_{x_{00}} S_{x_{01}}]$, $[S_x S_c S_y; S_{x_0} I_{x_1} I_{c_0} I_{y_0} I_{y_1}; S_{x_{00}} I_{x_{01}}]$, and $[S_x S_c S_y; S_{x_0} I_{x_1} I_{c_0} I_{y_0} I_{y_1}; I_{x_{00}} I_{x_{01}}]$. We make a closure at this level by assuming, to take the first of these as an example:

$$[S_x S_c S_y; S_{x_0} I_{x_1} I_{c_0} I_{y_0} I_{y_1}; I_{x_{00}} S_{x_{01}}] \approx \frac{[S_x S_c S_y; S_{x_0} I_{x_1} I_{c_0} I_{y_0} I_{y_1}] \times [S_{x_0} S_x S_c; I_{x_{00}} S_{x_{01}} I_{x_1} I_{c_0} S_y]}{[S_x S_c S_y; S_{x_0} I_{x_1} I_{c_0}]} \tag{3.72}$$

As we have not modelled x_{00} and x_{01} explicitly, the probability of state $[S_{x_0} S_x S_c; I_{x_{00}} S_{x_{01}} I_{x_1} I_{c_0} S_y]$ remains undefined. However, as we start from random initial conditions, and given that a k-regular network is isotropic, all extended triples within a k-regular network are equivalent. Because of this, we have:

$$[S_{x_0}S_xS_c; I_{x_{00}}S_{x_{01}}I_{x_1}I_{c_0}S_y] = [S_xS_cS_y; I_{x_0}S_{x_1}I_{c_0}I_{y_0}S_{y_1}] \tag{3.73}$$

Thus, we obtain an expression for this state by taking into account the symmetry of a k-regular network, and by relabelling individuals so that states containing individuals not explicitly modelled are defined in terms of explicitly modelled individuals exclusively.

We can now arrive at an expression for the external force of infection acting upon state A (λ_A), which is given by:

$$\lambda_A = \frac{\sum_{P,Q\in\{S,I\}}(1_{P=I} + 1_{Q=I}) \times [S_xS_cS_y; P_{x_0}Q_{x_1}I_{c_0}I_{y_0}S_{y_1}]}{\sum_{P,Q\in\{S,I\}}[S_xS_cS_y; P_{x_0}Q_{x_1}I_{c_0}I_{y_0}S_{y_1}]} \tag{3.74}$$

where $1_{P=I}$ and $1_{Q=I}$ are indicator functions.

Relabelling generally

The particular relabelling depends upon the particular state of the external triple, and upon the particular neighbouring individuals whose external force of infection you are considering. The requires labellings for the $k = 3$ case are given in Table 3.1, and the required relabellings for a general k is given in Table 3.2. The header row gives the neighbouring individual whose external force of infection we are considering, while the leftmost column gives the new positions of states in a given column now occupy. External vertices that contribute to the external force of infection always occupy the relabelled x_i positions.

Table 3.1: **Relabelling for $k = 3$.**

Individual	$\mapsto$	$x_0 = S$	$x_1 = S$	$c_0 = S$	$y_0 = S$	$y_1 = S$
x	$\mapsto$	X_0	X_1	C_0	Y_0	Y_1
c	$\mapsto$	X	X	C	Y	Y
y	$\mapsto$	C	C	Y	C	C
x_0	$\mapsto$	$\{S, I\}$	$\{S, I\}$	$\{S, I\}$	$\{S, I\}$	$\{S, I\}$
x_1	$\mapsto$	$\{S, I\}$	$\{S, I\}$	$\{S, I\}$	$\{S, I\}$	$\{S, I\}$
c_0	$\mapsto$	X_1	X_0	X	Y_1	Y_0
y_0	$\mapsto$	C_0	C_0	Y_0	C_0	C_0
y_1	$\mapsto$	Y	Y	Y_1	X	X

Constructing the extended triple model

To make the extended triple model, we begin by constructing the model for the relevant finite topology with SIS-dynamics, as outlined previously in this section. To construct a model approximating a k-regular network, we must add an external force of infection to individuals neighbouring the central triple. The procedure is as follows:

1. Construct ODEs for the SIS-dynamics for a graph of the relevant topology, with the central triple as the first three rows of the adjacency matrix.

2. Express each state N as a vector $\underline{b}$ (of length $l = 3k - 1$) with a 0 in position i of $\underline{b}$ representing that $i = S$ in that state, and with a 1 in position i of $\underline{b}$ representing that $i = I$ in that state.

3. For each vector b, loop through entries $i \in \{4, ..., l\}$. If $b(i) = 1$ calculate the external force of infection on this vertex, I_{ext}, by relabelling.

4. Subtract this, multiplied by τ and the state itself (i.e. $\tau N I_{ext}$), to that state's ODE (i.e. $\dot{N} = \dot{N} - \tau N I_{ext}$).

5. Let e be the binary vector obtained by changing $b(i)$ from 1 to 0, and let E be the state corresponding to this number. Add on the $\tau N I_{ext}$ to this ODE

(i.e. $\dot{E} = \dot{E} + \tau N I_{ext}$).

.

Table 3.2: **Relabelling for general k.** Subscripts of X and Y are modulo k, while subscripts of C are modulo $k-1$

Individual	$\mapsto$	$x_i = S$	$c_0 = S$	$c_i = S$	$y_0 = S$	$y_i = S$
x	$\mapsto$	X_i	C_0	C_i	Y_0	Y_i
c	$\mapsto$	X	C	C	Y	Y
y	$\mapsto$	C	Y	Y	C	C
x_i	$\mapsto$	$\{S, I\}$	$\{S, I\}$	$\{S, I\}$	$\{S, I\}$	$\{S, I\}$
c_0	$\mapsto$	X_{i+1}	X	X	Y_1	Y_{i+1}
c_j	$\mapsto$	X_{i+j+1}	C_j	C_{j+1}	C_{j+1}	C_{i+j+1}
y_0	$\mapsto$	Y	Y_0	Y_0	X	X
y_j	$\mapsto$	C_{j-1}	Y_j	Y_j	C_{j-1}	C_{j-1}

3.4.3 Stochastic simulations

We use explicit stochastic simulations as our final benchmark for the accuracy of our approximate models. It is not computationally possible to construct infinite loopless networks for simulations. Instead, large random graphs where each individual has k neighbours can be constructed using the Molloy-Reed algorithm [Molloy and Reed, 1995], which should behave similarly for very large network sizes. We use the methods outlined by Keeling et al. [2016] to remove short loops and to efficiently calculate the quasi-equilibrium prevalence of infection. This method does not capture the infection dynamics on the network through time. As this chapter uses endemic prevalence of infection as the primary metric for model comparison, stochastic simulations capturing infection dynamics through time are not included, but these could be obtained via numerical simulation using a Gillespie algorithm.

3.5 Comparing Models

In this section, we compare the previous described k-regular network models; in order of dimensionality, these are: the mean-field approximation model (Model 4), the pairwise approximation model (Model 5), the improved pairwise approximation model (Model 6), the neighbourhood approximation model (Model 7), and the extended triple approximation model. As we are considering a disease with SIS-dynamics, the models evolve to an endemic prevalence of infection (given a sufficiently high transmission rate) - we use this as the primary metric for model comparison. All of these models are approximations of the true system, where there are infinitely many individuals, but we expect as we increase the dimensionality of approximation we also increase the accuracy of the model. We compare all approximate models to explicit stochastic simulations on networks of 10,000 individuals.

3.5.1 Comparing models closed at different orders

In Figure 3.8, we compare the endemic prevalence generated by the four models that do not explicitly model α to stochastic simulations - the improved pairwise approximation (which utilises the dynamics of α) is considered in Figure 3.9 onwards. While we notice large differences between mean-field and pairwise models, the difference in prevalence between models decreases as we increase the dimensionality of the model. For $k = 3$, there is little difference between the neighbourhood and extended triple approximation models, and there is excellent agreement between the extended triple model and stochastic simulation. For $k = 4$ and $k = 10$, the extended triple model is omitted, as the neighbourhood approximation models match closely to stochastic simulations. This indicates that including further complexity into a model may be unnecessary, or may not be worth the increasing complexity or computational expense. For $k = 2$, there is still a significant difference be-

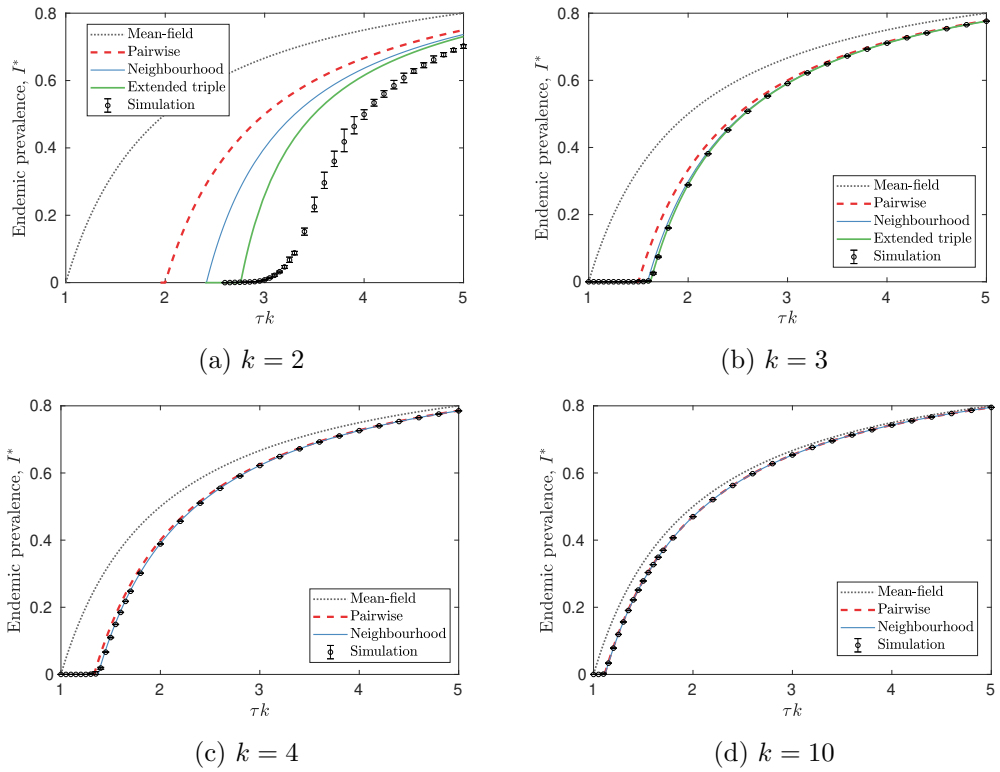

(a) $k = 2$ (b) $k = 3$

(c) $k = 4$ (d) $k = 10$

Figure 3.8: **Comparing approximate models for k-regular networks.** Here we compare endemic prevalence (I^*) against $\lambda = \tau k$ for mean-field (grey, dotted), pairwise (red), neighbourhood (blue), extended triple (green) approximations for k-regular networks against explicit stochastic simulations (points) for a) $k = 2$, (b) $k = 3$ (c) $k = 4$, and (d) $k = 10$. For $k = 3$ simulations are matched well by the extended triple model, while for $k > 3$ simulations are matched well by the neighbourhood model. As k increases, all models move closer to the mean-field approximation, and the difference in I^* for a given λ between approximate models decreases. For stochastic simulations, each I^* point is calculated as the average of 150 runs, and error bars indicate 95% confidence intervals.

tween simulation and the extended triple model. However, this is unsurprising, as previous research [Keeling et al., 2016] has shown that errors persist when much larger neighbourhoods are modelled explicitly. Figure 3.8 also illustrates that as we increase k, models tend towards the mean-field approximation (which can be considered the $k \to \infty$ limit), which we prove for the pairwise models below.

3.5.2 Convergence to the mean-field approximation as $k \to \infty$

We believe that as $k \to \infty$, all models converge to the mean-field approximation. In this section, we show this is true for both the pairwise and improved pairwise approximation models, and outline how this would be approached in the general case.

For all models, Equations (3.38) and (3.40) ($[\dot{S}]$ and $[\dot{SI}]$) hold exactly - only beginning to differ at the level of triples. Our contention is that as $k \to \infty$, $[SI] \to [S][I]$. First, we note that because $[SI] = [S] - [SS]$, $[SI] = [S][I] \iff [SS] = [S]^2$. We consider $[\dot{SS}]$,

$$[\dot{SS}] = 2\gamma[SI] - 2(k-1)\tau[SSI] \tag{3.75}$$

Now, we introduce $\lambda = \tau k$, which remains constant as k increases. We make the assumption that $[SS] = [S]^2$ initially and consider their time evolution:

$$([\dot{S}]^2) = 2[S][\dot{S}] = 2\gamma[S][I] - 2\lambda[S]^2[I] \tag{3.76}$$

$$[\dot{SS}] = 2\gamma[S][I] - 2\frac{(k-1)}{k}\lambda[SSI] \to 2\gamma[S][I] - 2\lambda[SSI] \text{ as } k \to \infty \tag{3.77}$$

These equations are equal, and therefore the relationship $[SS] = [S]^2$ continues to hold, conditional on $[SSI] = [S]^2[I]$. In general we need to show that the relationship $[SSI] = [S]^2[I]$ continues, given that it holds initially.

Convergence for the pairwise approximation model

Under the standard pairwise model, $[SSI] = [SS][SI]/[S]$. Assuming that $[SS] = [S]^2$, it is clear that $[SSI] = [S]^2[I]$. Given that at $t = 0, [SS] = [S]^2$, and that $[SS] = [S]^2 \Rightarrow [\dot{SS}] = [\dot{S}]^2$, the convergence of the standard pairwise model is proved by induction.

Convergence for the improved pairwise approximation model

Under this model $[SSI] = ([SS][SI] - \alpha_S)/[S]$, i.e. $[SSI] = [S]^2[I] \iff ([SS] = [S]^2, \alpha_S = 0)$. Let us assume that $[SS] = [S]^2$, $\alpha_S = 0$, and $\alpha_I = 0$. Then $[SSI] = [S]^2[I]$ and by examining Equations (3.54) and (3.57), we find that $\dot{\alpha_S} = 0$ and $\dot{\alpha_I} = 0$. Given that at $t = 0, [SS] = [S]^2, \alpha_S = 0, \alpha_I = 0$, and that $[SS] = [S]^2, \alpha_S = 0, \alpha_I = 0 \Rightarrow [\dot{SS}] = [\dot{S}], \dot{\alpha_S} = 0, \dot{\alpha_I} = 0$, the convergence of the improved pairwise model is proved by induction.

Convergence in the general case

More generally, we believe that as $k \to \infty$, spatial correlation at a particular level is only introduced by spatial correlations at a higher level. For example, correlations only enter the pairwise model if there are correlations at the level of pairs, correlations only enter the improved pairwise model if there are correlations at the level of pairs and triples (α terms), etc. Given that by assumption we start with no spatial correlation at any level, it follows that correlations are never introduced. However, we believe that the proof of this more general claim is beyond the remit of this chapter.

In Figure 3.8 we also see that as we increase k, the difference between pairwise and neighbourhood approximation models decreases, although the pairwise model consistently predicts higher endemic prevalences.

3.5.3 Exploring the shape of errors α_S and α_I

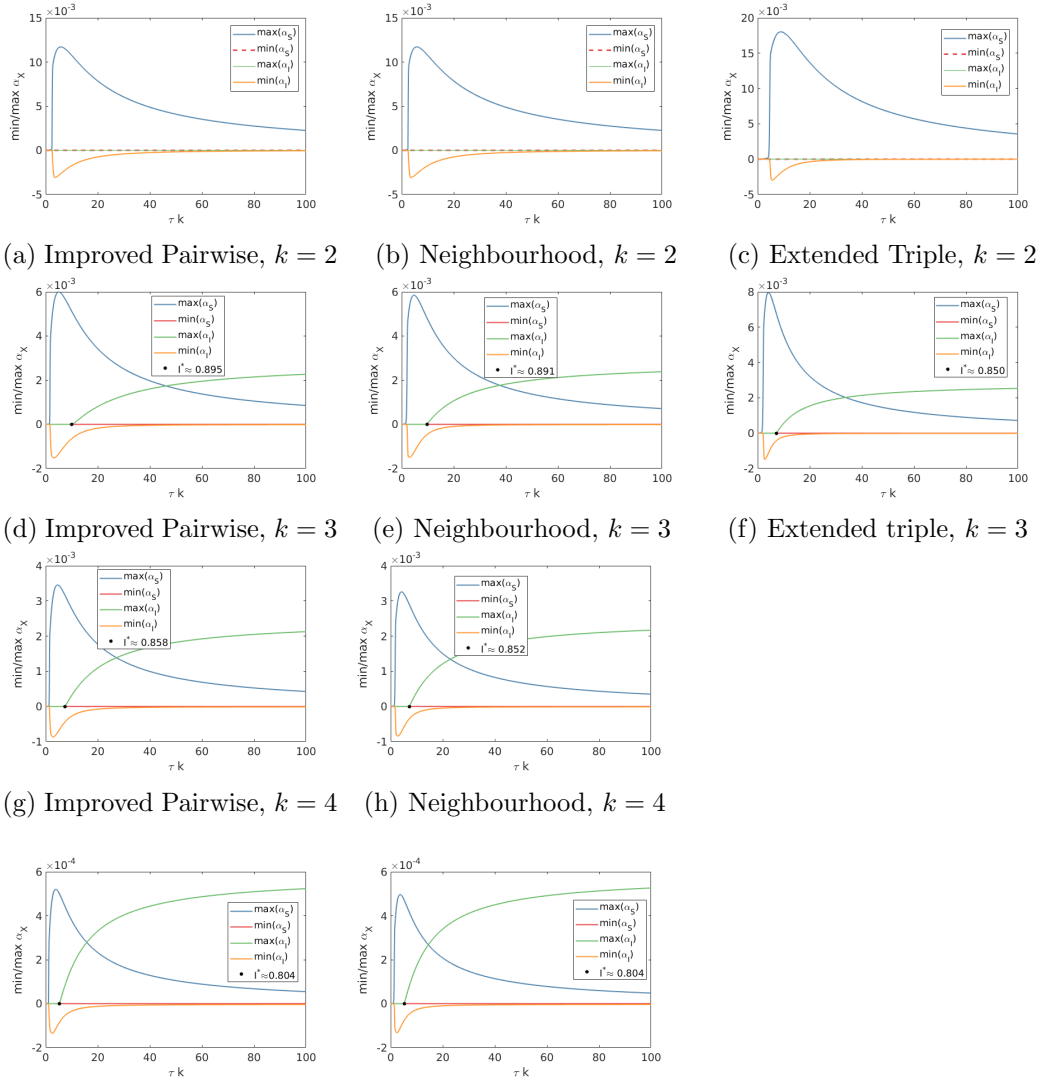

(a) Improved Pairwise, $k = 2$ (b) Neighbourhood, $k = 2$ (c) Extended Triple, $k = 2$

(d) Improved Pairwise, $k = 3$ (e) Neighbourhood, $k = 3$ (f) Extended triple, $k = 3$

(g) Improved Pairwise, $k = 4$ (h) Neighbourhood, $k = 4$

(i) Improved Pairwise,$k = 10$ (j) Neighbourhood, $k = 10$

Figure 3.9: **Numerical exploration of α_S and α_I for different approximate models of the k-regular network.** We consider how $min(\alpha_X)$ and $max(\alpha_X)$, $X \in \{S, I\}$ vary with τk for different approximate models of the k-regular network: Improved pairwise (left column), neighbourhood (centre column), extended triple (right column). These plots demonstrate the bound $\alpha_S \geq 0$ holds for all approximations of the k-regular network, but that $\alpha_I \leq 0$ only holds for the case $k = 2$. For $k > 2$, $max(\alpha_I) > 0$ given τ is sufficiently high. These transmission rates correspond to high endemic prevalences - in all cases $I^* > 0.8$. In all plots we set $\gamma = 1$.

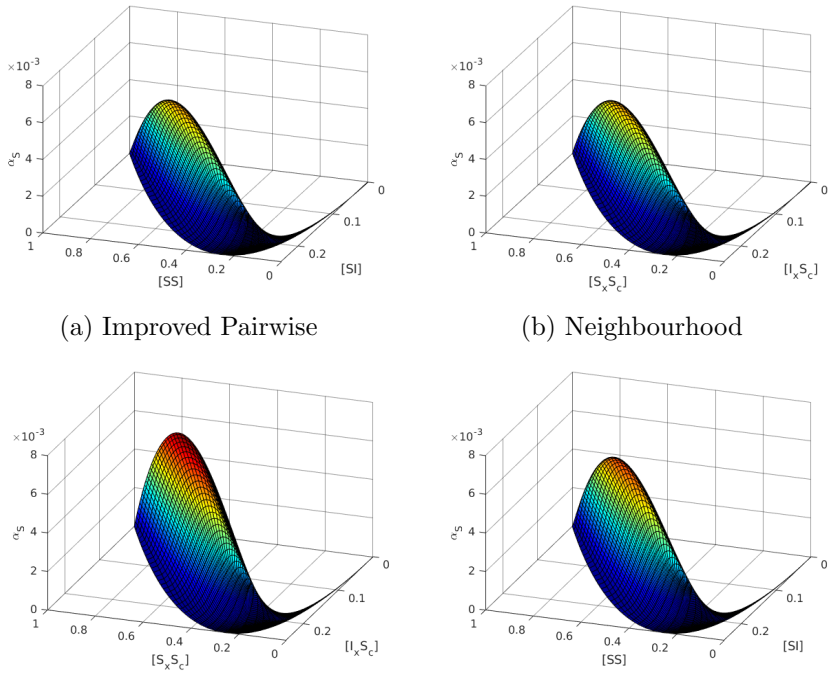

(a) Improved Pairwise (b) Neighbourhood

(c) Extended Triple (d) Improved Pairwise, $\alpha_I = 0$

Figure 3.10: **Exploring the shape of α_S for different approximate models.** Here we compare the shape of the error term α_S as a function of $[SS]$ and $[SI]$ for improved pairwise models ((a) and (d)), and as a function of $[S_xS_c]$ and $[I_xS_c]$ for neighbourhood and extended triple approximations ((b) and (c)), for the example $k = 3$. We observe that α_S in the improved pairwise (a) and the neighbourhood (b) approximation models are extremely similar, but that the improved pairwise approximation model underestimates this error compared to the extended triple approximation (c). By assuming $\alpha_I = 0$ and $\dot{\alpha_I} = 0$ (d), the resulting α_S surface more closely resembles that of the extended triple model. In all plots, we set $\tau = 1, \gamma = 1$.

Now, we turn our attention to the improved pairwise approximation (Model 6), which tracks the errors α_S and α_I explicitly. Here we focus on the examples $k = 2$ and $k = 3$, though comparable results are found for all higher values of k. The error in our pairwise model depends on only one term: α_S. This term captures the error between the 'true' value of triples and the standard pairwise approximation of their values. We can obtain estimates for α_S from each of our higher-order models, noting that the improved pairwise approximation (Model 6) is based on

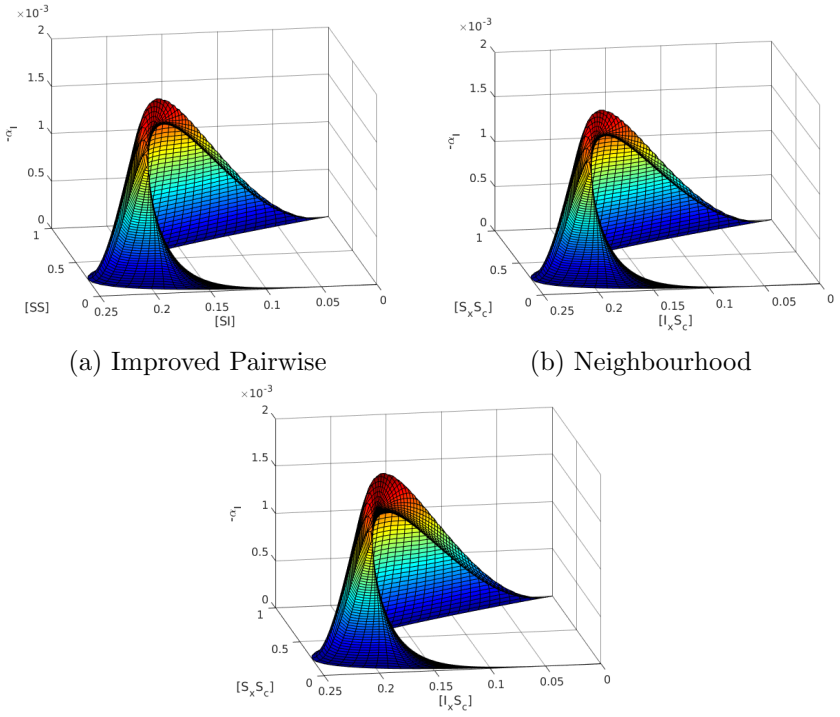

(a) Improved Pairwise

(b) Neighbourhood

(c) Extended Triple

Figure 3.11: **Exploring the shape of α_I for different approximate models.** Here we compare the shape of the error term $-\alpha_I$ as a function of $[SS]$ and $[SI]$ for the improved pairwise model (a), and as a function of $[S_xS_c]$ and $[I_xS_c]$ for neighbourhood and extended triple approximations ((b) and (c)), for the example $k = 3$. We observe that α_I surfaces in all three models are very similar, and that their magnitude is much smaller than their corresponding α_S surfaces (Figure 3.10). In all plots, we set $\tau = 1, \gamma = 1$.

consideration of four connected vertices. Comparing α_S between models allows us to assess the extent to which the improved pairwise approximation is successful in capturing the errors introduced to the pairwise approximation induced by dynamics of higher-order structures. Firstly, we observe that the numerical result $\alpha_S \geq 0$ that was true for the isolated open triple also holds true for each of these models (numerically demonstrated in Figure 3.9). Hence, the bounds obtained for triples $[S_xS_cS_y]$, $[I_xS_cI_y]$, and $[S_xS_cI_y]$ in Section 3.2 for the isolated open triple also hold for k-regular networks. Secondly, by plotting α_S as a function of the pairs $[SS]$ and $[SI]$ we obtain surfaces; their shape informing our intuition of the behaviour

of α_S as we move through $([SS],[SI])$-space (Figure 3.10). Surface plots are obtained by running each model over a range of initial conditions, varying the initial prevalence from 0 to 1. For each of these model runs, we plot the 3-D trajectory of $([SS],[SI],\alpha_S)$, with $[SS]$ values on the x-axis, $[SI]$ values on the y-axis and α_S values on the z-axis. By conjoining adjacent trajectories, we then visualise α_S as a surface. Doing so, we obtain similar α_S surfaces from the improved pairwise and neighbourhood approximation models. We do, however, see these are smaller than α_S from the extended triple. In other words, models that include higher-order correlations, such as the extended triple, have higher values of α_S than are obtained from the improved pairwise model.

3.5.4 Assessing the accuracy of improved pairwise models

Comparing the prevalence of infection obtained from these models, we observe only a minor difference between improved pairwise and neighbourhood approximations (Figure 3.12). By including just two more equations (for α_S and α_I), we arrive at a model with an endemic prevalence much closer to results obtained from stochastic simulation, with only a marginal increase in dimensionality. Unlike the isolated open triple, α_I can be positive when $k > 2$ in each of the approximate models. However, this only occurs at very high transmission rates - typically when endemic prevalence $I^* > 0.8$ (Figure 3.9).

In an attempt to further improve the accuracy, and to reduce the dimensionality, of the model, we consider the effect of ignoring α_I on the shape of α_S in the improved approximation; noting that the values of α_S from the extended triple approximation are consistently larger than from the other lower-order approximations (Figure 3.10). We do this by setting $\alpha_I = 0$, which is equivalent to using the standard pairwise approximation for triples with infected central individuals. This is in part justified by the fact that values of α_I are typically much smaller in magnitude

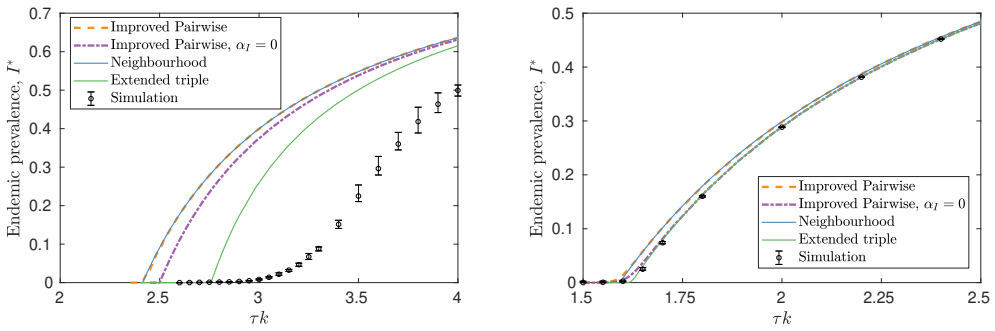

(a) $k = 2$ (b) $k = 3$

Figure 3.12: **Comparing improved pairwise approximations against higher-order approximations for $k = 2$ and $k = 3$-regular networks.** We compare endemic prevalence I^* obtained from improved pairwise model (full in orange; $\alpha_I = 0$ in purple) against neighbourhood (blue) and extended triple (green) approximations, as well as against explicit stochastic simulations (points), as we vary $\lambda = \tau k$, for (a) $k = 2$ and (b) $k = 3$-regular networks. In both (a) and (b) I^* obtained from the improved pairwise approximation is very similar to I^* obtained from the neighbourhood approximation. By assuming $\alpha_I = 0$ and $\dot{\alpha_I} = 0$, the dynamics of the improved pairwise approximation are closer to those of the extended triple approximation, and match I^* from stochastic simulations well for $k = 3$. For all models we set $\gamma = 1$. For stochastic simulations, each I^* point is calculated as the average of 150 runs, and error bars indicate 95% confidence intervals.

than α_S (Figure 3.11). This assumption further reduces the dimensionality of the system, as we have one less variable. Moreover, as α_I is typically ≤ 0, ignoring it will increase $\dot{\alpha_S}$, meaning we will generate higher values of α_S. (Positive values of α_I can only occur at very high values of τ; at such values, the disease dynamics on the k-regular network are already well approximated by the standard pairwise approximation). Indeed, comparing shapes of α_S (Figure 3.10), we see this assumption provides a closer match to the values from the extended triple. In Figure 3.12, we compare the endemic prevalence obtained using this $\alpha_I = 0$ assumption against the extended triple approximation, as well as against the improved pairwise approximation where α_I is a dynamic variable. Ignoring α_I provides an estimate closer to the extended triple approximation than accounting for α_I explicitly, which in the case of $k = 3$ matches stochastic simulations closely.

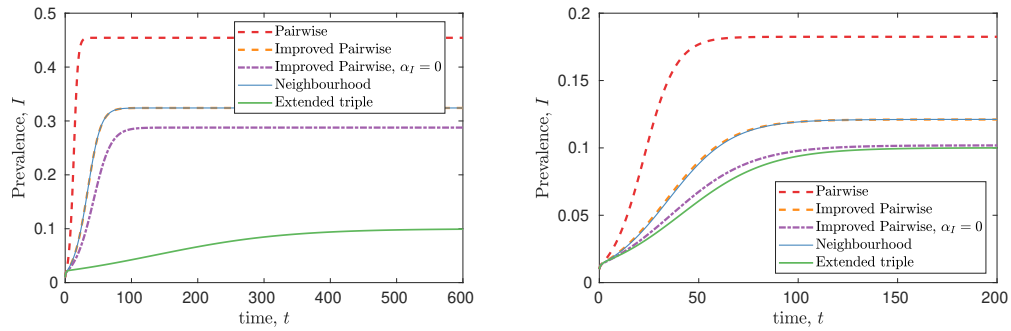

(a) $k = 2$ (b) $k = 3$

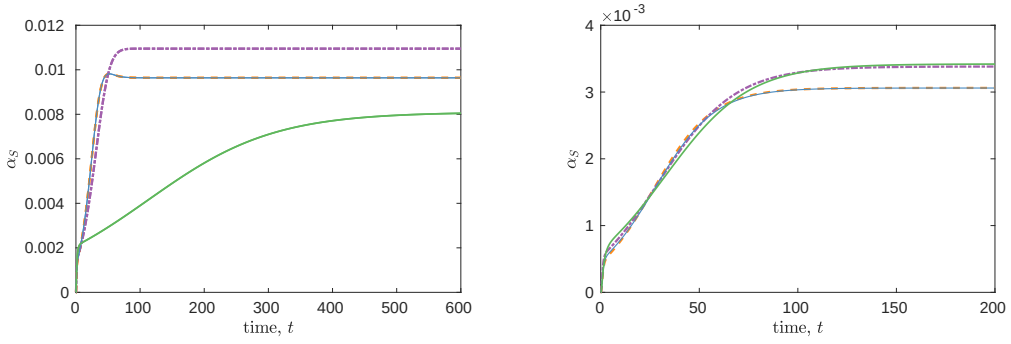

(c) $k = 2$ (d) $k = 3$

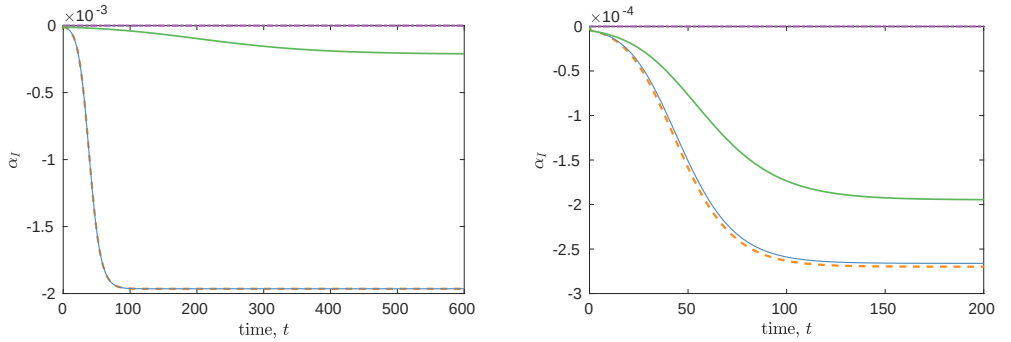

(e) $k = 2$ (f) $k = 3$

Figure 3.13: **Comparing the time-evolution of improved pairwise approximations against higher-order approximations for $k = 2$ and $k = 3$-regular networks.** (a) and (b) illustrate the performance of improved pairwise approximations compared to the higher-order neighbourhood (blue) and extended triple (green) approximations in matching prevalence through time, (c) and (d) show how α_S varies through time for each model, and (e) and (f) show how α_I varies through time for each model. We choose values τ s.t. $I^* = 0.1$ in the extended triple model ((a, c, e) $\tau = 1.4163$, (b, d, f) $\tau = 0.5744$). In both (a) and (b) there is little difference between the time-evolution of improved pairwise (orange) and neighbourhood model. In (b), while the improved pairwise model with $\dot{\alpha_I} = 0$ (purple) matches the endemic prevalence of the extended triple approximation closely, its evolution to this equilibrium state differs. In all plots we set $\gamma = 1$.

3.5.5 Exploring the time-evolution of approximate models for $k = 2$ and $k = 3$

Here, we present the time-evolution of improved pairwise models, as well as for the neighbourhood and extended triple approximation models, for $k = 2$ and $k = 3$, with the the improved pairwise approximation matching closely to that of the neighbourhood approximation models. We also see that while for $k = 3$ the improved pairwise model with $\dot{\alpha_I} = 0$ matches the endemic prevalence of the extended triple approximation closely, the same cannot be said about their time-evolution. For the parameters considered, the magnitude of α_S and α_I monotonically increases through time for all models for $k = 3$. For $k = 2$, $|\alpha_I|$ monotonically increases through time for all models; $|\alpha_S|$ increases monotonically for the extended triple approximation and improved pairwise for $\alpha_I = 0$, but $|\alpha_S|$ reaches a maximum value before slightly decreasing to its steady state value for the extended triple approximation and for the improved pairwise approximation with $\alpha_I = 0$.

3.6 Discussion

Whenever detailed information on underlying network structure is available, detailed stochastic simulation of an epidemic on a network is always the 'gold standard' for any real-world application. In the absence of such information, moment-closure approximation methods for the spread of infections promise relatively simple models that allow us to understand the effect of network structure on the dynamics of an epidemic. The success of such a method, however, depends upon understanding the errors introduced by moment-closure approximations, and upon refinements that minimise such errors. While this approach has been successfully applied to diseases with SIR-dynamics, the dynamic build-up of correlations between distant individuals for diseases with SIS-dynamics means success for infections with this

natural history has been more limited. However, as the dynamics of most STIs can be well approximated by the SIS-paradigm, and given the importance of network structure in this case, further research into this area is paramount. Indeed, there is already a considerable body of literature concerning moment-closure approximations for SIS-dynamics [Taylor et al., 2012; Taylor and Kiss, 2014; Keeling et al., 2016; House et al., 2009; Simon and Kiss, 2016], as well as other network approaches to diseases of this type [Floyd et al., 2012; Lee et al., 2013; Wilkinson and Sharkey, 2013], demonstrating this as an active research area.

This study improves upon the standard pairwise approximation by explicitly tracking the errors between the 'true' value of triples and their estimate from the standard pairwise approximation. We show that these errors are fully described by the quantity α_S for triples with susceptible central individuals, and by the quantity α_I for triples with infected central individuals. By tracking the time-evolution of these error terms, we improve upon the standard pairwise approximation by incorporating these terms into the modelling framework. For the isolated open triple (just three individuals connected in a line), both $\dot{\alpha_S}$ and $\dot{\alpha_I}$ are exactly described as functions of $[S_x S_c], [I_x S_c], \alpha_S$ and α_I; hence, in this case, the improved pairwise model is itself exact. For k-regular networks, $\dot{\alpha_S}$ and $\dot{\alpha_I}$ depend upon order-four structures. However, by approximating the prevalence of these structures via higher order moment-closures, we obtain expressions for $\dot{\alpha_S}$ and $\dot{\alpha_I}$ solely in terms of pairs, α_S and α_I. While such a model is not exact, explicitly modelling the time-evolution of these errors markedly improves upon the standard pairwise approximation for k-regular networks, obtaining prevalence estimates comparable both to models closed at even higher orders and to explicit stochastic simulations.

The findings of this chapter contribute towards understanding the shape and direction of errors introduced by pairwise approximations. We show that the errors between triples and their standard approximation are quantified by just two values: α_S and α_I. Interestingly, we find numerically that $\alpha_S \geq 0$ and $\alpha_I \leq 0$, which

inform us as to whether the standard pairwise approximation underestimates or overestimates the proportion of certain triples. While both bounds hold for the isolated open triple, only $\alpha_S \geq 0$ holds in general for k-regular networks. This result also appears to hold for the constituent triples of all other investigated topologies (line graphs up to length 10, star graphs with up to 10 neighbouring individuals, the extended triple with no external force of infection), while the result $\alpha_I \leq 0$ only appears to apply when central individuals in a triple have no other connections outside of the triple. We hence believe that an analytical exploration of such bounds could be fruitful, and would make an important contribution to this research area if such bounds could be proven generally. A deeper understanding of the shape, direction, and magnitude of such error terms is not only of interest to those concerned with using the improved pairwise approximation model described in this chapter, but to any researcher interested in applying the standard pairwise approximation to a network model of a disease where recovery from infection does not lead to immunity.

In this chapter, we compare approximations to the dynamics of k-regular networks closed at increasingly higher levels of complexity - from individual, to pair, to neighbourhood, to an extended neighbourhood. As we increase the dimensionality of a model, we expect to obtain more accurate results. On the other hand, models of high dimensionality are difficult to understand intuitively and are much more computationally expensive. Whether including such complexity is worthwhile depends on the task at hand. We believe that our improved pairwise approximation provides a reasonable compromise between intuition and complexity - this model is still described by a small number of ODEs, and has dynamics closely resembling those from the model closed at the level of neighbourhoods, more closely matching prevalence estimates obtained from stochastic simulations. An unexpected result is that by ignoring α_I, i.e. using the standard pairwise approximation for triples with infected central individuals, one appears to obtain a better approximation to the

true dynamics. It is important to establish if such a result holds generally, and if so why, or whether this result is a spurious convenience for k-regular networks.

The results here consider the two most ideal networks: the isolated open triple is the simplest possible network topology including three individuals, while in k-regular networks each individual has exactly k neighbours and there are no closed loops within the network. We consider these idealisations as it is in these networks that network structure is most dominant and the errors introduced by moment-closure approximations are most pronounced. But this means there is fertile ground for further exploration on both local and global scales. On a local scale, a taxonomy of the errors that occur for a variety of different small topologies, as has been done by Pellis et al. [2015b] for diseases with SIR-dynamics, would be useful contribution to understanding the impact of local moment-closures for diseases with SIS-dynamics. On a global scale, understanding whether tracking the dynamics of error terms explicitly would be worthwhile in heterogeneous networks (building upon the work of Simon and Kiss [2016]), and assessing whether the same techniques can be applied in the presence of clustering, are important next steps.

This chapter makes three assumptions common to the literature on the mathematics on epidemics on networks: first, that epidemiologically relevant contacts (the edges between vertices) are fixed throughout the epidemic and not dynamic; second, that these contacts are identical in kind, such that probability of infection for an individual from any partner of theirs is equal to any other partner; third, that individuals have exponentially distributed periods of infection (the Markovian assumption). Each of these are in some senses unrealistic: people's sexual partnerships change over time (it is a question of theoretical importance the extent to which the dynamics of epidemics on dynamic networks can by approximated by the dynamics of epidemics on static networks, which has begun to be explored [Volz and Meyers, 2007; Bansal et al., 2010]); for individuals in more than one partnership, the frequency of sexual contact will be different for each partnership, hence

the probability of transmission across partnerships will also be different; whilst periods of infection may be better modelled as having a constant duration. For SIR-dynamics, a variety of dynamic network models incorporating moment-closure approximations, or other low-dimensional ODE models have been developed [Ball and Neal, 2008; Volz, 2008]. So too are there a variety of dynamic network models for SIS-dynamics (e.g. Bauch and Rand [2000]; Leng and Keeling [2018]). Incorporating improved moment-closure approximations into such models, and exploring how the introduction of partnership formation and dissolution effects the errors introduced, are important next steps. While studies into the contribution of steady and casual partnerships to the spread of STIs has been explored [Xiridou et al., 2003; Hansson et al., 2019], heterogeneity in edge type is an underexplored topic for moment-closure approximations, even for diseases with SIR-dynamics. Assuming constant periods of infection, instead of making a Markovian assumption, can make closures exact for different network topologies in the case of SIR-dynamics [Pellis et al., 2015b]. Exploring this alternative assumption and its effect on errors α_S and α_I may prove interesting avenues of research.

3.7 Conclusion

In this chapter, we have detailed moment-closure approximations for the isolated open triple and for k-regular networks that improve upon standard pairwise approximations. We do so by accounting for the correlations in disease status between unconnected individuals within triples, through the α error terms now included. Our research highlights the importance of accounting for such correlations, and the relative simplicity of including such terms into a model. By considering a disease with SIS-dynamics on two ideal networks, our research illustrates the complexity of disease dynamics that occur in even the simplest systems, and that analytical insights remain hard to obtain for disease dynamics without immunity.

With regards to modelling the spread of STIs, it is clear that research should continue to develop more realistic and more sophisticated stochastic simulations. However, we believe that approximate methods have an important role to play, in both developing an intuitive understanding of the effect of network structure on the fate of the spread of STIs, and as a benchmark to compare such simulations against. It is in this context that improving the accuracy of such approximate methods is paramount, and it is in this context that we believe we make a valuable contribution to the literature.

Chapter 4

Concurrency of partnerships, consistency with data, and control of sexually transmitted infections

The research in this chapter has been presented in Leng and Keeling [2018].

4.1 Introduction

Controlling the spread of sexually transmitted infections (STIs) remains an important public health challenge globally. Each year, there are an estimated 357 million new infections from four common STIs: chlamydia, gonorrhoea, trichomoniasis, and syphilis [Newman et al., 2015]. Both chlamydia and gonorrhoea can lead to infertility and ectopic pregnancy [Cates Jr et al., 1990; Ankum et al., 1996], while syphilis can be fatal if untreated [Kent and Romanelli, 2008]. Further, these infections can increase the risk of transmission of another STI - the human immunodeficiency virus (HIV) [Gelmon and Piot, 1996; Cohen, 1998], which presently infects an estimated 36.7 million people globally [UNAIDS, 2017]. These common

STIs are usually treated with antibiotics. However, the increasing problem of antibiotic resistance [Cohen, 1992; Barry and Klausner, 2009] requires academics and public health professionals concerned with STIs to propose new and more effective control measures. As such, it has been suggested that the development of vaccines is required to abate the spread of many of the STIs where antibiotics are failing [Brunham and Rappuoli, 2013; Jerse et al., 2014; Cameron and Lukehart, 2014; Gottlieb et al., 2014]. For HIV, which cannot be treated by antibiotics, incidence levels globally remain high [UNAIDS, 2017], and hence much research has focussed on developing an HIV vaccine [Burton et al., 2004; rgp120 HIV Vaccine Study Group et al., 2005], albeit with limited success [Sekaly, 2008].

For one STI, human papillomavirus (HPV), a vaccine has been successfully developed and deployed [Markowitz et al., 2007]. HPV is the most common STI globally, with the majority of people being infected by the virus at some point in their lives [Koutsky, 1997]. Though most will recover with no serious health consequences, in a small proportion of cases, HPV infection (especially with strains 16 and 18) can lead to cancer later in life: principally cervical cancer [Muñoz et al., 2003] but also oropharyngeal, vulvar, anal, penile and vaginal cancers; in addition HPV (strains 6 and 11) can cause genital warts [Ljubojevic and Skerlev, 2014]. In many countries, including the UK [Jit et al., 2008] and the USA [Stokley et al., 2014], vaccination programmes targeted at young girls before the age of sexual debut have been implemented [Markowitz et al., 2012].

Due to its substantive public health impact, multiple predictive models have been developed to examine the effectiveness of vaccinating against HPV. These models range in complexity and sophistication, based on the questions they are attempting to address and the data that is available. The stochastic models developed by Kulasingam and Myers [2003], Goldie et al. [2004], and Canfell et al. [2012], while capturing individual-level behaviour in detail, do not consider population-level changes in prevalence and therefore cannot capture the impact of herd immu-

nity. In contrast, dynamic population-scale models capture this impact but require assumptions about partnership formation. For example, the model by Ribassin-Majed et al. [2014] assumed homogeneous random mixing throughout the population, while the models of Taira et al. [2004] and Barnabas et al. [2006] assumed sexual mixing patterns can be stratified between age-groups. The model by Jit et al. [2008], which provided health-economic policy advice to the UK, accounts for age, sex, risk-group and multiple strains of HPV. It has been observed previously that the differing assumptions between models for HPV control can lead to conflicting results [Van de Velde et al., 2010]. However, all such models assume implicitly that individuals have serially monogamous relationships. While this is a reasonable first approximation, it is a simplification of real-world sexual networks. In the UK, where detailed data is available, it is estimated that around 20% of sexually active adults aged 16-24 years engage in a *concurrent partnership* in a year [Johnson et al., 2001], that is, temporally overlapping sexual partnerships with two or more people. Intuitively, concurrency breaks the protective nature of a partnership, allowing an STI to enter an otherwise uninfected pairing. It is thus important to understand the extent to which the level of concurrent partnerships within a population impacts the success of vaccination efforts.

While concurrency is clearly an important feature of sexual transmission networks, and is epidemiologically important because it allows infection into otherwise closed partnerships, it is difficult to measure precisely. For example, the National Survey of Sexual Attitudes and Lifestyles (Natsal) questionnaires [Johnson et al., 2001] provide fine-scale details on sexual behaviour in the UK; for example capturing the number of sexual partners (and sexual behaviours) over multiple time scales. Such information allows for rich heterogeneous risk-structured models to be developed. In contrast, concurrency only features in limited number of questions; the third Natsal survey [Wellings and Johnson, 2013] only specifically asks about concurrency on two occasions: (i) a binary question about overlap between partners in last 5

years and (ii) a binary question about swinging couples. Other than these questions, concurrency is estimated from the dates of the last three sexual relationships. While this is likely to be the most detailed information on concurrency at the population scale, it is difficult to correlate this information with other risk factors and therefore difficult to robustly include concurrency in mathematical models. For these reasons, we test the sensitivity of predictive models for STI control by vaccination to the level of concurrency.

In this chapter, we develop three nested *pair-formation models* of STI spread. Pair-formation models, by explicitly modelling the formation and dissolution of partnerships, are particularly useful in modelling the spread of infections where the assumption of instantaneous contact is inappropriate. These dynamic models are particularly applicable to the spread of STIs, given sexual partnerships are often long lasting. Kretzschmar and Heijne [2017] provide a useful review on this approach and previous applications to modelling STIs. We begin by developing a model with no concurrency; this is a deterministic ordinary differential equation (ODE) model, where an infection with susceptible-infected-susceptible (SIS) dynamics can only be transmitted through stable sexual partnerships. We then extend this model to include casual partnerships, where single individuals can acquire infection from other single individuals who are infected without having to enter into a stable partnership. Finally, to this model we add concurrent partnerships, where those in stable partnerships can acquire infection from both single infected individuals and infected individuals in other partnerships. For all these models we also consider the addition of a protected (vaccinated) subpopulation that is immune to infection. In agreement with HPV vaccination programmes, these individuals are assumed to have been immunised before sexual debut and are also assumed to obtain life-long protection (although the data on the duration of protection offered by the vaccine is limited [De Vincenzo et al., 2014]). We use the models developed to explore the effect of concurrency on the transmission of an STI and on the critical

level of vaccination required to eliminate the infection from the population. We perform this analysis in two distinct scenarios: firstly, when the epidemiological and behavioural parameters are fixed and the level of concurrency is allowed to vary, mimicking changing patterns of sexual behaviour; and secondly, when models with and without concurrency are matched to available data, capturing the impact of model misspecification.

The effect of concurrent partnerships on the spread of STIs has been explored before: Watts and May [1992] develop a deterministic ODE model to explore the effects of concurrent partnerships on the dynamics of HIV; Kretzschmar and Morris (1996 and 1997) show that concurrent partnerships have a large impact upon the early growth rate of an epidemic through a stochastic simulation model; Bauch and Rand [2000] derive a moment closure approximation model of STI spread through a concurrent partnership network; Eames and Keeling [2004] compare their model of STI spread assuming serial monogamy against a model where individuals form short-term casual partnerships with others outside the relationship; and Leung et al. [2012] develop a dynamic partnership network model to explore the influence of concurrency. In particular, Xiridou et al. [2003, 2004] model concurrency in a similar approach to this chapter to assess the contribution of stable and casual partnerships to the spread of HIV. While all these models highlight the implications of concurrency on transmission and endemic prevalence of infection, to our knowledge, the implications that concurrency has on the control of STIs when parameters are matched to data has not been fully explored.

The model we develop is deliberately simplified, described by only a few ODEs and ignores many levels of real-world structure. For example, the formulation of our model assumes that partnerships occur via random mixing. In reality, sexual networks are highly heterogeneous, with sexual behaviours depending upon a large number of factors such as age, sex, sexual orientation, and cultural norms [Adimora and Schoenbach, 2005; Garnett et al., 1992]. Further, we do not specifically model

any particular STI; rather, we model some generic STI with SIS-dynamics. We use this generic formulation to observe the effects of concurrency on transmission and control, and hence to inform future researchers whether modelling concurrent partnerships explicitly is necessary in more sophisticated models of STI control.

4.2 The model

4.2.1 A model without concurrency

We first develop a simple model of STI transmission across partnerships without concurrency; this introduces our methodology and provides simple predictions to compare with our later more realistic model. A large number of STIs follow SIS dynamics – that is, recovering from infection does not provide immunity to an individual, but rather returns them to the susceptible population. Chlamydia [Garnett and Anderson, 1996] and gonorrhoea [Hethcote and Yorke, 1984] are generally assumed to exhibit these dynamics, although not HIV due to the lack of recovery [Anderson et al., 1986]. In addition, many of the models exploring the impact of vaccination against HPV also assume SIS-dynamics [Ribassin-Majed et al., 2014; Taira et al., 2004], although this may be an idealised view of the true behaviour [Beachler et al., 2016]. In common with these studies, we focus on infections with SIS-dynamics throughout.

We develop a deterministic ODE-model focussing on the behavioural aspects (formation and breaking of partnerships) onto which we graft the spread of infection – we label individuals by their infectious state: S for susceptible and I for infected. Single individuals, not in a partnership and represented by S or I, are assumed to form partnerships at a rate f; while sexual partnerships, represented by $[SS]$, $[SI]$ and $[II]$ break at a rate $2b$ (as each partner breaks up the partnership at a rate b). Once in a partnership, an infected partner will transmit an infection to

their susceptible partner at a rate τ. Infected individuals are assumed to recover at a rate γ, which could either represent natural recovery (as observed for HPV) or obtaining treatment. Table 4.1 describes all notation used in this chapter. We set the time scale of all parameters to be yearly, though we omit the suffix yr^{-1} throughout. We also insist that $S + I + 2([SS] + [SI] + [II]) = 1$, such that the model refers to proportions of the population.

Our model makes a number of simplifying assumptions: we assume a closed population without demography (i.e. no births or deaths), the recovery of individuals back into the susceptible class is sufficient to maintain infection in the population; we assume homogeneous mixing within the population (i.e. partnerships are formed uniformly at random) ignoring the impact of gender and sexual preference (all partnerships within the population are equally likely). These assumptions are clearly unrealistic – for example the number and pattern of sexual partners is highly heterogeneous between individuals [Johnson et al., 2001; Anderson, 1988] – however, the effects of such heterogeneities is not the focus of this study, and indeed has been studied extensively elsewhere [Garnett et al., 1992; Eames and Keeling, 2002; Gupta et al., 1989]. The simplifying assumptions we make are common to other studies exploring the effect of concurrency [Kretzschmar and Morris, 1996; Bauch and Rand, 2000] and allow us to highlight the likely impact of concurrency in a generic setting.

In our model, an individual leaves the class of susceptible individuals not in a partnership (S) if they form a partnership (which they do so at a rate f), or if any other individual not in a partnership forms a partnership with the susceptible individual (also at a rate f). Individuals enter the susceptible class from the class of infected individuals at a rate γ. Individuals enter the susceptible class from the $[SI]$ class at a rate of $2b$, as the susceptible individual will enter the S class if they break up the partnership (which they do so at a rate b) or if their infected partner breaks up the partnership (also at a rate b). Individuals enter the susceptible class

Table 4.1: **Chapter 4 table of notation.**

Term	**Meaning**
f	rate at which individuals form a stable partnership
b	rate at which individuals break up a stable partnership
τ	transmission rate across a stable partnership
γ	recovery rate
κ	rate at which single individuals form casual partnerships
K	rate at which individuals in partnerships form casual partnerships
p	probability of transmission via a casual partnership
S	susceptible individuals not in a partnership
I	infected individuals not in a partnership
V	vaccinated individuals not in a partnership
F	totality of individuals not in a partnership
$[SS]$	susceptible-susceptible partnerships
$[II]$	infected-infected partnerships
$[VV]$	vaccinated-vaccinated partnerships
$[SI]$	susceptible-infected partnerships
$[SV]$	susceptible-vaccinated partnerships
$[IV]$	infected-vaccinated partnerships
P	totality of individuals in a partnership
S_P	susceptible individuals currently in a partnership
I_P	infected individuals currently in a partnership
V_P	vaccinated individuals currently in a partnership
I_{tot}	totality of infected individuals
ν	proportion of population vaccinated
ν_C	critical level of vaccination required to eliminate the infection from the population
ρ	rate of new partnerships (including casual partnerships)
Y	individuals not in a partnership who have had a concurrent partnership
N	individuals not in a partnerships who have not had a concurrent partnership
$[YY]$	had concurrent partner - had concurrent partner partnerships
$[NN]$	no concurrent partner - no concurrent partner partnerships
$[YN]$	had concurrent partner - no concurrent partner partnerships
r	rate of vaccination
r_C	critical rate of vaccination required to eliminate the infection from the population
ω	rate of waning immunity

from the $[SS]$ class at a rate of $4b$, as either partner can break up the partnership, and both return to the susceptible class. Hence $\frac{dS}{dt}$ is given by

$$\begin{aligned}\frac{dS}{dt} &= -fS - fF\frac{S}{F} + \gamma I + 2b[SI] + 4b[SS] \\ &= -2fS + \gamma I + 2b[SI] + 4b[SS]\end{aligned} \tag{4.1}$$

Similar considerations give us the rest of the ODEs for Model 1, which are given in full below:

Model 1:

$$\frac{dS}{dt} = -2fS + \gamma I + 4b[SS] + 2b[SI] \tag{4.2}$$

$$\frac{dI}{dt} = -2fI - \gamma I + 4b[II] + 2b[SI] \tag{4.3}$$

$$\frac{d[SS]}{dt} = fS\frac{S}{S+I} - 2b[SS] + \gamma[SI] \tag{4.4}$$

$$\frac{d[SI]}{dt} = 2fS\frac{I}{S+I} - 2b[SI] - \tau[SI] - \gamma[SI] + 2\gamma[II] \tag{4.5}$$

$$\frac{d[II]}{dt} = fI\frac{I}{S+I} - 2b[II] + \tau[SI] - 2\gamma[II] \tag{4.6}$$

We note that in this simple formulation transmission only occurs within an $[SI]$ partnership. We can consider the behavioural dynamics if we sum appropriate terms to obtain the proportion of individuals who are single or in a partnership. We set $F := S+I$, denoting the proportion of individuals free to form a partnership, and $P := 2([SS] + [SI] + [II])$, denoting the proportion of individuals currently in partnerships.

$$\frac{dF}{dt} = -\frac{dP}{dt} = -2fF + 2bP \tag{4.7}$$

which has a non-trivial equilibrium at $F^* = \frac{b}{b+f}$, and $P^* = \frac{f}{b+f}$. The model developed here is similar to the deterministic model of Kretzschmar and Morris [1996], and yields the same equilibrium values for F and P. However, their model assumes a different disease dynamic - SI-dynamics as opposed to SIS-dynamics.

This is primarily because their model was focussed upon the effect of concurrency on the early growth rate of an STI.

Using the equilibrium values found for F and P, we can find the fixed points of the full system. The fixed points of the system are given by:

$$I^* = \frac{2bf\tau - (2bf\gamma + 3b\gamma^2 + 2b^2\gamma + b\gamma\tau + 2f\gamma^2 + \gamma^3)}{2f\tau(b+f)} \tag{4.8}$$

$$S^* = \frac{b}{b+f} - I^* \tag{4.9}$$

$$[SI]^* = \frac{\gamma(2b+2f+\gamma)}{2b\tau} I^* \tag{4.10}$$

$$[II]^* = \frac{\gamma\tau + 2f\tau - 2b\gamma - 2\gamma f - \gamma^2}{4b\tau} I^* \tag{4.11}$$

$$[SS]^* = \frac{f}{2(b+f)} - [SI]^* - [II]^* \tag{4.12}$$

From this, we are able to obtain the endemic prevalence of infection within the population. We denote the total prevalence as $I_{tot} := I + [SI] + 2[II]$. The non-trivial equilibrium value of I_{tot}, when it exists, is given by:

$$\begin{aligned} I^*_{tot} &= \frac{2b+2f+\gamma}{2b} I^* \\ &= \frac{(2b+2f+\gamma)(2bf\tau - (2bf\gamma + 3b\gamma^2 + 2b^2\gamma + b\gamma\tau + 2f\gamma^2 + \gamma^3))}{4bf\tau(b+f)}. \end{aligned} \tag{4.13}$$

Hence we obtain conditions for the existence of the non-trivial equilibrium, which is stable, when $I^* > 0$:

$$2bf\tau > 2bf\gamma + 3b\gamma^2 + 2b^2\gamma + b\gamma\tau + 2f\gamma^2 + \gamma^3 \tag{4.14}$$

Further, in the case where transmission is rapid (instantaneous) within a partnership, such that $[SI]$ partnerships do not exist, the expression for the endemic

prevalence simplifies to:

$$\lim_{\tau\to\infty} I^*_{tot} = \frac{(2b+2f+\gamma)(2f-\gamma)}{4f(b+f)} \tag{4.15}$$

In this limit it is clear that, the formation of new partnerships must be sufficiently rapid compared to the recovery from infection to allow persistence; in particular $\gamma < 2f$ to maintain the infection which acts as a lower bound for the persistence of the full model (Equations (4.2) to (4.6)). Figure 4.1 highlights the effects of the main parameters (γ, τ, f and b) on the endemic prevalence. As expected I^*_{tot} is a monotonic increasing function of the infectious period, the within partnership transmission rate and the rate at which single individuals form partnerships. However, the effects of breaking partnerships is more complex with infection maximised at an intermediate value of b; this is because persistence of infection requires a turnover of partnerships in order to infect new individuals, but if this is too rapid there is insufficient chance of transmission within the partnership and most individuals spend the majority of their time single.

4.2.2 Including casual partnerships

Model 1 describes a situation where individuals must enter into a stable partnership before they engage in sexual activity that could lead to disease transmission. However, for real-world populations, especially those at greater risk of contracting STIs, some sexual partnerships will be over a much shorter time-period - where the pair engage in a single instance of sexual activity, but do not form a stable partnership. We refer to such partnerships as *casual partnerships* and can include them through small additions to Model 1. Let κ denote the rate that single individuals have a casual partnership with another single individual, and let p denote the probability of transmission by a casual partnership. The equations for individuals in partnerships remains unchanged from Model 1, whereas the equations for single

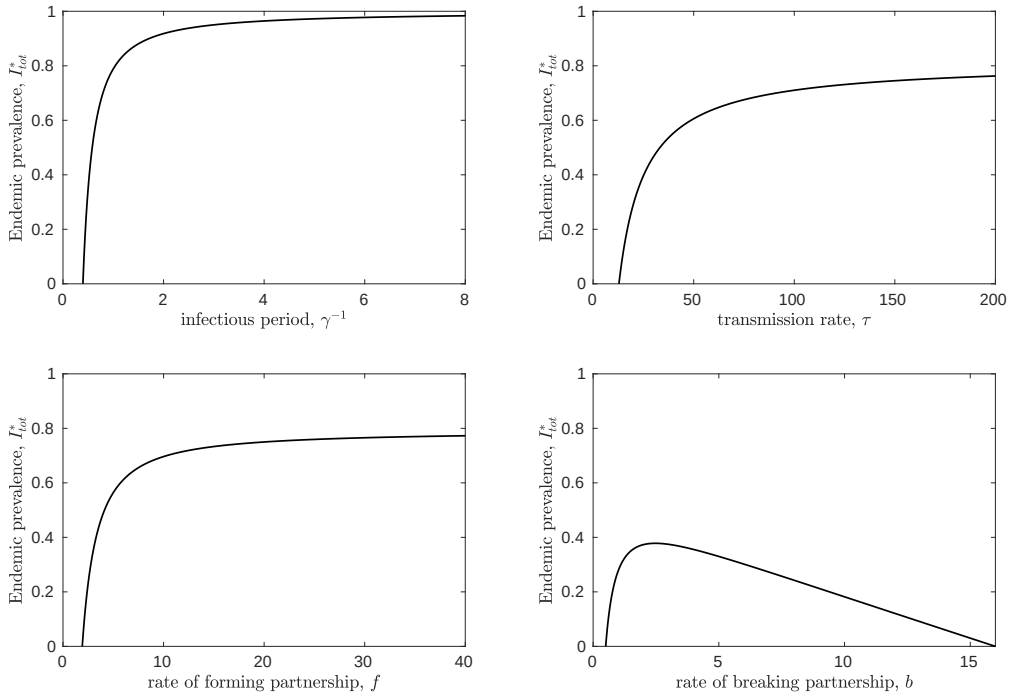

Figure 4.1: **The effect of varying parameters on endemic prevalence.** We plot the effects of varying γ, τ, f, and b against I^*_{tot} respectively. Default parameter values are $\gamma = 2$, $\tau = 22.50$, $f = 3$, $b = 1.5$, while the key parameter is varied. As we increase the infectious period γ^{-1} the total level of infection asymptotes to one, whereas for τ and f the asymptote is lower. For b we find that I^*_{tot} is maximised at intermediate values.

individuals are modified to:

Model 2:

$$\frac{dS}{dt} = -2fS + \gamma I + 4b[SS] + 2b[SI] - \kappa pS\frac{I}{F} \tag{4.16}$$

$$\frac{dI}{dt} = -2fI - \gamma I + 4b[II] + 2b[SI] + \kappa pS\frac{I}{F} \tag{4.17}$$

Although in this formulation it is only the product κp that influences the dynamics, it is useful to have a value for the probability of transmission across a casual partnership p. From Model 1 it is clear that the probability of transmission across the duration of a stable partnership is given by $\hat{p} = \frac{\tau}{2b+\gamma+\tau}$, and we assume that

this should reasonably place an upper bound on the casual transmission probability p. The precise relationship between p and $\hat{p}$ is complex and will depend on many factors including the number and type of sex acts involved. In addition, it has been observed that for some STIs, transmission occurs early on in a partnership or not at all [Peterman et al., 1988], suggesting that p should be close to $\hat{p}$. In the calculations that follow we assume that $p = \frac{1}{2}\hat{p}$, while acknowledging that this merely forms a scaling for the rate of casual partnerships κ. Once again, we can obtain the fixed points of Model 2:

$$I^* = \frac{b(2bf\tau + \kappa p(2b^2 + \gamma^2 + 3b\gamma + b\tau) - (3b\gamma^2 + 2b^2\gamma + 2\gamma^2 f + \gamma^3 + 2bf\gamma + b\gamma\tau))}{(b+f)(2bf\tau + \kappa p(2b^2 + \gamma^2 + 3b\gamma + b\tau))} \tag{4.18}$$

$$S^* = \frac{b}{b+f} - I^* \tag{4.19}$$

$$[SI]^* = \frac{\gamma f(2b + 2f + \gamma + \kappa p)}{2bf\tau + \kappa p(2b^2 + \gamma^2 + 3b\gamma + b\tau)} I^* \tag{4.20}$$

$$[II]^* = \frac{f(\hat{\kappa}(2b + \gamma + \tau) + \gamma\tau + 2f\tau - 2b\gamma - 2f\gamma - \gamma^2)}{2(2bf\tau + \hat{\kappa}(2b^2 + \gamma^2 + 3b\gamma + b\tau))} I^* \tag{4.21}$$

$$[SS]^* = \frac{f}{2(b+f)} - [SI]^* - [II]^* \tag{4.22}$$

Hence, for Model 2, I^*_{tot} is given by:

$$I^*_{tot} = \frac{f\tau(2b + 2f + \gamma) + \kappa p(2b^2 + 2bf + 3b\gamma + b\tau + 2f\gamma + f\tau + \gamma^2)}{2bf\tau + \kappa p(2b^2 + 3b\gamma + b\tau + \gamma^2)} I^* \tag{4.23}$$

Although not obvious from these equations, it is clear from the model formulation that the addition of these casual partnerships increases the prevalence of infection. The results of Model 1 are all regained by setting $\kappa = 0$.

4.2.3 Including concurrency

The models developed above (Models 1 and 2) describe populations where individuals are serially monogamous, and do not have overlapping partners: either they form a stable partnership, in which infection can be transmitted between partners, or they have a casual partnership - a one-time sexual partnership with another single individual. Here we develop two variations of the model that incorporate concurrent sexual partnerships - where an individual in a stable partnership can be involved in casual partnerships, with both single individuals and individuals in other stable partnerships. As such this breaks the protection of a partnership and can lead to greater transmission of infection. This approach is similar to that developed by Eames and Keeling [2004].

We now extend the model to allow both single individuals and those in stable partnerships to partake in casual sexual activity. We retain the parameter κ to be the rate at which any single individual takes part in a casual partnership, and include a new parameter K for the rate at which those in a stable partnership partake in an additional casual partnership. This leads to the following model:

Model 3:

$$\frac{dS}{dt} = -2fS + \gamma I + 4b[SS] + 2b[SI] - \kappa pS\hat{I} \tag{4.24}$$

$$\frac{dI}{dt} = -2fI - \gamma I + 4b[II] + 2b[SI] + \kappa pS\hat{I} \tag{4.25}$$

$$\frac{d[SS]}{dt} = fS\frac{S}{F} - 2b[SS] + \gamma[SI] - 2Kp[SS]\hat{I} \tag{4.26}$$

$$\frac{d[SI]}{dt} = 2fS\frac{I}{F} - 2b[SI] - \tau[SI] - \gamma[SI] + 2\gamma[II] + 2Kp[SS]\hat{I} - Kp[SI]\hat{I} \tag{4.27}$$

$$\frac{d[II]}{dt} = fI\frac{I}{F} - 2b[II] + \tau[SI] - 2\gamma[II] + Kp[SI]\hat{I} \tag{4.28}$$

where $\hat{I}$ refers to the level of infection for individuals engaging in such casual relationship:

$$\hat{I} = \frac{\kappa I + K(2[II] + [SI])}{\kappa F + KP}. \tag{4.29}$$

We define two variations of this model. In Model 3.1, we make the simplifying assumption that all individuals engage in casual relationships at an equal rate $K = \kappa$, which implies that $\hat{I} = I_{tot}$. In Model 3.2, we let K and κ take different values, but in all figures we set $\kappa = 2K$ capturing the intuition that singles should be more likely to partake in casual sexual activity. We note that we can regain Model 2 by setting $K = 0$.

4.2.4 Obtaining levels of concurrency

By considering the rate of formation of stable and casual partnerships, we are able to describe a system of equations to obtain the proportion of the population who are involved in concurrent partnerships for Model 3. To do so, we let Y denote individuals not in a partnership who have had a concurrent partnership, N denote individuals not in a partnership who have not had a concurrent partnership, $[YY]$ partnerships between individuals who have both had concurrent partnerships, and so on. We rescale parameters f, b, and K so that they are over the time scale of a day - i.e. they are $1/365$ of the corresponding parameters from the previous models. We assume that the proportion of individuals in partnerships is at equilibrium, and individuals begin in N classes, i.e. $N(0) = \frac{b}{f+b}, [NN](0) = \frac{f}{f+b}, Y(0) = [YN](0) = [YY](0) = 0$. The model is described as follows:

$$\frac{dN}{dt} = -2fN + 4b[NN] + 2b[YN] \tag{4.30}$$

$$\frac{dY}{dt} = -2fY + 4b[YY] + 2b[YN] \tag{4.31}$$

$$\frac{d[NN]}{dt} = fN\frac{N}{F} - 2b[NN] - 2K[NN] \tag{4.32}$$

$$\frac{d[YN]}{dt} = 2fY\frac{N}{F} - 2b[YN] + 2K[NN] - K[YN] \tag{4.33}$$

$$\frac{d[YY]}{dt} = fY\frac{Y}{F} - 2b[YY] + K[YN] \tag{4.34}$$

We obtain our estimates for K by running the ODEs for 365 days, and find the value of K that satisfies $Y+[YN]+2[YY]$ equalling the desired level of concurrency numerically.

4.2.5 Including vaccination

Now, we extend our model to include a vaccinated and hence immunised class. Here, we make the simplifying assumptions that these individuals are immunised before they enter the sexually active population and that the immunity is long-lived; hence individuals in this V-class play no active role in the epidemiological dynamics, but may limit the population spread on infection. Again, these assumptions are based on the natural history of HPV, where young girls (aged 12-13 years in the UK) are vaccinated. In Section 4.2.6 we consider a model including waning immunity.

We let V denote the vaccinated individuals not in a partnership and $[XV]$ denote a stable partnership between a vaccinated individual and someone in state-X . Further, we let $S_P = [SI] + [SV] + 2[SS]$, $I_P = [SI] + [IV] + 2[II]$, and $V_P = [SV]+[IV]+2[VV]$ - the susceptible, infected, and vaccinated individuals currently in a partnership. Assuming that a proportion ν of the population is vaccinated

initially, we amend Model 3 to include vaccination as follows:

$$\frac{dS}{dt} = -2fS + \gamma I + 2bS_P - \kappa pS\hat{I} \tag{4.35}$$
$$\frac{dI}{dt} = -2fI - \gamma I + 2bI_P + \kappa pS\hat{I} \tag{4.36}$$
$$\frac{dV}{dt} = -2fV + 2bV_P \tag{4.37}$$
$$\frac{d[SS]}{dt} = fS\frac{S}{F} - 2b[SS] + \gamma[SI] - 2Kp[SS]\hat{I} \tag{4.38}$$
$$\frac{d[SI]}{dt} = 2fS\frac{I}{F} - 2b[SI] - \tau[SI] - \gamma[SI] + 2\gamma[II] + Kp(2[SS] - [SI])\hat{I} \tag{4.39}$$
$$\frac{d[II]}{dt} = fI\frac{I}{F} - 2b[II] + \tau[SI] - 2\gamma[II] + Kp[SI]\hat{I} \tag{4.40}$$
$$\frac{d[VV]}{dt} = fV\frac{V}{F} - 2b[VV] \tag{4.41}$$
$$\frac{d[SV]}{dt} = 2fS\frac{V}{F} - 2b[SV] + \gamma[IV] - Kp[SV]\hat{I} \tag{4.42}$$
$$\frac{d[IV]}{dt} = 2fI\frac{V}{F} - 2b[IV] - \gamma[IV] + Kp[SV]\hat{I} \tag{4.43}$$

where now $\hat{I} = \frac{\kappa I + KI_P}{\kappa F + KP}$, $F = S + I + V$, and $P = 2([SS] + [SI] + [II] + [VV] + [SV] + [IV])$. We obtain the same differential equations for F and P as before. If we set $K = \kappa$, we obtain an analogue for Model 3.1 with vaccination, while analogues for Model 1 and Model 2 are recovered by setting $\kappa = K = 0$ or $K = 0$ respectively. With no vaccination, the infection remains endemic; when a large enough proportion of the population is vaccinated, the infection cannot persist - we refer to the smallest such proportion as the critical level of vaccination, denoted ν_C. We explain how ν_C is determined in Section 4.2.7.

4.2.6 Including waning immunity

In our main analyses, we consider the case of vaccination that confers lifelong immunity to an infection. In reality, protection against infection offered by vaccination often wanes over time. Previous HPV studies have shown that the duration of vaccine protection impacts the effectiveness of vaccination [Van de Velde et al., 2010].

To understand the impact that waning immunity has on our results, we developed a vaccination model for Model 3 that incorporates waning immunity.

We now vaccinate susceptible individuals at a constant rate r, and allow the vaccine to wane at a constant rate ω. This amended model is given by:

$$\frac{dS}{dt} = -2fS + \gamma I + 2bS_P - \kappa pS\hat{I} - rS + \omega V \tag{4.44}$$

$$\frac{dI}{dt} = -2fI - \gamma I + 2bI_P + \kappa pS\hat{I} \tag{4.45}$$

$$\frac{dV}{dt} = -2fV + 2bV_P + rS - \omega V \tag{4.46}$$

$$\frac{d[SS]}{dt} = fS\frac{S}{F} - 2b[SS] + \gamma[SI] - 2Kp[SS]\hat{I} - 2r[SS] + \omega[SV] \tag{4.47}$$

$$\frac{d[SI]}{dt} = 2fS\frac{I}{F} - 2b[SI] - \tau[SI] - \gamma[SI] + 2\gamma[II] + Kp(2[SS] - [SI])\hat{I} - r[SI] + \omega[IV] \tag{4.48}$$

$$\frac{d[II]}{dt} = fI\frac{I}{F} - 2b[II] + \tau[SI] - 2\gamma[II] + Kp[SI]\hat{I} \tag{4.49}$$

$$\frac{d[VV]}{dt} = fV\frac{V}{F} - 2b[VV] + r[SV] - 2\omega[VV] \tag{4.50}$$

$$\frac{d[SV]}{dt} = 2fS\frac{V}{F} - 2b[SV] + \gamma[IV] - Kp[SV]\hat{I} + 2r[SS] - \omega[SV] - r[SV] + 2\omega[VV] \tag{4.51}$$

$$\frac{d[IV]}{dt} = 2fI\frac{V}{F} - 2b[IV] - \gamma[IV] + Kp[SV]\hat{I} + r[SI] - \omega[IV] \tag{4.52}$$

We then determine the value of r required to eliminate the infection, r_C, by procedure outlined in Section 4.2.7. The endemic proportion of the population vaccinated is given by $\frac{r}{r+\omega}$, and so the critical level of vaccination is given by $\nu_C = \frac{r_C}{r_C+\omega}$.

4.2.7 Finding the critical level of vaccination

To determine the critical level of vaccination, we consider the stability of the disease free equilibrium. At this equilibrium, there is random mixing between susceptible and vaccinated individuals, so if we vaccinate ν of the population, the fixed points are given by $S^* = (1-\nu)F^*$, $V^* = \nu F^*$, $[SS]^* = (1-\nu)^2 P^*/2$, $[SV]^* = \nu(1-\nu)P^*$, $[VV]^* = \nu^2 P^*/2$, $I^* = [SI]^* = [II]^* = [IV]^* = 0$, where $F^* = \frac{b}{b+f}$, $P^* = \frac{f}{b+f}$. We then consider the Jacobian of the system evaluated at this equilibrium. The stability of the equilibrium is ensured given the real parts of all eigenvalues of the Jacobian are less than zero [Kretzschmar et al., 1994], thus varying ν we numerically determine when the largest real part of the Jacobian's eigenvalues is 0 to find the critical level of vaccination.

Note, we do not have to consider the Jacobian of the full system, only of the states including an infected individual. If we let $f_I = \frac{dI}{dt}$, and so on, the Jacobian is given by:

$$J = \begin{pmatrix} \frac{\partial f_I}{\partial I} & \frac{\partial f_I}{\partial [SI]} & \frac{\partial f_I}{\partial [II]} & \frac{\partial f_I}{\partial [IV]} \\ \frac{\partial f_{[SI]}}{\partial I} & \frac{\partial f_{[SI]}}{\partial [SI]} & \frac{\partial f_{[SI]}}{\partial [II]} & \frac{\partial f_{[SI]}}{\partial [IV]} \\ \frac{\partial f_{[II]}}{\partial I} & \frac{\partial f_{[II]}}{\partial [SI]} & \frac{\partial f_{[II]}}{\partial [II]} & \frac{\partial f_{[II]}}{\partial [IV]} \\ \frac{\partial f_{[IV]}}{\partial I} & \frac{\partial f_{[IV]}}{\partial [SI]} & \frac{\partial f_{[IV]}}{\partial [II]} & \frac{\partial f_{[IV]}}{\partial [IV]} \end{pmatrix}$$

Assuming no waning immunity, evaluated at the disease-free equilibrium, and letting $c = \frac{p}{\kappa F + KP}$, we obtain:

$$J = \begin{pmatrix} \kappa^2 c S^* - 2f - \gamma & \kappa K c S^* + 2b & 2(\kappa K c S^* + 2b) & \kappa K c S^* + 2b \\ 2\kappa K c [SS]^* + 2f(1-\nu) & 2K^2 c [SS]^* - 2b - \tau - \gamma & 2(2K^2 c [SS]^* + \gamma) & 2K^2 c [SS]^* \\ 0 & \tau & -2(b+\gamma) & 0 \\ \kappa K c [SV]^* + 2f\nu & K^2 c [SV]^* & 2K^2 c [SV]^* & K^2 c [SV]^* - 2b - \gamma \end{pmatrix}$$

Assuming that immunity can wane, we obtain:

$$J = \begin{pmatrix} \kappa^2 cS^* - 2f - \gamma & \kappa K c S^* + 2b & 2(\kappa K c S^* + 2b) & \kappa K c S^* + 2b \\ 2\kappa K c[SS]^* + 2f(1-\nu) & 2K^2 c[SS]^* - 2b - \tau - \gamma - r & 2(2K^2 c[SS]^* + \gamma) & 2K^2 c[SS]^* + \omega \\ 0 & \tau & -2(b+\gamma) & 0 \\ \kappa K c[SV]^* + 2f\nu & K^2 c[SV]^* & 2K^2 c[SV]^* + r & K^2 c[SV]^* - 2b - \gamma - \omega \end{pmatrix}$$

4.3 Results

4.3.1 Parameter inference

Our aim has been to develop a generic model of STI transmission and control by immunisation, rather than to model the specific details of any single infection. However, despite this generic approach, it is still important that we use parameters that reflect the general behavioural dynamics of human populations and the general epidemiology that is comparable with STIs. We do this by utilising data from surveys of sexual behaviour and estimates of HPV prevalence in England. We acknowledge that our simplified model cannot capture the complex heterogeneities of the true sexual network; for example, the rates of partnership, break-ups, and concurrent partnerships are not fixed, but rather are culturally situated social conventions [Adimora and Schoenbach, 2005], which change over time [Haavio-Mannila, 2001]. However, we inform our default parameter choices from available real-world data.

The parameters determining partnership dynamics (f, b, κ and K) are estimated from data contained within the National Survey of Sexual Attitudes and Lifestyles conducted in 2000 (Natsal-2) [Johnson et al., 2001] and the US National Longi-

tudinal Student of Adolescent Health (AddHealth) [Scott et al., 2011], focussing on the sexual behaviours of young adults (aged 16-24 years from Natsal-2, 18-25 years from AddHealth). We choose this group as they have, in general, a higher rate of sexual partnerships, are less likely to be in very long-term monogamous relationships, and report higher levels of concurrency [Johnson et al., 2001].

Males aged 16-24 years report an average of 1.45 new partnerships a year, while for females the average is 0.75. From this we assume an individual will average one new partnership a year. At equilibrium, the instantaneous rate of new partnership acquisition can be calculated: for Model 1 is given by $F^* f = \frac{fb}{b+f}$, while for Model 3.2 this becomes $F^* f + F^* \kappa + (1 - F^*)K$.

From AddHealth, we find that 67% of 18-25 year olds are in an exclusive relationship. This gives us $F^* \approx 1/3 \Rightarrow f = 2b$. We use this US data source as no comparable question is asked in the Natsal-2 for the UK. For Model 1, this relationship data together with the partnership information allows us to make the approximation that $f = 3$ and $b = 1.5$, as $f = 2b$, $\frac{fb}{b+f} = 1 \Rightarrow f = 3, b = 3/2$. We set these as our default values for f and b for all models.

Natsal-2 reports that, of individuals who have had a sexual partnership in the last year, 20.8% of males and 15.2% of females aged 16-24 years report to be involved in at least one concurrent partnership within the previous year. From this we take our default level of concurrency to be 20%. We estimate our values of κ and K by reformulating our infection models to simply capture whether or not individual have been involved in a concurrent partnership, and assess the level of concurrency after 1 year. This gives us $K = 0.335$ for Models 3.1 and 3.2 (with $\kappa = K$ and $\kappa = 2K$ respectively). Given this definitive value for K we introduced two parameter variations for Model 2: in Model 2.1 we set $\kappa = 0.335$ as above, such that single individuals partake in the same level of casual partnerships in both Model 2.1 and Model 3.1; in Model 2.2 we set $\kappa = 0.335/F^* = 1.005$, which is three

times as high, such that there are the same level of casual partnerships across the entire population in both Model 2.2 and Model 3.1. We note that keeping f and b constant, whilst adding in casual and concurrent partnerships, increases the overall rate of new partnerships: later we consider controlling for this.

We assume on average that within half a year of contracting the virus an individual will recover, i.e. we set $\gamma = 2$. We inform our default transmission rate τ by considering data on the prevalence of HPV in women aged 16-24 years in the UK prior to the introduction of the mass vaccination campaigns against the STI. Howell-Jones et al. [2012] report the prevalence of high-risk HPV substrains to be 35% for females of this age-group, which we set as our default endemic prevalence. For Models 1 and 2 we can derive a value of τ satisfying $I^*_{tot} = 0.35$ analytically - for Models 3.1 and 3.2 we obtain the appropriate value of τ numerically.

4.3.2 Comparing models with fixed behavioural and epidemiological parameters

First, we compare models when behavioural and epidemiological parameters are fixed, and allow the rate of casual partnerships to vary. For models that include casual partnerships (all but Model 1) we find an increasing non-linear relationship between the rate of casual partnerships and the total prevalence of infection in the population; unsurprisingly increasing this rate also leads to increasing prevalence. Allowing those in stable partnerships to partake in casual partnerships, hence introducing concurrency to the population, has the greatest impact upon the prevalence of infection as it breaks the protection afforded by uninfected partnerships; we observe that, other things being equal, the introduction of concurrency increases endemic prevalence (c.f. Model 2.2 and Model 3.1, where the total level of casual partnerships is equal between models).

Accordingly, the critical level of vaccination, ν_C, required to eliminate the disease

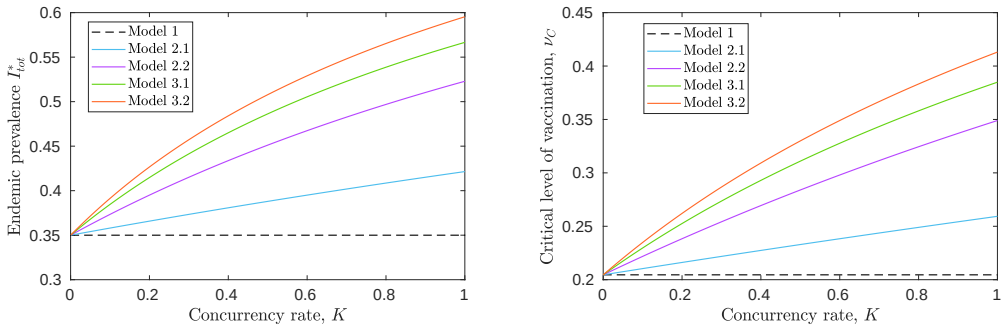

(a) (b)

Figure 4.2: **Comparing endemic prevalence and critical levels of vaccination across models.** In all models we maintain the same epidemiological and behavioural parameters while modifying the levels of concurrency (K). Model 1 does not allow for concurrency, so the endemic prevalence remains constant. In Model 2.1 (blue) and Model 3.1 (green), we insist that $\kappa = K$, while for Model 2.2 (purple) we set $\kappa = 3K$ and for Model 3.2 (orange) we set $\kappa = 2K$. In (a), we see the addition of casual partnerships increases endemic prevalence, and allowing individuals in stable partnerships to engage in casual sexual activity has a greater impact on endemic prevalence than allowing only individuals to engage in casual partnerships, even when the total rate of such partnerships remains equal (c.f. Model 2.2 and Model 3.1). In (b) we consider how this translates into the critical level of vaccination ν_C required to eradicate infection. ($f = 3$, $b = 1.5$, $\gamma = 2$, $\tau = 22.50$, $\Rightarrow\ p = 0.45$.)

from the population too has an increasing non-linear relationship between the rate of casual partnerships. With fixed parameters, the addition of concurrency can have a large impact upon ν_C: in the absence of casual partnerships (Model 1) only 22.45% of the population need to be protected by the vaccine to eliminate the disease, while at $K = 1$ ν_C is as high as 42.46% (Model 3.2).

4.3.3 Comparing models for a fixed endemic prevalence

In practice, we rarely have estimates of the transmission rate τ *a priori* which can be fed into our model. Rather, we generally need to estimate our value of τ to match the observed level of infection within the population. We can compare the models,

and hence different levels of concurrency, by altering τ and fixing I^*_{tot} (Figure 4.3). As expected, higher prevalences require higher levels of transmission, and this is non-linear due to the saturating nature of the dynamics. We also observe that the introduction of casual partnerships (going from Model 1 to Model 3.2) lowers slightly the transmission rate required to satisfy a given level of infection. Thus for a prevalence of 35%, which mimics reported levels of HPV, the fitted transmission rate drops from $\tau = 22.50$ to $\tau = 17.03$.

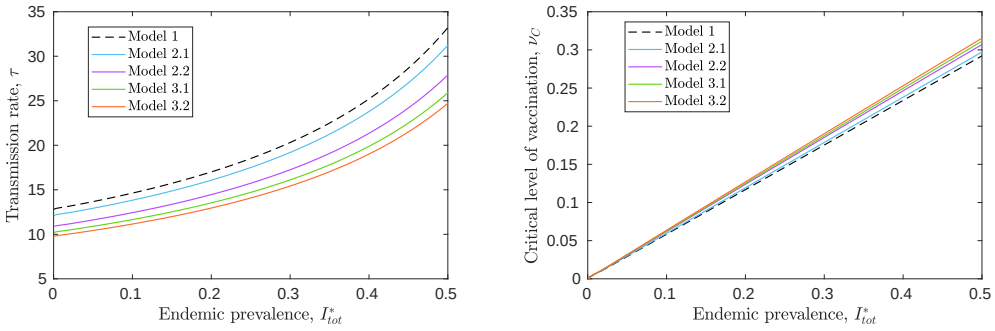

(a) (b)

Figure 4.3: **Impact of constraining all models to have the same endemic prevalence.** All models have their transmission rate τ set such that they reproduce the same prevalence of infection at equilibrium. In (a) we see that the models with less concurrency require a higher transmission rate to achieve the same endemic prevalence. In (b) we consider how this translates into the critical level of vaccination ν_C required to eradicate infection. (For all models we set $f = 3$, $b = 3/2$ and $\gamma = 2$; Model 2.1 $\kappa = 0.335$, Model 2.2 $\kappa = 1.005$, Model 3.1 $\kappa = K = 0.335$; and Model 3.2 $\kappa = 2K = 0.670$.)

We can now use these fitted values of τ to determine for each model ν_C, the critical level of vaccination required to eliminate infection. We find that when matching to the same endemic prevalence, the impact of model formulation is limited. We still find a ranked order of models (Model 1, Model 2.1, Model 2.2, Model 3.1, Model 3.2), with Model 3.2 needing a higher proportion of the population to be immunised in order to eliminate infection, but the differences between the models is minimal. At a prevalence of 35%, the critical proportions of the population that need to be protected by the vaccine range from 22.45% to 23.93%.

4.3.4 Controlling for the rate of new partnerships

As a further step to ensure agreement between models and data, we can aim to match both behavioural and demographic data. We therefore now insist that all models have both the same endemic prevalence of infection (I^*_{tot}) and the same total rate of new partnerships (both long-term and casual), which we denote as ρ. In Figure 4.3, as we move from Model 1 to Model 3.2, the introduction of more casual partnerships inevitably leads to an increase in the expected number of sexual partners of each individual.

For Model 3.2 (which is the most general of the models with all other models nested within), we find that the rate of new partnerships, ρ, is:

$$\rho = F^* f + F^* \kappa + (1 - F^*)K \qquad \Rightarrow \quad f = \frac{\rho - K}{F^*} - (\kappa - K) \tag{4.53}$$

Hence, we can determine the parameter f such that the expected number of new sexual partners per year agrees with reported values (here assumed to be approximately one per year). As previously described, to obtain $F^* = 1/3$ we require $f = 2b$. We then solve for the appropriate mix of K and κ (as prescribed by the model) and the parameter f, to obtain both 20% of individuals having a concurrent partnership within a year and to achieve a given partnership rate from Equation (4.53).

When we additionally control for the rate of new partnerships (ρ), a larger transmission rate is required to satisfy a given endemic prevalence for all versions of Models 2 and 3 (first panel of Figure 4.4). This is due to the corresponding lower rates of f and b for models with more casual partnerships, as these additional casual partnerships also contribute to ρ. In such models, individuals in $[SS]$ partnerships are offered a longer duration of relative isolation (they can only be infected through casual partnerships) due to the lower rate of stable partnership break-up. Similarly,

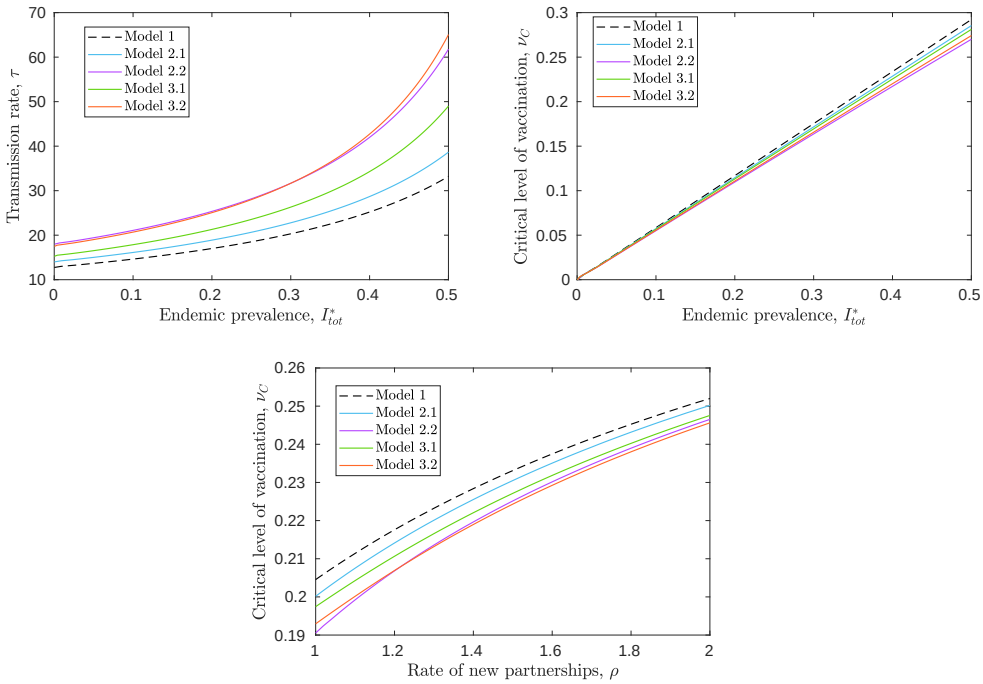

Figure 4.4: **Controlling τ for a fixed endemic prevalence and f to fix the rate of new partnerships.** In the top panel, for each model we choose values of f, b, K and κ such that $\rho = 1$, $F^* = 1/3$, and where appropriate 20% of the population will have a concurrent partnership in a year. We then find τ that satisfies the endemic prevalence, which is varied. In the bottom panel, a similar approach is taken but I^*_{tot} is fixed at 35%, and the total rate of new partnerships per year ρ is varied.

individuals in $[II]$ partnerships are retained in the stable partnership for longer and hence are less infectious to the population. This effect is sufficiently strong to change the ordering of transmission rates compared to the first panel of Figure 4.3; Model 1 now requires the lowest transmission rate, while the transmission rates needed for Model 2.2 and Model 3.2 are largest and comparable.

As we control for the rate of new partnerships, adding concurrency only has negligible impact upon the critical level of vaccination ν_C; moreover for higher endemic prevalences, Model 1 requires the largest ν_C while Model 2.2 requires the lowest. If we instead fix the prevalence $I^*_{tot} = 35\%$, and vary the rate of new partnerships

ρ, the differences between the five models is more clear, although the absolute differences in the required critical vaccination level are minimal. Larger partnership rates require slightly larger vaccination levels, but given that we are maintaining a constant infection prevalence even doubling the partnership rate invokes a relatively small change in ν_C. We consistently find that Model 1 (without any casual partnerships) requires the greatest level of vaccination, while either Model 2.2 or 3.2 requires the least depending on parameter values.

4.3.5 Impact of waning immunity

In the above figures, we have assumed that the immunity conferred via vaccination is lifelong. Here, we consider the impact of waning immunity, and the extent to which the duration of vaccine protection impacts previous results, i.e. whether for shorter durations of vaccine protection it still holds true that the addition concurrency has minimal impact upon the critical level of vaccination.

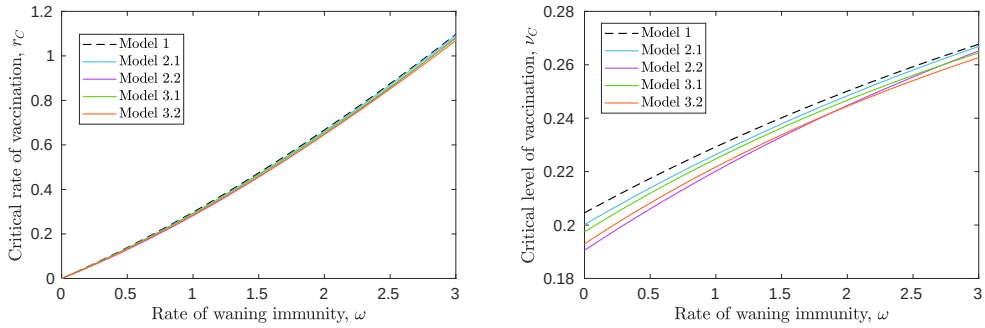

Figure 4.5: **Impact of including waning immunity.** For each model we choose values of f, b, K and κ such that $\rho = 1$, $F^* = 1/3$, and where appropriate 20% of the population will have a concurrent partnership in a year. We set τ such that $I^*_{tot} = 0.35$ for each model, and vary the rate of waning. immunity ω. In the left panel, we consider the critical rate of vaccination, while in the right panel we consider the critical level of vaccination, given by $\nu_C = \frac{r_C}{r_C+\omega}$.

As we increase the rate of waning ω, and hence decrease the duration of vaccine protection, the critical level of vaccination increases for all models. Importantly

however, we see that for any given value of ω, the values of obtained for ν_C remain within a small range between models; indeed, as we increase ω, this range decreases.

4.4 Discussion

Models for the spread of STIs play a critical role in public-health planning, allowing policy-makers to assess the impact of control measures. Of these, the control of HIV by increased behavioural awareness [Coates et al., 2008] or through antiretroviral drugs [Granich et al., 2009], and HPV by vaccination, are amongst the most studied. One factor that arises from many of these models is that increases in concurrency (extra sexual partnerships in addition to stable sexual relationships), while all other factors remain constant, lead to greater prevalence of infection and more difficulty in controlling the infection. This is intuitive as an increase in concurrency both increases the number of sexual partnerships in the population and breaks the protection otherwise afforded to stable partnerships. This might suggest that models which include concurrency, compared to those that do not, will also predict greater prevalence and the need for greater control. However, this neglects the fact that these models should first be matched to available data, before the implications of control are assessed. Here we have developed a range of models that include various amounts of casual partnerships and consider the behaviour as we match the model to both epidemiological and behavioural data.

If we assume a fixed transmission rate, then our models echo previous findings that concurrent partnerships have a significant impact on the effectiveness and appropriateness of interventions; the addition of concurrency to such models increases markedly the endemic prevalence of infection, and hence the critical level of vaccination required to eliminate the infection. This captures what we would expect to happen if the level of concurrency (and the number of short casual relationships)

increases in a population while all other aspects remains unperturbed.

To assess the importance of robustly measuring and capturing concurrency within a predictive model, we take an alternative approach. This is of public-health importance given the potential reluctance of individuals to disclose this behaviour and the difficulty of assessing how concurrency may correlate with other risk factors. To address this, we compared models with and without concurrency, that are matched to the same endemic prevalence of infection. When we adjust the transmission rate τ to obtain the same endemic prevalence for each model (as would occur if we were matching models to observations), the inclusion of concurrent partnerships has a much more limited impact upon vaccination. Further, when we also control for the total rate of new partnerships (including stable and casual partnerships), the difference between estimates of the critical level of vaccination is further reduced and the rank-order of the models is reversed: the model without concurrency requires the greatest level of vaccination to control the infection. Given that models without concurrent partnerships are in general simpler – in our examples (Models 1 and 2) are analytically tractable – our results would question the need for the additional complexity of modelling concurrency to achieve accurate predictions for public-health policy regarding vaccination.

This very weak dependence on the level of concurrency can be intuitively explained as follows. In the simple (one-dimensional) SIS model, that does not explicitly include partnerships, the critical vaccination level is equal to the endemic prevalence of infection. This precise relationship is only broken in models that capture partnerships due to the correlations that quickly develop between the status of individuals in partnerships due to transmission within the partnership. This simply introduces a linear scaling between prevalence and critical vaccination levels. The action of concurrent partnerships is effectively random across the population, so does not impact on the relationship between prevalence and critical vaccination levels. The analysis in this chapter has focused on vaccination, and it remains to

be seen whether the inclusion of concurrency has an impact on the success of more targeted interventions that depend more closely on the network structure of a population, such as contact tracing. Such interventions require a different modelling approach, and are considered in the next chapter.

Our models, and the data that underpin them, take a highly simplified form which is necessary to elucidate the behaviour. In our models we do not differentiate between sexes – individuals are equally likely to form a partnership with any other. This simplification not only ignores the obvious point that most partnerships are heterosexual, but also ignores parameter differences between sexes. In the UK, reported rates of new partnership and rates of concurrency are higher amongst men [Johnson et al., 2001] (although this may represent reporting bias), while in cultures where polygyny is the prevailing social norm, this difference is even more pronounced [Reniers and Tfaily, 2012]. Further, for a large number of STIs there can be asymmetric transmission between sexes [Hethcote and Yorke, 1984; Nicolosi et al., 1994; Nyitray et al., 2013]. Such factors are important to consider in an applied context, given that vaccination campaigns such as those against HPV are generally targeted to young girls.

Our model describes a situation where there is a simple asymmetry between the types of partnerships. Individuals are either in long-term stable partnerships, or they are involved in casual one-time partnerships akin to a single sexual encounter with another individual. Hence for our model when there are concurrent partnerships they are always of the form one stable partnership and one casual partnership. Our models do not describe a situation where an individual can be engaged in multiple stable sexual partnerships; nor do they capture the spectrum of partnership durations. When considering the appropriateness of this model it is therefore important to consider the appropriateness of this assumption. This simple asymmetry may not hold across all cultures - in some sub-Saharan countries (a focal point of the global HIV-epidemic) the reported proportion of individuals engaged in multi-

ple long-term partnerships is significant (reported to be as high as 55% in Lesotho, Southern Africa) [Carael, 1995]. Thus our models may be a closer approximation to the behaviour in UK and western Europe, although we again expect a spectrum of behaviours. Other models of concurrency that allow for individuals in multiple stable partnerships have been developed: of note for their analytic tractability are the models created by Leung et al. [2012] and Miller et al. [2012]. Our research could naturally be extended to such models, but carefully matching these models to data is paramount. When including multiple long-term partnerships, it may be important to consider the effect of *coital dilution* (as one engages in more sexual partnerships, they tend to have less frequent sexual contact with any one partner) on transmission parameters [Gaydosh et al., 2013].

Potentially the most substantial omission in our models is the lack of heterogeneity. Patterns of sexual partnerships are generally characterised by extreme levels of heterogeneity, such that some individuals have few lifetime partners while others have many [Anderson et al., 1986]; in addition it is likely that the rate of new partners is correlated with other factors such as the propensity to be involved in concurrent partnerships, the likelihood of being involved in higher-risk sexual activities, or lower rates of vaccine uptake. It is well understood that heterogeneities in the rate of new sexual partnerships play an important role in STI transmission and control [May and Anderson, 1987]. However, there is limited data, or theoretical studies, on the impact of the interaction between this heterogeneity and other elements of risk.

4.5 Conclusion

In summary, our simplified model highlights that the impact of casual partnerships (and hence concurrency) on the control of STIs by vaccination is limited, once the models are matched to infection prevalence and the rate of new partnerships. This

strongly suggests that we should question the need of including the complexity of concurrent partnerships in more complex models. Obviously, complex models that include a multitude of heterogeneities are vital when addressing public health problems that require accurate answers, but we should continue to question the role of complexity in these models.

Our results illustrate the role that relatively simple epidemiological models can play in understanding the importance of including network features in models for public health. While we believe our findings are generic, the inclusion of heterogeneity across multiple risk factors is an important next step, especially if greater realism is required. Understanding how this risk heterogeneity and concurrency interact is a key area of future work, and is the subject of the next chapter.

Chapter 5

Capturing partnership heterogeneity and concurrency in a dynamic heterosexual network model

5.1 Introduction

In Chapter 4, our results from a deterministic pair-formation model suggest that explicitly including concurrency may not be necessary to reliably forecast the impact of vaccination against sexually transmitted infections (STIs). However, this approach can only tell us so much. Our pair-formation model does not include many of the heterogeneities that exist within real-world sexual networks, nor does it account for the stochasticity of the dynamics of epidemics, nor does it consider the uncertainty in the underlying data. Moreover, state-based models are unsuitable for assessing the impact of control measures that require knowledge at an individual-level, such as contact tracing. In lieu of a vaccine, contact tracing is a key control measure against the many STIs [Clarke, 1998; FitzGerald et al., 1998; Golden et al., 2003]. In order to assess the impact heterogeneities have, and to assess a wider

range of control measures, in this chapter we take a different approach, modelling a dynamic heterosexual partnership network explicitly by simulating both the formation and dissolution of partnerships in a heterosexual population and fitting this simulation model to available behavioural data on heterosexual networks.

In order to obtain forecasts of the spread and control of STIs, models must capture heterogeneities in partnership behaviour that have a substantive impact on the dynamics of epidemics. While the impact of heterogeneity in the rate of sexual partnerships [Garnett et al., 1992; Eames and Keeling, 2002; Rozhnova et al., 2016], the impact of concurrency [Watts and May, 1992; Morris and Kretzschmar, 1997; Leng and Keeling, 2018], and the impact of heterosexual transmission [Gomez-Gardenes et al., 2008] are well documented, the impact of such heterogeneities in models matched to prevalence data, and the impact these have in conjunction with one another, is still an area relatively unexplored.

There have been many individual-based models used to forecast STI spread and control that capture some aspects of partnership behaviour. Inevitably, however, such models must make some assumptions. For example, the model of Datta et al. [2018] captures the observed degree distribution of partnerships across the population, but assumes that individuals are serially monogamous. At the other extreme, the models of Garnett and Anderson [1994] and Choi et al. [2010] assume that partnerships form independently of one another. Under this assumption, the resulting level of concurrency within the modelled population is unclear. Others still assume randomly mixing populations [Barnabas et al., 2006; Smid et al., 2018], and hence do not consider concurrency explicitly. While some models have been matched to concurrency data (e.g. Jenness et al. [2017]; Goodreau et al. [2018]), this is often of the form of instantaneous concurrency data rather than yearly concurrency data. These models also are not matched to yearly degree distribution data, and have typically focussed on populations of men who have sex with men (MSM).

Recently, Whittles et al. [2019] have described methods to obtain dynamic partnership network models capable of capturing the yearly degree distribution in populations of MSM. Such distributions are typically heavy-tailed, and have been observed to approximately obey a power-law degree distribution [Schneeberger et al., 2004]. These populations have been the focus of much of the literature surrounding the control of STIs, due to the higher prevalence of certain STIs within this population. However, for some STIs such as chlamydia, there are a larger number of diagnoses within the heterosexual population, while the incidence of gonorrhoea and syphilis has seen a sustained increase in recent years within this population [Public Health England, 2019]. Of particular interest are young people, aged 16-24 years, who accounted for 49.6% of STI diagnoses in 2019 among the heterosexual population in England [Public Health England, 2019].

As well as the public health motivation in modelling STIs in heterosexual populations, such populations are interesting and challenging from a theoretical perspective. While for MSM, a dynamic network model attempting to match yearly degree distribution data must capture one distribution, a dynamic network model of heterosexual partnership networks must be capable of capturing two distinct yearly degree distributions (one for males, one for females) from one dynamical process. Compounding this issue, observed male and female degree distribution data from surveys such as the National Survey of Sexual Attitudes and Lifestyle (Natsal) are often mutually inconsistent [Mercer et al., 2013; Mitchell et al., 2019]. While dynamic partnership models of heterosexual networks that capture some heterogeneity in the number of partnerships have been designed before [Garnett and Anderson, 1994; Gray et al., 2009], these models typically assume a pre-defined number of risk classes within the population, are not fitted to observed yearly degree distributions explicitly, and do not attempt to capture observed levels of concurrency.

In this chapter, we describe a stochastic individual-based dynamic model of a heterosexual network, consisting of an arbitrary number of male and female risk groups,

that is capable of being fitted to male and female yearly degree distributions simultaneously. This simulation model is also fitted to observed levels of concurrency and observed proportions of single individuals for each sex. We compare this simulation model, matched to concurrency data, to alternative models representing the two extremes of assumptions surrounding concurrency - at one extreme, individuals are serially monogamous and there is therefore no concurrency; at the other extreme, an individual's rate of forming new partnerships is independent of their relationship status, potentially leading to high levels of concurrency. At both extremes, the yearly degree distributions and expected proportion of singles can be obtained either analytically or numerically, and the methods of doing so are described in this chapter. By fitting these models using a Markov Chain Monte Carlo (MCMC) approach, and selecting models using the Deviance Information Criterion (DIC) [Spiegelhalter et al., 2002], we compare the optimal number of risk groups for these models, and we explore other aspects of network structure, that have not been explicitly fitted to, in the three models.

Acting on this dynamic network model, we explore the impact of a disease with susceptible-infected-susceptible (SIS) dynamics, which approximates the dynamics of many bacterial STIs, [Garnett and Anderson, 1996; Yorke et al., 1978] and has been used to model the spread of human papillomavirus (HPV) [Ribassin-Majed et al., 2014], although this may be an idealisation of its true behaviour [Beachler et al., 2016]. Doing so, we compare the resulting epidemiological dynamics in each of the three scenarios. By matching models to prevalence data, we compare the impact of the control measures vaccination and contact tracing in each of the dynamic models. By doing so, we not only assess the impact such measures have, but we also compare the extent to which the three models differ, and whether models not explicitly matched to levels of concurrency lead to underestimates or overestimates of different quantities. The methods described in this chapter therefore not only provide a flexible dynamic model capable of matching observed data, but also

provide an assessment of the merits of explicitly matching models of heterosexual populations to concurrency data in a realistic setting.

5.2 Defining the network model

5.2.1 Full simulation partnership model

Here, we present a stochastic individual-based model of partnership formation and dissolution for a heterosexual population with an arbitrary number of 'risk groups' for males and females. Individuals from different risk groups form and dissolve partnerships at different rates, and hence have different risks of transmitting and contracting infection. Letting k_M denote the number of distinct male risk groups, and letting k_F the number of distinct female risk groups, single individuals form partnerships at a yearly rate of $f_{sr}, s \in \{M, F\}, r \in \{1, ..., k_s\}$. As in Chapter 4, the total rate an individual forms a new partnership depends both on their rate of partnership formation and on the rate that other individuals partner with them. The number of individuals in each risk class also varies, and is denoted by N_{sr}.

We assume the rate at which partnerships dissolve depends upon the rate at which its constituent individuals form partnerships when single, i.e. a partnership between a male from risk group x and a female from risk group y dissolves at a rate $b \times g(f_{Mx}, f_{Fy})$, where b is a positive constant, and where g is some function of f_{Mx} and f_{Fy}. We assume that individuals who form partnerships at a high rate also dissolve partnerships at a high rate, and hence we consider $g(f_{Mx}, f_{Fy}) = f_{Mx} + f_{Fy}$. Alternative functions that could be considered are $g(f_{Mx}, f_{Fy}) = max(f_{Mx}, f_{Fy}), g(f_{Mx}, f_{Fy}) = min(f_{Mx}, f_{Fy})$, and $g(f_{Mx}, f_{Fy}) = (f_{Mx} + f_{Fy})^{\alpha}$, where $0 < \alpha < 1$, and $g(f_{Mx}, f_{Fy}) = 1$, though these alternative assumptions are not explored here.

As well as allowing single individuals to form new partnerships, we allow individuals within partnerships to form additional partnerships at a reduced rate, in order to capture concurrency within the model. Specifically, we introduce the concurrency parameters $c_s, s \in \{M, F\}$, where $0 \leq c_s \leq 1$, which scale the rate individuals form additional partnerships - an individual who forms a partnership when single at a rate f_{sr} forms additional partnerships when in a relationship at a rate $c_s f_{sr}$. We assume that individuals within partnerships form additional partnerships at this rate despite the number of partnerships they are already in - that is to say, the rate at which an individual who is currently in one partnership forms new partnerships is the same as the rate at which an individual who is currently in two partnerships forms new partnerships, and so on. This assumption is made by Kretzschmar and Morris [1996] for a population with only one sex. We assume that all individuals are capable of entering into concurrent partnerships - an alternative assumption could be that only a fraction c_{sr} of the population form concurrent partnerships, but they do so at their original rate f_{sr}, similar to the assumption made by Gray et al. [2009].

When an individual forms a new partnership, the probability of choosing a particular partner is proportional to the potential partner's rate of forming new partnerships. For example, if a single male forms new partnerships at a rate f_{Mr}, the probability a female chooses that male when they form a new partnership is f_{Mr} divided by the total rate that males form new partnerships. If that male is in a relationship, they form new partnersihps at a rate $c_M f_{Mr}$, and the probability a female chooses that male when they form a new partnership is $c_M f_{Mr}$ divided by the total rate that males form new partnerships.

In this model, we assume there is no distinction between the additional (concurrent) partnerships and the original partnerships, in contrast to Chapter 4, which assumed one stable partnership and one additional (instantaneous) casual partnership. At the extreme values $c_M = c_F = 1$, the rate individuals form partnerships

is independent of their relationship status (as in the public health model described by Choi et al. [2010] and the theoretical model described by Leung et al. [2012]), while at the extreme values $c_M = c_F = 0$, individuals are serially monagamous, and the model described is an extension to the partnership model described in Chapter 4.

From this model we can obtain several outputs, which can be used for comparison with real-world data. For each sex, we can obtain both instantaneous degree distributions (the number of partnerships individuals are in at any given time) and yearly degree distributions (the number of new partnerships individuals form within a year). We can also obtain yearly concurrency data for both sexes, i.e. the proportion of individuals who have engaged in a concurrent partnership in the past year. We could also obtain the duration of finished partnerships. Each of these can be disaggregated by risk group. In this chapter, we fit models to yearly degree distributions and the instantaneous proportion of single individuals. At both $c_M = c_F = 1$ and $c_M = c_F = 0$, the expected values of these can be obtained exactly, which is described in Section 5.2.2 and Section 5.2.3 respectively. For the full simulation model ($0 < c_S < 1$), we also fit to yearly concurrency data.

The model can be simulated using a Gillespie algorithm, which simulates each event and the time of that event explicitly. Doing so renders the most faithful simulation of the underlying process, but is computationally expensive, and the time for simulations grows exponentially with population size. Alternatively, it can be simulated with a τ-leap algorithm, where time progresses in discrete steps (e.g. days) and the number of each type of event is drawn from a Poisson distribution. However, such an algorithm only provides an approximation to the underlying process, as it excludes the possibility of multiple dependent events happening within the same time-step. For example, using this algorithm, partnerships that are formed within a time-step cannot dissolve in the same time-step, and individuals cannot form an additional concurrent partnership within the same time-step. The choice

of which algorithm to use is a trade-off between efficiency and accuracy. In this chapter, we a use a τ-leap algorithm with time-steps of 0.25 days for model fitting, and use a Gillespie algorithm for obtaining results from the fitted model.

5.2.2 Special case - $c_M = c_F = 1$

Assuming that $c_M = c_F = 1$, the rate individuals form partnerships is independent of their relationship status. In this special case, both the instantaneous proportion of single individuals and yearly degree distributions can be obtained analytically.

Obtaining proportion of single individuals for $c_M = c_F = 1$

By considering partnerships between different risk groups separately, we are able to calculate analytically the expected proportion of single individuals for $c_M = c_F = 1$. Because partnership formation and dissolution happen at constant rates, the underlying process is Markovian. By aggregating together individuals from the same sex and risk class, and considering the number of partnerships they are involved in with a given risk class from the opposite sex, we can obtain continuous-time Markov processes for which the Master equations can be feasibly defined and solved. Considering an arbitrary male from risk class r who is currently in i partnerships with females from risk class q, the male forms new partnerships at a rate independent of the number of partnerships they are involved in, while the rate of losing a partnership is proportional to the number of partnerships that individual is in. In fact, this situation is described in the theoretical literature as a $M/M/\infty$ server queue [Kulkarni, 2016]. Letting N^i_{MrFq} denote the number of men from risk class r who have i partnerships with women from risk class q, the situation can be visualised by the following state-space diagram:

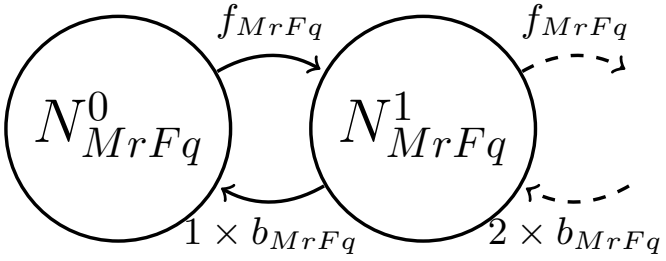

Figure 5.1: **Graphical representation of number of partnerships between males from risk class r and females from risk class q.**

Here, b_{MrFq} is given directly from our break-up function:

$$b_{MrFq} = b(f_{Mr} + f_{Fq}) \tag{5.1}$$

Considering the rate of partnership for an arbitrary male from risk class r, there are two ways a partnership could form. Either that male forms a partnership with a female from risk class q, which happens at a rate $f_{Mr}\frac{f_{Fq}N_{Fq}}{\sum_p f_{Fp}N_{Fp}}$, or a female from risk class q forms a partnership with that male, which happens at a rate $f_{Fq}N_{Fq}\frac{f_{Mr}}{\sum_p f_{Mp}N_{Fp}}$. Hence f_{MrFq} is given by:

$$f_{MrFq} = f_{Mr}f_{Fq}N_{Fq}\left(\frac{1}{\sum_p f_{Fp}N_{Fp}} + \frac{1}{\sum_p f_{Mp}N_{Mp}}\right) \tag{5.2}$$

We can obtain the expected number of males from risk class r with no partnerships with females from risk class q by solving the Master equations describing the above situation. This is achieved by considering the proportion of individuals in each state required to satisfy that the rate of exit from a particular state is equal to the rate of entry to that state, i.e. we must solve the system of equations via the principle of detailed balance:

$$(i \times b_{MrFq}) N^i_{MrFq} = f_{MrFq} N^{i-1}_{MrFq} \text{ for } i = 1, 2, ... \tag{5.3}$$

$$\iff N^i_{MrFq} = \left(\frac{f_{MrFq}}{b_{MrFq}}\right)^i \frac{1}{i!} N^0_{MrFq} \tag{5.4}$$

We can solve the above system of equations as we know that $\sum_i N^i_{MrFq} = N_{Mr}$, and so:

$$N_{Mr} = N^0_{MrFq} \sum_{i=0}^{\infty} \left(\frac{f_{MrFq}}{b_{MrFq}}\right)^i \frac{1}{i!} \tag{5.5}$$

$$\iff N^0_{MrFq} = N_{Mr} \times exp\left(-\frac{f_{MrFq}}{b_{MrFq}}\right) \tag{5.6}$$

So, the stationary distribution of number of partners for males of risk class r with females of risk class q is a Poisson distribution with mean f_{MrFq}/b_{MrFq}, multiplied by N_{Mr}. As the number of partnerships males of risk class r have with females of different risk classes are independent of one another, the stationary distribution for the number of partners for males of risk class r is a Poisson distribution with mean $\sum_q f_{MrFq}/b_{MrFq}$, and the expected number of single males from risk class r is given by:

$$N^0_{Mr} = N_{Mr} \times exp(-\sum_q \frac{f_{MrFq}}{b_{MrFq}}) \tag{5.7}$$

Finally, the expected number of single males is given by summing over all risk classes:

$$N_M^0 = \sum_r \left(N_{Mr} exp(- \sum_q \frac{f_{MrFq}}{b_{MrFq}} \right) \tag{5.8}$$

Analogously, the expected number of single females is given by:

$$N_F^0 = \sum_p \left(N_{Fp} exp(- \sum_r \frac{f_{FpMr}}{b_{FpMr}} \right) \tag{5.9}$$

The expected proportion of single males and females is then given by N_M^0/N_M and N_F^0/N_F respectively, where $N_M = \sum_r N_{Mr}$ and $N_F = \sum_q N_{Fq}$.

Obtaining yearly degree distributions for $c_M = c_F = 1$

Similarly, we can express the yearly degree distribution for males and females by summing the appropriate Poisson distributions. Considering an arbitrary male from risk class r, they enter into a partnership in two different ways. Either they themselves form a partnership, which they do so at a rate f_{Mr}, or a female forms a partnership with that individual, which occurs at a rate f'_{Mr}, where f'_{Mr} is given by:

$$f'_{Mr} = \sum_q \frac{f_{Fq} N_{Fq}}{N_{Mr}} \frac{f_{Mr} N_{Mr}}{\sum_p f_{Mp} N_{Mp}} \tag{5.10}$$

$$\iff f'_{Mr} = f_{Mr} \frac{\sum_q f_{Fq} N_{Fq}}{\sum_p f_{Mp} N_{Mp}} \tag{5.11}$$

The first fraction in Equation (5.10) is the rate of partnerships formed by females of

risk group q with any specific male from risk group r, while the second fraction is the probability of a female choosing a male from risk group r out of all possible males. As both cases (f_{Mr} and f'_{Mr}) are independent Poisson processes, the individual will enter into partnerships at a rate $f_{Mr} + f'_{Mr}$ Thus, the yearly degree distribution of males from risk group r, denoted Y_{Mr}, is given by:

$$Y_{Mr} = Pois\left(f_{Mr}\left(1 + \frac{\sum_q f_{Fq} N_{Fq}}{\sum_p f_{Mp} N_{Mp}}\right)\right) \tag{5.12}$$

The yearly degree distribution for all males, denoted Y_M, will be given by the sum of these degree distributions, relative to the size of that particular risk group, i.e.

$$Y_M = \frac{\sum_r N_{Mr} Y_{Mr}}{N_M} \tag{5.13}$$

Analogously, the yearly degree distribution for all females, Y_F, is given by:

$$Y_F = \frac{\sum_q N_{Fq} Y_{Fq}}{N_F}, \text{ where } Y_{Fq} = Pois\left(f_{Fq}\left(1 + \frac{\sum_r f_{Mr} N_{Mr}}{\sum_p f_{Fp} N_{Fp}}\right)\right) \tag{5.14}$$

Removing the free parameter

If we consider the case where there is only one risk class for both males and females, it is clear that the yearly degree distributions for men and women only depend on the sum of their rates of forming partnership, described by a Poisson distribution with mean $f_{M1} + f_{F1}$, rather than the values of the rates in and of themselves; in

other words, we are left with a free parameter. We constrain this free parameter by making the assumption that the total rate of males forming partnerships must equal the total rate of females forming partnerships, i.e. by setting:

$$\sum_r f_{Mr} N_{Mr} = \sum_q f_{Fq} N_{Fq} \tag{5.15}$$

This assumption does not impact the previous analyses, which holds for any valid parameter set. Instead, this assumption determines the value of the final parameter in a given parameter set. This constraint simplifies our expressions for $Y_{sr}, s \in \{M, F\}$ to:

$$Y_{sr} = Pois(2f_{sr}) \tag{5.16}$$

We assume that this free parameter persists for a higher number of risk classes of men and women, though we do not show this explicitly in this chapter. Accordingly, we make the above assumption in each of our models. Doing so, we arrive at the surprising result that for this model, under the assumption that the total rate of males forming partnerships is equal to the total rate of females forming partnerships, the yearly degree distribution of males is independent of the risk structure of the female population, and vice versa.

5.2.3 Special case - $c_M = c_F = 0$

Assuming that $c_M = c_F = 0$ implies that individuals are serially monogamous, and therefore we can obtain a closed set of ordinary differential equations describing

the underlying partnership dynamics of the population. Doing so, we obtain an extension of the pair-formation model described in Chapter 4. By solving these equations numerically, we are able to obtain both the instantaneous proportion of single individuals as well as the yearly degree distribution.

Obtaining proportion of single individuals for $c_M = c_F = 0$

We let $[s_r]$ denote the number of single individuals from sex s and risk class r, and let $[M_r F_q]$ denote the number of partnerships involving a male from risk class r and a female from risk class q.

Considering first the rate of change of $[M_r]$. A male from risk class r forms a partnership in two different ways: either they form a partnership themselves, which they do so at a rate f_{Mr} or a female forms a partnership with that individual, which occurs at a rate f'_{Mr} - here, the expression for f'_{Mr} can be obtained by replacing N_{Fr} terms in Equation (5.10) with $[F_r]$ terms, reflecting that only single individuals can form new partnerships. A male from risk class r in a relationship with a female from risk class q becomes single again at a rate $b(f_{Mr} + f_{Fq})$, and to obtain the total rate that males from risk class r re-enter the single population, we must sum over all female risk classes. Doing so, and by considering the analogous situation for females, we obtain the following equations:

$$\frac{d[M_r]}{dt} = - f_{Mr}[M_r]\left(1 + \frac{\sum_q f_{Fq}[F_q]}{\sum_p f_{Mp}[M_p]}\right) + b\sum_q (f_{Mr} + f_{Fq})[M_r F_q] \tag{5.17}$$

$$\frac{d[F_q]}{dt} = - f_{Fq}[F_q]\left(1 + \frac{\sum_r f_{Mr}[M_r]}{\sum_p f_{Fp}[F_p]}\right) + b\sum_r (f_{Mr} + f_{Fq})[M_r F_q] \tag{5.18}$$

Considering partnerships between males from risk class r and females from risk class q, partnerships are formed in two different ways, either a male from risk class

r forms a partnership with a female from risk class q, which happens at a rate $f_{Mr}\frac{f_{Fq}[F_q]}{\sum_p f_{Fp}[F_p]}$, or a female from risk class q forms a partnership with a male from risk class r, which happens at a rate $f_{Fq}\frac{f_{Mr}[M_r]}{\sum_p f_{Mp}[M_p]}$. Partnerships break up simply at a rate $b(f_{Mr} + f_{Fq})$. The equation describing the dynamics of partnerships is then given by:

$$\frac{d[M_rF_q]}{dt} = f_{Mr}[M_r]f_{Fq}[F_q]\left(\frac{1}{\sum_i f_{Fp}[F_p]} + \frac{1}{\sum_i f_{Mp}[M_p]}\right) - b(f_{Mr} + f_{Fq})[M_rF_q] \tag{5.19}$$

The above equations result in a system of $k_M + k_F + (k_M \times k_F)$ equations. These equations can be solved numerically until equilibrium, and the expected proportion of single males and females is given by $\sum_i [M_i]^*/N_M$ and $\sum_i [F_i]^*/N_F$ respectively.

Obtaining yearly degree distributions for $c_M = c_F = 0$

The above system can be extended to obtain yearly degree distributions for $c_M = c_F = 0$. Specifically, we extend the above system by explicitly tracking the number of new partnerships individuals have had, up to a maximum of n new partnerships. Letting $[s_r^i]$ denote the number of single individuals from sex s and risk group r who have had i new partnerships in the last year, and letting $[M_r^i F_q^j]$ denote partnerships between males of risk class r who have had i new partnerships in the last year and males of risk class q who have had j new partnerships in the last year. We initialise this by setting $[s_r^0](0) = [s_r]^*$ and $[M_r^0 F_q^0](0) = [M_rF_q]^*$, i.e. we set the initial values of all states indicating no new partnerships to be the equilibrium values obtained from the previous system, and set all other states to have an initial value of zero. Tracking the number of new partnerships individuals have, we arrive

at the following system of equations:

$$\frac{d[M_r^0]}{dt} = - f_{Mr}[M_r^0]\left(1 + \frac{\sum_i \sum_q f_{Fq}[F_q^i]}{\sum_j \sum_p f_{Mp}[M_p^j]}\right) + b\sum_q (f_{Mr} + f_{Fq})[M_r^0 F_q^0] \tag{5.20}$$

$$\frac{d[F_q^0]}{dt} = - f_{Fq}[F_q^0]\left(1 + \frac{\sum_j \sum_r f_{Mr}[M_r^j]}{\sum_i \sum_p f_{Fp}[F_p^i]}\right) + b\sum_r (f_{Mr} + f_{Fq})[M_r^0 F_q^0] \tag{5.21}$$

$$\begin{aligned}\frac{d[M_r^k]}{dt} =& - f_{Mr}[M_r^k]\left(1 + \frac{\sum_i \sum_q f_{Fq}[F_q^i]}{\sum_j \sum_p f_{Mp}[M_p^j]}\right) \\ &+ b\sum_i \sum_q (f_{Mr} + f_{Fq})[M_r^k F_q^i] \text{ for } 1 \le k \le n\end{aligned} \tag{5.22}$$

$$\begin{aligned}\frac{d[F_q^l]}{dt} =& - f_{Fq}[F_q^l]\left(1 + \frac{\sum_j \sum_r f_{Mr}[M_r^j]}{\sum_i \sum_p f_{Fp}[F_p^i]}\right) \\ &+ b\sum_j \sum_r (f_{Mr} + f_{Fq})[M_r^j F_q^l] \text{ for } 1 \le l \le n\end{aligned} \tag{5.23}$$

$$\frac{d[M_r^0 F_q^0]}{dt} = - b(f_{Mr} + f_{Fq})[M_r^0 F_q^0] \tag{5.24}$$

$$\begin{aligned}\frac{d[M_r^k F_q^l]}{dt} =& f_{Mr}[M_r^{k-1}] f_{Fq}[F_q^{l-1}]\left(\frac{1}{\sum_i \sum_p f_{Fp}[F_p^i]} + \frac{1}{\sum_j \sum_p f_{Mp}[M_p^j]}\right) \\ &- b(f_{Mr} + f_{Fq})[M_r^k F_q^l] \text{ for } 1 \le k, l < n\end{aligned} \tag{5.25}$$

$$\begin{aligned}\frac{d[M_r^n F_q^l]}{dt} =& f_{Mr}([M_r^{n-1}] + [M_r^n]) f_{Fq}[F_q^{l-1}]\left(\frac{1}{\sum_i \sum_p f_{Fp}[F_p^i]} + \frac{1}{\sum_j \sum_p f_{Mp}[M_p^j]}\right) \\ &- b(f_{Mr} + f_{Fq})[M_r^n F_q^l] \text{ for } 1 \le l < n\end{aligned} \tag{5.26}$$

$$\begin{aligned}\frac{dM_r^k F_q^n}{dt} =& f_{Mr}[M_r^{k-1}] f_{Fq}([F_q^{n-1}] + [F_q^n])\left(\frac{1}{\sum_i \sum_p f_{Fp}[F_p^i]} + \frac{1}{\sum_j \sum_p f_{Mp}[M_p^j]}\right) \\ &- b(f_{Mr} + f_{Fq})[M_r^k F_q^n] \text{ for } 1 \le k < n\end{aligned} \tag{5.27}$$

$$\begin{aligned}\frac{dM_r^n F_q^n}{dt} =& f_{Mr}([M_r^{n-1}] + [M_r^n]) f_{Fq}([F_q^{n-1}] + [F_q^n])\left(\frac{1}{\sum_i \sum_p f_{Fp}[F_p^i]} + \frac{1}{\sum_j \sum_p f_{Mp}[M_p^j]}\right) \\ &- b(f_{Mr} + f_{Fq})[M_r^n F_q^n]\end{aligned} \tag{5.28}$$

We obtain yearly degree distributions by running this system of equations for a year. The above equations result in a system of $(n+1)(k_M + k_F) + (n^2+1)(k_m \times k_F)$

equations. Because of this, the computational benefits of this approach diminish rapidly. However, the benefit of this method is that the expected yearly degree distribution can be derived exactly in the case of $c_M = c_F = 0$. In Figure 5.2, we demonstrate the soundness of the methods to obtain yearly degree distributions for $c_M = c_F = 1$ and $c_M = c_F = 0$ by comparing them to yearly degree distributions obtained from explicit stochastic simulation.

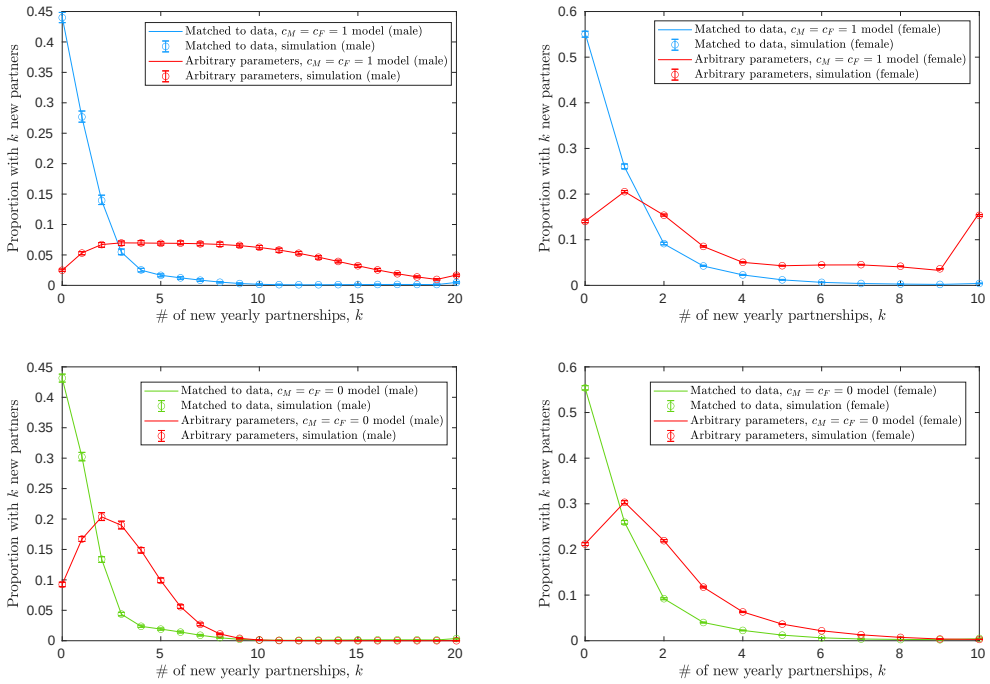

Figure 5.2: **Comparing yearly degree distributions obtained from exact methods and from simulation for $c_M = c_F = 1$ and $c_M = c_F = 0$.** Here we demonstrate the accuracy of the exact methods described for $c_M = c_F = 1$ (above) and $c_M = c_F = 0$ (below) by comparing their results against yearly degree distributions obtained from direct simulation (circles). For both sexes, we see excellent agreement between exact methods and simulation, both for models fitted to Natsal data (blue for $c_M = c_F = 1$ and green for $c_M = c_F = 0$) and for models with formation rates and risk group sizes chosen arbitrarily (red). Simulated degree distributions here are obtained from 100 simulation runs, and error bars refer to 95% prediction intervals.

5.3 Fitting the network model

5.3.1 Natsal data

The Natsal is a decennial survey, asking a representative sample of participants across the UK a range of questions concerning their sexual behaviour [Mercer et al., 2013]. These surveys can be used to inform underlying behavioural parameters in epidemiological models of STI spread, as done by Datta et al. [2018], Choi et al. [2010], and Smid et al. [2018].

In this chapter we use data from Natsal-3, a survey of 15,162 adults between September 2010 and August 2012. Specifically, we consider data from the Natsal-3 concerning heterosexual 16-24 year olds. We focus on this age bracket owing to the disproportionate number of STI diagnoses. Considering heterosexual males diagnosed in 2019 in England, 53.5% of chlamydia diagnoses, 42.2% of gonorrhoea diagnoses, and 31.5% of anogenital herpes diagnoses were aged 15-24 years; considering heterosexual females diagnosed in 2019 in England, 69.2% of chlamydia diagnoses, 60.8% of gonorrhoea diagnoses, and 45.5% of anogenital herpes diagnoses were aged 15-24 years [Public Health England, 2019]. To consider a heterosexual population, we constrain the data to include only those who have ever had a heterosexual sexual partnership (coded `everhet`). Using this definition, we capture the sexually active population of this age range. This definition is not based on sexual orientation, and therefore includes individuals who do not identify as exclusively heterosexual. Restricting to this age bracket, using this criterion to determine the sexually active heterosexual population, and filtering out respondents with anomalous answers, we are left with a sample of 1432 females and 1091 males.

Of these individuals, we can obtain the number of new (heterosexual) partnerships each individual has had in the previous year (coded `hetnonew`), from which we can construct the yearly degree distributions for both males and females. For both

sexes, the majority of respondents report having either 0 or 1 new partnerships - (73.2% of males and 80.5% of females). Only 6.7% of males and 3.2% of females report having five or more new partnerships, 2.0% of males and 0.63% of females report having 10 or more new partnerships, and 0.64% of males and 0.07% of females (only one respondent) report having 20 or more new partnerships.

We obtain the number of single male and female individuals from their response to the question of whether they are likely to have sex again with their most recent partner (coded `r1sexagn`). If respondents answered 'Yes' or 'Probably', we assumed that individuals were involved in a sexually active partnership, otherwise we assumed that individuals were single. Using this criterion, we find that 31.9% of male respondents and 21.9% of female respondents are defined as single. Regarding concurrency, we obtain whether individuals have been involved in a concurrent partnership within the last year, coded `lypartn2` - finding that 13.8% of male respondents and 11.4% of female respondents report being involved in such a partnership within the last year.

5.3.2 Fitting to Natsal data

Balancing degree distributions

While yearly degree distributions of males and females will differ, within a closed population the total number of new heterosexual partnerships that males have will necessarily equal the total number of new heterosexual partnerships that females have. This is a necessary feature of the individual-based model described in this chapter. However, this is in general not a feature of observed yearly degree distributions, where typically the male population report a higher number of new partnerships than females [Mitchell et al., 2019]. Under the assumption of a closed population, and that the size of the sexually active population of males aged 16-24 years is equal to that of females 16-24 years, then the average number of partners

reported from males should approximately equal the average number of partners reported from females. However, from the data we consider, males report an average of 1.43 ($CI_{95\%} = [1.27, 1.60]$) new partners, while females report an average of 0.927 ($CI_{95\%} = [0.76, 1.09]$) new partners. Several suggestions have been made to explain this persistent discrepancy, including undersampling of female sex workers [Brewer et al., 2000], the cumulative impact of rounding errors [Brown and Sinclair, 1999], and cultural factors that cause either the exaggeration of partnerships by males or the understatement of partnerships by females [Fisher, 2009]. To fit to our model, we make the simplifying assumption that females underreport the true number of new partnerships they make, while male estimates are accurate. While doing so has some justification within the literature [Alexander and Fisher, 2003], we also do so because it is a conservative assumption, in the sense that making such an assumption will result in a model with a larger number of partnerships, where consequently infection will spread more rapidly. Doing so is also convenient mathematically. Letting $\rho = 0.927/1.43$ be the probability that a new partnership is reported by a female, letting n be the largest number of partnerships obtained from a simulation, and letting Y_F denote the female yearly degree distribution obtained from a model, then the adjusted female degree distribution, Y_F^ρ can be obtained by assuming that reported new partnerships are binomially distributed, i.e.

$$Y_F^\rho(i) = \sum_{j=i}^{n} \binom{j}{i} \rho^j (1-\rho)^{j-i} Y_F(j) \tag{5.29}$$

In the case of $c_M = c_F = 1$, the yearly degree distributions of each risk class r are Poisson distributed. Accordingly, adjusted female degree distributions in this instance can be given by adjusting Equation (5.16) :

$$Y_{Fr}^{\rho} = Pois(\rho \times 2f_{Fr}) \tag{5.30}$$

Fitting models via MCMC

In this chapter, we use a basic Metropolis-Hastings (MH) algorithm for fitting [Metropolis et al., 1953; Hastings, 1970]. While using this type of algorithm can be slow to converge, especially for high parameter models, we find that this fitting regime works adequately for convergence for all models fitted. For models consisting of k_M male risk groups and k_F female risk groups with $c_M = c_F = 0$ or $c_M = c_F = 1$, $2k_M + 2k_F - 2$ parameters must be fitted: $k_S - 1$ parameters specify the proportion of the population in each risk group (with the size of the last risk group specified by $1 - \sum_{j=1}^{k_s-1} N_{sj}$), $k_M + k_F - 1$ parameters specify the formation rates of each risk group (with the formation rate of one risk group determined to satisfy $\sum_r f_{Mr}N_{Mr} = \sum_q f_{Fq}N_{Fq}$), and one parameter specifies the partnership dissolution parameter b. For the full simulation model, c_M and c_F must also be fitted, meaning $2k_M + 2k_F$ parameters must be fitted.

MCMC approaches require defining the likelihood function of a model given the data, $L(\theta|x)$, where θ denotes the parameters of the model and where x denotes the observed data. We let Y_s denote the yearly degree distribution of sex s obtained from the model (expressed in terms of proportions), letting x_s^Y denote the observed yearly degree distribution of sex s (expressed in terms of numbers), and letting $X_s = \sum_i x_s^Y(i)$, i.e. the sample size of sex s , then the likelihood of obtaining the sampled degree distribution x_s^Y from the degree distribution Y_s is given by the probability mass function of the multinomial distribution:

$$L_{Y_s} = \frac{X_s!}{\prod_i (x_s^Y(i)!)} \prod_i Y_s(i)^{x_s^Y(i)} \tag{5.31}$$

While the multiplicative constant $\frac{X_s!}{\prod_i (x_s^Y(i)!)}$ cannot be feasibly calculated owing to the large factorial terms, we can use the above definition to calculate the *log* likelihood of obtaining the sampled degree distribution:

$$\log(L_{Y_s}) = (\sum_i x_s^Y(i) \log(Y_s(i))) + K_s^Y \tag{5.32}$$

where K_s^Y is some constant that only depends on the data. Because K_s^Y only depends on data, it is irrelevant when conducting our MCMC fitting approach, as it does not affect the probability of choosing a new set of parameters.

Letting S_s denote the proportion of single individuals of sex s obtained from the model, and let x_s^S denote the observed number of single individuals of sex S, the likelihood of sampling x_s^S given that S_s individuals in the population are single is given by the probability mass function of the binomial distribution with parameters X_s and S_s. Again, the likelihood cannot be computed directly, but the log likelihood is easily computable:

$$\log(L_{S_s}) = x_s^S \log(S_s) + (X_s - x_s^S) \times \log(1 - (S_s)) + K_s^S \tag{5.33}$$

Similarly, letting C_s denote the proportion of individuals of sex s who had a concurrent partnership in the past year obtained from the model, and x_s^C denote the observed number of individuals of sex s reporting a concurrent partnership, the

likelihood of sampling x_s^C given C_s is given by the probability mass function of the binomial distribution with parameters N_s and C_s.

$$\log(L_{C_s}) = x_s^C \log(C_s) + (X_s - x_s^C) \times \log(1 - (C_s)) + K_s^C \tag{5.34}$$

For the instances $c_M = c_F = 1$ and $c_M = c_F = 0$, where concurrency is not fitted to explicitly, the log likelihood used for the MCMC approach is given by summing the log-likelihoods of the observed degree distributions and number of singles for both sexes. For the full simulation model, the log-likelihoods from the observed levels of concurrency are also added:

$$\log(L) = \sum_s \log(L_{Y_s}) + \log(L_{S_s}) + \log(L_{C_s}) \tag{5.35}$$

For fitting, male degree distributions are counted up to 20 new partnerships (i.e. individuals reporting 20 or 21 new partnerships in a year are both classified as '20 or more') while female degree distributions are counted up to 10 new partnerships. For both sexes, $\approx 99.4\%$ of sampled individuals fall below their respective cut-offs. These are specified, rather than the maximum number reported by both males and females, so that the full simulation model consistently returns finite estimates of $log(L)$. If the chance of observing an individual within the model with n partnerships is too low, then on some runs there will be no such individuals, and in which case the log likelihood will return a value of $-\infty$. Doing so also reduces the computational intensity of running the $c_M = c_F = 0$ model. While for $c_M = c_F = 1$, we do not encounter the same problems, we still use the same cut-offs for consistency between models.

To fit models, we start at an arbitrary initial parameter set θ. The next candidate parameter set θ' is sampled from a multivariate distribution with mean θ, covari-

ances equal to zero, and variances equal to $0.05 \times \theta$, but are restricted to parameter sets that do not violate the underlying assumptions of the parameters (e.g. parameter sets that suggest $\sum_r N_{Mr} > N_M$, $f_{F1} > f_{F2}$ or $b < 0$ are not considered). We let the algorithm run for a burn-in period of 100,000 parameter sets. After which, the next 100,000 parameter sets are taken as the posterior distribution of the parameters given the data. In all cases, doing so allows the log likelihood to stabilise around a constant value.

5.3.3 Model selection

Increasing the number of risk groups within each model should always improve the fit to the underlying data. However, this comes at a cost - as the number of model parameters increases, so does the time it takes to fit the parameters of the model. Moreover, by increasing the number of risk groups, one runs the risk of *overfitting* the model, meaning the model may generalise badly to other scenarios. To assess the optimal number of risk groups, we use an information criterion, a standard method of model selection within the literature. While the Akaike Information Criterion and Bayesian Information Criterion are the most commonly used, these measures only assess the quality of a model at its maximum likelihood estimate [Kuha, 2004]. As we obtain a distribution of possible parameter sets that could generate the underlying data, we wish to use a criterion that accounts for the quality of a distribution. Methods that account for the quality of distributions, such as Watanabe-Akaike-Information Criterion [Watanabe, 2013], and leave-one-out cross-validation [Vehtari et al., 2017], require calculation of the likelihood explicitly, rather than just the log-likelihood. Because of this, we use the DIC, a criterion for model selection that applies to distributions, and can be calculated solely from log likelihoods [Spiegelhalter et al., 2002]. Defining the *deviance* as $D(\theta) = -2log(L) + C$, where C is some constant, the DIC can be calculated as:

$$DIC = 2\overline{D(\theta)} - D(\bar{\theta}) \tag{5.36}$$

For each model, we select the number of risk groups that produces the lowest DIC. It is important to note that the DIC is only valid when posterior distributions are approximately multivariate normal - a property satisfied for the posterior distributions of our models (Figures 5.3, B.1 and B.2). DIC values here should only be used to assess the optimal number of risk groups for each model, not to select *between* the three models. The the log-likelihood for the full simulation model includes log-likelihoods from the observed levels of concurrency, resulting in higher DIC values in cirtue of this. Further, while the $c_M = c_F = 0$ and $c_M = c_F = 1$ log-likelihoods are comprised of the same components, the most suitable model is likely more influenced by the suitability of the underlying assumption regarding concurrency. While there has been recent concerns about the DIC as a model selection criterion [Celeux et al., 2006; Pooley and Marion, 2018], we believe this criterion is sufficient for our purposes.

5.3.4 Fitted models

By comparing the DIC obtained for each model, we obtained the optimal number of risk groups for males and females to match the data for each of our three models. Here, we only explore situations where $k_M = k_F$, i.e. where there is the same number of risk groups for both males and females, although this need not necessarily be the case.

In Table 5.1, we compare the DICs obtained for different models. We stress that the DIC values here should only be used to assess the optimal number of risk groups for each model, not to select *between* the three models. Selecting between models

Table 5.1: **DIC values and summary statistics for a varying number of risk groups.** Bold typeface within the table indicates the optimal number of risk groups for each model, given by the number of risk groups that minimises the DIC.

Model	No. of risk groups	DIC + constant	KS statistic (male)	absolute Δ in singles (male)	KS statistic (female)	absolute Δ in singles (female)
$c_M = c_F = 1$	1	1777.6	0.180	0.057	0.140	0.043
	2	210.7	0.031	0.056	0.022	0.045
	3	77.7	0.003	0.060	0.009	0.041
	4	**36.1**	**0.022**	**0.021**	**0.004**	**0.010**
	5	80.7	0.021	0.022	0.007	0.011
Full model	**3**	**1963.4**	**0.008**	**0.038**	**0.008**	**0.031**
	4	1969.4	0.008	0.041	0.007	0.035
$c_M = c_F = 0$	1	3241.1	0.253	0.202	0.21	0.102
	2	235.3	0.030	0.076	0.019	0.024
	3	**59.15**	**0.007**	**0.056**	**0.006**	**0.044**
	4	59.24	0.009	0.055	0.007	0.045

depends on the suitability of the underlying assumptions around concurrency, and its impact on transmission dynamics. Additionally, the DIC is inevitably higher for the full model, where $0 < c_M, c_F < 1$, as in this instance we are also fitting to observed concurrency levels. In this table, we also include values obtained for the the absolute differences between the proportion of singles from the models and observed in data, and the Kolmogorov-Smirnov (KS) statistics for the yearly degree distributions of each sex, defined as:

$$KS_s = \sup_i |Y_s(i) - x_s^Y(i)| \tag{5.37}$$

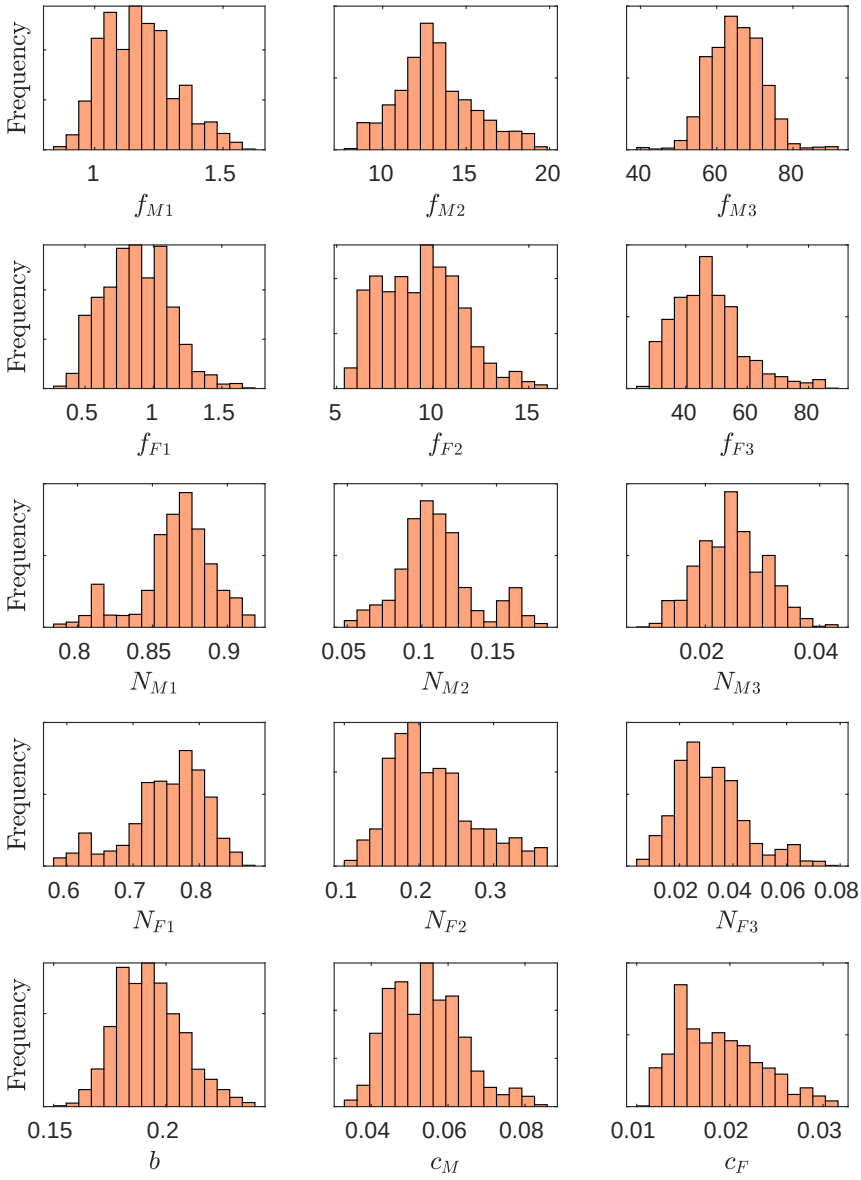

Figure 5.3: **Posterior distribution obtained from MCMC for the full model.** Here, we plot the posterior parameter distributions obtained via a MH-algorithm for the full model (where $0 < c_M, c_F < 1$). We observe that the distributions are approximately normally distributed. Distributions are obtained from 100,000 iterations of a MH-algorithm, after an initial burn-in period of 100,000 iterations.

For the $c_M = c_F = 0$ model and the full simulation model, only three risk groups

are optimal, while for the $c_M = c_F = 1$ models, four risk groups are optimal. Upon inspection of the posterior parameters, we see that the size of one of the female risk groups is extremely small, while the formation rate of the least active male risk group is almost zero. The $c_M = c_F = 1$ model is thus best fitted by assuming that there are three sexually active risk male and female risk groups, and one additional sexually inactive male risk group. The improved fit from including an extra risk group primarily comes from being able to capture the observed proportion of singles better, as evidenced by the absolute difference in singles for both males and females.

Table 5.2 contains the mean parameter values obtained for each of the optimal models, seeing similar trends in the size and formation rates of risk groups between models. Each model contains a large group of low or very-low risk individuals for both males and females, constituting between $86.6 - 89.8\%$ of the male and $75.4 - 79.7\%$ of the female population respectively, who form partnerships at a relatively modest rate (in the $c_M = c_F = 1$ model, this includes a subgroup of extremely inactive males). Each model contains a smaller group for each sex of medium-risk individuals, and a yet smaller group of high-risk individuals. These results signify a long established feature of sexual networks - a 'core' group of more sexually active individuals who are integral in driving the spread of sexually transmitted infections [Yorke et al., 1978]. Naturally, partnership formation rates are lower for the $c_M = c_F = 1$ model than the full model and $c_M = c_F = 0$ model, as in this instance individuals do not have to wait until they are single to form partnerships at a high rate.

From fitting the full model, we obtain very low values of c_M and c_F as the optimal choice to match observed concurrency levels (Table 5.2 and Figure 5.3). This result agrees with our intuition that in general, there is a strong social preference for monogamous relationships within the heterosexual population of the UK. Accordingly, the values of the other fitted parameters are relatively similar to those

Table 5.2: **Mean parameter values for optimal models.** Note that N_M and N_F values presented in the table refer to the *proportion* of each sex belonging to each risk class, as opposed to the absolute numbers.

Parameter	Risk group	$c_M = c_F = 1$ model mean (sd)	full model mean (sd)	$c_M = c_F = 0$ model mean (sd)
f_M	Very low	4×10^{-7} (1×10^{-7})	-	-
	Low	0.48 (0.03)	1.16 (0.13)	1.12 (0.13)
	Medium	2.47 (0.25)	13.09 (2.28)	16.18 (1.42)
	High	8.29 (0.57)	65.45 (7.16)	80.49 (7.03)
N_M	Very low	0.167 (0.022)	-	-
	Low	0.731 (0.023)	0.866 (0.025)	0.868 (0.013)
	Medium	0.083 (0.013)	0.109 (0.026)	0.111 (0.013)
	High	0.019 (0.003)	0.025 (0.006)	0.021 (0.004)
f_F	Very low	0.32 (0.03)	-	-
	Low	1.09 (0.30)	0.74 (0.25)	1.10 (0.19)
	Medium	1.78 (0.32)	9.39 (2.10)	10.09 (1.48)
	High	6.00 (0.79)	47.31 (11.27)	50.43 (6.17)
N_F	Very low	0.797 (0.032)	-	-
	Low	4×10^{-4} (1×10^{-4})	0.754 (0.058)	0.755 (0.045)
	Medium	0.179 (0.030)	0.216 (0.054)	0.217 (0.042)
	High	0.023 (0.007)	0.031 (0.013)	0.029 (0.007)
b	-	0.375 (0.021)	0.194 (0.015)	0.191 (0.010)
c_M	-	1	0.054 (0.009)	0
c_F	-	1	0.019 (0.005)	0

obtained from the $c_M = c_F = 0$ model, which assumes serial monogamy. Histograms describing the posterior distributions for the $c_M = c_F = 1$ model and $c_M = c_F = 0$ model are included as an appendix (Figures B.1 and B.2). For most parameters, we observe little correlation between fitted parameters for the full model (Figure 5.4). However, we observe a clear trade-off between the sizes of the first two risk groups for both males and females - i.e. larger values of N_{M1} or N_{F1} imply smaller values of N_{M2} or N_{F2}, and vice versa.

Compared to observed data, the $c_M = c_F = 0$ model underestimates the proportion of single males and overestimates the proportion of single females. This is a necessary feature of this model - in a serially monogamous heterosexual population, with equal numbers of males and females, the number of single males is necessarily

the number of single females. This underestimation of single males and overestimation of single females also occurs in the full model, owing to the low values of c_M and c_F that emerge from the fitting process that dictate that partnerships are predominantly monogamous. However, we see that each of the models produces yearly degree distributions that fit closely to observed data (Figure 5.5).

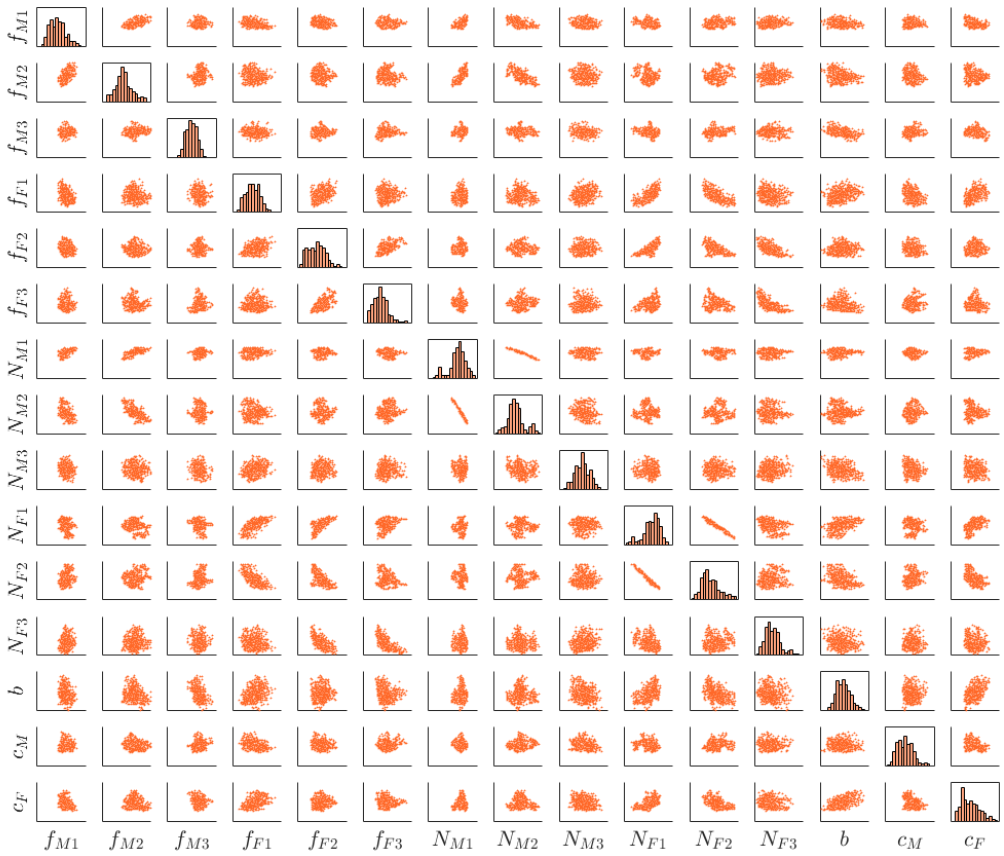

Figure 5.4: **Pairwise scatter plot of posterior distribution for the full model.** By comparing scatter plots of the fitted values of each parameter for the full model ($0 < c_M, c_F < 1$), we observe that there is little correlation between most parameters. Notable exceptions are N_{M1} against N_{M2}, N_{F1} against N_{F2}, which are negatively correlated with one another. Distributions are obtained from 100,000 iterations of a MH-algorithm, after an initial burn-in period of 100,000 iterations.

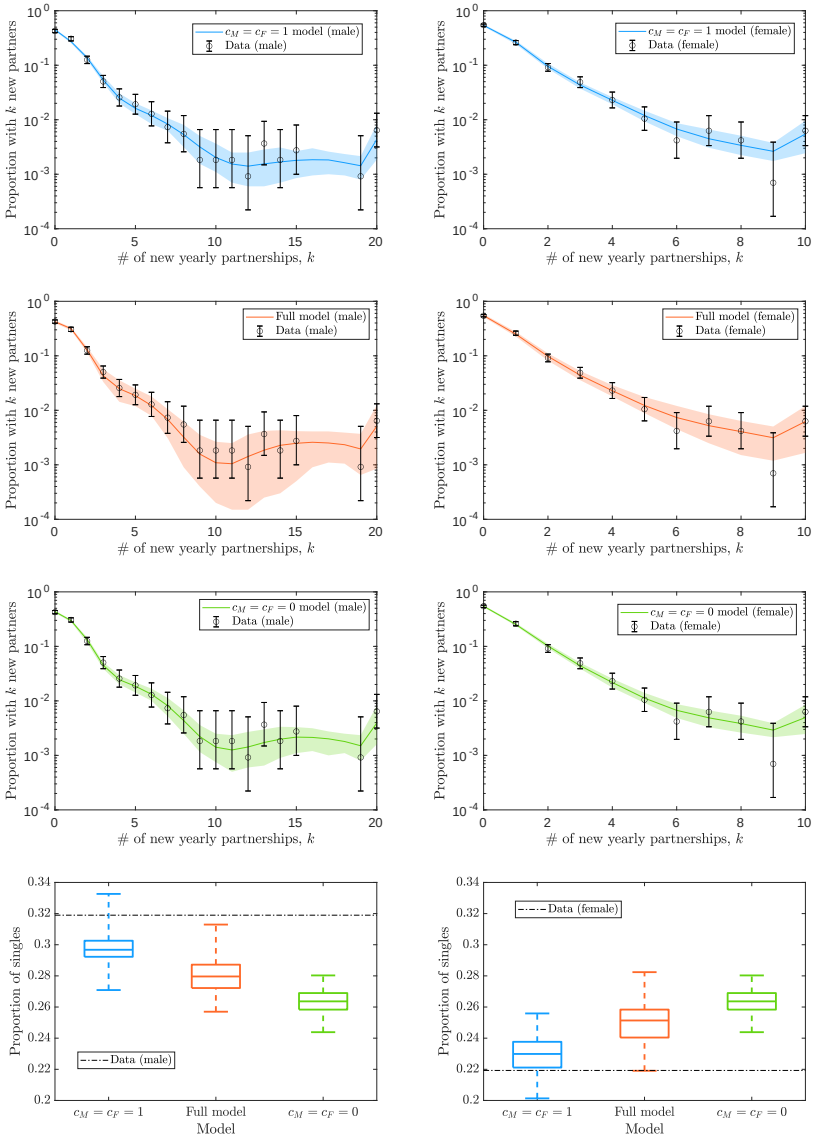

Figure 5.5: **Fitting models to yearly degree distributions and proportion of singles.** In the first three rows, we compare the yearly degree distributions obtained from the fitted models (blue - $c_M = c_F = 1$, orange - full model, green $c_M = c_F = 0$) and yearly degree distributions reported from Natsal-3 (circles). There is close agreement between models and observed data for each model for both males (left) and females (right). Shaded areas refer to 95% prediction intervals and error bars refer to 95% confidence intervals. In the last row, we compare the proportion of singles obtained from the fitted models against the reported proportion of singles from Natsal-3, observing that the fitted models in general underestimate the proportion of single males and overestimate the proportion of single females. Results are generated from 100 parameter sets sampled from fitted posterior distributions. Whiskers refer to maximum and minimum values.

5.3.5 Network characteristics

We can compare the emergent network characteristics that are present in each of the fitted models. In particular, we can compare the levels of concurrency present in the $c_M = c_F = 1$ model, which assumes that partnership formation rates are independent of relationship status, to the full model, which has been explicitly fitted to yearly concurrency data (the $c_M = c_F = 0$ model assumes that there are no concurrent partnerships). For the $c_M = c_F = 1$ model, on average 47.5% of males and 47.2% of females engage in a concurrent partnership in a year, markedly higher than both the observed levels from Natsal-3 (13.8% for males and 11.4% for females) and the levels obtained from full model (15.8% for males and 10.6% for females), which has been explicitly fitted to concurrency. Further, in the $c_M = c_F = 1$ model, a significant proportion of both the male and female population are engaged in multiple active relationships at any given time - at equilibrium, 25.5% of males and 22.8% of females are engaged in three or more partnerships in the $c_M = c_F = 1$ model. In contrast, individuals engaged in more than two partnerships at any given time are extremely rare in the full model (0.3% of males and 0.08% of females). As a consequence, large connected components of individuals interconnected by sexual relationships emerge in the $c_M = c_F = 1$ model, while in the full model the population consists of islands of individuals, pairs, and very small connected components.

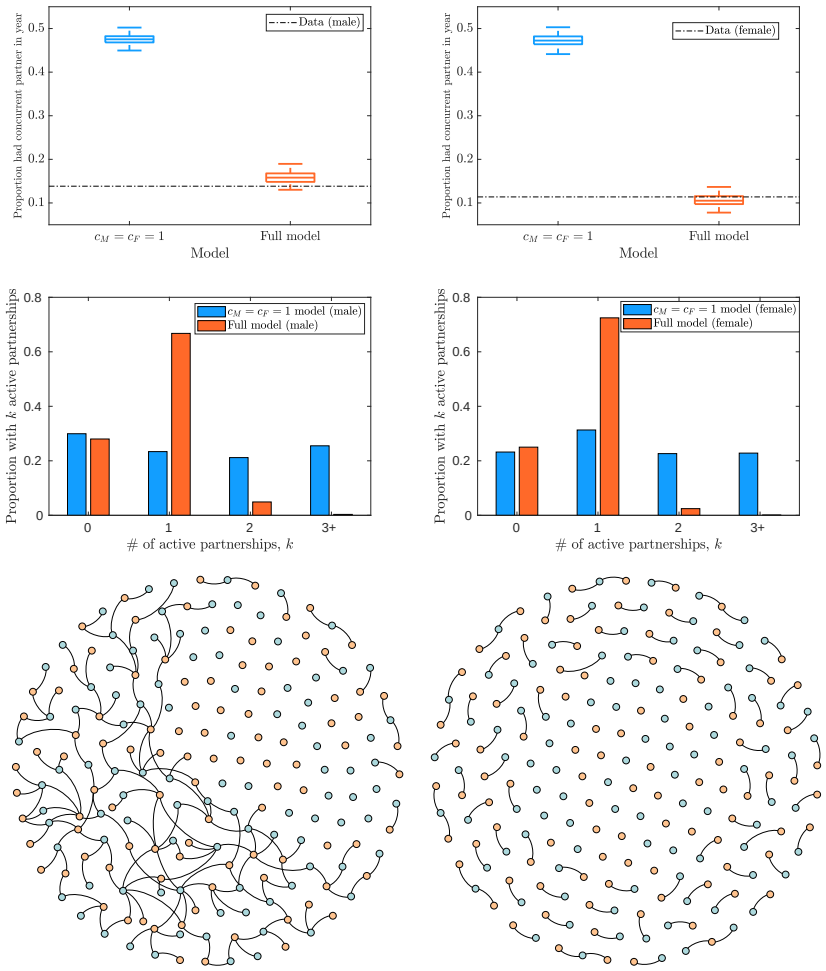

Figure 5.6: **Comparing instantaneous and yearly levels of concurrency between the full model and the $c_M = c_F = 1$ model** Top row - we compare the proportion of individuals who have engaged in a concurrent partnership in a year in the $c_M = c_F = 1$ model (blue) and the full model (orange) to for both sexes (males left, females right) against reported levels of concurrency from Natsal-3. Middle row - we compare the instantaneous levels of concurrency in each of these models by plotting the instantaneous degree distributions of both males and females - observing that individuals in many partnerships are commonplace in the $c_M = c_F = 1$ model. Results for the first four plots are generated from 100 parameter sets sampled from fitted posterior distributions. Bottom row - we generate illustrative networks of 200 individuals for the $c_M = c_F = 1$ model (left) and the full model (right), observing that large interconnected components can emerge from the underlying behavioural assumptions of the $c_M = c_F = 1$ model. Here, light blue designates males and yellow designates females.

The proportion of both males and females who are low, medium, or high risk is roughly the same across models. Accordingly, we can compare the proportions of singles and levels of yearly concurrency within each risk group to assess the difference between these models. For each model, the probability of being single decreases with increasing risk behaviour. Only a very small proportion of medium or high risk individuals are single at equilibrium in the $c_M = c_F = 1$ model; as illustrated in Figure 5.6, these individuals are typically engaged in multiple relationships at any given time. This is in contrast to the full model and $c_M = c_F = 0$ model, where a larger proportion are single at equilibrium. Within risk-group levels of concurrency also vary drastically between models (Figure 5.7). While clearly there are no concurrent partnerships in any risk group in the $c_M = c_F = 0$ model, for the other two models the proportion of individuals engaged in a yearly concurrent partnership increases with risk group. In both of these models, males are more likely to have been involved in a concurrent partnership than females. However, the $c_M = c_F = 1$ model sees a larger proportion of individuals engaged in concurrent partnerships in every risk group - in this model, almost all medium or high risk male individuals will engage in a concurrent partnership in a year. In the full model, low-risk males and females only rarely engage in concurrent partnerships (6.4% of low-risk males and 2.1% of low-risk females), while concurrency is fairly common among low-risk individuals within the $c_M = c_F = 1$ model.

5.4 Modelling transmission and control

5.4.1 Transmission dynamics

Acting on this dynamic partnership network, we consider a disease with SIS-dynamics. While many studies assume that transmission within a partnership is a Poisson process, i.e. with infection happening at a constant rate over time across

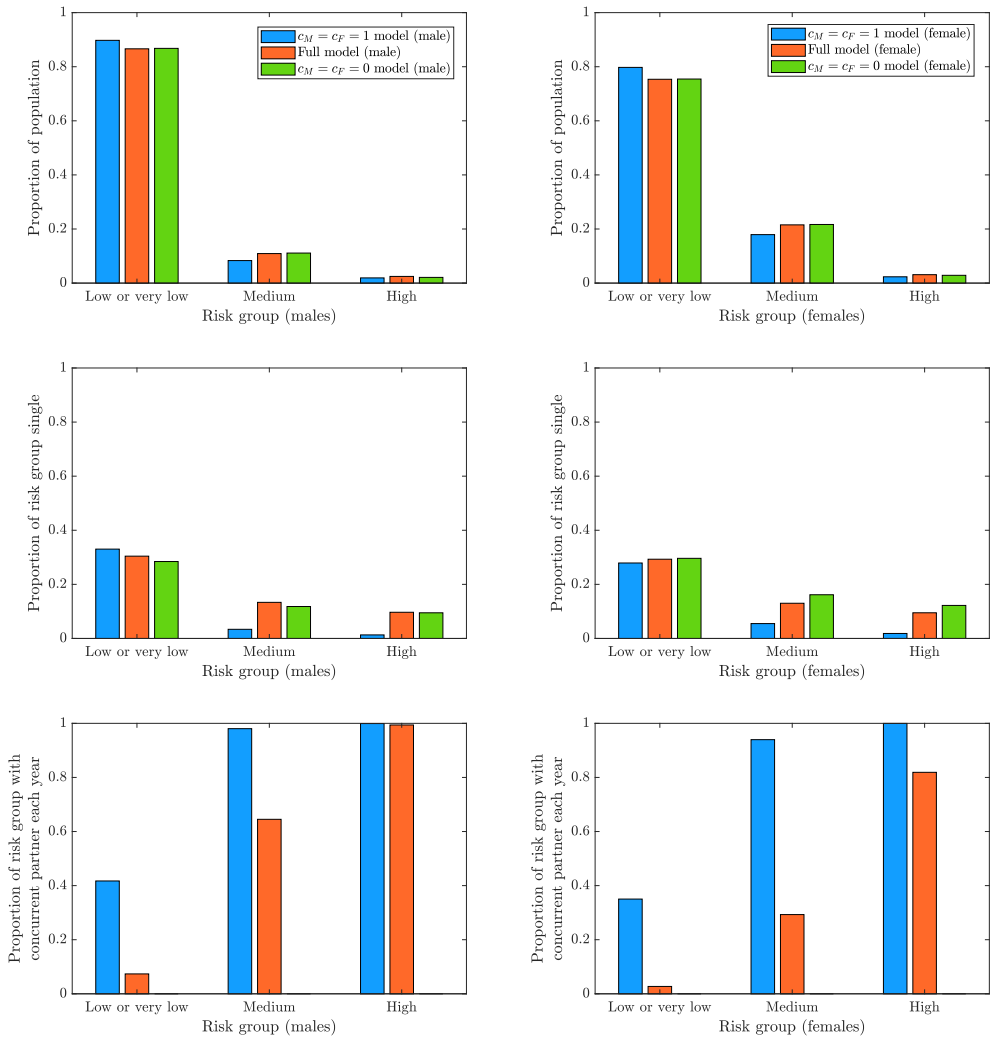

Figure 5.7: **Comparing levels of singles and levels of concurrency across models delineated by risk group.** Top row - we compare the proportion of the population who belong to 'low or very low', 'medium', of 'high' risk groups, for each model - $c_M = c_F = 1$ (blue) full model (orange) $c_M = c_F = 0$ (green), for both males (left) and females (right), observing that similar proportions fall into each risk group across models. In the middle row, we consider the proportion of individuals within each risk group who are single, while in the bottom row, we consider the proportion of individuals within each risk group who have been involved in a concurrent partnership in a year. Plotted results are averages obtained from 100 parameter sets sampled from fitted posterior distributions.

partnerships, for HIV it has been observed that within partnerships infection happens predominantly in the early stages of a relationship [Peterman et al., 1988], although the specific infectivity profile of different STIs will depend both upon biological and social factors. Because of this, in this chapter, we make the simplifying assumption that upon partnership formation, an infected individual infects their partner with a probability p_τ. A newly infected individual then infects each of their other (susceptible) partners with that probability, and so on until no new infections are recorded. Thus, at each time step infection percolates outward from a newly infected individual. This assumption also captures that the probability of infection across partnerships will also strongly depend on behaviour within a partnership, such as condom use - it is unclear how such behaviour varies over time in real-world relationships. However, this assumption may underestimate the probability of infection across longlasting partnerships and overestimate the probability of infection across shorter partnerships. Using this assumption omits the duration from partnership formation to infection onset, which may have some impact the trajectory of incidence through time. Our results focus on the endemic prevalence obtained through the model, rather than the time-evolution, which we would not expect to be largely effected by this assumption. Recovery from infection occurs at a constant rate γ, which we set as $\gamma = 2year^{-1}$, mirroring the assumption made in Chapter 4. Upon recovery from infection, an individual is reinfected with probability p_τ from each of their infected partners.

5.4.2 Transmission results

All simulations consist of a population of 2000 males and 2000 females. Before infection is introduced to the population, simulations run for 20 years, in order to reach an equilibrium of partnership dynamics. After this, infection and any control measures are introduced to the populations, and simulations have a further burn-in period of 10 years. When infection is introduced, all individuals are infected

- we find that this assumption reaches an endemic prevalence more quickly than assuming a small initial infected population, and also avoids the issue of stochastic extinction early on in simulations. Prevalence estimates are then taken as the mean values over that following year. For each model considered, 100 different parameter sets sampled from the obtained posterior distribution are simulated. Results show the mean value of these simulations, while bounds refer to 95% prediction intervals.

As these models differ in their underlying network structure, it is natural to assume that epidemics acting upon these dynamic networks would have different epidemiological dynamics. We compare the endemic prevalence obtained from each model as we vary the probability of infection across a partnership (Figure 5.8). For each model, the prevalence of infection is higher within the female population than in the male population, consistent with observed levels of STIs within heterosexual populations [Public Health England, 2019]. While this trend must emerge due to the different behaviours of males and females, which result in differing yearly degree distributions, an intuitive reason why this occurs is less clear. Medium- and high-risk females form partnerships at a lower rate than medium- and high-risk males, but there are more medium- and high-risk females than males. Females also engage in less concurrent partnerships than males. An answer may, in part, be found by considering that an individual's risk of infection is largely determined by their partner's behaviour, rather than their own.

Infection persists within the population at much lower probabilities of infection in the $c_M = c_F = 1$ model. For example, at a 30% probability of infection, the disease does not survive in either the full model or the $c_M = c_F = 0$ model, but in the $c_M = c_F = 1$ model, around 20% of individuals are infected. While the prevalence of the disease is higher in the full model than in the $c_M = c_F = 0$ model, the endemic prevalence follows a similar trajectory in these models. At a 100% probability of infection across contacts, the emergent endemic prevalence is similar

across all three models.

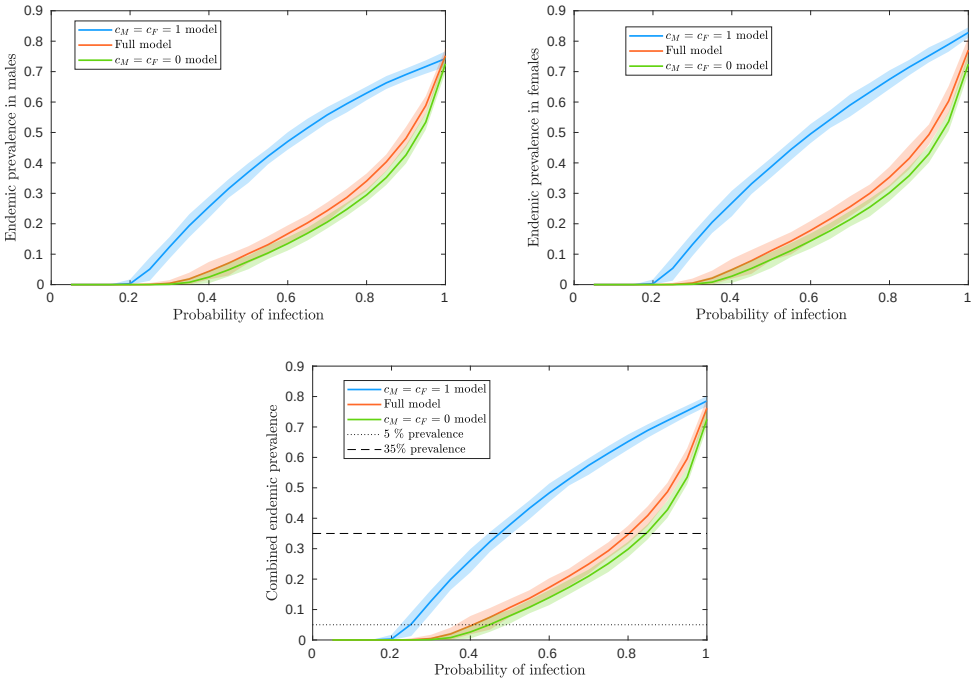

Figure 5.8: **Comparing prevalence across models.** Here we plot how the endemic prevalence within the population varies for each model as we increase the probability of infection across partnerships, p_τ. Above left, we consider the endemic prevalence in males; above right, we consider the endemic prevalence in females; Below, we consider the combined endemic prevalence. While for all models, females in general have a higher endemic prevalence than males, both follow similar trends as p_τ is increased. We observe that the trajectory of the $c_M = c_F = 1$ model (blue) differs substantially from that of the full model (orange) or the $c_M = c_F = 0$ model (green). Plotted results are averages of 100 epidemics generated from parameters sampled from the fitted posterior distributions.

In practice, instead of considering a disease with a fixed probability of infection, models are more likely to be calibrated to observed prevalence within the population. From Figure 5.8, we can obtain the probability of infection required to satisfy a given endemic prevalence. For the $c_M = c_F = 1$ model, the full model, and the $c_M = c_F = 0$ model respectively, transmission probabilities of 0.474, 0.803, and 0.846 are required to obtain a 35% prevalence, the level of infection used to assess the impact of vaccination, while transmission probabilities of 0.248, 0.407, and

0.448 are required to obtain a 5% prevalence, the level of infection used to assess the impact of contact tracing.

At these prevalences, we can compare the within risk group prevalence in each of the models (Figure 5.9). In all models prevalence increases with risk group, as expected. At 35% population prevalence the within risk group prevalence is similar. At 5% population prevalence, high risk males and females have a lower prevalence in the $c_M = c_F = 1$ than in the full model or $c_M = c_F = 0$ models, indicating that prevalence is less concentrated in high-risk individuals. There is considerable variation in within-risk group prevalence at 5% prevalence for medium and high risk groups. The large prediction intervals in the top panel of Figure 5.9 are, in part, a consequence of the variability in endemic prevalence between simulations - while transmission probabilities are set to obtain an average 5% prevalence, there is variability between the prevalence obtained for a given parameter set (indicated by the prediction intervals in Figure 5.8c).

5.4.3 Modelling control measures

We consider the impact of two different control measures on disease prevalence: vaccination and contact tracing. To consider the impact of vaccination, we assume that individuals are vaccinated with a probability p_V at time $t = 0$, and have full immunity from the modelled pathogen. We assume that immunity conferred through vaccination is longlasting and does not wane over the period of the simulation. We consider the impact of vaccination both when it occurs uniformly at random across the population, and when higher risk individuals are vaccinated first. To assess the impact of contact tracing, we consider a situation where only individuals recover following treatment, i.e. there is no spontaneous recovery. After individuals have been treated, each of their partners in the last T_{trace} years is contacted with a probability p_{trace}, and all contacted infected individuals seek treatment and recover from

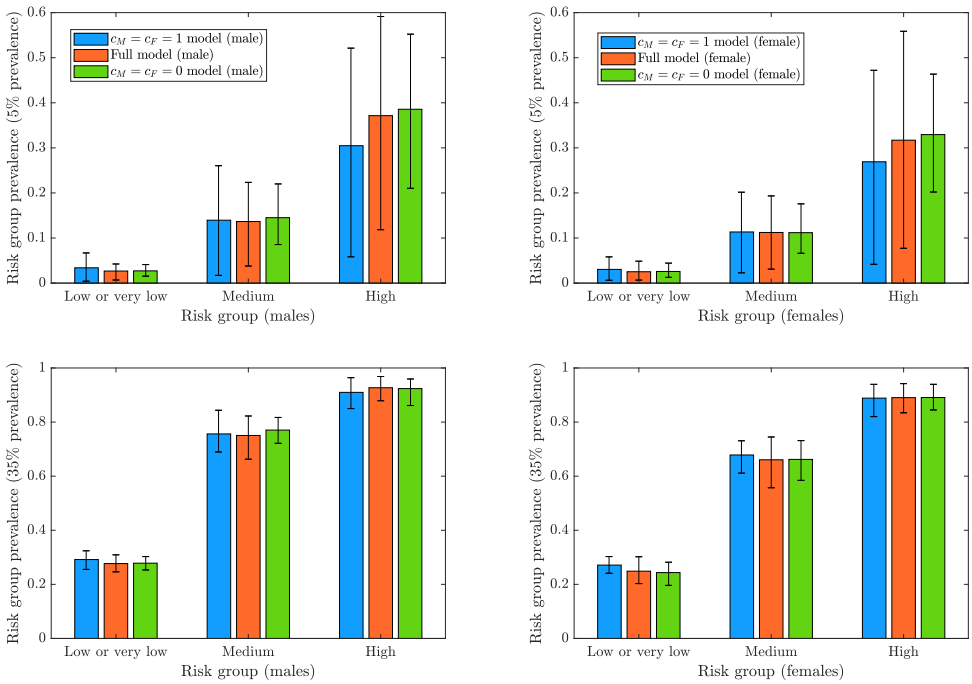

Figure 5.9: **Comparing within risk group prevalence across models.** Here, we compare the differences between within risk-group prevalences across models, when there is an average endemic prevalence of 5% (above) and an average endemic prevelance of 35% (below). In all models, at both prevalences, and across both sexes, within risk-group prevalence increases with risk group. At 5% prevalence, we see a lower prevalence in the high risk males and females for the $c_M = c_F = 1$ model (blue) compared to the full model (orange) or the $c_M = c_F = 0$ model (green), suggesting infection is more diffuse across the population in this model. At 35% prevalence, within risk-group prevalence is fairly consistent across models, despite the different underlying model assumptions. Plotted results are averages of 100 epidemics generated from parameters sampled from the fitted posterior distributions, while error bars indicate 95% prediction intervals.

infection. If individuals are successfully traced, and are infected, their partners in the last T_{trace} years are then contact traced. In this instance, similarly to infection, contact tracing percolates outward from a newly recovered individual.

To compare the impact of control measures acting on the full simulation model against results obtained from $c_M = c_F = 0$ and $c_M = c_F = 1$ models, we match models to prevalence data, finding the probability of infection required to obtain

a certain mean endemic prevalence for each model. To assess the impact of vaccination, we consider a sexually transmitted infection where there is 35% endemic prevalence, reflecting the pre-vaccination prevalence of HPV of females aged 16-24 years in England prior to vaccination [Howell-Jones et al., 2012]. To assess the impact of contact tracing, we consider a sexually transmitted infection where there is 5% endemic prevalence, a prevalence comparable to that of chlamydia [Gray et al., 2009; Public Health England, 2019].

5.4.4 Control by vaccination results

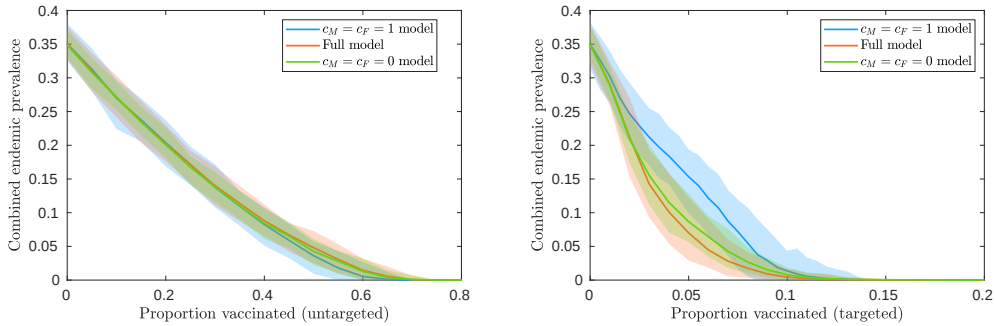

Figure 5.10: **Comparing the impact of untargeted and targeted vaccination across models.** Here,we compare the impact of untargeted (left) and targeted (right) vaccination on combined endemic prevalence, for the $c_M = c_F = 1$ model (blue), the full model (orange), and the $c_M = c_F = 0$ model (green). For untargeted vaccination, as the proportion of the population who are vaccinated, all three models similar trends. For targeted vaccination, while models follow different trends, the required level of targeted vaccination to eliminate the disease is similar across models. Plotted results are means of 100 epidemics generated from parameters sampled from the fitted posterior distributions, with shaded areas referring to 95% prediction intervals.

Setting the probability of infection for each model to be such that there is 35% endemic prevalence within each model, we consider the impact of vaccination. First, we consider the impact of untargeted vaccination, where vaccinated individuals are chosen at random across the population. Prevalence within the population follows similar trajectories in all three models, in particular the full model and $c_M = c_F = 0$

models (Figure 5.10). For the $c_M = c_F = 1$ model, a slightly lower proportion of the population is required to bring the disease to below 0.1% prevalence - (70.7%, while the full model and the $c_M = c_F = 0$ model both require 74.7% to be vaccinated), although all required levels of vaccination fall into a small range. This echoes our previous finding from Chapter 4 that models assuming serial monogamy and models matched to observed levels of concurrency require similar levels of vaccination to eliminate a disease, when models are matched to prevalence data. More novel, and perhaps more surprising given the radically different underlying network structure, is the result that same holds true for models that assume partnership formation rates are independent of relationship status, as in the $c_M = c_F = 1$ model.

We also considered the impact of targeted vaccination, whereby those in high-risk groups are vaccinated first, followed by those in medium-risk groups, and so on. Under this strategy, the trajectory of prevalence as the proportion of the population vaccinated increases does differ between models, although the full model and $c_M = c_F = 0$ model remain fairly similar. For a given proportion of the population vaccinated, there is a higher prevalence in the $c_M = c_F = 1$ model, followed by the $c_M = c_F = 0$ model, followed by the full model. Strikingly, the required level of vaccination to eliminate the disease is similar across models, despite these different trajectories of prevalence. To bring prevalence below 0.1%, 13.3% are required to be vaccinated in the full model, compared to 13.4% in the $c_M = c_F = 1$ model and 14.3% in the $c_M = c_F = 0$ model. Notably, this is approximately the combined proportion of medium- and high-risk males in each model, indicating that vaccinating all medium- or high-risk males along with a sufficient number of medium- or high-risk females is enough to eliminate the disease from the population in each model.

The trends in prevalence in males and females mirrors their combined trend for both untargeted and targeted vaccination - this is included in the appendix as Figure B.3.

5.4.5 Control by contact tracing results

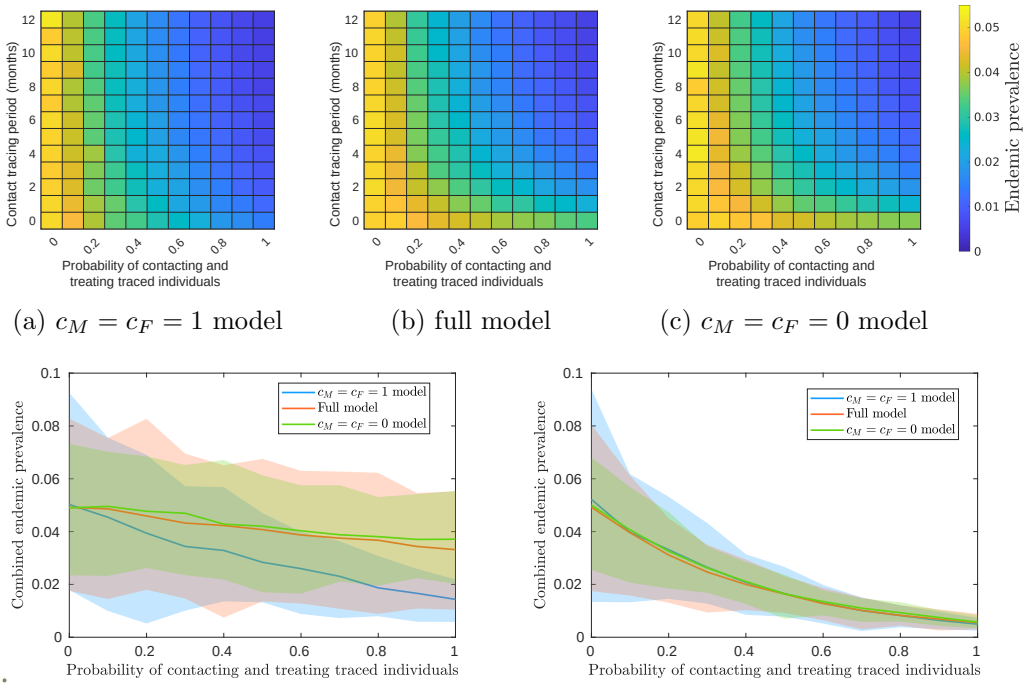

(a) $c_M = c_F = 1$ model (b) full model (c) $c_M = c_F = 0$ model

(d) Current contacts (e) Contacts over 1 year

Figure 5.11: **Comparing the impact of contact tracing across models.** Above, we plot heat maps showing the impact that contact tracing period and the probability of contacting and treating traced individuals has on the combined endemic prevalence, for each model. Below, we focus on the impact of contacting and tracing traced individuals has on prevalence when the tracing period is (d) 0 years and (e) 1 year . Thus the lines in the plots below correspond to first and last rows of the heat maps above. While the impact of a contact tracing with a tracing period of 0 years diverges between models, the impact of contact tracing with a tracing period of 1 year is similar across models. Plotted results are means of 100 epidemics generated from parameters sampled from the fitted posterior distributions, with shaded areas referring to 95% prediction intervals.

In Figure 5.11, we consider the impact of contact tracing, setting the endemic prevalence to be 5% for each model. For higher prevalence infections, contact tracing programmes would likely be logistically unfeasible. A contact tracing programme only contacting current partnerships is least effective in the $c_M = c_F = 0$ model; supposing that all contacts that fall within the contact tracing period are suc-

cessfully traced and treated, such a programme would reduce prevalence to 3.7%. Under the full model, such a strategy reduces prevalence to 3.3%, a slight reduction. While the impact of such a contact tracing programme is similar between these models, a contact tracing programme that only traces current partners is much more effective at reducing prevalence in the $c_M = c_F = 1$ model, reducing prevalence to 1.4%, owing to the larger connected components within the sexual network at any given time and the recursive nature of contact tracing. While the success of contact tracing improves as the period of contact tracing is extended for all models, this improvement is more modest in the $c_M = c_F = 1$ model than in the full model or $c_M = c_F = 0$ model. However, a contact tracing programme that contacts partners over the past year has a very similar impact on population prevalence across models. The trends in prevalence as a consequence of contact tracing in males and females mirrors their combined trend - this is included in the appendix as Figure B.4.

5.5 Discussion

Mathematical models are a vital tool for assessing the impact of public-health control measures against STIs. While models used to assess the adequacy of real-world interventions always aspire to realism, they must necessarily make some simplifying assumptions. Knowing which modelling assumptions have a significant impact on epidemiological outcomes, and which features have little bearing on the final outcomes of modelled interventions, is therefore of particular interest to the applied modeller.

The implications of differing assumptions surrounding concurrent partnerships are of particular interest. Different public health models of STI spread make different assumptions surrounding concurrent partnerships, some assuming serial monogamy (e.g. Datta et al. [2018]), others assuming partnership formation rates independent

of relationship status (e.g. Choi et al. [2010]), but the implications this has on the underlying network structure is relatively unexplored [Leng and Keeling, 2018]. In this chapter, we introduce a heterosexual simulation model that is capable of being fitted to concurrency, and compare it to alternative models either assuming serial monogamy or partnership formation rates that are independent of relationship status. After fitting these models to observed yearly degree distributions and the proportion of singles, we find that the underlying structure of the population is similar in some respects, but differs drastically in others. While fitted models share a similar risk structure - with similar proportions of low-, medium-, and high-risk males and females across models, they differ significantly in their instantaneous network structure. In particular, assuming that formation rates are independent of relationship status leads to a significant proportion of individuals being involved in multiple partnerships at once, which may lead to large connected components within the sexual network at any given time. In contrast, individuals involved in three partnerships scarcely occur when models are fitted to yearly concurrency data, resulting in a sexual network dominated by islands of very small connected components.

While these models differ in their underlying network structure, the vital question for public health is whether these differences impact the success of interventions. While previous studies have confirmed that, other things being equal, increased levels of concurrency within a population results in a higher prevalence of infection [Watts and May, 1992; Morris and Kretzschmar, 1997], our previous work has shown that when models are matched to prevalence data, pair-formation models matched to concurrency data give similar predictions on required levels of vaccination to pair-formation models assuming serial monogamy [Leng and Keeling, 2018]. Here, we extend this work by considering the impact of concurrency in a more realistic setting, using models that account for the heterogeneity in the number of new partnerships individuals form in a year. This chapter confirms that the main

result of Chapter 4 holds despite the inclusion of greater realism - that models explicitly matched to concurrency data yield similar results to those not matched to concurrency, when all models are matched to prevalence data. Given the uncertainty surrounding available concurrency data, this result should be reassuring for modellers interested in public health.

All models considered yielded similar levels of vaccination required to eliminate the disease from the population, when vaccination is untargeted. Perhaps more surprisingly, the same is true when considering targeted vaccination, where individuals who form partnership at a higher rate are vaccinated first - in this instance, around $10-15\%$ of the population must be vaccinated. This proportion is roughly equal to the combined proportion of males in medium- and high-risk groups, meaning that in the models considered vaccinating all medium- or high-risk males and enough medium- or high-risk females was sufficient to eliminate the disease from the population. This reiterates the standard result that the spread of sexually transmitted infections is driven by a 'core group' of active individuals [Yorke et al., 1978]. Further, it underlines the importance of capturing heterogeneity in the number of partnerships in models of sexual networks, which appears to be a key determinant of the critical level of vaccination.

The results from our three models diverge when it comes to contact tracing, when only current contacts are traced. Because of the interconnected structure of the network that emerges from assuming partnership formation is independent of relationship status, contact tracing is much more successful in this model than either the model assuming serial monogamy or the model that has been fitted to yearly concurrency data. However, when contacts from the previous year are traced, the results are extremely similar across models. In some ways, this is unsurprising - all models have been fitted to yearly degree distribution data, hence the distribution of number of partnerships are the same across models. However, models deviate significantly both in their instantaneous network structure and in their yearly

levels of concurrency. This reiterates the point above - that the success of control measures appears to be largely determined by the underlying heterogeneity in risk, and accurate of models of concurrency may not be needed to obtain reliable results.

Heterosexual network models face the specific challenge of satisfying two distinct degree distributions from just one dynamic process. This chapter introduces a generic framework for modelling heterosexual networks, capable of being fitted to arbitrary observed male and female degree distributions. At the extremes of concurrency behaviour (serial monogamy or formation rates independent of relationship status), we provide methods to obtain the expected yearly degree distributions exactly. While these models are capable of having a large number of risk groups, we find that the optimal choice of risk groups is relatively modest (three or four risk groups for males and females). This suggests it may be feasible to design deterministic models, such as pair-formation models [Kretzschmar and Heijne, 2017], that are capable of capturing the required heterogeneity in risk, that have a manageable number of equations.

This study has several limitations regarding the underlying population. Firstly, the models do not account for age structure explicitly, assuming a closed population of 16-24 year olds. In reality, individuals age. As individuals age, their sexual behaviour, which translates to their rate of forming new partnerships, changes. Furthermore, 16-24 year olds do not exclusively form relationships with individuals who are the same age, as detailed by Smid et al. [2018]. While we believe that our framework is robust and flexible enough to incorporate age structure, doing so is beyond the remit of this study. Secondly, we only consider heterosexual contacts. While many individuals will be exclusively heterosexual, some individuals will also have homosexual sexual partners. The interplay between these populations may be necessary to realistically model the spread of many STIs in heterosexual populations, particularly those STIs that have a higher prevalence among MSM.

This study also makes several simplifying assumptions surrounding the underlying disease dynamics - considering no specific STI, but a generic STI with SIS-dynamics. In particular, by assuming that infected individuals recover at a constant rate, we assume that durations of infection are exponentially distributed. While this assumption is common within the literature, for some STIs this may be unrealistic. Further, this model does not model sex acts explicitly - we assume that individuals are infected at the start of relationships or not at all, according to some fixed probability. While this does capture an observed feature of sexual transmission, it overlooks that individuals may be more likely to engage in riskier behaviour, such as sex without a condom, as a relationship progresses. It also overlooks the potential impact of coital dilution, i.e. if an individual is engaged in multiple relationships, they may engage in fewer sex acts with any one of those relationships [Gaydosh et al., 2013]. When constructing realistic models for public health, the above factors should be considered.

In summary, in this chapter we define a generic dynamic network simulation model, consisting of an arbitrary number of male and female risk groups, that can be fitted to observed yearly degree distribution and concurrency data. Additionally, we describe two exact methods for obtaining the yearly degree distribution data, at either of the extreme assumptions surrounding concurrency. Moreover, we use these models to assess the impact of concurrency on control measures in a realistic setting, when models are matched to prevalence data. Our results provide further evidence that the impact of concurrency on control measures is relatively limited - for all interventions considered, similar results are garnered from the model assuming serial monogamy and the one matched explicitly to concurrency. Doing so, this chapter provides further insight into the behavioural features of sexual networks most important to capture when designing models for public health.

5.6 Conclusion

The research in this chapter provides a further evaluation of the importance of capturing concurrency when modelling public-health interventions to control the spread of STIs. The findings corroborate the results from Chapter 4 - that explicitly matching models to concurrency may not be necessary to obtain forecasts for the control of STIs. However, it should be stressed that the importance of capturing concurrency, or any other network property, will depend both on the question being asked, and the data available. If data concerning the probability of infection across partnerships is more readily available than prevalence data, and if one is interested in inferring the early growth rate of an epidemic, then capturing concurrency will still be vital.

To evaluate the importance of capturing concurrency, we have created a flexible framework for modelling dynamic heterosexual networks, capable of being fitted to data from surveys such as Natsal. While this model does not include age-structure, or interactions between heterosexual and homosexual populations, we believe that this framework is capable of being extended to include such heterogeneities. While we consider a generic STI with relatively simple disease dynamics, incorporating the infectivity and recovery profile of a specific STI should also be achievable. With the advent of the next Natsal survey, Natsal-4, this framework may provide a useful tool for both researchers interested in modelling public health interventions and researchers interested in exploring the impact of explicitly fitting models to other features of network structure.

Chapter 6

Clustering: the effectiveness of social bubbles as part of a COVID-19 lockdown exit strategy

The research in this chapter has been presented in Leng et al. [2020].

6.1 Introduction

In this chapter, we move away from sexually transmitted infections (STIs), and consider the application of network modelling to a pathogen operating on an altogether different underlying contact network - severe acute respiratory syndrome coronavirus 2 (SARS-CoV-2), the virus responsible for coronavirus disease 2019 (COVID-19). SARS-CoV-2 is a respiratory pathogen, transmitted via respiratory droplets generated from coughing, sneezing, and breathing [Huang et al., 2020]. Because of this, an infected individual has the potential to infect their friends, their family, their colleagues, and their chance encounters, in contrast to the much more restricted relevant contact network in the case of STIs. As discussed in Chapters 1

and 2, because of the transience and uncertainty of aspects of the underlying relevant contact network, modelling the spread of such pathogens is not easily amenable to a network modelling approach.

This changed in March 2020. In response to the ensuing COVID-19 pandemic, and informed by modelling suggesting that inaction would result in health services being overwhelmed and a large number of deaths [Ferguson et al., 2020; Davies et al., 2020], governments across the world imposed strict restrictions on people's social interactions, colloquially known as 'lockdown'. In the UK, individuals were told to stay at home as much as possible - measures included the closure of schools, non-essential retail, bars, restaurants, and leisure facilities, asking all those who were able to work from home to do so (alongside furloughing a large proportion of the work force), as well as restricting households from mixing with one another. People's social interactions, previously transitory and varied, had become fixed and limited.

By severely restricting these social interactions, the UK was successful in reducing transmission of SARS-CoV-2, alleviating the burden on the healthcare system [Flaxman et al., 2020]. However, such stringent restrictions come at a high societal, economic, and wider health cost [Cluver et al., 2020; Forman et al., 2020; Appleby, 2020]. As infection incidence has declined, countries have had to consider ways to ease restrictions that still ensure that the epidemic remains under control [Gilbert et al., 2020; Keeling et al., 2021]. Multiple options have been suggested and implemented in different countries, including the widespread use of contact tracing in conjunction with testing and household isolation [Ferretti et al., 2020; Kucharski et al., 2020], expanded random testing in order to detect asymptomatic and presymptomatic individuals [Liu et al., 2020; Peto et al., 2020], quarantining travellers on arrival to a different country [Clifford et al., 2020; Kraemer et al., 2020], and the use of face masks [Clase et al., 2020; Lustig et al., 2020]. While the stringent lockdown from March to June of 2020 was successful in reducing

transmission, as restrictions have eased infection levels have increased.

Another option that has been suggested, and has been implemented to some extent in several countries such as Germany, New Zealand, and the UK, has been the clustering of contacts beyond the household - referred to as the social bubble strategy. Under this strategy, a household is allowed to enter into a cohesive and exclusive unit with other households. Doing so allows individuals to increase their social interactions beyond their household, but is intended to limit the risk of infection through the exclusivity of the bubble and the clustering such a strategy imposes.

Previous studies have shown that, because of a reduced number of new contacts in the second and subsequent generations, the average number of secondary infections from an infected individual is smaller in clustered populations [Keeling, 1999; Keeling and Eames, 2005]. Accordingly, control measures that increase the clustering of contacts have the potential to be an effective way of reducing transmission. Some studies have considered strategies aiming to increase the clustering of social networks specifically as a way of controlling the COVID-19 epidemic. Block et al. [2020] suggest several social reorganisation measures that result in more clustered social networks as a potential way to flatten the curve of an epidemic, while in a parallel study to our own Willem et al. [2021] consider the impact social bubble strategies would have on a population with the structure of Belgium.

Under the social bubble strategy, people's social interactions remain fixed and relatively limited - the only warranted social interactions are within household and within bubble. Because of this, we can use available census data to construct a network of the population's household contacts, and additionally we can use this to define the resulting network of bubble contacts from a given social bubble strategy. By doing so, and by defining an epidemic process on the resulting networks, we can assess the likely impact different social bubble strategies would have on infection

and mortality rates. By comparing these social bubble strategies to unclustered increases in contacts, we can assess the effectiveness of social bubbles induced by the clustering the strategy imposes.

In this chapter, using a stochastic generation-based static network model, we assess the likely increase in transmission resulting from various plausible social bubble strategies. As well as comparing the impact of allowing all households to enter into a social bubble with another household, we consider the impact of limiting bubbles to households who are likely to benefit most. While many adults are able to compensate for the lack of physical interaction with increased social interaction, doing so is harder for young children, for whom verbal interaction is only a small part of their communication with peers. Further, their carers have often had to balance working from home with childcare and homeschooling without the support networks of extended family, friends, and childminders usually available [Minello, 2020]. Single occupancy and single parent households will have also been disproportionately effected as the absence of meaningful face-to-face interaction may negatively impact mental wellbeing [Feys et al., 2020].

Using this model, we assess both the likely increase in transmission and in mortality induced by different social bubbles. By comparing populations under social bubble strategies to populations who have increased their contacts by an equivalent but unclustered amount, we assess the effectiveness of these different social bubble strategies. We assess the sensitivity of our results to a range of alternative model assumptions and parameterisations. By doing so, this chapter informs the potential value of social bubble strategies in the event of future social restrictions. Several studies have suggested that in order to avoid large casualties resulting from the COVID-19 epidemic, intermittent use of further lockdowns, either on a local or national scale, may be necessary over a period of years until a viable exit strategy to the epidemic is found [Keeling et al., 2021; Ferguson et al., 2020]. With this as a possibility, countries must find strategies that control the spread of an epidemic but

allow some semblance of normality in people's social lives. Clarifying the extent to which social bubbles are such a strategy is the aim of this chapter.

6.2 Methods

6.2.1 Population

Constructing household contacts

In order to assess the impact of social bubbles, we created a synthetic population, similar in structure to that of the UK, which we could implement social bubble strategies onto. The model's synthetic population was created by generating individuals who are residents of one of 10,000 households. We assume that each individual belongs to exactly one household, and that households are non-overlapping. The size of households, as well as the age distribution within households, was sampled to match the most recent census of England and Wales 2011 [Office for National Statistics, 2020a]. Specifically, we used data from this census to construct a distribution of age-stratified household compositions in terms of 10-year age bands, with the final age band designating ages 80 years and above. A probability was assigned to each composition observed in the census data based on the frequency of its appearance, and then used these probabilities to construct our simulated household population. This gave us a synthetic population whose age structure was comparable with that of England and Wales and whose household compositions reflected the observed correlations between the ages of household occupants. Of particular importance, doing so should accurately capture the generational structure of households in England and Wales, expected to be an important factor in transmission among age classes, and of interest due to the disproportionate health impact COVID-19 has on older individuals.

Recalling that a network can be represented as an adjacency matrix, the population of household contacts can be represented by the matrix A_H:

$$A_H(i,j) = \begin{cases} 1, & \text{if } i \text{ and } j \text{ are within the same household} \\ 0, & \text{otherwise} \end{cases} \tag{6.1}$$

In this model, we consider a situation similar to the UK lockdown in May 2020, where stringent physical distancing has been implemented, with schools, non-essential retail, and leisure facilities closed. As such, household contacts (prior to the introduction of social bubbles) are the only close contacts individuals have.

Constructing bubble contacts

With the synthetic population defined, we consider a number of potential 'social bubble' strategies, targeting different types of household. The population of social bubble contacts can be represented by the matrix A_B, which can be obtained straightforwardly with an algorithm joining eligible households:

$$A_B(i,j) = \begin{cases} 1, & \text{if } i \text{ and } j \text{ are within the same bubble (but not the same household)} \\ 0, & \text{otherwise} \end{cases} \tag{6.2}$$

Here, we can note some properties of the household and social bubble adjacency matrices A_H and A_B. Social bubbles imply that all members of the same household enter into a social bubble with the same household, which can be expressed as

$$A_H(i,j) = 1, A_B(i,k) = 1 \Rightarrow A_B(j,k) = 1 \tag{6.3}$$

Similarly, an individual being part of a social bubble with one household precludes them from being part of a social bubble with another household:

$$A_B(i,j) = 1, A_H(j,k) = 0 \Rightarrow A_B(i,k) = 0 \tag{6.4}$$

In this chapter, we consider a number of different feasible social bubble strategies, outlined in Section 6.2.5. All scenarios assume that pairing occurs at random between permitted households. In reality, it is likely that social bubbles form in a non-random way, but it is unclear the direction this non-randomness would act in. To some extent households of similar ages, may be more likely to form a bubble with one another - something explicitly accounted for by Willem et al. [2021]. On the other hand, families may choose to form social bubbles with elderly relatives, and young adults may choose to form social bubbles with their parents, resulting in a disassortativity between age groups.

6.2.2 Transmission model

Because SARS-CoV-2 is a novel pathogen, first identified in December 2019 [Huang et al., 2020], it is not known in the long term whether recovery from infection from COVID-19 leads to immunity. However, this appears likely to be the case at least in the short term. Serological studies on other coronaviruses, such as SARS, report immune periods of 2 years [Wu et al., 2007]. Studies estimate that SARS-CoV-2 has a median latent period from infection to infectivity of 5.2 days [Lauer et al., 2020] , followed by a median infectious period of 4-9.5 days [Byrne et al., 2020]. In this chapter, we consider an epidemic over its first 10 generations, i.e. over a period of months since the first infected case in the model. Because of this, in this chapter we model SARS-CoV-2 as a disease with Susceptible-Infected-

Figure 6.1: **An overview of the social bubble model.** Top panel: schematic of model structure and its stratification into different household sizes with three components of transmission dynamics, community transmission, bubble transmission and household transmission. Left panel: household size distribution for all households in England and Wales, for those households with at least one child younger than 20-years-old and for those with at least one child younger than 10-years-old (about primary school age or younger). Right panel: illustrative transmission probability matrix P_A, composed of household and bubble contacts and including community transmission.

Recovered (SIR) dynamics. While an exposed class is common to models of COVID-19 [Keeling et al., 2021; Davies et al., 2020; Ferguson et al., 2020], including such a class in unnecessary for our purposes, as in both SIR-models and SEIR-models the average number of secondary infections from an infected individual is the same, with the distinction only altering the time-evolution of the epidemic [Keeling and Rohani, 2011].

In this model, individuals have three potential sources of transmission: firstly, via

Table 6.1: **Chapter 6 summary of notation.**

Symbol	**Meaning**
A_H	Adjacency matrix of household contacts
A_B	Adjacency matrix of bubble contacts
$C(i)$	Age-dependent susceptibility scaling factor of individual i
$T(i)$	Age-dependent transmissibility scaling factor of individual i
$N_H(i)$	Number of household contacts an individual i has
τ_H	Baseline transmission rate across household contact
P_H	Matrix of transmission probabilities across household contacts
$\rho_H(i,j)$	Household transmission rate from individual j to individual i
τ_B	Baseline transmission rate across bubble contact, $\tau_B = k\tau_H, k \in [0\ 1]$
P_B	Matrix of transmission probabilities across bubble contacts
$\rho_B(i,j)$	Bubble transmission rate from individual j to individual i
ϵ	Baseline mean-field transmission rate
$\epsilon(i)$	Mean-field transmission rate to an individual i
$I_g(i)$	Infection status of individual i at generation g $I_g(i) = 0$ if i is susceptible at generation g $I_g(i) = 1$ if i has been infected by generation g (so includes recovered individuals)
$S_g(i)$	1 - $I_g(i)$, i.e. the susceptibility status of an individual i at generation g
N	Size of population

a household contact; secondly, if they are in a social bubble with another household then via a bubble contact; and finally, via the general population through mean-field transmission. We define a baseline transmission rate across household contacts as τ_H, a baseline transmission rate across bubble contacts as τ_B, and a baseline mean-field transmission rate ϵ. For all routes of transmission, we assume that susceptibility *to* infection as well as transmissibility *of* infection is potentially age dependent. We let $T(i)$ denote the (age-dependent) transmissibility of an individual i, a factor which scales the rate at which i transmits infection. Similarly, we let $C(i)$ denote the (age-dependent) susceptibility of an individual i, which scales the rate at which i becomes infected from an infected contact of theirs. We consider transmission across close contacts (household or bubble) and transmission from the general population separately. The notation used in this section is summarised in Table 6.1.

Transmission across close contacts

Transmission rates across household contacts are derived by assuming that interaction between close contacts is frequency dependent, in line with observational studies showing that an individual's risk of SARS-CoV-2 infection from a specific household member decreases with household size [Streeck et al., 2020]. Frequency dependent transmission across household contacts has also been assumed in household models of influenza [Cauchemez et al., 2004]. We also assume that transmission is frequency dependent across bubble contacts. In this instance, care must be taken, as bubble contacts i and j in general do not have the same set or number of bubble contacts (recall that i is a bubble with contacts with every member of j's household, and vice versa). This is similar to Chapter 5 when considering the rate of partnership formation in a heterosexual population, and has an analogous solution. We do so by decomposing interaction between individuals i and j into interactions led by i and interactions led by j. The amount of interaction led by i (or j) depends on the number of other close contacts i (or j) has. The total amount of interaction, hence the rate of transmission, is given by summing these interactions. Finally, to obtain the specific transmission rate from j to i, we multiply this rate of interaction by the rate of transmission given interaction between the two individuals. Letting $N_X(i)$ denote the number of relevant social contacts an individual i has, the transmission rate across close contacts $\rho_X, X \in \{H, B\}$ is given by:

$$\rho_X(i,j) = T(j)C(i)\tau_X \times \left(\frac{A_X(i,j)}{N_X(i)} + \frac{A_X(i,j)}{N_X(j)} \right) \tag{6.5}$$

For transmission across household contacts, this becomes:

$$\rho_H(i,j) = \begin{cases} \frac{2T(j)C(i)\tau_H}{N_H(i)}, & \text{if } A_H(i,j) = 1 \\ 0, & \text{otherwise} \end{cases} \tag{6.6}$$

an expression equivalent to the standard frequency dependence transmission formula. For transmission across bubble contacts however, we obtain the following expression (after noting that $N_B(j) = N_H(i) + 1$):

$$\rho_B(i,j) = \begin{cases} T(j)C(i)\tau_B(\frac{1}{N_H(i)+1} + \frac{1}{N_H(j)+1}), & \text{if } A_B(i,j) = 1 \\ 0, & \text{otherwise} \end{cases} \tag{6.7}$$

Assuming transmission occurs at a constant rate across relevant contacts over the course of an individual's infectious period, and with an individual's infectious period equalling one generation, we obtain the elements of the probability matrices P_H and P_B, the matrices of within household and within bubble transmissions respectively by taking:

$$P_X(i,j) = 1 - e^{-\rho_X(i,j)}, X \in \{H, B\} \tag{6.8}$$

We obtain the overall probability matrix of the close contacts for the population by taking $P_A = P_H + P_B$. This is used to drive forward the stochastic dynamics of the simulated epidemics via a next-generation approach, described in the Model set-up.

To obtain equations assuming density-dependent transmission, the dividing N_H terms are omitted from from Equations (6.6) and (6.7), which is an assumption considered in the sensitivity analysis.

Community transmission

The exact expression determining an individual's rate of transmission from the community depends on whether we assume that individuals interact with the population at large at a constant rate or whether we assume that households interacts with the population at a constant rate. If we assume the former, then mean-field transmission to an individual i, denoted $\epsilon(i)$, is given by standard frequency dependence assumption, once the relative susceptibility and transmissibility of individuals is taken into account:

$$\epsilon(i) = C(i)\epsilon\frac{\sum_j T(j)(I_g(j) - I_{g-1}(j))}{N} \tag{6.9}$$

However, we consider a situation where we assume that households are adhering to lockdown restrictions and social distancing, and therefore largely act as a coherent and largely isolated unit. Because of this, we assume that the risk of a household acquiring infection from the community is independent of its number of occupants as observed in a cross-sectional serological study for SARS-CoV-2 in Germany in March and April [Streeck et al., 2020]. To capture this, we assume that the mean-field transmission to an individual, as well as an individual's contribution to mean-field infection, is inversely proportional to the number of individuals in their household:

$$\epsilon(i) = \frac{C(i)\epsilon}{N_H(i)}\frac{\sum_j T(j)(I_g(j) - I_{g-1}(j))N_H^{-1}(i)}{\sum_i N_H^{-1}(i)} \tag{6.10}$$

Model set-up

To simulate an epidemic, we begin by randomly sampling the probability matrix P_A, i.e. the connection from individual j to individual i is retained with probability $P_A(i,j)$. Doing so, we retain only the infectious connections between individuals that will lead to an infection. These sampled probability matrices therefore represent *potential* transmission networks (though the exact transmission network for a given simulation will depend upon who is initially infected). Because these sampled matrices refer to transmission events rather than contacts, this matrix may be unsymmetric. We refer to the sampled matrix as P'_A. $P'_A(i,j) = 1$ denotes that individual j will infect individual i with probability 1, given individual j is infected. Initially infected individuals are chosen with probability proportional to their mean-field interaction, i.e. with a probability inversely proportional to their household size. Letting I_g be the vector of infection statuses of individuals in generation g, we obtain the next generation by:

$$I_{g+1} = sign((P'_A + \mathbb{I}) \times I_g) \tag{6.11}$$

where $\mathbb{I}$ is the identity matrix, and where $sign()$ is an element-wise function equal to 1 for each positive element and 0 otherwise. Via this matrix multiplication, every newly infected individual in generation g infects all of their infectious contacts that generation. Here, the identity matrix is added to impose that individuals do not become susceptible again after one generation, while the sign function is used to impose that individuals cannot be infected more than once. This process can be iterated until equilibrium is reached, and the epidemic has ended. To this, we also mean-field transmission. Each generation, the number of new infections is calculated in order to calculate $\epsilon(i)$ for each susceptible individual i, who is infected from mean-field transmission with probability $1 - e^{\epsilon(i)}$ each generation.

Recovery from infection is not explicitly modelled in the simulation, but rather is

implicitly built into the structure of the model. If an individual i is infected in generation g, they will infect all of their transmission contacts in generation $g+1$ via the matrix multiplication. They also only contribute to community infection in generation $g+1$. While individual i remains 'infected' (with value 1), they no longer play any role in the infection dynamics, nor can they be reinfected. Hence, the simulation model assumes that individuals are infectious for one generation, before recovering with immunity.

While in this chapter, we consider a disease in which recovery from infection leads to immunity, this modelling framework could be easily adapted to diseases with other dynamics. For example, to consider a disease where recovery from infection does not lead to immunity (i.e. SIS-dynamics) $\mathbb{I}$ can be omitted from Equation (6.11).

6.2.3 Outcome metrics

We assess the epidemiological impact of interventions in our simulation model using two key metrics. Firstly, the net reproduction number, R, which relates to epidemic risk, and secondly the relative increase in mortality, a measure of adverse health outcomes. Results are averages obtained from simulations of 1000 epidemics for 10 different sampled epidemic networks, hence results are averages of 10000 simulations. The value of R and the number of fatalities obtained from any single simulation varies considerably owing to the stochasticity of the underlying dynamics, while there is much less variability between average values from 1000 epidemics values obtained for different sampled networks (Figure 6.2). The variation in R values obtained from single simulations does not imply different rates of onward transmission between simulations; rather, this variability is a consequence of the small number of infected individuals in the generation used to measure R as well as the contact structure of those particular individuals.

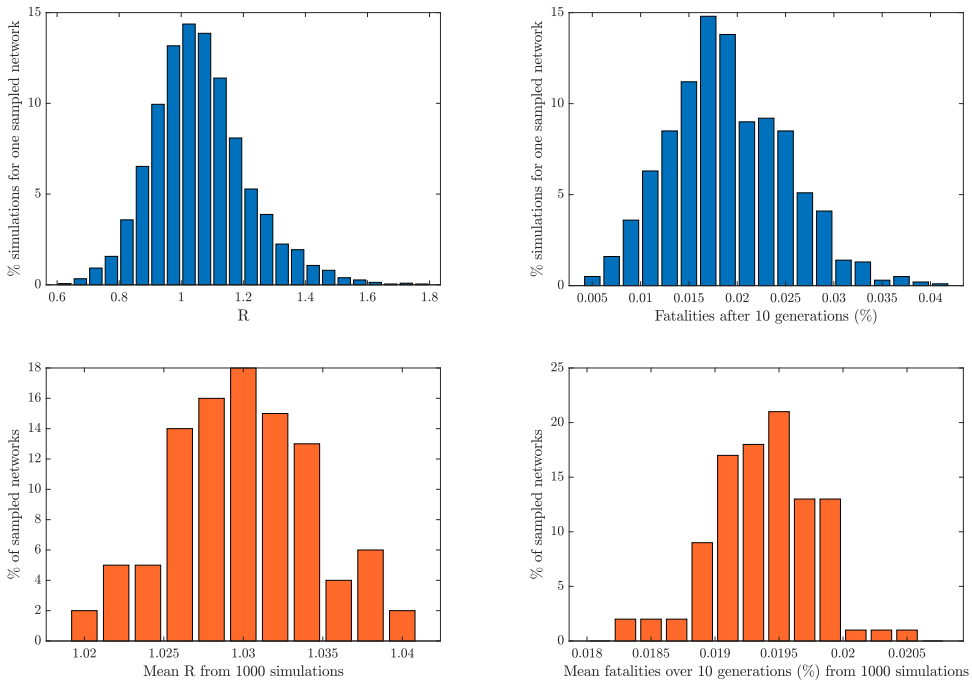

Figure 6.2: **Exploring the variability of R and fatalities.** Above, we explore the variability in outcome metrics between simulated runs on one sampled network, using Scenario 6 as an example. We plot histograms of R and the percentage of fatalities over 10 generations obtained from 1000 single simulated epidemics over one sampled network. Below, we explore the variability between in outcome metrics between sampled networks, where obtained values are averages of 1000 epidemics. We plot histograms of the mean values R and the percentage of fatalities over 10 generations obtained from 1000 simulations, for 100 different sampled networks.

Net reproduction number

Reproduction numbers are quantities central to the study of infectious diseases, all of which try to capture the average number of secondary infections generated by an infected individual, though there are numerous definitions applicable to different scenarios. Central to the concept of reproduction numbers are their thresholding properties - a value greater than 1 is required for an epidemic to occur. For randomly mixing populations, the basic reproduction number, R_0, is defined as the expected number of infected individuals infected by an initially infected individ-

ual, over the course of their entire infectious period. In this instance, R_0 can be calculated by taking the dominant eigenvalue of the next-generation matrix, the method developed by Diekmann et al. [1990]. However, such a method is unsuitable when considering a population with households. In this instance, the dominant eigenvalue does not possess the threshold property desired of reproduction numbers, and does not account for the early local depletion of susceptibles household structure imposes [Pellis et al., 2009]. Accordingly, alternative metrics have been proposed for populations composed of households [Pellis et al., 2012] . However, even in simpler models than ours, the formal derivation of R for households can be involved. Therefore, we take a numerical approach to calculating R. We wish to capture the number of secondary infections generated by a *typical* case. In models incorporating household structure, the typical case is effectively an average over the probability that such a case is the first, second, third or later generation case within the household [Ball et al., 2009]. Following the principle of Pellis et al. [2012], using an approach similar to House and Keeling [2011a], we determine the net reproduction number R numerically as the ratio of the number of new infections in the fifth to the fourth model generation, adjusted to account for the partial depletion of susceptibles. We obtain this by rearranging the equation for I from the standard SIR model, expressed as a difference equation [Allen, 1994]:

$$I_{n+1} = I_n(1 - \gamma\Delta t + \frac{\alpha\Delta t}{N}S_n) \tag{6.12}$$

where γ is the probability of removal in a time period Δt and α is the average number of individuals an infected individual would infect if all of their contacts were susceptible. In such a case, $R = \alpha/\gamma$. Our model progresses in steps of 1 generation (i.e. $\Delta t = 1$ generation), and individuals recover with probability 1 in a generation (i.e. $\gamma = 1$). Hence, in our model $\alpha = R$, and by substituting terms

and rearranging we obtain:

$$I_{n+1} = I_n \times R\frac{S_n}{N} \iff R = \frac{I_{n+1}}{I_n} \times \frac{N}{S_n} \tag{6.13}$$

Expressing time in terms of generations, g, and recalling in our model I_g (S_g) refers to the vector of infection (susceptible) statuses in generation g, we thus define $R(g)$ as

$$R(g) = \frac{\sum_i I_{g+1}(i)}{\sum_i I_g(i)} \times \frac{N}{\sum_i S_g(i)} \tag{6.14}$$

In all scenarios we observed that $R(g)$ decreases markedly in the first generation. In most cases, we observed that $R(g)$ continued to decrease by a much smaller amount over the next couple of generations, but in some cases $R(g)$ increased by a small amount between the second and third generation. In all scenarios, we observed $R(g)$ stabilises at a value that persists over several generations (Figure 6.3) by the fourth generation. Because of this, we take $R(4)$ as our estimate of R.

Relative mortality

Our second metric is the relative mortality (i.e. number of deaths), compared to a baseline scenario of isolated household with no social bubble strategy implemented. Doing so provides a measure of adverse health impacts as a result of the increased contact rates caused by the implementation of a given social bubble strategy. We use age-stratified infection fatality rates (IFR) estimated from repatriation flights early in the COVID-19 pandemic [Verity et al., 2020] to predict the mortality risk from the fourth to the ninth generation, i.e. once R has stabilised. Roughly,

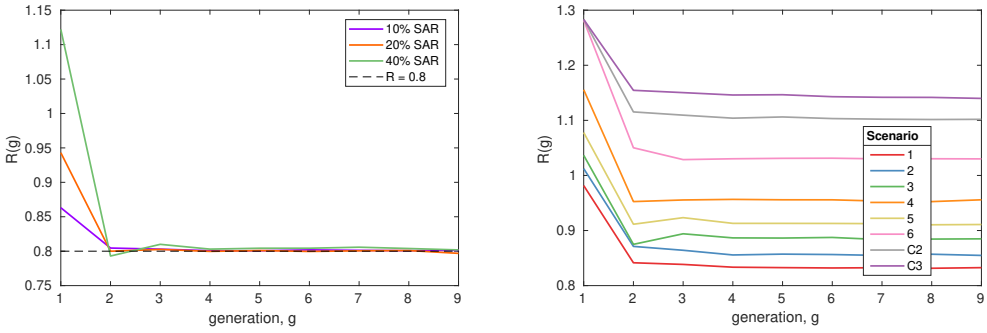

Figure 6.3: **Numerical exploration of R by generation**. Left shows examples of the method for which ϵ was fitted to satisfy $R(4) = 0.8$ under our baseline parameters for different household secondary attack rates. Right shows $R(g)$ by generation from each of our scenarios from our baseline parameterisation. In both plots, $R(g)$ decreases over the first few generations, before reaching an equilibrium value that persists over multiple generations.

this measures the relative mortality in the second month after social bubbles were initiated.

Each simulation is initiated with the required number of infectious individuals for 1% of the population to be infected by generation 4, in order for the fatalities following this generation to be meaningfully compared. This is achieved by choosing arbitrary an initial number of infected individuals, $I_{init}(1)$, and observing the resulting proportion of the population infected by generation 4, $I_{init}(4)$. Doing so, we obtain an estimate of the required number of initial infected individuals for a prevalence of 1% in generation 4, given by $(0.01 \times I_{init}(1))/I_{init}(4)$, a strategy we find works well.

6.2.4 Parameterisation

To parameterise the COVID-19 transmission dynamics in the model we need to define the infection dynamics within a household, within a bubble and from the community. To parameterise the within household transmission we assume that the secondary household attack rate, SAR_{HH}, is 20%. This is in line with observations

from contact tracing [Koh et al., 2020; Bi et al., 2020] while accounting for some underreporting. This is achieved by finding the value of τ_H which results in 20% of connections between individuals remaining after sampling the probability matrix, which is achieved through tuning. In this chapter, we consider a situation similar to the lockdown in the UK of May 2020. At this time, R was estimated to be approximately between 0.7 and 1 [GOV.UK, 2020a]. Accordingly, we assume that community transmission is such that, in combination with household transmission, the model generates an overall reproduction number of 0.8. As a base case, we assume that transmission between social bubble contacts, i.e. between households within the same bubble, is 50% lower than between household contacts, i.e. $\tau_B = 0.5\tau_H$.

The role that age plays in an individual's susceptibility and transmissibility is complex. While it has been observed that children are more likely to experience mild or no symptoms, meaning that they may have a lower transmission rate, cases with more severe symptoms are likely to self-isolate, reducing their infectious period. Consequently, children that are asymptomatic or mildly symptomatic may continue to transmit for longer. In our base parameterisation, we assume that children (less than 20-years-old) are half as susceptible to infection as adults (20 to 59-years-old) or older adults (60-years-old or above) but assume that transmissibility is independent of age, echoing the assumptions of a previous study [Davies et al., 2020]. An alternative parameterisation based on other work [Keeling et al., 2021] is considered as part of our sensitivity analysis, where transmissibility is age-dependent.

Under this parameterisation, we find that a 3.75-fold increase in community contacts yielded a reproduction number of about 2.5, in line with an approximate 70% reduction in contacts during lockdown and a reproduction number of about 2.5 in the early phase of the pandemic, when little to no distancing measures were in place [Jarvis et al., 2020].

Table 6.2: **Key model parameters and assumptions.**

Parameter	**Description**	**Value (base case)**	**Value (sensitivity)**	**Source**
-	Household structure and age distribution	-	-	Office for National Statistics [2020]
τ_H	Baseline household transmission rate	0.345 (20% SAR)	0.155 (10% SAR) 0.86 (40% SAR)	Matched to SAR Koh et al. [2020] Bi et al. [2020]
τ_B	Baseline bubble transmission rate	$0.5 \times \tau_H$	τ_H $0.1 \times \tau_H$	Assumption
$T(i)$	Relative transmissibility compared to adult	1 (child) 1 (older adult)	0.64 (child) 2.9 (older adult)	Davies et al. [2020] Keeling et al. [2021]
$C(i)$	Relative susceptibility compared to adult	0.5 (child) 1 (older adult)	0.79 (child) 1.22 (older adult)	Davies et al. [2020] Keeling et al. [2021]
-	Infection fatality rate	In 10 year age bands	-	Verity et al. [2020]
R	net reproduction number	0.8	0.7, 0.9	GOV.UK [2020a]
ϵ	Baseline mean-field transmission rate	1.13 (20% SAR)	1.29 (10% SAR) 0.925 (40% SAR)	Matched to R given τ_H

We additionally assume that all eligible households would take up the opportunity to expand their contacts and enter into a social bubble with one other household, and that they would adhere to the exclusivity of this bubble. The impact of only partial uptake is explored in our results, and , the impact of non-adherence, incorporated by allowing 50% of eligible households to form an additional social bubble, is explored in our sensitivity analyses. Table 6.2 summarises the key model parameters and assumptions, as well as alternative parameterisations and their sources.

6.2.5 Scenarios modelled

In this chapter, we consider six different feasible social bubble strategies, which we refer to as Scenarios, targeted at different types of households.

1. Allow households with children younger than 10-years-old (about primary school age or younger) to pair up.

2. Allow households with children younger than 20-years-old to pair up.

3. Allow single occupancy households to pair up with another single occupancy household.

4. Allow adults who live alone or with dependent children only to pair up with another household of any size in a 'support bubble' - the social bubble strategy implemented in the UK as of June 2020.

5. A combination of Scenarios 1 and 3.

6. Allow all households to pair up with another household.

Another potential strategy we began to consider was to allow all households with two or fewer adults to form a bubble with households of any size - an extension to the current situation in England. However, as 87.7% of households have two or fewer adults, we found that such a policy would result in 98% of households forming bubbles, such a policy would have largely the same impact as allowing all households to form bubbles.

To assess the impact social bubbles strategies have, we compare our results to three counterfactual scenarios:

C1. Perfect adherence to the household-only contact strategy (other than the background transmission risk from the community), i.e. a scenario where no social bubbles are implemented.

C2. Individuals increase their number of contacts, making the same number of infectious contacts as in Scenario 6, but contacts are unclustered and chosen at random. In this scenario, contacts are fixed, staying the same for each generation.

C3. Individuals increase their number of contacts, making the same number of infectious contacts as in Scenario 6, but contacts are unclustered and chosen at random. In this scenario, contacts vary over time, changing each generation.

Counterfactual scenarios C2 and C3 maintain the same number of infectious contacts each individual makes. Both scenarios are obtained by taking the sampled probability matrix of bubble connections, P'_B, from Scenario 6 and *rewiring* contacts. We do this by swapping edges in the adjacency matrix. The sampled probability matrix P'_B is a directed and asymmetric adjacency matrix - just because an infected individual j would infect an individual i, the same is not necessarily true vice versa, as the probabilities $P_B(i,j)$ and $P_B(j,i)$ are sampled independently. However, $P_B(i,j)$ and $P_B(j,i)$ are often both sampled due to i and j being close contacts. To capture this correlation when rewiring for counterfactual C2, we rewire directed edges (where $P'_B(i,j) = 1$ but $P'_B(j,i) = 0$) and undirected edges (where $P'_B(i,j) = P'_B(j,i) = 1$) separately. For counterfactual C3, no such correlation exists, as an individual chooses new contacts each generation, and hence all connections are treated as directed edges and rewired independently. As well as generating these counterfactual scenarios, we can also use this method to generate scenario specific counterfactual Scenarios, e.g. a C2 and C3 for Scenario 1, to assess the specific effectiveness of social bubbling in that instance.

6.2.6 Sensitivity analyses

Other than the previously described base case, we performed a number of univariate sensitivity analyses to test the robustness of our findings to the underlying assumptions. Specifically, we consider:

1. that the current value of R prior to the introduction of social bubbles is 0.7 and 0.9, instead of 0.8 [GOV.UK, 2020a].

2. that the secondary attack rate within the household is 10% or 40%, instead of 20% [Koh et al., 2020].

3. that $\tau_B = \tau_H$ or $\tau_B = 0.1\tau_H$, instead of $\tau_B = 0.5\tau_H$

4. that a household's risk of infection from the community increases with household size, as in Equation (6.9), instead of being independent from household size, as Equation (6.10).

5. that transmission across close contacts is density dependent rather than frequency dependent.

6. that 50% of eligible bubbles do not adhere to the recommendations, forming bubbles with an additional household, instead of perfect adherence.

7. that households including an individual over 70-years-old do not form bubbles.

8. that the relative susceptibility to infection of children and older adults compared to adults is 79% and 125% while the relative transmissibility is 64% and 290%, respectively [Keeling et al., 2021].

We model non-adherence to the strategy by allowing 50% of eligible households to enter into close contact with an additional household. Doing so means that bubbles are no longer mutually exclusive, and that chains of transmission could potentially span many households. Letting P_{B2} denote the probability matrix of additional bubbles through non-adherence, P_A is now obtained by the sum of P_H, P_B and P_{B2}.

6.3 Results

6.3.1 Households

We begin by observing several relevant descriptive statistics we can obtain by analysis of the age-distribution data of households obtained from the 2011 census of England and Wales [Office for National Statistics, 2020a]. Considering all households, the average size of a household was 2.36 persons. When we consider households

with at least one child under 10-years-old, the average household size increases to 3.89 persons, and 30.4% of the population live in such households. For households with at least one child under 20-years-old, the average household size is 3.73 persons, and 49.5% live in such households. In total, 37% of households are occupied by someone over the age of 60 years, and 50% of single occupancy households were occupied by such older adults. Single occupancy households comprise 30.2% of households. There is limited multi-generational mixing, with only 3.6% of households having both a child aged under 10 years and an adult aged over 60 years. Less than 0.7% of households are occupied by more than 6 persons, and less than 0.03% are occupied by more than 10 persons. The largest household in our modelled population comprises of 15 persons. An infected individual in a large household may result in a high number of secondary infections, particularly under the assumption of density dependence, but such households represent a very small proportion of all households, both in our model and in the 2011 census of England and Wales.

6.3.2 Impact of social bubbles on epidemic risk

Here, we consider the impact different social bubble scenarios have on R. Under our base parameterisation, we find that Scenarios targeting households with children (Scenarios 1 and 2) have the smallest impact on R, increasing R to a value of 0.83 and 0.86 respectively. The relatively small impact of social bubbles in these instances is owed to a combination of the lower susceptibility of children to infection and the assumption that households act as a cohesive unit when interacting with the community, reducing any given individual within that household's interaction with the community. Strategies that exclusively target single-person households (Scenario 3) also do not increase transmission substantially, increasing R to a value of 0.89. Scenario 5, the combination of Scenario 3 and Scenario 1 (the more conservative scenario allowing households with children to enter social bubbles) increases R to a value of 0.91. For these two targeted strategies, even under conservative

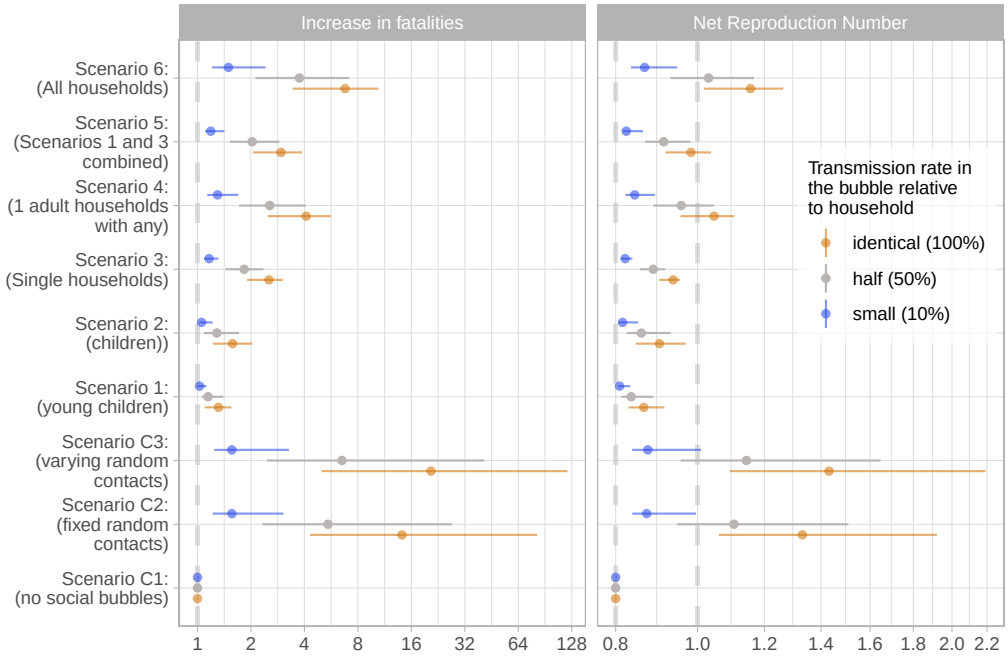

Figure 6.4: **The impact of bubbling scenarios on R and fatalities.** Here, we show the increase in fatalities (left) and the estimated reproduction number (right) for the considered scenarios under the assumption that all eligible households pair up and thereby form exclusive social bubbles and that transmission rates within a social bubble are the same as within the household. Central estimates are assuming $SAR_{HH} = 20\%$ and the upper and lower limits represent the respective 10% and 40% assumption.

assumptions ($SAR_{HH} = 40\%$, $\tau_H = \tau_B$), the increase in transmission is unlikely to lead to substantial spread of COVID-19, with an R of 0.95 and 0.91 for Scenario 1 and 3, respectively.

However, allowing all households to form bubbles (Scenario 6) is estimated to increase the reproduction number to 1.03, and hence marginally beyond the critical threshold value of 1 for the base case parameterisation (Figure 6.4). In general, it appears that the fewer households deemed eligible to expand their social bubble under a specific strategy, the smaller the average household size eligible to form social bubbles, and the smaller the risk of onward transmission within the bub-

ble determined by the age composition of a household, the smaller the increase in transmission as a result.

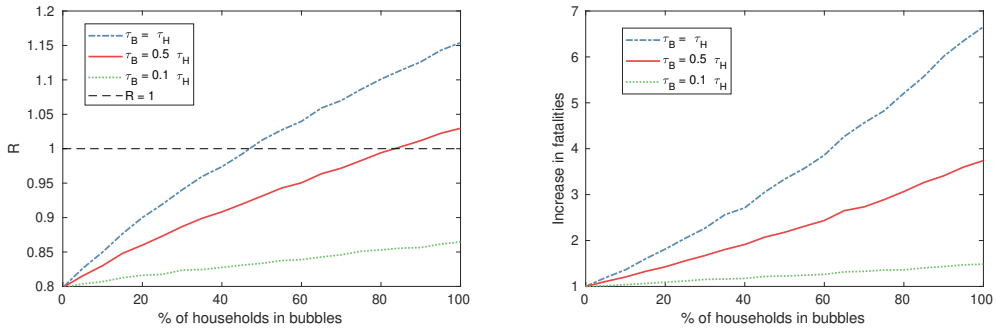

Figure 6.5: **The impact of uptake on R and fatality.** Here we consider the impact varying levels of uptake has on the reproduction number, R, and relative mortality. We consider this for our baseline parameters, at varying levels of transmission across bubble contacts ($\tau_B = \tau_H$ in blue, $\tau_B = 0.5\tau_H$ in red, $\tau_B = 0.1\tau_H$ in green). We observe that R scales sublinearly with uptake, with the gradient of increase dependent on transmission rate across bubble contacts.

As well as considering a situation in which all eligible households entered into a social bubble, we also consider the impact uptake has on R for Scenario 6. We find that R scales *sublinearly* with uptake (Figure 6.5). For example, this means that the increase in uptake from 0% to 20% has a larger R than an increase in uptake from 80% to 100%. Under our base parameterisation, if half of all households entered into a social bubble, R would increase to 0.93, as opposed to 1.03 under full uptake. However, assuming $\tau_H = \tau_B$, i.e. that transmission across bubble contacts occurs at the same rate as across household contacts, half of all entering into social bubbles would increase R above the epidemic threshold.

The impact bubbles have on epidemic risk depends upon the levels of transmission within the population prior to introducing a bubble strategy. We find that the impact of bubble strategies on transmission scales linearly with the prior R value, For all scenarios considered, this linear increase scales with a gradient ≈ 1, meaning the absolute increase in R from allowing social bubbles (Figure 6.6) remains relatively constant over a range of levels of community transmission within

the population.

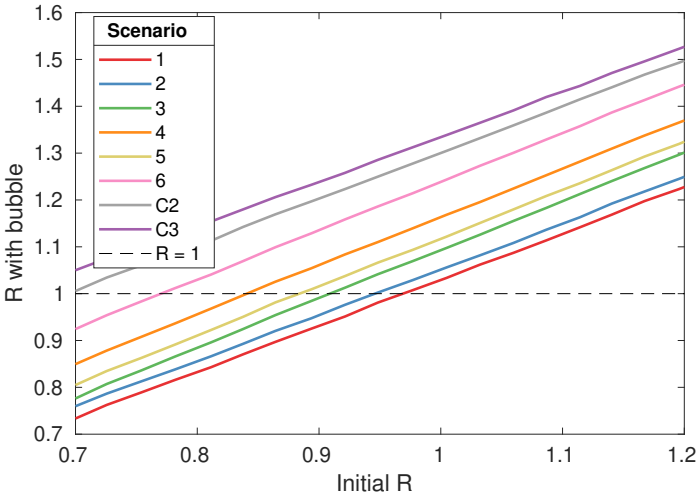

Figure 6.6: **The relationship between initial R and R under different bubble scenarios.** Here we consider the impact different bubble strategies have on the reproduction number, R. We consider this for our baseline parameters. For all scenarios, we find that R with bubbles increases linearly with initial R with a gradient approximately equal 1.

6.3.3 Impact of social bubbles on mortality risk

In all scenarios, the increased number of contacts lead to both excess infections and fatalities. Excess risk of *infection* compared to Scenario C1 was seen in both eligible and ineligible households under each scenario. This increased risk of infection in ineligible households occurs due to community transmission from eligible households. However, as expected the relative risk of infection was higher in eligible households (Figure 6.7).

The mortality risk associated with a social bubble strategy will not only depend on the increase in R associated with that strategy, but also on the demographic affected by the increased rate of infections. The average age in the households eligible to form social bubbles in scenarios 1 to 6 was 21.8, 25.6, 58.1, 40.2, 32.2,

and 39.4 years, hence the average infection fatality risk in an average household member eligible under such a strategy was 0.09%, 0.14%, 2.36%, 1.05%, 0.74%, and 0.93%. Because mortality risk to an individual depends on their age, the average age of eligible households to form social bubbles is relevant to the associated increase in mortality. For example, while social bubbles among households with young children (Scenario 1) saw similar increases in infections to increases in deaths (with a risk ratio of 1.13 and 1.14 for infections and deaths respectively), social bubbles targeting single occupancy households saw a larger increase in deaths than infections (with a risk ratio of 1.26 and 1.83 for infections and deaths respectively) due to the older targeted demographic. In scenarios targeting families, the mortality risk was largely attributed to households not eligible to form social bubbles, as a consequence of limited multigenerational mixing in UK households.

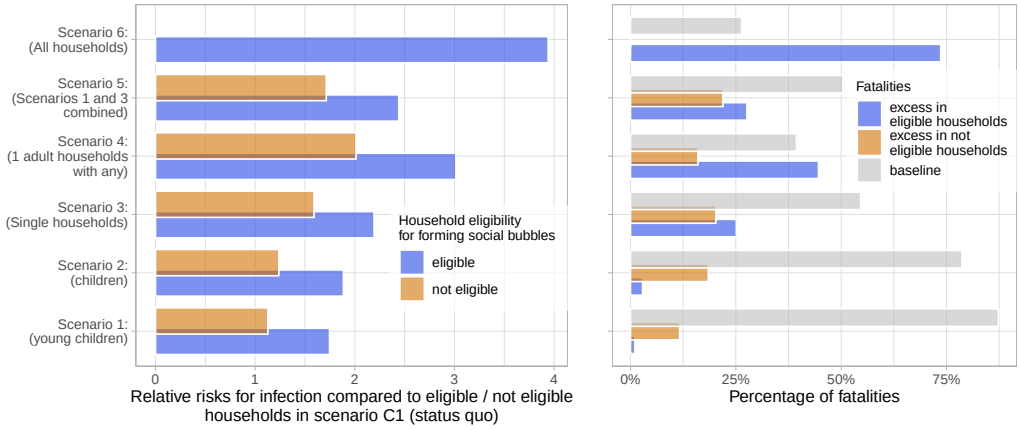

Figure 6.7: **Relative risk of infection and fatality.** Left panel: the relative risks of infection in the considered scenarios if compared to the status quo with no social bubbles (Scenario C1), stratified into the risks in households eligible and not eligible for forming social bubbles. Right panel: the population attributable fraction of fatalities in the considered scenarios. The overall mortality risk is stratified into the baseline risk, and the excess risk from forming social bubbles in both eligible and ineligible households.

6.3.4 Effectiveness of social bubbles

Here we consider the effectiveness of social bubbles, by considering the reduction in mortality risk compared to counterfactual scenarios where individuals increased their contacts in an unclustered fashion. Under our base parameterisation, allowing all households to form social bubbles reduced the mortality risk by 30.9% when compared to individuals making the same number of fixed infectious contacts at random across the population (Scenario C2). When compared to individual's making new unclustered infectious contacts every generation, social bubbles reduced the mortality risk by 42.4%.

We also considered scenario specific counterfactual scenarios. In general, the added benefit of social bubbles increases with a higher proportion of eligible households, alongside targeting riskier demographics. For example, social bubbles for households with young children (Scenario 1) reduced mortality risk by 4.2% and 8.1% compared to those households increasing contacts randomly and time-varying. In contrast, allowing households with one adult to form a support bubble with another household (Scenario 4) results in 51% of the households entering into a bubble, and leads to a 27.7% and 39.3% reduced mortality risk compared to individuals from those households increasing their contacts randomly but fixed and individuals from those households increasing their contacts randomly but varying each generation respectively (Figure 6.8).

6.3.5 Sensitivity analyses

We test the robustness of our findings to a number of alternative assumptions governing the spread of SARS-CoV-2 and the implementation of the social bubble strategy (Figure 6.9). Unsurprisingly, a lower initial value of R and a lower than observed household secondary attack rate, and a lower rate of transmission across bubble contacts, lowers epidemic risk in all scenarios. Excluding households includ-

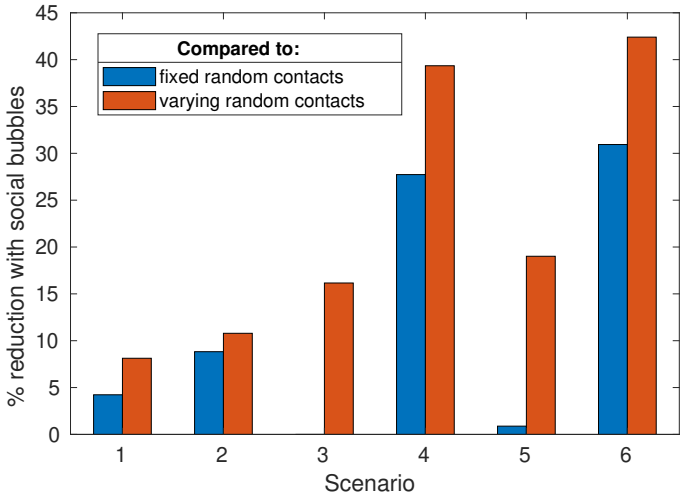

Figure 6.8: **Scenario specific effectiveness of social bubbles.** Here we compared the effectiveness of social bubbles in reducing mortality risk, when compared to other ways of increasing social contacts - where individuals from eligible households either make fixed random contacts (blue) or varying random contacts every generation (orange). In each comparison, individuals make the same number of infectious contacts, so the reduction in fatalities can be attributed to the clustering implied by social bubbles.

ing adults over 70 years also lowers epidemic risk, although in general to a smaller extent than the factors mentioned above. Conversely, a higher initial value of R, a higher than observed secondary attack rate, and a higher rate of transmission across bubble contacts increased epidemic risk in all scenarios. Households not adhering to social bubble guidelines, modelled by allowing 50% of eligible households, also increased epidemic risk.

For Scenarios 1-3, R did not exceed 1 under any of the univariate sensitivity analyses considered. For Scenario 4, all four factors leading to increased epidemic risk mentioned above pushed R above 1. For Scenario 5, R only exceeded 1 when there was a higher initial value of R prior to implementing social bubbles. For Scenario 5, all four factors leading to reduced epidemic risk mentioned above dropped R below 1.

The alternative assumptions on age-stratified susceptibility and transmissibility lowering epidemic risk in Scenarios 1 and 2, i.e. households with children, while for all other scenarios this alternative assumption increased epidemic risk. The opposite is true when considering the alternative assumptions on close-contact transmission and community transmission; these alternative assumption increased epidemic risk in Scenarios 1 and 2 and lowered epidemic risk for all other scenarios. This effect was sufficient to change the ordering of risk of social bubble strategies. Under our baseline assumption, Scenario 1, targeting families with young children, resulted in the lowest increase in R; under these alternative assumptions, Scenario 3, targeting single-occupancy households, resulted in the lowest increase in R.

The effectiveness of social bubbles also varied according to the underlying parametric assumptions. Assuming our alternative assumptions around susceptibility and infectivity, the effectiveness of social bubbles was as large as a 46.1% and a 58.5% reduction in mortality risk compared to adding the same amount of contacts randomly (Scenario C2) and time varying (Scenario C3). Under our most conservative assumptions, the reductions in mortality risk compared to C2 and C3 were 87.2% and 91.3%.

Alongside the parameter sensitivity scenarios considered, we also consider each scenario where older adults were shielded and excluded from being allowed to form a bubble as a sensitivity analysis. This only has a small impact on the effect of social bubbles for families with children (Scenarios 1 and 2), because of the small amount of multi-generational mixing between households in the UK, but does reduce R for social bubbles for single occupancy households or all households (Scenarios 3-6). While shielding older individuals does decrease overall mortality risk, the increase in infection resulting from social bubble strategies still impacts older individuals; bubbling strategies increase overall cases, which in turn increases risk to older individuals through community transmission.

(a) Scenario 1

(b) Scenario 2

(c) Scenario 3

(d) Scenario 4

(e) Scenario 5

(f) Scenario 6

(g) Scenario C2

(h) Scenario C3

Figure 6.9: **Sensitivity analyses.** Each tornado diagram shows the univariate sensitivity analysis on the expected increase in fatalities and the net reproduction number for a given scenario. The colour coding is based on factors determining higher risk (orange) and lower risk (blue) for Scenario 1. The base case estimate is indicated through the dashed grey vertical line. The sensitivity scenarios are (from top to bottom): transmission across individuals of households sharing a bubble is 90% or 0% lower than that within a household instead of 50%; the relative susceptibility to infection of children and older adults compared to adults is 79% and 125% while the relative transmissibility is 64% and 290%; the secondary attack rate in the household is 10% or 40% instead of 20%; R is 0.7 or 0.9 instead of 0.8; that households including an adult over 70-years-old are excluded from forming bubbles; that transmission across close contacts is density dependent; that 50% of bubbles do not adhere to the recommendations but pair up with an additional household; and that the risk of a household to get infected from the community is proportional to the household size instead of being the same across households.

6.4 Discussion

In this chapter, we find that contact clustering via the formation of social bubbles can limit the additional risk of transmission from allowing individuals to increase their social contacts beyond their own household. Under our base parameterisation, social bubbles reduced mortality risk by 42% compared to allowing individuals to make an equivalent number of infectious contacts in an unclustered manner, and under some alternative parameterisations this risk reduction was even greater. We find that allowing all households to form social bubbles may increase R above the epidemic threshold and hence may lead to an exponential increase in cases. Strategies that target households that may be in the highest need of additional social contacts only result in a limited increase in epidemic risk, increasing R by less than 11% individually and less than 15% in combination. Individually, these targeted strategies remained below the epidemic threshold under all sensitivity analysis scenarios considered. We find that adverse health outcomes resulting from a social bubble strategy are largely proportional to epidemic risk, but find that this will disproportionately affect households with older adults irrespective of whether they are eligible to enter into a social bubble.

This chapter investigates the effectiveness of social bubbles as a potential exit strategy from a successful period of lockdown, when stringent physical distancing measures have been imposed that have successfully reduced R to below the epidemic threshold. While we consider the impact of social bubbles in isolation, such a policy would only form one component of a multivariable exit strategy. Because of this, our comparisons of social bubble strategies should be interpreted cautiously and with regard to other relaxation measures implemented that allow social contact beyond the household. Such measures may have a non-linear impact on the increased epidemic risk caused by social bubbles. As social contacts increase in other ways, the benefits gained from the exclusivity of bubbles diminishes. Of particular

relevance, if schools are kept open, now seen as a priority for future lockdown situations, the resulting increase in social contact may impact the viability of strategies that include families with children.

Numerous countries, such as Germany, New Zealand, and the UK, have implemented social bubbles strategies similar to those considered in this chapter. In the UK, since June 2020, adults who live alone or with dependent children can form a 'support bubble' with another household of any size [GOV.UK, 2020b], since November 2020 households with a child aged 14 years or younger have been allowed to form a 'childcare bubble' with another household of any size [GOV.UK, 2021], and for Christmas Day only all households were allowed to form an exclusive bubble with two other households. Throughout lockdown in New Zealand, single occupancy households were allowed to pair up with a 'lockdown buddy' in another single occupancy household, and key workers were allowed to identify 'childcare buddies'. On 27 April 2020, New Zealand relaxed some of its restrictions, allowing residents to extend their household bubbles to reconnect with close family, bring in caregivers and support isolated members in the community, while recommending that such extended household bubbles remain exclusive [New Zealand Government, 2020]. A subsequent survey found that allowing households to reconnect, above reopening of schools, shops, churches and fitness centres, would result in the largest increase in quality of life [Long et al., 2020].

We identify three key risks impacting the success of social bubble strategies in maintaining R below the epidemic threshold. Firstly, if R is close to the epidemic threshold prior to the introduction of a social bubble strategy, implementing such a strategy may increase R above 1 even if the policy has a small impact. If the aim is to suppress the growth of cases, in such instances a social bubble strategy may be unsuitable. Secondly, if there is a higher than observed household secondary attack rate, then a policy allowing social bubbles will result in a larger increase in epidemic risk. There remains some uncertainty surrounding the house-

hold attack rate of COVID-19, with high household attack rates observed in some instances. However, our base case assumptions are in line with an increasingly consistent picture emerging in the contemporary academic literature [Koh et al., 2020]. Also, superspreading events have been raised as a potentially important source for sustained transmission of SARS-CoV-2, which would further imply a rather low secondary household attack rate in most instances. However, household attack rates may vary between different types of household, and may be larger for some households with unusual network structures [Potter and Hens, 2013], such as large student households. Thirdly, a lack of adherence to social bubble strategies could undermine their effectiveness. A lack of adherence allows potentially long chains of transmission through the population. While we find that some degree of non-adherence would not necessarily hinder the success of a strategy, if there is a perception within the population that exclusivity is unimportant, this could lead to individuals rebuilding their contact networks, resulting in a large increase in epidemic risk.

Alongside these, we have identified key opportunities to minimise the risk resulting from allowing social bubble strategies. If there is only partial uptake of social bubble strategies, this results in a lower increase to the epidemic risk. A survey in New Zealand found that only 50% of households took up the opportunity to expand their social bubbles as measures were relaxed [Long et al., 2020]. Under our base parameterisation, such a reduction would be enough to reduce R well below 1. We also find epidemic risk is reduced further if the risk of transmission across bubble contacts is low in comparison to household contacts. Hence, our research highlights that the messaging surrounding any social bubble policy could play an important role. In New Zealand, social bubbles were not framed as a relaxation of social distancing rules but rather as a source of support for those who are at a higher risk of social isolation or with needs for care, including childcare [Long et al., 2020]. Framed in this way, social bubbles may result in a minimal increase in epidemic

risk.

The expansion of contacts resulting from social bubbles will naturally lead to some increase in transmission when compared to a situation where social interaction is confined to within a household. However, perfect adherence to such stringent restrictions is not guaranteed over long periods of time. Eventually, adherence may decline, leading to individuals increasing their contacts in an unclustered fashion. To illustrate such a scenario, we include counterfactual scenarios capturing the effects of unclustered increases in contacts. Under Scenarios C2 and C3, we consider situations where individuals make the same number of infectious contacts as in Scenario 6, but these contacts are unclustered. In Scenario C2, these contacts stay fixed over time, while in Scenario C3, these contacts vary every generation. We show that the clustering reduces the epidemic and reduces the number of infections and subsequent fatalities by 30.9% and 42.4% in the base case and even more in some of the parametric sensitivity analysis. Because of this, social bubbles may actually help to reduce epidemic and mortality risk, if such a strategy is given as guidance to households struggling to cope with the distancing measures imposed in lockdown, who may end up increasing their social contacts anyway.

As in any epidemiological modelling study, we must make some assumptions surrounding transmission. Firstly, we assumed that transmission across close contacts was frequency dependent, informed by previous studies that indicate the probability of infection across two specific members of the same household decreases with household size for COVID-19 [Streeck et al., 2020] and other communicable diseases like influenza [Cauchemez et al., 2004]. However, there remains uncertainty surrounding the nature of close-contact transmission for COVID-19, and the assumption of frequency dependence may not accurately capture transmission across all settings. Secondly, we assumed that the risk of a household acquiring infection from the community is independent of its number of occupants. While this assumption may be appropriate for some households (e.g. families where one adult

leaves the household to do shopping), it may not hold true in other contexts (e.g. student households comprising of largely independent individuals). Because of this we tested the sensitivity of our results to these assumptions by alternatively considering close contact transmission as density dependent, and allowing the risk of household infection to increase with household size. These alternative assumptions do not qualitatively change our findings, but do change the ordering of the risk of social bubble strategies. In particular, under either of these alternative assumptions, social bubble strategies targeting single occupancy households result in a lower increase in R than strategies targeting families with children. Reports on the antibody prevalence in England found household size associated with antibody prevalence, suggesting that household size may play a role in the probability of acquiring infection [Ward et al., 2021]; a more detailed understanding of the nature of close contact and community transmission may help inform more precise evaluations of the effectiveness of social bubbles. We do not consider the risk of community transmission depending on bubble size. However, if bubbles were to act as cohesive units, and as a consequence reduce their interaction with the community, this may further increase the effectiveness of social bubble strategies.

Our analyses have a number of limitations. Firstly, this chapter assessed the risk associated with social bubble strategies, and their effectiveness compared to unclustered increases in contacts, but did not attempt to assess the benefits social bubbles could have. As noted previously, allowing individuals to have social interactions is important for their mental wellbeing and will have a disproportionate benefit for particular households, though this is not something we attempt to quantify. Social bubbles would also likely to have indirect benefits related to epidemic risk. Social bubbles would likely benefit any contact tracing efforts as the clustering imposed through social bubbles would mean that relevant close contacts would become easier to identify [House and Keeling, 2010]. Social bubbles could also amplify the beneficial impact of self-isolation measures, if all individuals within a bubble are

advised to self-isolate if a member of the bubble tests positive. Secondly, we did not include the possibility to form bigger social bubbles that would cluster together three or more households. While this has been implemented in some countries, the complexity of creating an exclusive cluster of three or more households could lead to a loss of adherence. Thirdly, we did not consider further heterogeneity within society that may affect both risk of transmission and adverse health outcomes. For example, about 20% of the working population is classified as key workers and will have an increased risk for infection from the community, while adverse health outcomes have disproportionately affected men, individuals of low socioeconomic status, and individuals from particular ethnic backgrounds [Kirby, 2020; Raisi-Estabragh et al., 2020]. Incorporating such information would require combining these factors with distributions of household compositions, which would not be a trivial task. Fourthly, we did not consider the impact immunity may have on our results. If a significant proportion of the population had some level of immunity, this would likely decrease the risk associated with the social bubble strategies. On the other hand, if the duration of protection via immunity is very short-lived, then this may affect our results considerably.

6.5 Conclusion

The modelling in this chapter highlights both the potential of a social bubble approach in relaxing lockdown measures as well as the continued need for social distancing measures even if social bubble strategies are implemented. While social bubble strategies are an effective way of limiting the risk from expanding individuals' social contacts compared to unclustered increases in contacts, the resulting increase in infections may result in R crossing the epidemic threshold. If social bubbles are recommended only for those particularly struggling with lockdown, while reinforcing the message that some level of social distancing even within social

bubbles is recommended, this may be an effective way of striking a balance between minimising the negative impact lockdowns must have on mental health and minimising the risk of a resurgence of cases. At the time of writing, the UK is currently in its third lockdown, a pattern echoed across Europe. As countries emerge from current and future lockdowns, social bubbles may again become a vital tool to provide social interactions to those that need it most, whilst keeping R below one.

While much is still uncertain around COVID-19, its treatment, and its control, one thing is sure: this virus and the control measures implemented to abate its spread will continue to effect us for a period of years. When considering future control policies, policy makers are in an unenviable position, having to balance effectiveness of measures against their proportionality, consistency, and simplicity. Ultimately though, whatever decisions are taken should be underpinned by thorough research, and in the context of epidemics this must include mathematical modelling. We believe this chapter contributes to this research effort, providing one of the first studies assessing the impact of social bubble strategies as a way of controlling the COVID-19 epidemic.

Chapter 7

Concluding thoughts

This thesis has utilised a variety of network modelling approaches. A network approach to mathematical modelling can provide important insights into a wide range of theoretical and applied questions. To understand the suitability or feasibility of such an approach, it is important to understand the impact that network structure has on epidemiological outcomes. Throughout this thesis, we have demonstrated that network models can elucidate the importance of different aspects of network structure in epidemiological modelling.

We began by investigating the correlations in infection status of individuals within a network that occur because of underlying network structure. Standard pairwise models assume the infection status of outer individuals in an open triple are conditionally independent given the infection status of the central individual. While this approach can lead to an exact description of the underlying epidemiological dynamics for diseases with Susceptible-Infected-Recovered (SIR) dynamics [Sharkey et al., 2015], the correlations induced by the possibility of reinfection means that these closures are only approximate for diseases with Susceptible-Infected-Susceptible (SIS) dynamics. In Chapter 3, we introduced improved pairwise approximation models for diseases with SIS-dynamics by explicitly tracking the time-evolution of the *er-*

rors between standard pairwise approximations of triples and their 'true' values. Doing so, we obtained a number of valuable insights: into the size and direction of errors introduced by standard pairwise approximations; into the small number of error terms required to capture the errors between approximations and their true values; and into a generic approach to improve the accuracy of pairwise approximation methods for diseases without immunity.

Chapter 3 focussed on a disease with idealised dynamics in two idealised settings. Firstly, we considered an improved pairwise closure for an isolated open triple, and we found that by explicitly tracking error terms, we could arrive at a model capable of describing exactly the underlying disease dynamics. Secondly, we considered a closure for k-regular networks which, while approximate, is capable of matching closely the results from higher-order approximation models and explicit stochastic simulations. We did so because in these settings the correlations between infected individuals are not disturbed by other features in a network, providing us with an ideal setting to understand the specific errors induced by SIS-dynamics. Even in these idealised settings, the disease dynamics are non-trivial and analytical tractability is limited. Our work in Chapter 3 highlights the complexity of disease dynamics that can arise on even the simplest network structures, the importance of basic models to understand these complexities, and the challenge of designing accurate network models of diseases without immunity.

The network structures considered in Chapter 3 are clear departures from epidemiologically relevant contact networks in the real world. However, we believe that this approach has the potential to be extended in a variety of ways to more realistically capture the structure of real-world networks. As discussed in Chapter 3, we believe that incorporating these improved closures into networks that are both heterogeneous and dynamic is possible. However, a key question going forward will be whether the improvement in accuracy from explicitly tracking errors is worth the additional complexity. We believe that this approach also has the potential to

illuminate some identified outstanding challenges for static network models. Pellis et al. [2015a] note that there has been little research into more complicated disease dynamics where reinfection is possible, such as Susceptible-Infected-Recovered-Susceptible (SIRS) dynamics or Susceptible-Exposed-Infected-Susceptible (SEIS) dynamics. In both cases, we believe our approach could be easily extended, and that doing so would only require one additional error term. Doing so could provide a valuable insight into the suitability and accuracy of pairwise approximation methods for a wide range of disease dynamics.

In Chapters 4 and 5 we considered the importance of accurately capturing levels of concurrency when modelling the control of sexually transmitted infections (STIs). We did so using two distinct modelling approaches. In Chapter 4, we used a relatively simple deterministic pair-formation model. Doing so has clear benefits. As there are a relatively small number of equations we can obtain an intuitive understanding of the underlying disease dynamics, and for models without concurrency we can obtain analytical expressions for the equilibrium values of different states of the system. Because pair-formation models are an extension of random-mixing models, it is possible to find the critical level of vaccination numerically, by finding the required level to bring the value of the real parts of all eigenvalues of the Jacobian matrix to be less than zero to ensure the stability of the disease-free equilibrium [Kretzschmar et al., 1994]. Through this modelling approach, we showed that when models are matched to prevalence data, models with and without concurrency require similar levels of vaccination, highlighting that accurately capturing concurrency may not always be necessary in models of STI control. This result appears to go against the received wisdom that concurrency has a large impact on epidemiological dynamics. However, the two are not mutually inconsistent. It is true that the presence of concurrent partnerships in a network will have a large impact on the prevalence of an STI, but given we know the prevalence of an STI, including concurrency in models that have been matched explicitly to prevalence

will have little bearing on the success of control by vaccination.

However, the simplicity of this model is also its limitation. In particular, these models are not naturally suited to include concurrent partnerships where additional partnerships have any duration (the models of Leung et al. [2012, 2015] address this problem, but assume that individuals form partnerships at a rate independent of their relationship status). In Chapter 5, to consider the impact of concurrent partnerships in a more realistic setting, we constructed a dynamic simulation model of a heterosexual population, with an arbitrary number of male and female risk groups, that we fitted to observed behavioural data from the National Survey of Sexual Attitudes and Lifestyle (Natsal). By inspecting the network at a snapshot in time, we were able to more fully understand the implications of different assumptions surrounding concurrent partnership on network structure, observing a stark difference between models assuming partnerships form at a rate independent of relationship status and models explicitly matched to observed levels of concurrency. Despite this difference, we once again observed that the impact of concurrency on the success of control measures is modest when models are matched to prevalence data, and is particularly similar to models assuming serial monogamy. The results from Chapter 5 confirm that the results from Chapter 4 hold true in a more realistic setting, and that the impact of concurrency does not have some non-linear interaction with other heterogeneities present in real-world sexual networks.

We believe that both the pair-formation models of Chapter 4 and the individual-based models of Chapter 5 have the potential to be extended in illuminating ways. As only a small number of male and female risk-groups are required to fit to observed yearly degree distributions, it would be feasible to define pair-formation models that more realistically capture the dynamics of heterosexual networks. Given that models with and without concurrency require similar levels of vaccinations, a pair-formation model assuming serial monogamy that is fitted to yearly degree distribution data could be used to understand the potential impact of vaccina-

tions. Doing so may achieve a good balance between complexity and tractability. With the prospect of future vaccines against STIs, such an approach may become a useful tool in the future [Gottlieb et al., 2014; Abraham et al., 2019]. For the individual-based model of Chapter 5, yet greater realism may be possible to include, including age-structure, the interaction between heterosexual and homosexual populations, more realistic disease dynamics, and a wider range of interventions. The results from the next Natsal survey, Natsal-4, will arrive in the next few years. Our individual-based modelling framework, fitted to behavioural data from this survey, could provide a basis to modelling the impact of STI control strategies in the UK in the coming decade.

While mathematical models that aim to predict the outcome of potential public health interventions always aspire to realism, they must inevitably make some simplifying assumptions. These chapters demonstrate an important task for researchers interested in network approaches to modelling the spread of epidemics: to understand which features of network structure have a significant impact on epidemiological outcomes, and must be included explicitly, as well as to understand which features have little impact on the resulting dynamics, and may be omitted without significantly changing outcomes. These chapters demonstrate that, when considering the impact of STI control measures and sexual network models are matched to prevalence data, concurrency falls into the latter category.

In Chapter 6, we moved away from STIs, and applied a network approach to answer an applied question about COVID-19 lockdown relaxation measures. In the context of a lockdown within the UK, we were able to utilise a rich data source, the most recent census of England and Wales, to obtain the underlying network and age structure of our synthetic population. By comparing a scenario where households form exclusive 'social bubbles' to scenarios where individuals make a comparable number of unclustered additional contacts, we were able to quantify the extent to which social bubbles were an effective way of minimising the risk from increasing

contacts. We were also able to compare a range of different potential social bubble policies, where only some households are eligible to form social bubbles, and we were able to test the sensitivity of our results to a range of alternative assumptions. By doing so, we were able to provide an assessment as to which social bubbles strategies were unlikely to increase transmission above the epidemic threshold. Our work in this chapter demonstrates the capacity of even relatively simple network models to provide insights into applied questions of importance to public health.

As we considered a situation where individual's social contacts were severely restricted to those within their household, we were able to utilise a static network model, as we could reasonably assume that an individual's household contacts comprised the majority of an individual's social contacts. While our model was capable of answering a specific question in a specific context, the extent to which this modelling approach could be extended to other contexts is unclear. It is unclear whether our approach could be adapted to consider a non-lockdown situation, where individual's contacts are dynamic and diverse, or indeed whether there would be appropriate data to parameterise such a model. However, adding another layer of static contacts could be relatively straightforward. For example, our framework may be able to consider a lockdown situation where schools are open. Given that further lockdowns are likely in the future, understanding the impact of social bubbles remains relevant, and network approaches such as ours may well be important tools in understanding their impact, and in understanding their interaction with other relaxation measures.

Overall, this thesis has demonstrated the capacity for network models to answer a variety of theoretical and applied questions. Doing so, we hope to have demonstrated the diversity of mathematical models that exist, and the diversity of questions they try to answer. From basic models to understand the correlations that result from network structure, to assessing the importance of including aspects of network structure in public health models, to quantifying the impact that specific

policies affecting network structure may have, network models are an invaluable tool. Given their capacity to answer such questions, and given the many open questions that exist, network models will remain important tools in the mathematical study of epidemics.

Appendix A

Appendix to Chapter 3

While we find that considering proportions is a more convenient way to express the results from Section 3.3, we appreciate that others may prefer to use our results under the convention of terms referring to numbers of motifs. In this appendix, we provide a conversion table to transform the terms from this section from proportions to numbers, and derive the improved pairwise model in terms of numbers. We stress that the improved pairwise model presented here is *equivalent* to the model presented in Section 3.3.2.

A.1 Converting the improved pairwise model for k-regular networks from proportions to numbers

First, to express the quantities in Section 3.3.2 in terms of numbers, we must be able to count the number of motifs relative to every individual. In a k-regular network, for every individual there are k pairs, for every pair there are $(k-1)$ triples, and for every triple there are $(k-1)$ line graphs of length 4 and $(k-2)$ 4-stars. Using straight line brackets $|X|$ to denote the *number* of individuals in

Table A.1: Conversion table between proportions and numbers.

Motif	Ratio to # of individuals	Term (proportion)	Equivalent term (numbers)
Individual	1	$[X]$	$\|X\|/N$
Pair	k	$[XY]$	$\|XY\|/kN$
Triple	$k(k-1)$	$[XCY]$	$\|XCY\|/k(k-1)N$
Line graph (length 4)	$k(k-1)^2$	$[A_aX_xC_cY_y]$	$\|A_aX_xC_cY_y\|/k(k-1)^2N$
4-star	$k(k-1)(k-2)$	$[X_xC_cY_yZ_z]$	$\|X_xC_cY_yZ_z\|/k(k-1)(k-2)N$

state X etc. Table A.1 below outlines equivalent terms:

Using these conversions for example on Equations (3.38) and (3.40), we obtain the formally derived equations obtained by Taylor et al. [2012] (Theorem 1). We can also use these to convert our closures from proportions to numbers. Applying these, we obtain the unintuitive result that the closure $[XCY] \approx [XC][CY]/[C]$ in terms of proportions is equivalent to the closure $|XYZ| \approx (k-1)/k \times |XC||CY|/|C|$ in terms of numbers. Applying these conversions to this and to Equations (3.60) and (3.61) we obtain:

$$|XCY| \approx \frac{k-1}{k}\frac{|XC||CY|}{|C|} \tag{A.1}$$

$$|A_xS_cB_yI_z| \approx \frac{k(k-2)}{(k-1)^2}\frac{|ASB||BSI||ASI||S|}{|AS||BS||IS|} \tag{A.2}$$

$$|I_aS_xA_cB_y| \approx \frac{|ISA||SAB|}{|SA|} \tag{A.3}$$

To obtain the improved pairwise approximation in terms of numbers, we again consider the term α between a triple and its approximation. Below we consider $\alpha_{|ISI|}$:

$$\alpha_{|ISI|} = k|ISI||S| - (k-1)|SI|^2 \tag{A.4}$$

$$= k|ISI|\frac{|SSS| + 2|SSI| + |ISI|}{k(k-1)} - (k-1)\frac{(|SSS| + |SSI|)^2}{(k-1)^2} \tag{A.5}$$

$$= \frac{\alpha_{|S|}}{k-1} \text{ where } \alpha_{|S|} = |SSS||ISI| - |SSI|^2 \tag{A.6}$$

As before, we find $\alpha_{|ISI|} = \alpha_{|SSS|} = -\alpha_{|SSI|} = \alpha_{|S|}/(k-1)$. Defining $\alpha_{|I|}$ as $|III||SIS| - |SII|^2$, we similarly find $\alpha_{|SIS|} = \alpha_{|III|} = -\alpha_{|SII|} = \alpha_{|I|}/(k-1)$. By applying the conversions from Table A.1 to Equations (3.44) to (3.49), we can obtain expressions for the rate of change of $\alpha_{|S|}$ and $\alpha_{|I|}$:

$$\dot{\alpha_{|S|}} = \gamma(\phi_{|S|} - 2\alpha_{|S|}) + \tau(\beta_{|S|} - 2\alpha_{|S|}) \tag{A.7}$$

$$\text{where } \phi_{|S|} = |SSS||III| + |SIS|ISI| - 2|SSI||SII| \tag{A.8}$$

$$\text{and where } \beta_{|S|} = 2(k-1)(|I_a S_x S_c I_y||SS| - |I_a S_x S_c S_y||SI|) + 2|S_x S_c I_y I_z||SSI| \tag{A.9}$$

$$- |S_x S_c S_y I_z||ISI| - |I_x S_c I_y I_z||SSS|$$

$$\dot{\alpha_{|I|}} = -4\gamma\alpha_{|I|} + \tau(\beta_{|I|} + 2\phi_{|I|} - 2\alpha_{|I|}) \tag{A.10}$$

$$\text{where } \phi_{|I|} = 2|SIS||ISI| - 2|SSI||SII| \tag{A.11}$$

$$\text{and where } \beta_{|I|} = 2(k-1)(|I_a S_x I_c I_y||SI| - |I_a S_x I_c S_y||II|) - 2|S_x S_c I_y I_z||SII| \tag{A.12}$$

$$+ |I_x S_c I_y I_z||SIS| + |S_x S_c S_y I_z||III|$$

Finally, rearranging Equation (A.4) and its analogues, substituting in $\alpha_{|X|}$ we can obtain the closure for triples in the improved pairwise approximation:

$$|ABA| \approx \frac{(k-1)^2|AB|^2 + \alpha_{|B|}}{k(k-1)|B|} \qquad |ABC| \approx \frac{(k-1)^2|AB||BC| - \alpha_{|B|}}{k(k-1)|B|} \tag{A.13}$$

Thus we arrive at the improved pairwise approximation for k-regular networks, expressed in terms of numbers rather than proportions:

Model 6 in terms of numbers - The improved pairwise approximation for k-regular networks

$$|\dot{SS}| = 2\gamma|SI| - 2\tau\frac{(k-1)^2|SS||SI| - \alpha_{|S|}}{k(k-1)|S|} \tag{A.14}$$

$$|\dot{SI}| = \gamma(|II| - |SI|) - \tau|SI| + \tau\frac{(k-1)^2|SS||SI| - \alpha_{|S|}}{k(k-1)|S|} - \tau\frac{(k-1)^2|SI|^2 + \alpha_{|S|}}{k(k-1)|S|} \tag{A.15}$$

$$\dot{\alpha_{|S|}} = \gamma(\phi_{|S|} - 2\alpha_{|S|}) + \tau(\beta_{|S|} - 2\alpha_{|S|}) \tag{A.16}$$

$$\dot{\alpha_{|I|}} = -4\gamma\alpha_{|I|} + \tau(\beta_{|I|} + 2\phi_{|I|} - 2\alpha_{|I|}) \tag{A.17}$$

Appendix B

Appendix to Chapter 5

This appendix provides supporting plots to Chapter 5.

In Figures B.1 and B.2 we provide posterior distributions obtained for the fitted $c_M = c_F = 1$ models and $c_M = c_F = 0$ models, analogous to Figure 5.3 in the main text. As for the full simulation model, we find that posterior distributions are approximately multivariate normal distributed.

In Figure B.3 we explore the impact of untargeted and targeted vaccination on endemic prevalence in males and females, with similar trends emerging for both sexes.

In Figure B.4 we explore the impact of contact tracing on endemic prevalence in males and females. Again, we see the combined trend mirrored in the trend of each individual sex.

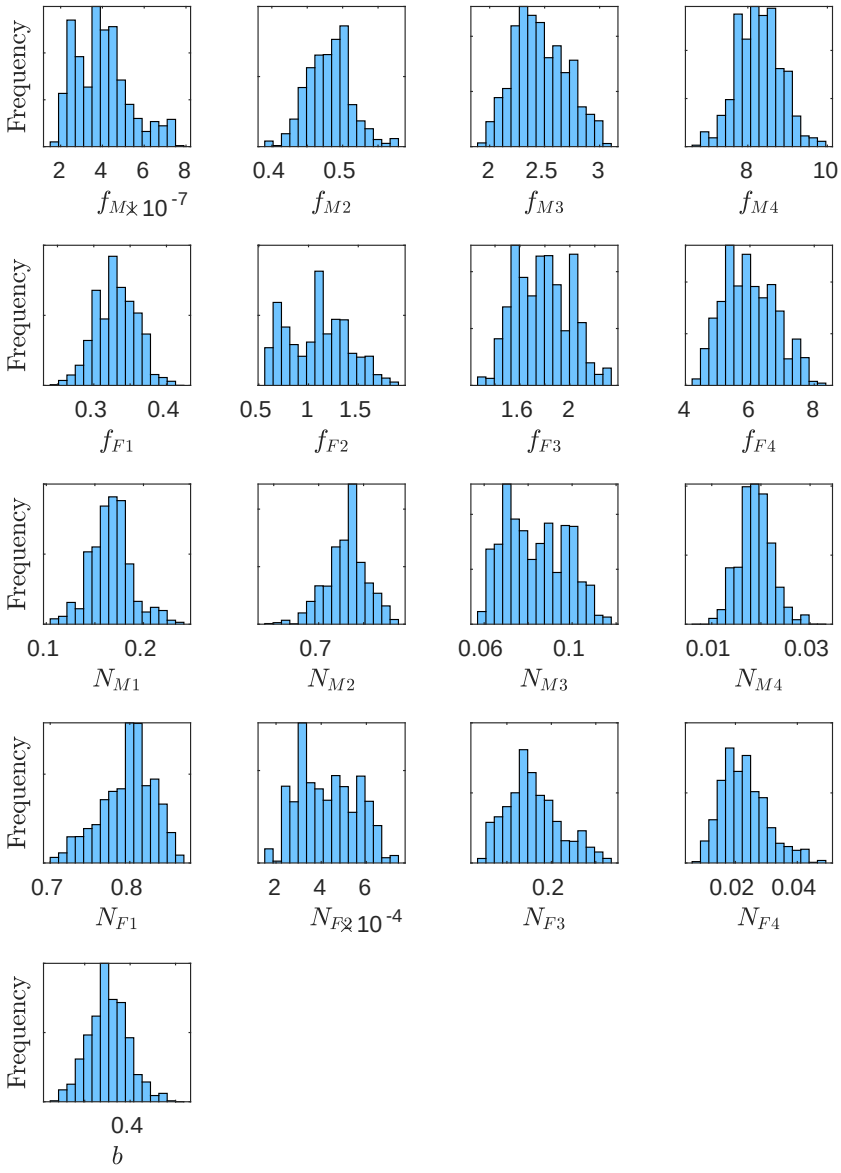

Figure B.1: **Posterior distribution obtained from MCMC for the $c_M = c_F = 1$ model.** Here, we plot the posterior parameter distributions obtained via a MH-algorithm for the $c_M = c_F = 1$ model. We observe that the distributions are approximately normally distributed. Distributions are obtained from 100,000 iterations of an MH-algorithm, after an initial burn-in period of 100,000 iterations.

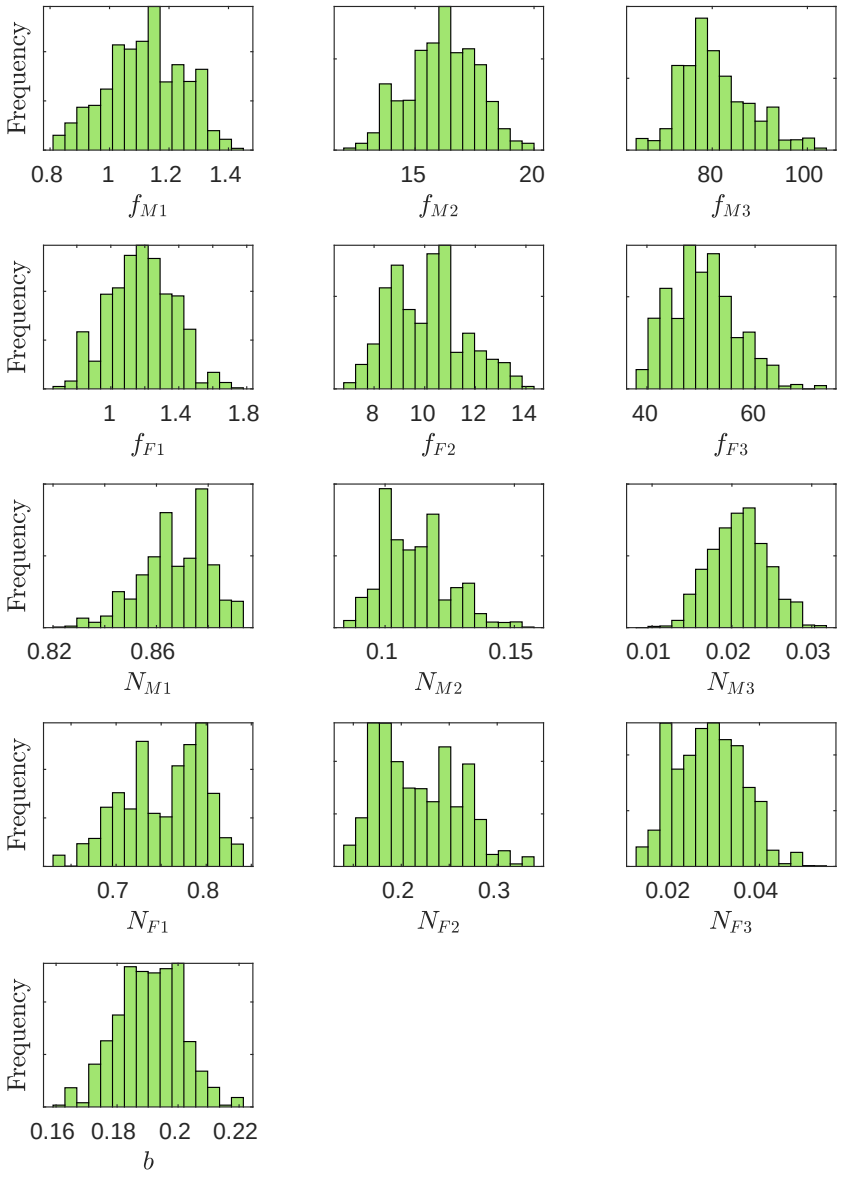

Figure B.2: **Posterior distribution obtained from MCMC for the $c_M = c_F = 0$ model.** Here, we plot the posterior parameter distributions obtained via a MH-algorithm for the $c_M = c_F = 0$ model. We observe that the distributions are approximately normally distributed. Distributions are obtained from 100,000 iterations of a MH-algorithm, after an initial burn-in period of 100,000 iterations.

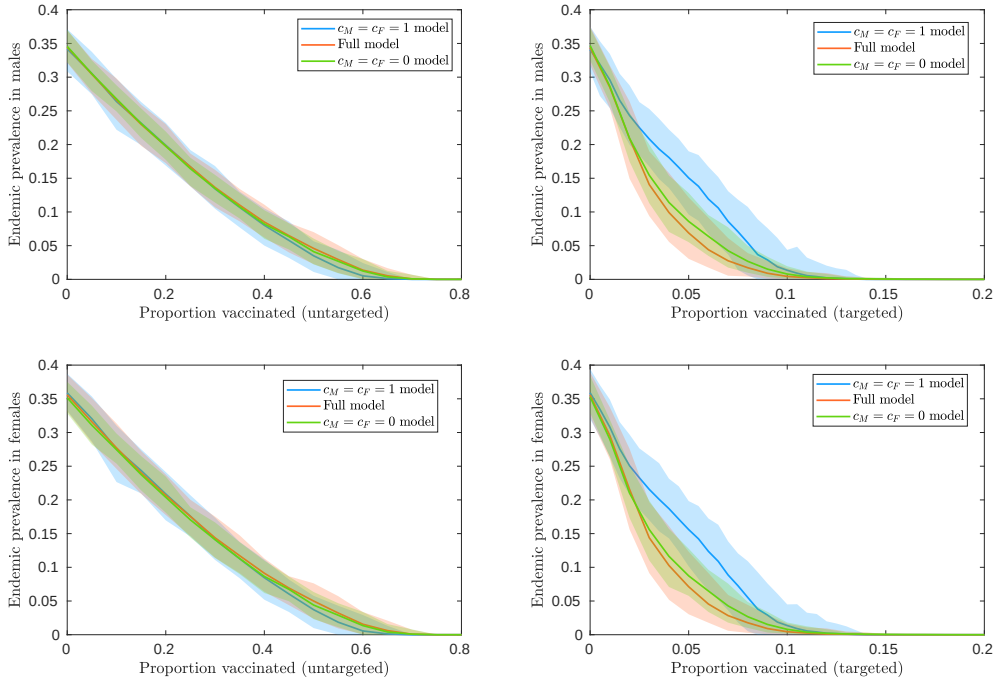

Figure B.3: **Sex-specific comparison the impact of untargeted and targeted vaccination across models.** In the top panel, we compare the impact of untargeted (left) and targeted (right) vaccination on endemic prevalence in males, for the $c_M = c_F = 1$ model (blue), the full model (orange), and the $c_M = c_F = 0$ model (green). Similarly, in the bottom panel, we compare the impact of untargeted (left) and targeted (right) vaccination on endemic prevalence in females. The trends resulting from vaccination in different models are similar for both sexes. Plotted results are means of 100 epidemics generated from parameters sampled from the fitted posterior distributions, with shaded areas referring to 95% prediction intervals.

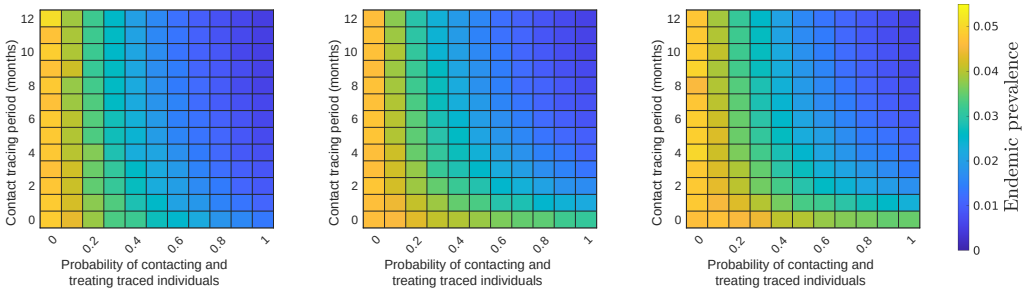

(ai) $c_M = c_F = 1$ model (aii) full model (aiii) $c_M = c_F = 0$ model

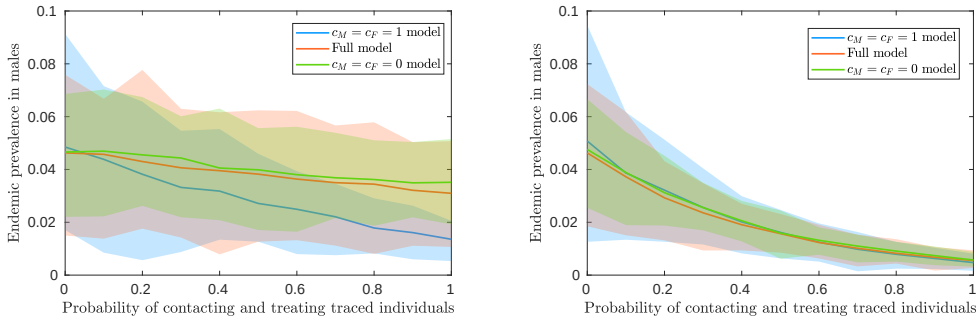

(aiv) Current contacts (av) Contacts over 1 year

(a) Prevalence in males

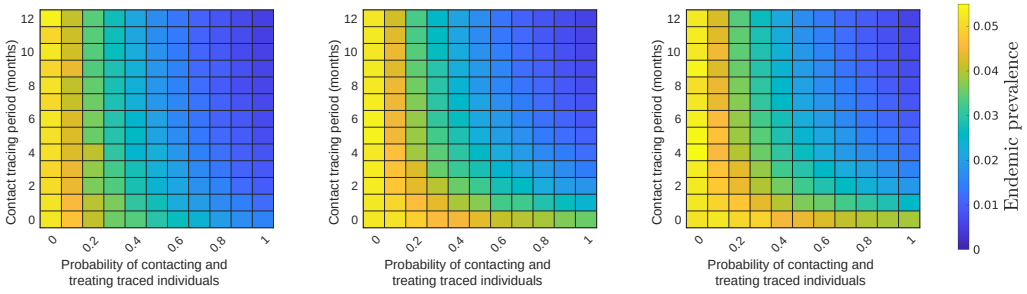

(bi) $c_M = c_F = 1$ model (bii) full model (biii) $c_M = c_F = 0$ model

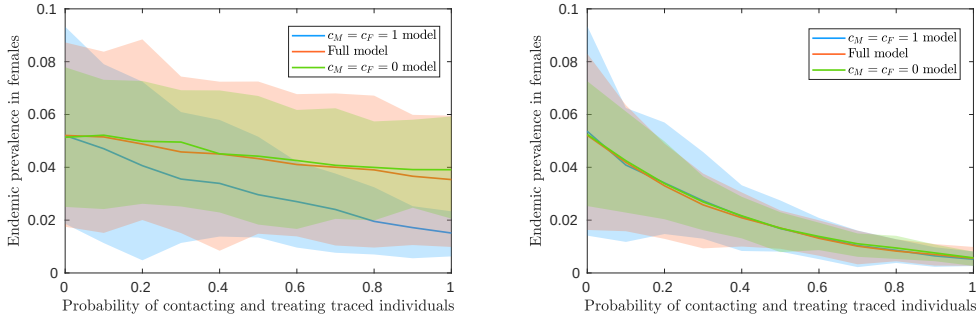

(biv) Current contacts (bv) Contacts over 1 year

(b) Prevalence in females

Figure B.4: **Sex-specific comparison of the impact of contact tracing across models.** For (a) males and (b) females, in (i-iii) we plot heat maps showing the impact that contact tracing period and the probability of contacting and tracing traced individuals has on endemic prevalence for each model. In (iv) and (v) we focus on the impact of contacting and tracing traced individuals has on prevalence when the tracing period is (iv) 0 years and (v) 1 year . Plotted results are means of 100 epidemics generated from parameters sampled from the fitted posterior distributions, with shaded areas referring to 95% prediction intervals.

Bibliography

S. Abraham, H. B. Juel, P. Bang, H. M. Cheeseman, R. B. Dohn, T. Cole, M. P. Kristiansen, K. S. Korsholm, D. Lewis, A. W. Olsen, et al. Safety and immunogenicity of the chlamydia vaccine candidate CTH522 adjuvanted with CAF01 liposomes or aluminium hydroxide: a first-in-human, randomised, double-blind, placebo-controlled, phase 1 trial. *The Lancet Infectious Diseases*, 19(10):1091–1100, 2019.

A. A. Adimora and V. J. Schoenbach. Social context, sexual networks, and racial disparities in rates of sexually transmitted infections. *The Journal of Infectious Diseases*, 191(Supplement_1):S115–S122, 2005.

R. Albert, H. Jeong, and A.-L. Barabási. Diameter of the world-wide web. *Nature*, 401(6749):130–131, 1999.

M. G. Alexander and T. D. Fisher. Truth and consequences: Using the bogus pipeline to examine sex differences in self-reported sexuality. *Journal of Sex Research*, 40(1):27–35, 2003.

L. J. Allen. Some discrete-time SI, SIR, and SIS epidemic models. *Mathematical Biosciences*, 124(1):83–105, 1994.

R. M. Anderson. The epidemiology of HIV infection: variable incubation plus infectious periods and heterogeneity in sexual activity. *Journal of the Royal Statistical Society: Series A (Statistics in Society)*, 151(1):66–93, 1988.

R. M. Anderson and R. M. May. Population biology of infectious diseases: Part i. *Nature*, 280(5721):361–367, 1979.

R. M. Anderson, G. F. Medley, R. M. May, and A. M. Johnson. A preliminary study of the transmission dynamics of the human immunodeficiency virus (HIV), the causative agent of AIDS. *Mathematical Medicine and Biology: a Journal of the IMA*, 3(4):229–263, 1986.

W. M. Ankum, B. W. J. Mol, F. Van der Veen, and P. M. M. Bossuyt. Risk factors for ectopic pregnancy: a meta-analysis. *Fertility and Sterility*, 65(6):1093–1099, 1996.

J. Appleby. Tackling COVID-19: are the costs worth the benefits? *The British Medical Journal*, 369, 2020.

B. Armbruster, L. Wang, and M. Morris. Forward reachable sets: Analytically derived properties of connected components for dynamic networks. *Network Science*, 5(3):328–354, 2017.

J. Badham and R. Stocker. The impact of network clustering and assortativity on epidemic behaviour. *Theoretical Population Biology*, 77(1):71–75, 2010.

M. Baguelin, A. J. Van Hoek, M. Jit, S. Flasche, P. J. White, and W. J. Edmunds. Vaccination against pandemic influenza A/H1N1v in England: a real-time economic evaluation. *Vaccine*, 28(12):2370–2384, 2010.

F. Ball and P. Neal. A general model for stochastic SIR epidemics with two levels of mixing. *Mathematical Biosciences*, 180(1-2):73–102, 2002.

F. Ball and P. Neal. Network epidemic models with two levels of mixing. *Mathematical Biosciences*, 212(1):69–87, 2008.

F. Ball, D. Mollison, and G. Scalia-Tomba. Epidemics with two levels of mixing. *The Annals of Applied Probability*, pages 46–89, 1997.

F. Ball, D. Sirl, and P. Trapman. Threshold behaviour and final outcome of an epidemic on a random network with household structure. *Advances in Applied Probability*, 41(3):765–796, 2009.

S. Bansal, J. Read, B. Pourbohloul, and L. A. Meyers. The dynamic nature of contact networks in infectious disease epidemiology. *Journal of Biological Dynamics*, 4(5):478–489, 2010.

R. V. Barnabas, P. Laukkanen, P. Koskela, O. Kontula, M. Lehtinen, and G. P. Garnett. Epidemiology of HPV 16 and cervical cancer in Finland and the potential impact of vaccination: mathematical modelling analyses. *PLoS Medicine*, 3 (5):e138, 2006.

P. M. Barry and J. D. Klausner. The use of cephalosporins for gonorrhea: the impending problem of resistance. *Expert Opinion on Pharmacotherapy*, 10(4): 555–577, 2009.

D. S. Bassett and O. Sporns. Network neuroscience. *Nature Neuroscience*, 20(3): 353–364, 2017.

C. Bauch and D. Rand. A moment closure model for sexually transmitted disease transmission through a concurrent partnership network. *Proceedings of the Royal Society of London. Series B: Biological Sciences*, 267(1456):2019–2027, 2000.

D. C. Beachler, G. Jenkins, M. Safaeian, A. R. Kreimer, and N. Wentzensen. Natural acquired immunity against subsequent genital human papillomavirus infection: a systematic review and meta-analysis. *The Journal of Infectious Diseases*, 213(9):1444–1454, 2016.

L.-G. Bekker, Z. Moodie, N. Grunenberg, F. Laher, G. D. Tomaras, K. W. Cohen, M. Allen, M. Malahleha, K. Mngadi, B. Daniels, et al. Subtype C ALVAC-HIV and bivalent subtype C gp120/MF59 HIV-1 vaccine in low-risk, HIV-uninfected, South African adults: a phase 1/2 trial. *The Lancet HIV*, 5(7):e366–e378, 2018.

Q. Bi, Y. Wu, S. Mei, C. Ye, X. Zou, Z. Zhang, X. Liu, L. Wei, S. A. Truelove, T. Zhang, et al. Epidemiology and transmission of COVID-19 in 391 cases and 1286 of their close contacts in Shenzhen, China: a retrospective cohort study. *The Lancet Infectious Diseases*, 20(8):911–919, 2020.

P. Block, M. Hoffman, I. J. Raabe, J. B. Dowd, C. Rahal, R. Kashyap, and M. C. Mills. Social network-based distancing strategies to flatten the COVID-19 curve in a post-lockdown world. *Nature Human Behaviour*, 4(6):588–596, 2020.

D. D. Brewer, J. J. Potterat, S. B. Garrett, S. Q. Muth, J. M. Roberts, D. Kasprzyk, D. E. Montano, and W. W. Darrow. Prostitution and the sex discrepancy in reported number of sexual partners. *Proceedings of the National Academy of Sciences*, 97(22):12385–12388, 2000.

N. R. Brown and R. C. Sinclair. Estimating number of lifetime sexual partners: Men and women do it differently. *Journal of Sex Research*, 36(3):292–297, 1999.

R. C. Brunham and R. Rappuoli. Chlamydia trachomatis control requires a vaccine. *Vaccine*, 31(15):1892–1897, 2013.

D. R. Burton, R. C. Desrosiers, R. W. Doms, W. C. Koff, P. D. Kwong, J. P. Moore, G. J. Nabel, J. Sodroski, I. A. Wilson, and R. T. Wyatt. HIV vaccine design and the neutralizing antibody problem. *Nature Immunology*, 5(3):233–236, 2004.

A. W. Byrne, D. McEvoy, A. B. Collins, K. Hunt, M. Casey, A. Barber, F. Butler, J. Griffin, E. A. Lane, C. McAloon, et al. Inferred duration of infectious period of SARS-CoV-2: rapid scoping review and analysis of available evidence for asymptomatic and symptomatic COVID-19 cases. *BMJ Open*, 10(8):e039856, 2020.

C. E. Cameron and S. A. Lukehart. Current status of syphilis vaccine development: need, challenges, prospects. *Vaccine*, 32(14):1602–1609, 2014.

K. Canfell, H. Chesson, S. L. Kulasingam, J. Berkhof, M. Diaz, and J. J. Kim. Modeling preventative strategies against human papillomavirus-related disease in developed countries. *Vaccine*, 30:F157–F167, 2012.

M. Carael. Sexual behaviour. In J. G. Cleland and B. Ferry, editors, *Sexual Behaviour and AIDS in the Developing World*, chapter 4. Taylor & Francis, 1995.

W. Cates Jr, R. T. Rolfs Jr, and S. O. Aral. Sexually transmitted diseases, pelvic inflammatory disease, and infertility: an epidemiologic update. *Epidemiologic Reviews*, 12(1):199–220, 1990.

S. Cauchemez, F. Carrat, C. Viboud, A. Valleron, and P. Boelle. A Bayesian MCMC approach to study transmission of influenza: application to household longitudinal data. *Statistics in Medicine*, 23(22):3469–3487, 2004.

S. Cauchemez, A.-J. Valleron, P.-Y. Boelle, A. Flahault, and N. M. Ferguson. Estimating the impact of school closure on influenza transmission from sentinel data. *Nature*, 452(7188):750–754, 2008.

G. Celeux, F. Forbes, C. P. Robert, D. M. Titterington, et al. Deviance information criteria for missing data models. *Bayesian Analysis*, 1(4):651–673, 2006.

M. I. Chen and A. C. Ghani. Populations and partnerships: insights from metapopulation and pair models into the epidemiology of gonorrhoea and other sexually transmitted infections. *Sexually Transmitted Infections*, 86(Suppl 3):iii63–iii69, 2010.

H. W. Chesson, S. Kidd, K. T. Bernstein, R. N. Fanfair, and T. L. Gift. The cost-effectiveness of syphilis screening among men who have sex with men: an exploratory modeling analysis. *Sexually Transmitted Diseases*, 43(7):429, 2016.

T. Chin, C. O. Buckee, and A. S. Mahmud. Quantifying the success of measles vaccination campaigns in the rohingya refugee camps. *Epidemics*, 30:100385, 2020.

Y. H. Choi, M. Jit, N. Gay, A. Cox, G. P. Garnett, and W. J. Edmunds. Transmission dynamic modelling of the impact of human papillomavirus vaccination in the United Kingdom. *Vaccine*, 28(24):4091–4102, 2010.

J. Clarke. Contact tracing for chlamydia: data on effectiveness. *International journal of STD & AIDS*, 9(4):187–191, 1998.

C. M. Clase, E. L. Fu, M. Joseph, R. C. Beale, M. B. Dolovich, M. Jardine, J. F. Mann, R. Pecoits-Filho, W. C. Winkelmayer, and J. J. Carrero. Cloth masks may prevent transmission of COVID-19: An evidence-based, risk-based approach, 2020.

S. Clifford, C. A. Pearson, P. Klepac, K. Van Zandvoort, B. J. Quilty, CMMID COVID-19 working group, R. M. Eggo, and S. Flasche. Effectiveness of interventions targeting air travellers for delaying local outbreaks of SARS-CoV-2. *Journal of Travel Medicine*, 27(5):taaa068, 2020.

L. Cluver, J. M. Lachman, L. Sherr, I. Wessels, E. Krug, S. Rakotomalala, S. Blight, S. Hillis, G. Bachman, O. Green, et al. Parenting in a time of COVID-19. *The Lancet*, 395(10231), 2020.

T. J. Coates, L. Richter, and C. Caceres. Behavioural strategies to reduce HIV transmission: how to make them work better. *The Lancet*, 372(9639):669–684, 2008.

M. L. Cohen. Epidemiology of drug resistance: implications for a post-antimicrobial era. *Science(Washington)*, 257(5073):1050–1055, 1992.

M. S. Cohen. Sexually transmitted diseases enhance HIV transmission: no longer a hypothesis. *The Lancet*, 351:S5–S7, 1998.

A. J. Conlan, K. T. Eames, J. A. Gage, J. C. von Kirchbach, J. V. Ross, R. A. Saenz, and J. R. Gog. Measuring social networks in British primary schools

through scientific engagement. *Proceedings of the Royal Society B: Biological Sciences*, 278(1711):1467–1475, 2011.

K. L. Cooke and J. A. Yorke. Some equations modelling growth processes and gonorrhea epidemics. *Mathematical Biosciences*, 16(1-2):75–101, 1973.

L. Danon, A. P. Ford, T. House, C. P. Jewell, M. J. Keeling, G. O. Roberts, J. V. Ross, and M. C. Vernon. Networks and the epidemiology of infectious disease. *Interdisciplinary Perspectives on Infectious Diseases*, 2011, 2011.

L. Danon, L. Lacasa, and E. Brooks-Pollock. Household bubbles and covid-19 transmission: insights from percolation theory. *medRxiv*, 2020.

S. Datta, C. H. Mercer, and M. J. Keeling. Capturing sexual contact patterns in modelling the spread of sexually transmitted infections: Evidence using Natsal-3. *PloS one*, 13(11):e0206501, 2018.

S. Datta, J. Pink, G. F. Medley, S. Petrou, S. Staniszewska, M. Underwood, P. Sonnenberg, and M. J. Keeling. Assessing the cost-effectiveness of HPV vaccination strategies for adolescent girls and boys in the UK. *BMC Infectious Diseases*, 19 (1):552, 2019.

E. Davidson and M. Levin. Gene regulatory networks. *Proceedings of the National Academy of Sciences*, 102(14):4935–4935, 2005.

N. G. Davies, A. J. Kucharski, R. M. Eggo, A. Gimma, W. J. Edmunds, T. Jombart, K. O'Reilly, A. Endo, J. Hellewell, E. S. Nightingale, et al. Effects of non-pharmaceutical interventions on COVID-19 cases, deaths, and demand for hospital services in the UK: a modelling study. *The Lancet Public Health*, 5(7): e375–e385, 2020.

R. De Vincenzo, C. Conte, C. Ricci, G. Scambia, and G. Capelli. Long-term efficacy and safety of human papillomavirus vaccination. *International Journal of Women's Health*, 6:999, 2014.

O. Diekmann and J. Heesterbeek. Mathematical epidemiology of infectious diseases: model building, analysis and interpretation (vol. 5). In *Wiley Series in Mathematical and Computational Biology*. John Wiley & Sons, 2000.

O. Diekmann, J. A. P. Heesterbeek, and J. A. Metz. On the definition and the computation of the basic reproduction ratio R0 in models for infectious diseases in heterogeneous populations. *Journal of Mathematical Biology*, 28(4):365–382, 1990.

O. Diekmann, K. Dietz, and J. A. P. Heesterbeek. The basic reproduction ratio for sexually transmitted diseases: I. theoretical considerations. *Mathematical Biosciences*, 107(2):325–339, 1991.

K. Dietz and K. Hadeler. Epidemiological models for sexually transmitted diseases. *Journal of Mathematical Biology*, 26(1):1–25, 1988.

J. P. Dodds, A. Nardone, D. E. Mercey, and A. M. Johnson. Increase in high risk sexual behaviour among homosexual men, London 1996-8: cross sectional, questionnaire study. *British Medical Journal*, 320(7248):1510–1511, 2000.

K. Eames, S. Bansal, S. Frost, and S. Riley. Six challenges in measuring contact networks for use in modelling. *Epidemics*, 10:72–77, 2015.

K. T. Eames and M. J. Keeling. Modeling dynamic and network heterogeneities in the spread of sexually transmitted diseases. *Proceedings of the National Academy of Sciences*, 99(20):13330–13335, 2002.

K. T. Eames and M. J. Keeling. Monogamous networks and the spread of sexually transmitted diseases. *Mathematical Biosciences*, 189(2):115–130, 2004.

R. Edwards, S. Kim, and P. van den Driessche. A multigroup model for a heterosexually transmitted disease. *Mathematical Biosciences*, 224(2):87–94, 2010.

N. Ferguson, D. Laydon, G. Nedjati Gilani, N. Imai, K. Ainslie, M. Baguelin, S. Bhatia, A. Boonyasiri, Z. Cucunuba Perez, G. Cuomo-Dannenburg, et al.

Report 9: Impact of non-pharmaceutical interventions (NPIs) to reduce COVID-19 mortality and healthcare demand. 2020.

N. M. Ferguson, D. A. Cummings, S. Cauchemez, C. Fraser, S. Riley, A. Meeyai, S. Iamsirithaworn, and D. S. Burke. Strategies for containing an emerging influenza pandemic in Southeast Asia. *Nature*, 437(7056):209–214, 2005.

L. Ferretti, C. Wymant, M. Kendall, L. Zhao, A. Nurtay, L. Abeler-Dörner, M. Parker, D. Bonsall, and C. Fraser. Quantifying SARS-CoV-2 transmission suggests epidemic control with digital contact tracing. *Science*, 368(6491), 2020.

F. Feys, S. Brokken, and S. De Peuter. Risk-benefit and cost-utility analysis for COVID-19 lockdown in belgium: the impact on mental health and wellbeing. 2020.

T. D. Fisher. The impact of socially conveyed norms on the reporting of sexual behavior and attitudes by men and women. *Journal of Experimental Social Psychology*, 45(3):567–572, 2009.

M. FitzGerald, D. Thirlby, and C. Bedford. The outcome of contact tracing for gonorrhoea in the United Kingdom. *International Journal of STD & AIDS*, 9 (11):657–660, 1998.

S. Flaxman, S. Mishra, A. Gandy, H. J. T. Unwin, T. A. Mellan, H. Coupland, C. Whittaker, H. Zhu, T. Berah, J. W. Eaton, et al. Estimating the effects of non-pharmaceutical interventions on COVID-19 in europe. *Nature*, 584(7820): 257–261, 2020.

W. Floyd, L. Kay, and M. Shapiro. A covering-graph approach to epidemics on SIS and SIS-Like networks. *Bulletin of Mathematical Biology*, 74(1):175–189, 2012.

R. Forman, R. Atun, M. McKee, and E. Mossialos. 12 lessons learned from the management of the coronavirus pandemic. *Health Policy*, 2020.

G. P. Garnett and R. M. Anderson. Balancing sexual partnership in an age and activity stratified model of hiv transmission in heterosexual populations. *Mathematical Medicine and Biology: A Journal of the IMA*, 11(3):161–192, 1994.

G. P. Garnett and R. M. Anderson. Sexually transmitted diseases and sexual behavior: insights from mathematical models. *Journal of Infectious Diseases*, 174(Supplement_2):S150–S161, 1996.

G. P. Garnett, J. Swinton, R. C. Brunham, and R. M. Anderson. Gonococcal infection, infertility, and population growth: Ii. the influence of heterogeneity in sexual behaviour. *Mathematical Medicine and Biology: A Journal of the IMA*, 9 (2):127–144, 1992.

L. Gaydosh, G. Reniers, and S. Helleringer. Partnership concurrency and coital frequency. *AIDS and Behavior*, 17(7):2376–2386, 2013.

L. J. Gelmon and P. Piot. The interactions between HIV and other sexually transmitted infections. In J. Mann and D. Tarantola, editors, *AIDS in the World II*, volume 99, chapter 6, pages 99–101. New York New York Oxford University Press 1996., 1996.

M. Gilbert, M. Dewatripont, E. Muraille, J.-P. Platteau, and M. Goldman. Preparing for a responsible lockdown exit strategy. *Nature Medicine*, 26(5):643–644, 2020.

M. R. Golden, M. Hogben, H. H. Handsfield, J. S. S. Lawrence, J. J. Potterat, and K. K. Holmes. Partner notification for HIV and STD in the United States: Low coverage for gonorrhea, chlamydial infection, and HIV. *Sexually Transmitted Diseases*, 30(6):490–496, 2003.

S. J. Goldie, M. Kohli, D. Grima, M. C. Weinstein, T. C. Wright, F. X. Bosch, and E. Franco. Projected clinical benefits and cost-effectiveness of a human papillomavirus 16/18 vaccine. *Journal of the National Cancer Institute*, 96(8): 604–615, 2004.

J. Gomez-Gardenes, V. Latora, Y. Moreno, and E. Profumo. Spreading of sexually transmitted diseases in heterosexual populations. *Proceedings of the National Academy of Sciences*, 105(5):1399–1404, 2008.

L. A. Goodman. Snowball sampling. *The Annals of Mathematical Statistics*, pages 148–170, 1961.

S. M. Goodreau, J. A. Kitts, and M. Morris. Birds of a feather, or friend of a friend? using exponential random graph models to investigate adolescent social networks. *Demography*, 46(1):103–125, 2009.

S. M. Goodreau, E. S. Rosenberg, S. M. Jenness, N. Luisi, S. E. Stansfield, G. A. Millett, and P. S. Sullivan. Sources of racial disparities in HIV prevalence in men who have sex with men in Atlanta, GA, USA: a modelling study. *The Lancet HIV*, 4(7):e311–e320, 2017.

S. M. Goodreau, S. E. Stansfield, J. T. Murphy, K. C. Peebles, G. S. Gottlieb, N. F. Abernethy, J. T. Herbeck, and J. E. Mittler. Relational concurrency, stages of infection, and the evolution of HIV set point viral load. *Virus Evolution*, 4(2): vey032, 2018.

S. L. Gottlieb, N. Low, L. M. Newman, G. Bolan, M. Kamb, and N. Broutet. Toward global prevention of sexually transmitted infections (STIs): the need for STI vaccines. *Vaccine*, 32(14):1527–1535, 2014.

GOV.UK. The R number in the UK. https://www.gov,uk/guidance/the-r-number-in-the-uk, 2020a.

GOV.UK. Meeting people from outside your household, 2020b.

GOV.UK. Making a childcare bubble with another household. https://www.gov.uk/guidance/making-a-childcare-bubble-with-another-household, 2021.

R. M. Granich, C. F. Gilks, C. Dye, K. M. De Cock, and B. G. Williams. Universal voluntary HIV testing with immediate antiretroviral therapy as a strategy for elimination of HIV transmission: a mathematical model. *The Lancet*, 373(9657): 48–57, 2009.

R. T. Gray, K. W. Beagley, P. Timms, and D. P. Wilson. Modeling the impact of potential vaccines on epidemics of sexually transmitted chlamydia trachomatis infection. *The Journal of Infectious Diseases*, 199(11):1680–1688, 2009.

B. Grenfell and J. Harwood. (Meta) population dynamics of infectious diseases. *Trends in Ecology & Evolution*, 12(10):395–399, 1997.

B. T. Grenfell, O. N. Bjørnstad, and J. Kappey. Travelling waves and spatial hierarchies in measles epidemics. *Nature*, 414(6865):716–723, 2001.

S. Gupta, R. M. Anderson, and R. M. May. Networks of sexual contacts: Implication for the pattern of spread. *AIDS*, 3(12), 1989.

E. Haavio-Mannila. *Trends in sexual life: Measured by national sex surveys in Finland in 1971, 1992 and 1999, and a comparison to a sex survey in St. Petersburg in 1996.* (STAKES, Services for Independent Living), 2001.

D. Hansson, K. Leung, T. Britton, and S. Strömdahl. A dynamic network model to disentangle the roles of steady and casual partners for HIV transmission among MSM. *Epidemics*, 27:66–76, 2019.

W. K. Hastings. Monte Carlo sampling methods using Markov chains and their applications. 1970.

D. D. Heckathorn. Respondent-driven sampling: a new approach to the study of hidden populations. *Social Problems*, 44(2):174–199, 1997.

J. C. Heijne, C. L. Althaus, S. A. Herzog, M. Kretzschmar, and N. Low. The role of reinfection and partner notification in the efficacy of chlamydia screening programs. *Journal of Infectious Diseases*, 203(3):372–377, 2011.

J. C. Heijne, S. A. Herzog, C. L. Althaus, N. Low, and M. Kretzschmar. Case and partnership reproduction numbers for a curable sexually transmitted infection. *Journal of Theoretical Biology*, 331:38–47, 2013.

H. W. Hethcote and J. A. Yorke. *Gonorrhea transmission dynamics and control*, volume 56. Springer, 1984.

J. Hilton and M. J. Keeling. Incorporating household structure and demography into models of endemic disease. *Journal of the Royal Society Interface*, 16(157): 20190317, 2019.

J. Horn, O. Damm, M. Kretzschmar, Y. Deleré, O. Wichmann, A. Kaufmann, E. Garbe, A. Krämer, W. Greiner, and R. Mikolajczyk. Estimating the long-term effects of HPV vaccination in germany. *Vaccine*, 31(19):2372–2380, 2013.

T. House. Algebraic moment closure for population dynamics on discrete structures. *Bulletin of Mathematical Biology*, 77(4):646–659, 2015.

T. House and M. J. Keeling. Deterministic epidemic models with explicit household structure. *Mathematical Biosciences*, 213(1):29–39, 2008.

T. House and M. J. Keeling. The impact of contact tracing in clustered populations. *PLoS Computational Biology*, 6(3):e1000721, 2010.

T. House and M. J. Keeling. Epidemic prediction and control in clustered populations. *Journal of Theoretical Biology*, 272(1):1–7, 2011a.

T. House and M. J. Keeling. Insights from unifying modern approximations to infections on networks. *Journal of The Royal Society Interface*, 8(54):67–73, 2011b.

T. House, G. Davies, L. Danon, and M. J. Keeling. A motif-based approach to network epidemics. *Bulletin of Mathematical Biology*, 71(7):1693–1706, 2009.

R. Howell-Jones, N. de Silva, M. Akpan, P. Oakeshott, C. Carder, L. Coupland, M. Sillis, H. Mallinson, V. Ellis, D. Frodsham, et al. Prevalence of human papillomavirus (HPV) infections in sexually active adolescents and young women in England, prior to widespread HPV immunisation. *Vaccine*, 30(26):3867–3875, 2012.

S. Hsiang, D. Allen, S. Annan-Phan, K. Bell, I. Bolliger, T. Chong, H. Druckenmiller, L. Y. Huang, A. Hultgren, E. Krasovich, et al. The effect of large-scale anti-contagion policies on the COVID-19 pandemic. *Nature*, 584(7820):262–267, 2020.

C. Huang, Y. Wang, X. Li, L. Ren, J. Zhao, Y. Hu, L. Zhang, G. Fan, J. Xu, X. Gu, et al. Clinical features of patients infected with 2019 novel coronavirus in Wuhan, China. *The Lancet*, 395(10223):497–506, 2020.

R. Huerta and L. S. Tsimring. Contact tracing and epidemics control in social networks. *Physical Review E*, 66(5):056115, 2002.

L. Isella, M. Romano, A. Barrat, C. Cattuto, V. Colizza, W. Van den Broeck, F. Gesualdo, E. Pandolfi, L. Ravà, C. Rizzo, et al. Close encounters in a pediatric ward: measuring face-to-face proximity and mixing patterns with wearable sensors. *PloS one*, 6(2):e17144, 2011.

C. I. Jarvis, K. Van Zandvoort, A. Gimma, K. Prem, P. Klepac, G. J. Rubin, and W. J. Edmunds. Quantifying the impact of physical distance measures on the transmission of COVID-19 in the UK. *BMC Medicine*, 18:1–10, 2020.

S. M. Jenness, K. M. Weiss, S. M. Goodreau, T. Gift, H. Chesson, K. W. Hoover, D. K. Smith, A. Y. Liu, P. S. Sullivan, and E. S. Rosenberg. Incidence of gonorrhea and chlamydia following human immunodeficiency virus preexposure prophylaxis among men who have sex with men: a modeling study. *Clinical Infectious Diseases*, 65(5):712–718, 2017.

S. M. Jenness, S. M. Goodreau, and M. Morris. EpiModel: an R package for mathematical modeling of infectious disease over networks. *Journal of Statistical Software*, 84, 2018.

A. E. Jerse, M. C. Bash, and M. W. Russell. Vaccines against gonorrhea: current status and future challenges. *Vaccine*, 32(14):1579–1587, 2014.

M. Jit, Y. H. Choi, and W. J. Edmunds. Economic evaluation of human papillomavirus vaccination in the united kingdom. *British Medical Journal*, 337, 2008.

A. M. Johnson, C. H. Mercer, B. Erens, A. J. Copas, S. McManus, K. Wellings, K. A. Fenton, C. Korovessis, W. Macdowall, K. Nanchahal, et al. Sexual behaviour in Britain: partnerships, practices, and HIV risk behaviours. *The Lancet*, 358(9296):1835–1842, 2001.

S. Johnson, V. Domínguez-García, L. Donetti, and M. A. Muñoz. Trophic coherence determines food-web stability. *Proceedings of the National Academy of Sciences*, 111(50):17923–17928, 2014.

M. J. Keeling. The effects of local spatial structure on epidemiological invasions. *Proceedings of the Royal Society of London. Series B: Biological Sciences*, 266 (1421):859–867, 1999.

M. J. Keeling and K. T. Eames. Networks and epidemic models. *Journal of the Royal Society Interface*, 2(4):295–307, 2005.

M. J. Keeling and P. Rohani. *Modeling infectious diseases in humans and animals*. Princeton university press, 2011.

M. J. Keeling, T. House, A. J. Cooper, and L. Pellis. Systematic approximations to susceptible-infectious-susceptible dynamics on networks. *PLoS Computational Biology*, 12(12):e1005296, 2016.

M. J. Keeling, E. M. Hill, E. E. Gorsich, B. Penman, G. Guyver-Fletcher, A. Holmes, T. Leng, H. McKimm, M. Tamborrino, L. Dyson, et al. Predic-

tions of COVID-19 dynamics in the uk: short-term forecasting and analysis of potential exit strategies. *PLoS Computational Biology*, 17(1):e1008619, 2021.

M. E. Kent and F. Romanelli. Reexamining syphilis: an update on epidemiology, clinical manifestations, and management. *Annals of Pharmacotherapy*, 42(2): 226–236, 2008.

W. O. Kermack and A. G. McKendrick. A contribution to the mathematical theory of epidemics. *Proceedings of the Royal Society of London. Series A, Containing papers of a mathematical and physical character*, 115(772):700–721, 1927.

J.-H. Kim, R. L. Riolo, and J. S. Koopman. HIV transmission by stage of infection and pattern of sexual partnerships. *Epidemiology (Cambridge, Mass.)*, 21(5):676, 2010.

T. Kirby. Evidence mounts on the disproportionate effect of COVID-19 on ethnic minorities. *The Lancet Respiratory Medicine*, 8(6):547–548, 2020.

J. G. Kirkwood. Statistical mechanics of fluid mixtures. *The Journal of Chemical Physics*, 3(5):300–313, 1935.

I. Z. Kiss, C. G. Morris, F. Sélley, P. L. Simon, and R. R. Wilkinson. Exact deterministic representation of Markovian epidemics on networks with and without loops. *Journal of Mathematical Biology*, 70(3):437–464, 2015a.

I. Z. Kiss, G. Röst, and Z. Vizi. Generalization of pairwise models to non-markovian epidemics on networks. *Physical Review Letters*, 115(7):078701, 2015b.

I. Z. Kiss, J. C. Miller, P. L. Simon, et al. Mathematics of epidemics on networks. *Cham: Springer*, 598, 2017.

A. S. Klovdahl. Social networks and the spread of infectious diseases: the AIDS example. *Social Science & Medicine*, 21(11):1203–1216, 1985.

A. S. Klovdahl, J. J. Potterat, D. E. Woodhouse, J. B. Muth, S. Q. Muth, and W. W. Darrow. Social networks and infectious disease: The colorado springs study. *Social Science & Medicine*, 38(1):79–88, 1994.

W. C. Koh, L. Naing, L. Chaw, M. A. Rosledzana, M. F. Alikhan, S. A. Jamaludin, F. Amin, A. Omar, A. Shazli, M. Griffith, et al. What do we know about SARS-CoV-2 transmission? a systematic review and meta-analysis of the secondary attack rate and associated risk factors. *PloS One*, 15(10):e0240205, 2020.

L. Koutsky. Epidemiology of genital human papillomavirus infection. *The American Journal of Medicine*, 102(5):3–8, 1997.

M. U. Kraemer, C.-H. Yang, B. Gutierrez, C.-H. Wu, B. Klein, D. M. Pigott, L. Du Plessis, N. R. Faria, R. Li, W. P. Hanage, et al. The effect of human mobility and control measures on the COVID-19 epidemic in China. *Science*, 368(6490):493–497, 2020.

M. Kretzschmar and J. C. Heijne. Pair formation models for sexually transmitted infections: a primer. *Infectious Disease Modelling*, 2(3):368–378, 2017.

M. Kretzschmar and M. Morris. Measures of concurrency in networks and the spread of infectious disease. *Mathematical Biosciences*, 133(2):165–195, 1996.

M. Kretzschmar, J. C. Jager, D. P. Reinking, G. Van Zessen, and H. Brouwers. The basic reproduction ratio R0 for a sexually transmitted disease in pair formation model with two types of pairs. *Mathematical Biosciences*, 124(2):181–205, 1994.

M. Kretzschmar, K. M. Turner, P. M. Barton, W. J. Edmunds, and N. Low. Predicting the population impact of chlamydia screening programmes: comparative mathematical modelling study. *Sexually Transmitted Infections*, 85(5):359–366, 2009.

M. Kretzschmar, R. G. White, and M. Caraël. Concurrency is more complex than it seems. *AIDS (London, England)*, 24(2):313, 2010.

A. J. Kucharski, P. Klepac, A. J. Conlan, S. M. Kissler, M. L. Tang, H. Fry, J. R. Gog, W. J. Edmunds, J. C. Emery, G. Medley, et al. Effectiveness of isolation, testing, contact tracing, and physical distancing on reducing transmission of SARS-CoV-2 in different settings: a mathematical modelling study. *The Lancet Infectious Diseases*, 20(10):1151–1160, 2020.

J. Kuha. AIC and BIC: Comparisons of assumptions and performance. *Sociological Methods & Research*, 33(2):188–229, 2004.

S. L. Kulasingam and E. R. Myers. Potential health and economic impact of adding a human papillomavirus vaccine to screening programs. *Jama*, 290(6):781–789, 2003.

V. G. Kulkarni. *Modeling and analysis of stochastic systems*. Crc Press, 2016.

S. A. Lauer, K. H. Grantz, Q. Bi, F. K. Jones, Q. Zheng, H. R. Meredith, A. S. Azman, N. G. Reich, and J. Lessler. The incubation period of coronavirus disease 2019 (COVID-19) from publicly reported confirmed cases: estimation and application. *Annals of Internal Medicine*, 172(9):577–582, 2020.

H. K. Lee, P.-S. Shim, and J. D. Noh. Epidemic threshold of the susceptible-infected-susceptible model on complex networks. *Physical Review E*, 87(6): 062812, 2013.

T. Leng and M. J. Keeling. Concurrency of partnerships, consistency with data, and control of sexually transmitted infections. *Epidemics*, 25:35–46, 2018.

T. Leng and M. J. Keeling. Improving pairwise approximations for network models with susceptible-infected-susceptible dynamics. *Journal of Theoretical Biology*, 500:110328, 2020.

T. Leng, C. White, J. Hilton, A. Kucharski, L. Pellis, H. Stage, N. G. Davies, et al. The effectiveness of social bubbles as part of a covid-19 lockdown exit strategy, a modelling study. *Wellcome open research*, 5, 2020.

K. Y. Leung, M. Kretzschmar, and O. Diekmann. Dynamic concurrent partnership networks incorporating demography. *Theoretical Population Biology*, 82(3):229–239, 2012.

K. Y. Leung, M. Kretzschmar, and O. Diekmann. Infection on a dynamic partnership network: characterization of R0. *Journal of Mathematical Biology*, 71(1): 1–56, 2015.

B. Lewin, K. Fugl-Meyer, G. Helmius, A. Lalos, and S.-A. Månsson. *Sex i Sverige; Om sexuallivet i Sverige 1996*. Folkhälsoinstitutet, 1998.

T. M. Liggett. *Stochastic interacting systems: contact, voter and exclusion processes*, volume 324. springer science & Business Media, 2013.

F. Liljeros, C. R. Edling, L. A. N. Amaral, H. E. Stanley, and Y. Åberg. The web of human sexual contacts. *Nature*, 411(6840):907–908, 2001.

J. Lindquist, J. Ma, P. Van den Driessche, and F. H. Willeboordse. Effective degree network disease models. *Journal of Mathematical Biology*, 62(2):143–164, 2011.

Y. Liu, S. Funk, S. Flasche, and CMMID COVID-19 working group. The contribution of pre-symptomatic infection to the transmission dynamics of covid-2019. *Wellcome Open Research*, 5, 2020.

S. Ljubojevic and M. Skerlev. HPV-associated diseases. *Clinics in Dermatology*, 32(2):227–234, 2014.

N. J. Long, P. J. Aikman, N. S. Appleton, S. G. Davies, A. Deckert, E. Holroyd, N. Jivraj, M. Laws, N. Simpson, R. Sterling, et al. Living in bubbles during the coronavirus pandemic: insights from New Zealand. 2020. URL `http://orapp.aut.ac.nz/handle/10292/13334`.

S. R. Lustig, J. J. Biswakarma, D. Rana, S. H. Tilford, W. Hu, M. Su, and M. S. Rosenblatt. Effectiveness of common fabrics to block aqueous aerosols of virus-like nanoparticles. *ACS Nano*, 14(6):7651–7658, 2020.

L. E. Markowitz, E. F. Dunne, M. Saraiya, H. W. Lawson, H. Chesson, and E. R. Unger. Quadrivalent human papillomavirus vaccine. *Morbidity and Mortality weekly report*, 56(RR-2):1–24, 2007.

L. E. Markowitz, V. Tsu, S. L. Deeks, H. Cubie, S. A. Wang, A. S. Vicari, and J. M. Brotherton. Human papillomavirus vaccine introduction–the first five years. *Vaccine*, 30:F139–F148, 2012.

R. M. May and R. M. Anderson. Commentary˜ transmission dynamics of hiv infection. *Nature*, 326:137, 1987.

S. McCormack, D. T. Dunn, M. Desai, D. I. Dolling, M. Gafos, R. Gilson, A. K. Sullivan, A. Clarke, I. Reeves, G. Schembri, et al. Pre-exposure prophylaxis to prevent the acquisition of HIV-1 infection (PROUD): effectiveness results from the pilot phase of a pragmatic open-label randomised trial. *The Lancet*, 387 (10013):53–60, 2016.

C. H. Mercer, C. Tanton, P. Prah, B. Erens, P. Sonnenberg, S. Clifton, W. Macdowall, R. Lewis, N. Field, J. Datta, et al. Changes in sexual attitudes and lifestyles in britain through the life course and over time: findings from the national surveys of sexual attitudes and lifestyles (natsal). *The Lancet*, 382(9907): 1781–1794, 2013.

N. Metropolis, A. W. Rosenbluth, M. N. Rosenbluth, A. H. Teller, and E. Teller. Equation of state calculations by fast computing machines. *The Journal of Chemical Physics*, 21(6):1087–1092, 1953.

L. A. Meyers, B. Pourbohloul, M. E. Newman, D. M. Skowronski, and R. C. Brunham. Network theory and SARS: predicting outbreak diversity. *Journal of Theoretical Biology*, 232(1):71–81, 2005.

J. C. Miller. Percolation and epidemics in random clustered networks. *Physical Review E*, 80(2):020901, 2009.

J. C. Miller, A. C. Slim, and E. M. Volz. Edge-based compartmental modelling for infectious disease spread. *Journal of the Royal Society Interface*, 9(70):890–906, 2012.

A. Minello. The pandemic and the female academic. *Nature*, 17:2020, 2020.

K. R. Mitchell, C. H. Mercer, P. Prah, S. Clifton, C. Tanton, K. Wellings, and A. Copas. Why do men report more opposite-sex sexual partners than women? analysis of the gender discrepancy in a british national probability survey. *The Journal of Sex Research*, 56(1):1–8, 2019.

H. Mohammed, P. Blomquist, D. Ogaz, S. Duffell, M. Furegato, M. Checchi, N. Irvine, L. A. Wallace, D. R. Thomas, A. Nardone, et al. 100 years of STIs in the UK: a review of national surveillance data. *Sexually Transmitted Infections*, 94(8):553–558, 2018.

M. Molloy and B. Reed. A critical point for random graphs with a given degree sequence. *Random structures & algorithms*, 6(2-3):161–180, 1995.

C. Moore and M. E. Newman. Epidemics and percolation in small-world networks. *Physical Review E*, 61(5):5678, 2000.

M. Morris and M. Kretzschmar. Concurrent partnerships and transmission dynamics in networks. *Social Networks*, 17(3-4):299–318, 1995.

M. Morris and M. Kretzschmar. Concurrent partnerships and the spread of HIV. *AIDS*, 11(5):641–648, 1997.

M. Morris and M. Kretzschmar. A microsimulation study of the effect of concurrent partnerships on the spread of HIV in Uganda. *Mathematical Population Studies*, 8(2):109–133, 2000.

J. Mossong, N. Hens, M. Jit, P. Beutels, K. Auranen, R. Mikolajczyk, M. Massari, S. Salmaso, G. S. Tomba, J. Wallinga, et al. Social contacts and mixing patterns relevant to the spread of infectious diseases. *PLoS Medicine*, 5(3):e74, 2008.

N. Muñoz, F. X. Bosch, S. De Sanjosé, R. Herrero, X. Castellsagué, K. V. Shah, P. J. Snijders, and C. J. Meijer. Epidemiologic classification of human papillomavirus types associated with cervical cancer. *New England Journal of Medicine*, 348(6): 518–527, 2003.

M. Nath, Y. Ren, Y. Khorramzadeh, and S. Eubank. Determining whether a class of random graphs is consistent with an observed contact network. *Journal of Theoretical Biology*, 440:121–132, 2018.

New Zealand Government. Covid-19 alert system. unite covid-19, 2020.

L. Newman, J. Rowley, S. Vander Hoorn, N. S. Wijesooriya, M. Unemo, N. Low, G. Stevens, S. Gottlieb, J. Kiarie, and M. Temmerman. Global estimates of the prevalence and incidence of four curable sexually transmitted infections in 2012 based on systematic review and global reporting. *PloS one*, 10(12):e0143304, 2015.

M. Newman. *Networks: an introduction*. Oxford University Press, 2010.

M. E. Newman. Random graphs as models of networks. *Handbook of Graphs and Networks*, 1:35–68, 2003.

A. Nicolosi, M. L. C. Leite, M. Musicco, C. Arici, G. Gavazzeni, and A. Lazzarin. The efficiency of male-to-female and female-to-male sexual transmission of the human immunodeficiency virus: a study of 730 stable couples. *Epidemiology*, pages 570–575, 1994.

A. G. Nyitray, H.-Y. Lin, W. J. Fulp, M. Chang, L. Menezes, B. Lu, M. Abrahamsen, M. Papenfuss, C. Gage, C. M. Galindo, and A. R. Giuliano. The role of monogamy and duration of heterosexual relationships in human papillomavirus transmission. *The Journal of Infectious Diseases*, 209(7):1007–1015, 2013.

Office for National Statistics. Census ad hoc household composition (age groups)

safeguarded tables (lower layer super output area): England and Wales. http://doi.org/10.5255/UKDA-SN-8637-1, 2020a.

Office for National Statistics. STI diagnoses and rates in England by gender, 2010 to 2019, 2020b.

J. T. Parsons, T. J. Starks, S. DuBois, C. Grov, and S. A. Golub. Alternatives to monogamy among gay male couples in a community survey: Implications for mental health and sexual risk. *Archives of Sexual Behavior*, 42(2):303–312, 2013.

L. Pellis, N. Ferguson, and C. Fraser. Threshold parameters for a model of epidemic spread among households and workplaces. *Journal of the Royal Society Interface*, 6(40):979–987, 2009.

L. Pellis, F. Ball, and P. Trapman. Reproduction numbers for epidemic models with households and other social structures. i. definition and calculation of R0. *Mathematical Biosciences*, 235(1):85–97, 2012.

L. Pellis, F. Ball, S. Bansal, K. Eames, T. House, V. Isham, and P. Trapman. Eight challenges for network epidemic models. *Epidemics*, 10:58–62, 2015a.

L. Pellis, T. House, and M. J. Keeling. Exact and approximate moment closures for non-Markovian network epidemics. *Journal of Theoretical Biology*, 382:160–177, 2015b.

A. S. Perelson and R. M. Ribeiro. Modeling the within-host dynamics of HIV infection. *BMC Biology*, 11(1):1–10, 2013.

T. A. Peterman, R. L. Stoneburner, J. R. Allen, H. W. Jaffe, and J. W. Curran. Risk of human immunodeficiency virus transmission from heterosexual adults with transfusion-associated infections. *Jama*, 259(1):55–58, 1988.

J. Peto, N. A. Alwan, K. M. Godfrey, R. A. Burgess, D. J. Hunter, E. Riboli, P. Romer, I. Buchan, T. Colbourn, C. Costelloe, et al. Universal weekly testing

as the UK COVID-19 lockdown exit strategy. *The Lancet*, 395(10234):1420–1421, 2020.

C. Pooley and G. Marion. Bayesian model evidence as a practical alternative to deviance information criterion. *Royal Society open science*, 5(3):171519, 2018.

G. E. Potter and N. Hens. A penalized likelihood approach to estimate within-household contact networks from egocentric data. *Journal of the Royal Statistical Society. Series C, Applied statistics*, 62(4):629, 2013.

K. A. Powers, A. C. Ghani, W. C. Miller, I. F. Hoffman, A. E. Pettifor, G. Kamanga, F. E. Martinson, and M. S. Cohen. The role of acute and early HIV infection in the spread of HIV and implications for transmission prevention strategies in lilongwe, malawi: a modelling study. *The Lancet*, 378(9787):256–268, 2011.

D. J. D. S. Price. Networks of scientific papers. *Science*, pages 510–515, 1965.

Public Health England. Sexually transmitted infections and screening for chlamydia in England, 2019. *London, UK: Public Health England*, 2019.

Z. Raisi-Estabragh, C. McCracken, M. S. Bethell, J. Cooper, C. Cooper, M. J. Caulfield, P. B. Munroe, N. C. Harvey, and S. E. Petersen. Greater risk of severe COVID-19 in Black, Asian and Minority Ethnic populations is not explained by cardiometabolic, socioeconomic or behavioural factors, or by 25 (OH)-vitamin D status: study of 1326 cases from the UK Biobank. *Journal of Public Health*, 42 (3):451–460, 2020.

D. Rand. Correlation equations and pair approximations for spatial ecologies. *Advanced Ecological Theory: Principles and Applications*, pages 100–142, 1999.

J. M. Read and M. J. Keeling. Disease evolution on networks: the role of contact structure. *Proceedings of the Royal Society of London. Series B: Biological Sciences*, 270(1516):699–708, 2003.

G. Reniers and R. Tfaily. Polygyny, partnership concurrency, and HIV transmission in Sub-Saharan Africa. *Demography*, 49(3):1075–1101, 2012.

G. Reniers and S. Watkins. Polygyny and the spread of HIV in Sub Saharan Africa: a case of benign concurrency. *AIDS (London, England)*, 24(2):299, 2010.

rgp120 HIV Vaccine Study Group et al. Placebo-controlled phase 3 trial of a recombinant glycoprotein 120 vaccine to prevent HIV-1 infection. *Journal of Infectious Diseases*, 191(5):654–665, 2005.

L. Ribassin-Majed, R. Lounes, and S. Clémençon. Deterministic modelling for transmission of human papillomavirus 6/11: impact of vaccination. *Mathematical Medicine and Biology: a Journal of the IMA*, 31(2):125–149, 2014.

T. Rogers. Maximum-entropy moment-closure for stochastic systems on networks. *Journal of Statistical Mechanics: Theory and Experiment*, 2011(05):P05007, 2011.

M. M. Rönn, C. Testa, A. R. Tuite, H. W. Chesson, T. L. Gift, C. Schumacher, S. L. Williford, L. Zhu, M. Bellerose, R. Earnest, et al. The potential population-level impact of different gonorrhea screening strategies in Baltimore and San Francisco: an exploratory mathematical modeling analysis. *Sexually Transmitted Diseases*, 47(3):143, 2020.

G. Rozhnova, M. F. S. van der Loeff, J. C. Heijne, and M. E. Kretzschmar. Impact of heterogeneity in sexual behavior on effectiveness in reducing HIV transmission with test-and-treat strategy. *PLoS Computational Biology*, 12(8):e1005012, 2016.

G. Rozhnova, J. C. Heijne, M. Basten, C. den Daas, A. Matser, and M. Kretzschmar. Impact of sexual trajectories of men who have sex with men on the reduction in HIV transmission by pre-exposure prophylaxis. *Epidemics*, 28:100337, 2019.

M. Salathé, M. Kazandjieva, J. W. Lee, P. Levis, M. W. Feldman, and J. H. Jones. A high-resolution human contact network for infectious disease transmission. *Proceedings of the National Academy of Sciences*, 107(51):22020–22025, 2010.

I. Sarbu, C. Matei, V. Benea, and S. Georgescu. Brief history of syphilis. *Journal of Medicine and Life*, 7(1):4, 2014.

A. Schneeberger, C. H. Mercer, S. A. Gregson, N. M. Ferguson, C. A. Nyamukapa, R. M. Anderson, A. M. Johnson, and G. P. Garnett. Scale-free networks and sexually transmitted diseases: a description of observed patterns of sexual contacts in Britain and Zimbabwe. *Sexually Transmitted Diseases*, 31(6):380–387, 2004.

M. E. Scott, N. R. Steward-Streng, J. Manlove, E. Schelar, and C. Cui. Characteristics of young adult sexual relationships: Diverse, sometimes violent, often loving. *Child Trends*, 18:1–8, 2011.

R.-P. Sekaly. The failed HIV Merck vaccine study: a step back or a launching point for future vaccine development? *Journal of Experimental Medicine*, 205(1):7–12, 2008.

K. J. Sharkey. Deterministic epidemiological models at the individual level. *Journal of Mathematical Biology*, 57(3):311–331, 2008.

K. J. Sharkey. Deterministic epidemic models on contact networks: correlations and unbiological terms. *Theoretical Population Biology*, 79(4):115–129, 2011.

K. J. Sharkey, C. Fernandez, K. L. Morgan, E. Peeler, M. Thrush, J. F. Turnbull, and R. G. Bowers. Pair-level approximations to the spatio-temporal dynamics of epidemics on asymmetric contact networks. *Journal of Mathematical Biology*, 53 (1):61–85, 2006.

K. J. Sharkey, I. Z. Kiss, R. R. Wilkinson, and P. L. Simon. Exact equations for SIR epidemics on tree graphs. *Bulletin of Mathematical Biology*, 77(4):614–645, 2015.

P. L. Simon and I. Z. Kiss. Super compact pairwise model for SIS epidemic on heterogeneous networks. *Journal of Complex Networks*, 4(2):187–200, 2016.

P. L. Simon, M. Taylor, and I. Z. Kiss. Exact epidemic models on graphs using graph-automorphism driven lumping. *Journal of Mathematical Biology*, 62(4): 479–508, 2011.

J. H. Smid, V. Garcia, N. Low, C. H. Mercer, and C. L. Althaus. Age difference between heterosexual partners in britain: Implications for the spread of chlamydia trachomatis. *Epidemics*, 24:60–66, 2018.

D. J. Spiegelhalter, N. G. Best, B. P. Carlin, and A. Van Der Linde. Bayesian measures of model complexity and fit. *Journal of the Royal Statistical Society: Series B (Statistical Methodology)*, 64(4):583–639, 2002.

S. Stokley, J. Jeyarajah, D. Yankey, M. Cano, J. Gee, J. Roark, R. C. Curtis, and L. Markowitz. Human papillomavirus vaccination coverage among adolescents, 2007-2013, and postlicensure vaccine safety monitoring, 2006-2014–united states. *MMWR. Morbidity and Mortality Weekly Report*, 63(29):620–624, 2014.

H. Streeck, B. Schulte, B. M. Kümmerer, E. Richter, T. Höller, C. Fuhrmann, E. Bartok, R. Dolscheid-Pommerich, M. Berger, L. Wessendorf, et al. Infection fatality rate of SARS-CoV-2 in a super-spreading event in Germany. *Nature Communications*, 11(1):1–12, 2020.

A. V. Taira, C. P. Neukermans, and G. D. Sanders. Evaluating human papillomavirus vaccination programs. *Emerging Infectious Diseases*, 10(11):1915, 2004.

M. Taylor, P. L. Simon, D. M. Green, T. House, and I. Z. Kiss. From Markovian to pairwise epidemic models and the performance of moment closure approximations. *Journal of Mathematical Biology*, 64(6):1021–1042, 2012.

T. J. Taylor and I. Z. Kiss. Interdependency and hierarchy of exact and approximate

epidemic models on networks. *Journal of Mathematical Biology*, 69(1):183–211, 2014.

P. Trapman. Reproduction numbers for epidemics on networks using pair approximation. *Mathematical Biosciences*, 210(2):464–489, 2007.

A. R. Tuite, M. M. Rönn, E. E. Wolf, T. L. Gift, H. W. Chesson, A. Berruti, K. Galer, N. A. Menzies, K. Hsu, and J. A. Salomon. Estimated impact of screening on gonorrhea epidemiology in the United States: insights from a mathematical model. *Sexually Transmitted Diseases*, 45(11):713, 2018.

UNAIDS. Fact sheet – latest statistics on the status of the aids epidemic. `http://www.unaids.org/en/resources/fact-sheet`, 2017. Online; accessed July 2017.

N. Van de Velde, M. Brisson, and M.-C. Boily. Understanding differences in predictions of HPV vaccine effectiveness: A comparative model-based analysis. *Vaccine*, 28(33):5473–5484, 2010.

P. Van Mieghem and R. Van de Bovenkamp. Non-Markovian infection spread dramatically alters the susceptible-infected-susceptible epidemic threshold in networks. *Physical Review Letters*, 110(10):108701, 2013.

A. Vehtari, A. Gelman, and J. Gabry. Practical Bayesian model evaluation using leave-one-out cross-validation and WAIC. *Statistics and Computing*, 27(5):1413–1432, 2017.

R. Verity, L. C. Okell, I. Dorigatti, P. Winskill, C. Whittaker, N. Imai, G. Cuomo-Dannenburg, H. Thompson, P. G. Walker, H. Fu, et al. Estimates of the severity of coronavirus disease 2019: a model-based analysis. *The Lancet Infectious Diseases*, 20(6):669–677, 2020.

E. Volz. SIR dynamics in random networks with heterogeneous connectivity. *Journal of Mathematical Biology*, 56(3):293–310, 2008.

E. Volz and L. A. Meyers. Susceptible–infected–recovered epidemics in dynamic contact networks. *Proceedings of the Royal Society B: Biological Sciences*, 274 (1628):2925–2934, 2007.

E. Volz and L. A. Meyers. Epidemic thresholds in dynamic contact networks. *Journal of the Royal Society Interface*, 6(32):233–241, 2009.

E. M. Volz, J. C. Miller, A. Galvani, and L. A. Meyers. Effects of heterogeneous and clustered contact patterns on infectious disease dynamics. *PLoS Computational Biology*, 7(6):e1002042, 2011.

C. Von Ferber, T. Holovatch, Y. Holovatch, and V. Palchykov. Public transport networks: empirical analysis and modeling. *The European Physical Journal B*, 68(2):261–275, 2009.

J. Wallinga, P. Teunis, and M. Kretzschmar. Using data on social contacts to estimate age-specific transmission parameters for respiratory-spread infectious agents. *American Journal of Epidemiology*, 164(10):936–944, 2006.

H. Ward, C. Atchison, M. Whitaker, K. E. Ainslie, J. Elliott, L. Okell, R. Redd, D. Ashby, C. A. Donnelly, W. Barclay, et al. Sars-cov-2 antibody prevalence in england following the first peak of the pandemic. *Nature communications*, 12(1): 1–8, 2021.

S. Watanabe. A widely applicable Bayesian information criterion. *Journal of Machine Learning Research*, 14(Mar):867–897, 2013.

C. H. Watts and R. M. May. The influence of concurrent partnerships on the dynamics of HIV/AIDS. *Mathematical Biosciences*, 108(1):89–104, 1992.

D. J. Watts and S. H. Strogatz. Collective dynamics of small-worldnetworks. *Nature*, 393(6684):440–442, 1998.

K. M. Weiss, S. M. Goodreau, M. Morris, P. Prasad, R. Ramaraju, T. Sanchez, and S. M. Jenness. Egocentric sexual networks of men who have sex with men in the United States: Results from the ARTnet study. *Epidemics*, 30:100386, 2020.

K. Wellings and A. M. Johnson. Framing sexual health research: adopting a broader perspective. *The Lancet*, 382(9907):1759–1762, 2013.

L. K. Whittles, P. J. White, and X. Didelot. A dynamic power-law sexual network model of gonorrhoea outbreaks. *PLoS Computational Biology*, 15(3):e1006748, 2019.

R. R. Wilkinson and K. J. Sharkey. An exact relationship between invasion probability and endemic prevalence for Markovian SIS dynamics on networks. *PloS one*, 8(7):e69028, 2013.

R. R. Wilkinson and K. J. Sharkey. Message passing and moment closure for susceptible-infected-recovered epidemics on finite networks. *Physical Review E*, 89(2):022808, 2014.

L. Willem, S. Abrams, P. J. Libin, P. Coletti, E. Kuylen, O. Petrof, S. Møgelmose, J. Wambua, S. A. Herzog, C. Faes, et al. The impact of contact tracing and household bubbles on deconfinement strategies for COVID-19. *Nature Communications*, 12(1):1–9, 2021.

F. Wu, S. Zhao, B. Yu, Y.-M. Chen, W. Wang, Z.-G. Song, Y. Hu, Z.-W. Tao, J.-H. Tian, Y.-Y. Pei, et al. A new coronavirus associated with human respiratory disease in China. *Nature*, 579(7798):265–269, 2020.

L.-P. Wu, N.-C. Wang, Y.-H. Chang, X.-Y. Tian, D.-Y. Na, L.-Y. Zhang, L. Zheng, T. Lan, L.-F. Wang, and G.-D. Liang. Duration of antibody responses after severe acute respiratory syndrome. *Emerging Infectious Diseases*, 13(10):1562, 2007.

J. L. Wylie and A. Jolly. Patterns of chlamydia and gonorrhea infection in sexual networks in Manitoba, Canada. *Sexually Transmitted Diseases*, 28(1):14–24, 2001.

M. Xiridou, R. Geskus, J. de Wit, R. Coutinho, and M. Kretzschmar. The contribution of steady and casual partnerships to the incidence of HIV infection among homosexual men in Amsterdam. *AIDS*, 17(7):1029–1038, 2003.

M. Xiridou, R. Geskus, J. de Wit, R. Coutinho, and M. Kretzschmar. Primary HIV infection as source of HIV transmission within steady and casual partnerships among homosexual men. *AIDS*, 18(9):1311–1320, 2004.

J. A. Yorke, H. W. Hethcote, A. Nold, et al. Dynamics and control of the transmission of gonorrhea. *Sexually Transmitted Diseases*, 5(2):51–56, 1978.